Journal of Physical and Chemical Reference Data

Protocol for Structure Determination of Unknowns by EI Mass Spectrometry. I. Diagnostic Ions for Acyclic Compounds with up to One Functional Group

Cite as: J. Phys. Chem. Ref. Data **51**, 031501 (2022); https://doi.org/10.1063/5.0091956
Submitted: 18 March 2022 • Accepted: 08 June 2022 • Published Online: 13 September 2022

Anzor Mikaia

Journal of Physical and Chemical Reference Data REVIEW scitation.org/journal/jpr

Protocol for Structure Determination of Unknowns by EI Mass Spectrometry. I. Diagnostic Ions for Acyclic Compounds with up to One Functional Group

Cite as: J. Phys. Chem. Ref. Data 51, 031501 (2022); doi: 10.1063/5.0091956
Submitted: 18 March 2022 • Accepted: 8 June 2022 •
Published Online: 13 September 2022

View Online Export Citation CrossMark

Anzor Mikaia[a)]

AFFILIATIONS

National Institute of Standards and Technology, 100 Bureau Drive, Gaithersburg, Maryland 20899, USA

[a)]Author to whom correspondence should be addressed: anzor.mikaia@nist.gov

ABSTRACT

This Review covers wide-ranging electron ionization (EI) dissociation reactions for various acyclic compounds and their derivatives, such as alcohols, aldehydes, ketones, carboxylic acids, amines, halides, thiols, thiones, esters, thioesters, amides, and more. Common derivatives of monofunctional compounds, such as trialkylsilyl, acyl, perfluoroacyl, oxazoline, and nicotinyl derivatives, are also discussed. The behavior of these under mass spectrometry (MS) conditions is determined, structures and stabilities of product ions are considered, and the ions of diagnostic power in their EI spectra are highlighted. Characteristic dissociation pathways for specific structural elements and their application for spectra/structure correlations are presented. Fundamental approaches for identifying unknowns are given. The advantages and limitations of EI-MS are emphasized. This knowledge is the key for successful applications of the exceptional capabilities of EI-MS for initial structure elucidation and then reliable structure determination of unknowns.

Key words: acids; alcohols; aldehydes; aliphatic hydrocarbons; amides; amines; derivatives; electron ionization; identification of unknowns; ketones; mass spectra; thiols; thiones.

CONTENTS

List of Tables

List of Figures

1. Introduction

Mass spectrometry (MS) is the most powerful instrumental method for the analysis of chemicals at a molecular level due to its high sensitivity and the ability to be employed in combination with various separation techniques. The first use of a MS approach in analytical chemistry goes back to 1913 when Thomson separated the neon isotopes[1] and to the beginning of 1930 when the first mass spectra of alkanes were recorded.[2] Since then, MS instruments have been developing rapidly, mainly due to the growing interest in the areas of environmental chemistry, petrochemistry, and biological science. At the present time, researchers have access to a wide variety of ionization methods, such as chemical ionization, electrospray ionization, matrix-assisted laser desorption/ionization, photoionization, ambient MS ionization, and more.[3] Ultimately, MS has become

both the science and the technology of ions employed for fundamental physical quantifications, for the study of ion chemistry, and for chemical analysis. Among all, electron ionization (EI), the oldest ionization technique, remains the most efficient and popular for structure determination of components within mixtures of natural and synthetic origin.

The analytical and physical aspects in this field are well represented in many books in light of rapid expansion of MS and its applications.[4–21] Additionally, presently there are two major mass spectral databases in the market: the NIST/NIH/EPA mass spectral library[22] and the Wiley Registry of Mass Spectral Data.[23] The high quality and reliability of mass spectral data and the presence of additional gas chromatography (GC) retention index data make the NIST Library the "gold standard" among major and many special mass spectral databases. Software tools for structure determination and the inclusion of artificial intelligence in the data analysis process are beneficial.[24–27]

When we use the term "unknowns," this includes three classes of "unknown compounds": (1) "known not expected substances," (2) "unknown but expected substances," and (3) "unknown and unexpected substances."

The present protocol is designed for the identification of unknowns by EI-MS to be used for "bottom-up" (identification of unknowns via computer assisted manual examination of data) and "top-down" (database search followed by a manual evaluation) data analysis. The backbone of the protocol encompasses categorized diagnostic ions for selected classes of compounds of organic and bioorganic origin as well as notes on the potential and limitations of the EI-MS method. The goal of this protocol is to assist in the development of logical thinking skills to utilize known ion fragmentation rules and to generate structures of unknown entities by establishing relations between a spectrum and the structure or structural elements.

This protocol provides general concepts of EI-MS, such as the description of types of ions, and general MS rules and established basic fragmentation regularities. Emphasis is made on the examination of stability of classes of chemicals under EI, analysis of their dissociation pathways, systematization of general and specific dissociation patterns, identification of diagnostically important ions, organization of typical ions for recognition of specific structural elements, and summation of approaches to correlate fragmentation patterns and characteristic ions with molecular structures. Methodological approaches that can be utilized to extend the analytical potential of the MS method are presented.[28]

Chemicals under discussion are organized in increasing chemical functionality. The mass spectral characteristics of simple saturated hydrocarbons are followed by their mono- and poly-unsaturated homologs and then their mono- and poly-heteryl analogs are examined. Behavior under EI for each group of compounds is examined along with their mono-functional derivatives containing oxygen (alcohols, ethers, carbonyl compounds, and acids), sulfur (mercaptanes, sulfides, and thiones), and nitrogen (amines, hydrazines, diazenes, and azides), and halogen (chlorine, bromine, and iodine) containing substituents as well as sulfoxides, sulfones, amides, hydroxylamines, cyanides, and isocyanides. The mass spectral characteristics of chemical modification products for specific classes of compounds are also discussed in recognition of derivatization as one of the strategies to control fragmentation and to improve the performance of MS methods in order to expand its efficiency, adaptability, and effectiveness.

This is Paper I and the other parts are in preparation. The first three parts (Papers I–III) will discuss potential of the MS method for structure elucidation of relatively simple compounds, Papers IV and V will examine complex molecules containing multifunctional groups, and Paper VI will provide a guide for the effective use of reference data and software tools for computer assisted examination of data containing unknowns.

We present in this paper, Paper I of the protocol, which explores the mass spectral characteristics of compounds with the simplest backbone aliphatic (acyclic) hydrocarbons and their mono- and poly-heteryl analogs along with their monofunctional derivatives.

In Paper II, we will consider behavior under EI of monocyclic hydrocarbons with three, four, five, six, and seven plus membered rings. Unsaturated will follow the saturated hydrocarbons. Mass spectra of hetero-atom(s) containing analogs are examined for each group of monocyclic hydrocarbons.

Paper III will discuss more complex compounds containing a monocyclic moiety with an aliphatic chain and one of the functional groups that are listed above for aliphatic compounds.

Papers IV and V will analyze carbo- and hetero-polycyclic compounds along with their unsaturated and aromatic analogs with mono- and multi-functional groups. Emphasis will be made on mass spectral characteristics of environmentally important compounds (such as pesticides and herbicides) as well as drugs and drug metabolites (including drugs of abuse). Special sections will be reserved for mass spectra of polyols (sugars), polyamines, hydroxyl acids, oxo acids, amino acids, steroids, and selected groups of alkaloids. Dissociation patterns of these compounds under EI may encompass pathways observed for unsubstituted and mono-substituted acyclic, alicyclic, heterocyclic, and aromatic mono ring compounds in Papers I–III. Additional decomposition routes for these multifunctional chemicals may include dissociation due to the interactions of substituents and various structural elements that may change the reaction directions and generate diagnostically important ions. Some of these products may be due to "*peri* effect," "*ortho* effect," and "*para* effect." Note that multiple dissociation patterns generate a set of competing fragmentation patterns. Some of these can be dominant for one type of compound and the other type of patterns is unfavorable and may not participate in the decomposition process. The favorability of a decomposition reaction under EI depends on the driving force of a reaction; it depends on the thermochemistry of a process, kinetic factors, and stability of ions. The role of these aspects will be outlined in Papers IV and V along with the revelation of potentially successful fragmentation patterns for specific groups of chemicals.

Paper VI will summarize analytically important dissociation patterns of chemicals under EI and diagnostically important ions in their mass spectra, will explore their correlation with MS theories/concepts and bond dissociation processes, and will recap the criteria for establishing the consistency between mass spectra and molecular structures. The potential of tools provided by artificial intelligence, effectiveness of search engines, software systems for the extraction and analysis of data, and special algorithms for computer assisted manual evaluation of data will be reviewed. The efficiency of comprehensive mass spectral databases and their content as well

as related databases, which provide data on gas chromatographic retention and thermochemistry, and IR spectra will be considered.[29]

Plots of mass spectra presented in the protocol for illustration originate from the NIST/NIH/EPA mass spectral library.[22] These spectral data along with mass spectra published in the open literature are used for analysis and interpretation. For that reason, a special section of Paper VI will provide information on the history of the NIST/NIH/EPA mass spectral library,[30] the content of data, the origin of data, step-by-step critical evaluation procedures of data for this library,[31] search engines, software tools for the analysis of data, and more.

Conclusions are made during the examination of spectra for homologous series and comparison of the findings to known fragmentation patterns that are described in special reviews and books in MS. Basically, MS provides a good estimation of a general structure, including the molecular weight and selected structural elements. However, the best practice includes the selection and utilization of additional instrumental methods. In addition, a molecular structure may be fully decoded via the combined use of various spectral and non-spectral methods.[32,33] It is important to note that structure determination by MS does not always imply complete structure elucidation and differentiation of regioisomers, conformational isomers, diastereomers, and enantiomers.

2. General Concepts

During MS experiments, a sample is destroyed completely, whereas an analyte remains intact after the analysis by other spectroscopy methods. Fragmentation of molecular and product ions is the key to mass spectra interpretation of unknowns. The determination of the elemental composition and possible structure of these ions, as well as the identification of eliminating neutral fragments, followed by the formulation of decomposition pathway mechanisms, leads to an accurate characterization and virtual reconstruction of the molecular structure of the initial analyte.

The EI-MS experiment involves shooting energetic electrons carrying 50–80 eV kinetic energy on a neutral, and ionization is achieved by knocking off an electron from the analyte. This classical procedure instigates the transfer of some of the energy of an electron to the neutral. The transferred energy usually exceeds the ionization energy (IE) of the neutral, which is usually about 4–14 eV for most organic molecules and elements of the Periodic Table (see Table S1); the IE value is higher for a few elements (from 15 to 25 eV), such as argon, fluorine, neon, and helium. Only positively charged ions are registered at positive mode EI (Scheme 1):

(1) odd-electron (commonly abbreviated as OE) or open-shell ions that are termed "radical cations,"
(2) even electron (commonly abbreviated as EE) or closed-shell ions that are termed "cations,"
(3) doubly charged (EE) and triply charged (OE) ions, and
(4) metastable ions (earlier referred to as "diffuse peaks") that are generated on the way from an ionization chamber to the ion detector.

Neutral species and radicals are suggested based on mass differences between the precursor and product ions. Negatively charged species are not considered in positive mode EI.

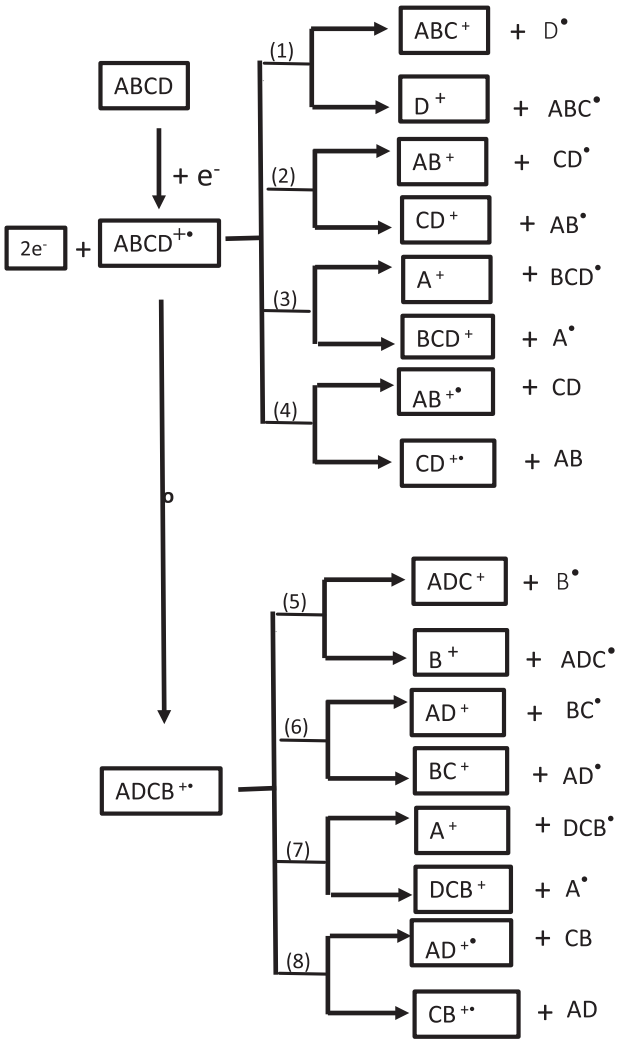

SCHEME 1. Ionization of a sample and formation of ions.

2.1. Molecular ion

Molecular ion ($M^{+\cdot}$) refers to the neutral molecule that has lost an electron. Its mass reveals a combination of elements in the analyte and equals the sum of nominal masses of constituents. Accurate mass measurements may be applied for the determination of the elemental formula. The $M^{+\cdot}$ peak candidate may show a high intensity peak or may not appear in the spectrum at all. The diagnostic criteria for the selection of a molecular ion peak include the following parameters:

(1) The peak that has the highest mass value in the spectrum refers to the most abundant natural isotope.
(2) It shall correspond to an ion with a single charge.
(3) The mass shall agree with the "nitrogen rule" stating that organic molecules containing an odd number of nitrogen atoms have an odd nominal molecular mass and molecules

containing an even number of nitrogen atoms (or without nitrogen atoms) show an even nominal molecular mass.

(4) Mass differences 4–14 Da from the molecular ion to fragment ion peaks are improbable; additionally, peaks with 21–25 Da differences are unlikely to appear.

(5) The isotope profile of the $M^{+\cdot}$ peak shall be reasonable for the suggestion of the elemental composition of an analyte.

The generated molecular ions (and isomeric cation radicals produced as a result of rearrangement reactions) decompose strictly via competing unimolecular dissociations due to low pressure and higher dissociation rate than the frequency of ion–molecule collisions.

2.2. Distonic radical cations

Chemical species that contain charge and radical sites on separate atoms of the same "molecule" are named distonic ions. They can be differentiated according to the location of the charge and the radical site as α-, β-, γ-, δ-, and ε-distonic ions. In α-distonic ions, the charge and the radical site are placed on adjacent atoms, and they are separated by one atom in β-distonic ions, by three atoms in γ-distonic ions, and so forth. Distonic ions are generated by the rearrangement of radical cations, and they may not dissociate similar to the conventional radical cations.

2.3. "The EE rule"[34]

The "EE rule" states that OE ions (radical cations) can eliminate a radical or neutral species. The loss of radicals from OE ions leads to the formation of EE cations [pathways (1)–(3) and (5)–(7)] as shown in Scheme 1, and OE radical cations are formed [pathways (4) and (8)], as a result of the elimination of neutral species. The resulting EE (closed-shell) ions predominantly lose a neutral molecule and produce an EE ion—cation (no odd–odd electron combinations). The "EE rule" forbids successive loss of radicals. OE ions may eliminate either a radical or an EE neutral species, but EE ions do not usually lose a radical to form an OE ion.[34] The exception to the rule is addressed when discussing fragmentation patterns of specific compounds.

2.4. "Nitrogen rule"

OE radical cations, including molecular ions of all organic compounds, with an even number of nitrogen atoms (or no nitrogen atoms) have an even nominal mass, whereas radical cations with an odd number of nitrogen atoms have an odd nominal mass. On the contrary, the EE cations containing an even number of nitrogen atoms (or no nitrogen atoms) have an odd nominal mass, and cations with an odd number of nitrogen atoms have an even nominal mass. This rule is valuable for determining the content of nitrogen in an unknown and for interpreting fragmentation patterns of nitrogen-containing compounds.

2.5. Isotope patterns

Elements present in a molecule demonstrate their natural isotopic occurrences by producing clusters in mass spectra. The intensity ratios of peaks in these clusters are unique (see Table 7) and are used for the identification of polyisotopic constituents in a molecule and the number of these elements.[35,36] Figure 1 demonstrates very different profiles of the molecular ion peaks for alkane, perfluoroalkane, carborane, cyclopentasilane, and octathiocane as well as for chloro-, bromo-, and iodo-form. Similar differences are successfully employed for the determination of the elemental composition of an unknown. A useful approach for determining possible molecular formula(s) of a compound from its molecular mass is the "rule of 13."[37] The rule states that the C_nH_{n+r} formula of a compound is a multiple "n" of 13 (mass of CH) plus remainder "r"; the latter may represent the count of additional hydrogen atoms. Formula adjustment is required for the inclusion of heteroatoms: (a) CH_4 is subtracted from the formula with the addition of each oxygen, (b) CH_2 is subtracted from the formula with the addition of each nitrogen, and (c) C_2H_{11} is subtracted from the formula with the addition of chlorine. Along with the "rule of 13," the intensity ratios of the candidate $M^{+\cdot}$ peaks and their minor naturally occurring stable isotopes of ^{13}C, ^{34}S, and ^{30}Si may suggest candidate elemental formulas of an unknown.

MS can characterize natural isotopes qualitatively and quantitatively and determine the difference in their masses. The difference

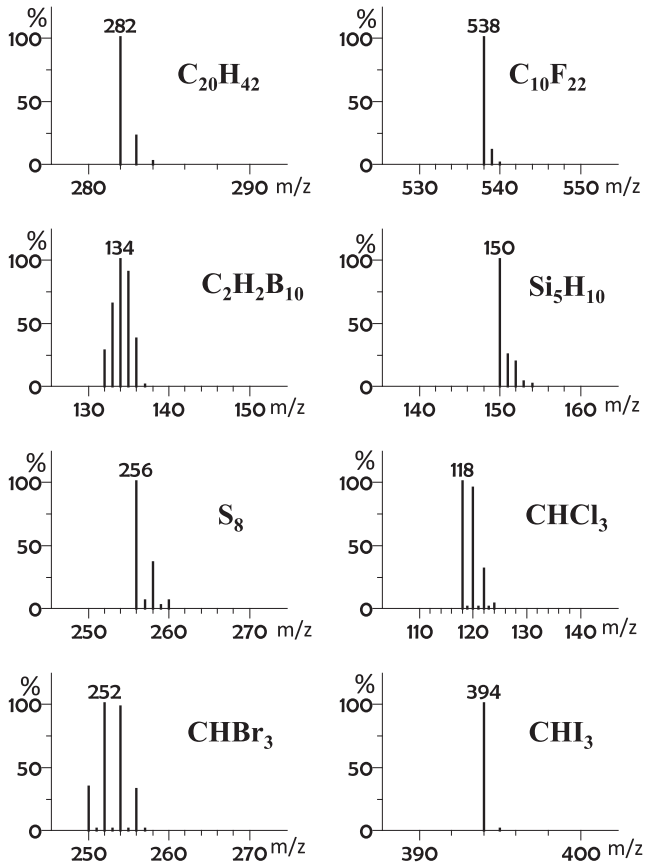

FIG. 1. Molecular ions in the mass spectra (m/z/relative intensity) of eicosane ($C_{20}H_{42}$), perfluorodecane ($C_{10}F_{22}$), o-carborane ($C_2H_2B_{10}$), cyclopentasilane (Si_5H_{10}), octathiocane (S_8), chloroform ($CHCl_3$), bromoform ($CHBr_3$), and iodoform (CHI_3).

in masses of the isotopes of an element causes the difference in their reaction rates. The latter determines the difference in chemical properties of isotopes of an element. The simplest example is the hydrogen isotope effect: the mass of deuterium is twice as heavy as that of hydrogen; usually, the kinetic isotope effects observed by MS differ than the theoretically predicted data obtained by quasi-equilibrium theory (QET), Rice–Ramsperger–Kassel–Marcus (RRKM) theories, and Quantum Chemical EIMS (QCEIMS).

2.6. Stevenson–Audier rule

This rule is based on the application of ionization and appearance energies to understand, interpret, and predict charged species in EI spectra. The Stevenson–Audier rule[38] states that among competing species the positive charge remains on the fragment with the lowest ionization energy.

2.7. Unimolecular organic reactions

Molecular ions that obtained sufficient energy can dissociate via competing unimolecular fragmentations. The charge and the radical locations in $M^{+\cdot}$ usually represent the ground state of a molecule; however, an electron may be removed from various sites during rapid transitions between excited electronic states and the electronic ground state. In the case of monofunctional compounds, several primary fragmentation reactions are established for dissociation of $M^{+\cdot}$: (a) a simple bond cleavage, such as homolytic cleavage and heterolytic cleavage; (b) cleavages of two σ-bonds without the formation of new bonds, such as the retro-Diels–Alder (rDA) reaction and water molecule elimination reaction; (c) a simple bond cleavage with the formation of a new bond between the previously unconnected atoms; and (d) skeletal rearrangements, including hydrogen transfer (e.g., McLafferty rearrangement), halogen transfer, oxygen transfer, and more.

2.7.1. Homolytic cleavage

The term homolytic derives from the Greek "homoios" ("equal") and "lysis" ("loosening"). Typically, the radical site is responsible for a symmetrical bond breaking that occurs in homolytic cleavage in such a way that each fragment gets one of the shared electrons. The positive charge does not move during the homolytic dissociation; the movement of single electrons is specified by a single "fish hook" half-arrow. As shown in Scheme 2, three competing homolytic cleavages are available for 3-methylhexanol-3 to produce homologous oxocarbenium cations $[M\text{-}CH_3]^+$ (101 Da), $[M\text{-}C_2H_5]^+$ (87 Da), and $[M\text{-}C_3H_7]^+$ (73 Da). The tendency of radicals with greater mass to leave is favorable; therefore, the intensities of peaks of the product ions depend on the size of the radical lost: $I_{73\ Da} > I_{87\ Da} > I_{101\ Da}$.

2.7.2. Heterolytic cleavage

Heterolytic cleavages are controlled by the ability of the positive charged atoms to attract a shared electron pair, and the tendency is determined by the electronegativity of an element (χ): **F** (3.98) > **O** (3.44) > **Cl** (3.16) > **N** (3.04) > **Br** (2.96) > **I** (2.66) > **S** (2.58) > **C** (2.55) > **P** (2.19) > **Si** (1.90). The charge site inspires heterolytic fission that involves heterolytic capture of both electrons out of the bond. These electrons migrate to the positive charge and neutralize the charge at the original site. Synchronously, an electron deficiency

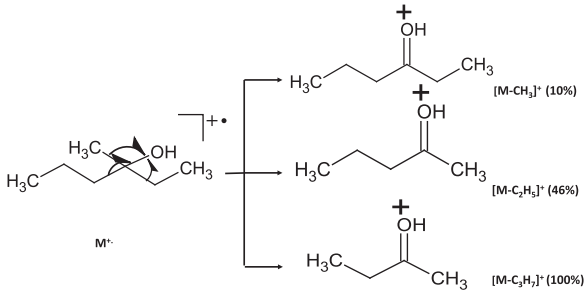

SCHEME 2. Homolytic cleavages in $M^{+\cdot}$ of 3-methylhexanol-3.

emerges on the other part of $M^{+\cdot}$; it is reflected by the positive charge developing on the carbon atom that previously formed the C–Br bond (see Scheme 3). A synonymous term "inductive cleavage" is also used to describe this reaction. The movement of two electrons and charge relocation is indicated by a doubly barbed arrow.

2.7.3. Bond cleavage and formation of a new bond

This type of dissociation occurs in $M^{+\cdot}$ of primary chloro-, bromo-, mercapto-, amino-, and cyano-alkanes as a result of σ-bond cleavage at the δ-, ε-, or ζ-carbon atom in the alkyl chain. For chlorides and bromides, prominent peaks correspond to cyclic chloronium or bromonium EE ions $[C_4H_8X]^+$ (Scheme 4); the homologous six-membered $[C_5H_{10}X]^+$ cations are less prominent. The same is true for 1-thiols, and a six membered ring is typical for 1-aminoalkanes. For long-chain nitriles, eight-membered cyclic cations are favorable among six- to nine-membered EE ions present in the spectra. Chain branching may significantly reduce this reaction.

2.7.4. Two bond cleavages without formation of a new bond

2.7.4.1. retro-Diels–Alder reaction. The term "retro-Diels–Alder" (rDA) reaction best describes the fragmentation of $M^{+\cdot}$ of a variety of compounds that contain cyclohexene structural units with

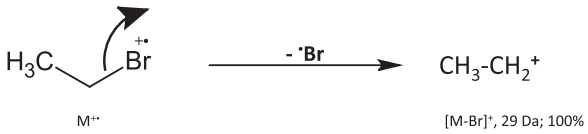

SCHEME 3. Heterolytic cleavage of the C–Br bond in $M^{+\cdot}$ of ethylbromide.

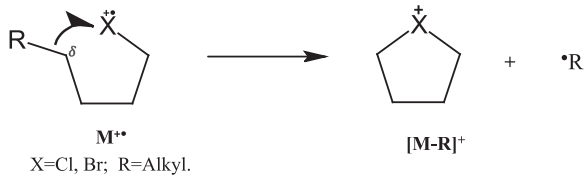

SCHEME 4. Alkyl radical elimination at δ-C in $M^{+\cdot}$ of alkyl chlorides and bromides.

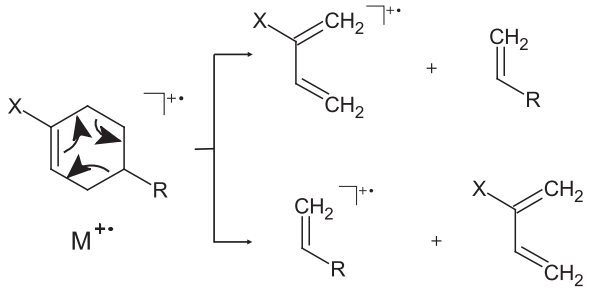

SCHEME 5. retro-Diels–Alder reaction in $M^{+\cdot}$ of 1,4-disubstituted cyclohexene.

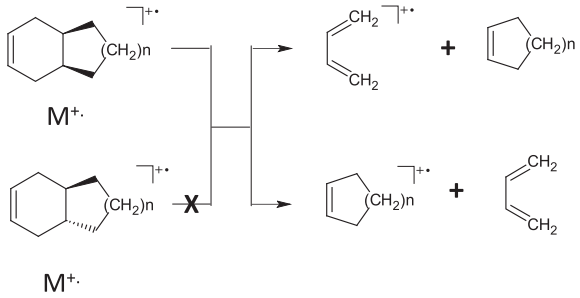

SCHEME 6. rDA reaction in $M^{+\cdot}$ of stereoisomeric bicycloalkanes.

the formation of the "starting materials"—cycloreversion reaction products. Cyclohexenes and their multiple heteroatom-containing analogs formally formed from a diene and an olefin via [4 + 2] cycloaddition, and the products of the dissociation of cyclohexene $M^{+\cdot}$ are the corresponding dienes and the olefins (Scheme 5); the charge may be localized on either of the fragments. According to the Stevenson–Audier rule, the charge site is controlled by the ionization energies of the fragments in their neutral forms, i.e., the charge is retained by the species with lower ionization energy. Identification of the radical cations produced via the rDA reaction enables a reliable double bond location in the six-membered ring.

The rDA reaction is not relevant for *trans*-bi- and polycyclic systems, and only *cis* isomers would undergo the rDA fragmentation controlled by stereochemistry. Thus, the presence or absence of rDA products is diagnostically important for the differentiation of (*E*)- and (*Z*)-isomers as shown in Scheme 6.

2.7.4.2. Symmetric ring scission in cyclobutanes. Four-membered ring compounds (such as cyclobutane, sila- and germacyclobutanes, thietane, oxetanes, and azetidine) are formally products of [2 + 2] cycloaddition and their $M^{+\cdot}$ dissociation products are two olefins (Scheme 7). Similar to cyclohexenes, the charge may be localized on either of the fragments.

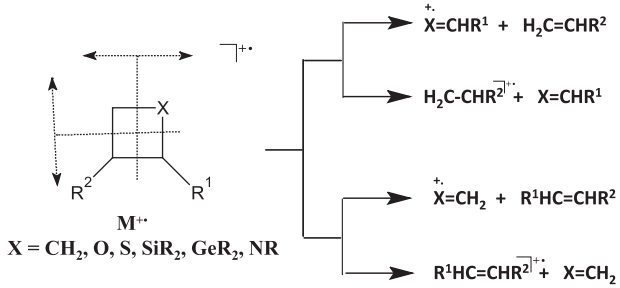

SCHEME 7. Typical reactions in ionized four-membered ring compounds.

2.7.5. H_2O, H_2S, HCl elimination from $M^{+\cdot}$

The synchronous loss of a functional group and an H-atom from $M^{+\cdot}$ may not always be considered a rearrangement process. Thus, dehydrochlorination of 1-alkylchlorides predominantly proceeds via 1,3-elimination (five-membered transition state), while primary alkanols demonstrate an exclusive preference for 1,4-elimination (90%, six-membered transition state). Neutral hydrogen sulfide is equally eliminated via 1,3- and 1,4-elimination reactions in dissociation of 1-alkanethiol molecular ions (Scheme 8).[39,40]

2.7.6. Skeletal rearrangement

Rearrangements of $M^{+\cdot}$ via (a) McLafferty rearrangements of monofunctional compounds that involve 1,6-hydrogen shift and (b) skeletal rearrangements of hetero compounds via three-, four-, five-, and six-centered transition states are discussed in this section.

2.7.6.1. 1,6-Hydrogen shifts—McLafferty rearrangement. The McLafferty rearrangement refers to the formation of distonic intermediates from $M^{+\cdot}$ of monounsaturated molecules containing γ-hydrogen relative to the double bond followed by the transfer of γ-hydrogen via a six-membered transition state and the β-bond

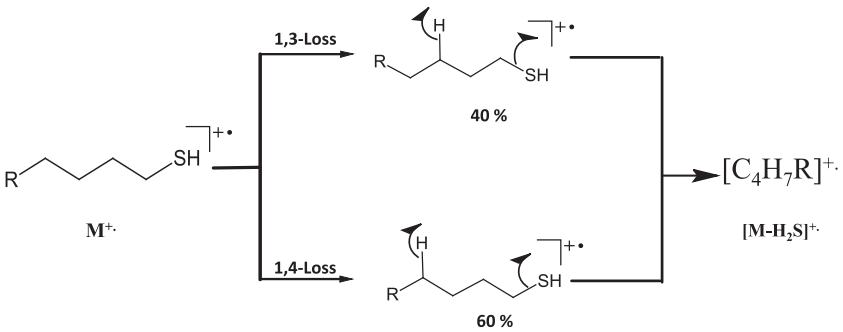

SCHEME 8. Mechanisms of H_2S elimination from alkanethiols.

cleavage resulting in the elimination of neutral species (Scheme 9). The hydrogen transfer and β-cleavage in distonic ions may be a synchronized process or proceed via an initial γ-hydrogen transfer followed by β-cleavage. The reaction was first observed and reported by Nicholson and later generalized and named after McLafferty. It is accepted that the distance between carbonyl oxygen and γ-hydrogen for carbonyl compounds shall not exceed 1.8 Å, and an angle of 50° or less is a requirement for the McLafferty rearrangement to proceed. Secondary γ-hydrogen atoms shift more favorable than the primary atoms. Compounds containing an additional γ-hydrogen relative to the double bond may undergo parallel and/or second McLafferty rearrangement. This process is similar to the photochemical intramolecular abstraction of a γ-hydrogen known as Norrish reaction, type II.

2.7.6.2. Smiles-type skeletal rearrangements. Smiles-type rearrangement usually takes place in $M^{+\cdot}$ of sulfides, sulfones, arylthiocarbamates, imidates, thioacids, nitro compounds, and more.

2.7.6.3. Nitro-compounds. It is established that nitro–nitrito isomerization is much faster than the spontaneous nitro–nitrito rearrangement and $M^{+\cdot}$ of nitro compounds undergo partial isomerism (Scheme 10). The "nitrito form" of $M^{+\cdot}$ further loses NO in one step. The elimination of NO proceeds via both homolytic and heterolytic cleavages.

2.7.6.4. Sulfones and sulfoxides. Rearrangement of $M^{+\cdot}$ and the formation of distonic ions are common for sulfides, sulfoxides, sulfonyls, thiones, and arylthiols.[41] $M^{+\cdot}$ of sulfoxides and sulfonyls demonstrate explicit *ipso* attack of sulfoxide (or sulfonyl) oxygen (Scheme 11) and "double *ipso*-attack"—aryl to aryl migration

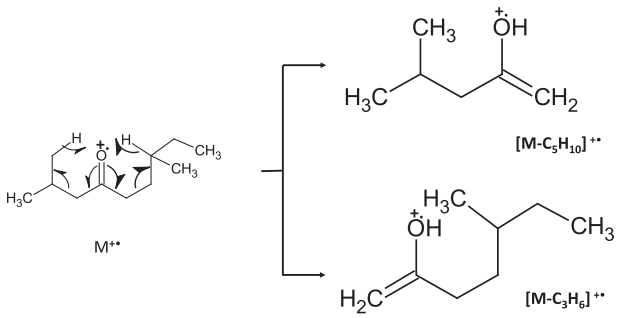

9. McLafferty rearrangement in ionized 3,8-dimethylnonan-6-one.

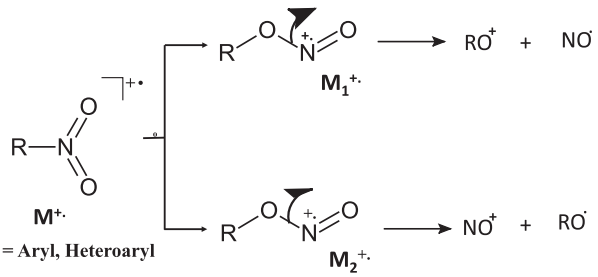

SCHEME 10. Nitro–nitrito isomerization.

(Scheme 12). They are summarized in Schemes 11 and 12, and the resulting product ions are depicted. These reactions are remarkably sensitive to structural details. The product ions may be dominant or almost disappear depending on the nature of the substituents in the aromatic systems.

2.7.6.5. 1,6-Halogen shift. Dissociation of $M^{+\cdot}$ of δ-chloroallenes and acetylenes resulting in the formation of $[M\text{-}C_2H_4]^{+\cdot}$ is good evidence of chlorine migration via a six-membered transition state (Scheme 13). Similar shifts are proceeding in $M^{+\cdot}$ of δ-bromo and δ-hydroxyl analogs.

Other diagnostically important fragmentation patterns, such as α-cleavage, β-cleavage, "allylic cleavage," "benzylic cleavage," and more, will be discussed along with the analysis of specific classes of compounds.

3. Hydrocarbons and Their Group IV Element Analogs

3.1. Saturated hydrocarbons

n-Alkane molecules do not possess distinctive sites for charge localization, and they undergo random σ-bond ionization. The $M^{+\cdot}$ peak of an *n*-octane [Fig. 2(a)] shows a weak abundance in the spectrum. This is typical for all straight-chain alkanes, and the $M^{+\cdot}$ intensity is even lower for the branched analogs. There are eight carbon atoms connected by seven σ-bonds in the *n*-octane molecule. Each σ-bond weakened equivalently in $M^{+\cdot}$, and each bond participates evenly in dissociation of $M^{+\cdot}$. In essence, $M^{+\cdot}$ of alkanes undergo (a) simple C–H and C–C bond cleavages and (b) extensive rearrangement reactions: hydrogen shifts and skeletal rearrangements.

(a-1) The percentage of product ions formed by breaking of C–H bonds (without rupture of C–C bonds) decreases from 84% in the case of ethane to less than 1% for *n*-octane; this statement is true for homologous C_2–C_8 alkanes.

(a-2) σ-C–C bond rupture at every methylene moiety in the carbon backbone of *n*-alkane produces a typical series of $[C_nH_{2n+1}]^+$ cations with monotonous intensities that decrease from the base peak up toward $M^{+\cdot}$ [Fig. 2(a)]. About 80% of these ions are formed by direct σ-cleavage of C–C bonds when the "n" number is above the number of carbon atoms in a given alkane. For *n*-alkanes, the maximum intensity corresponds to $[C_3H_7]^+$ (43 Da) or $[C_4H_9]^+$ (57 Da) EE ions. The introduction of additional one or two alkyl groups to an internal/external carbon weakens the α-C–C bond. The stability of the produced EE alkyl cations increases from methyl to (trialkyl)methyl: $[CH_3]^+ < [RCH_2]^+ < [R_2CH]^+ < [R_3C]^+$. Two or more peaks with maximum intensities in a spectrum are distinctive for branched alkanes.

Note that the sum of the intensities of peaks of $[C_nH_{2n+1}]^+$ cations is used for qualitative and semi-quantitative determination of the composition of "paraffins" in naphtha-paraffin fractions of oil.

(b) The major documented rearrangements occurring in alkanes include (1) hydrogen shifts in $M^{+\cdot}$ and product ions, (2) the loss of a hydrogen molecule from OE and EE product

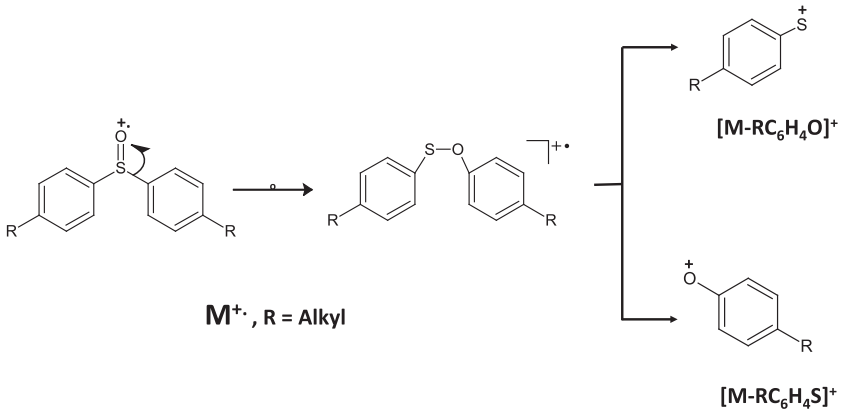

SCHEME 11. Sulfoxide–sulfite isomerization.

ions and $M^{+\cdot}$, and (3) synchronous hydrogen and skeletal rearrangement.

(b-1) The loss of a hydrogen molecule is not a major dissociation pathway for alkanes, and the abundance of $[M\text{-}H_2]^{+\cdot}$ ions is low in the spectra. However, a series of homologous $[M\text{-}C_nH_{2n+1}\text{-}H_2]^+$ ion peaks are prominent in the spectra; see ion peaks at m/z 27, m/z 41, and m/z 55 in the spectrum of *n*-octane [Fig. 2(a)]. This process includes rearrangements and proceeds further: $[C_3H_7]^+ \longrightarrow H_2 + [C_3H_5]^+ \longrightarrow H_2 + [C_3H_3]^+$. The abundance of peaks of $[M\text{-}C_nH_{2n-1}]^+$ cations relative to the intensities of others in a given cluster are higher in the low mass region (27–71 Da) of an alkane spectrum, as seen in Fig. 2(a).

(b-2) Elimination of a methane molecule along with the $^{\cdot}CH_3$ radical from $M^{+\cdot}$ of lower *n*-alkanes, ethane to *n*-heptane, is one of the examples of skeletal rearrangements. Two pathways for this reaction have been identified: (1) loss of a terminal methyl group and hydrogen at α- or β-carbon atoms and (2) σ-bond cleavage and a series of internal rearrangements with participation of methylene moieties in the carbon skeleton. The role of internal rearrangements rises with the increase in the length of an alkyl chain, and they are more characteristic for linear alkanes than for branched ones.

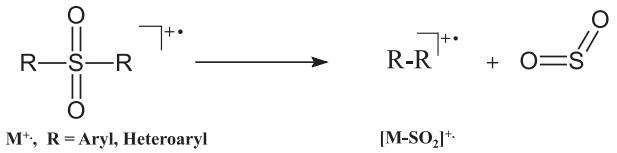

SCHEME 12. "Double *ipso*-attack" in $M^{+\cdot}$ of sulfones.

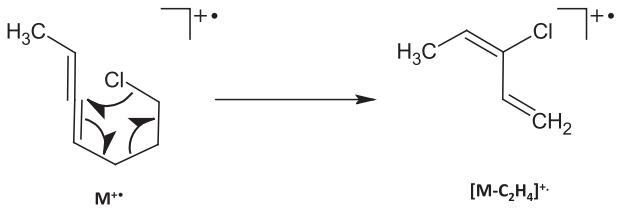

SCHEME 13. Chlorine shift in molecular radical cations of allenic chlorides.

The other type of rearrangement is associated with the dissociation of secondary and tertiary carbenium cations produced from $M^{+\cdot}$ of branched alkanes. Thus, the EE carbenium ion $[M\text{-}CH_3]^+$ in the case of 2,3,4-trimethylpentane [Fig. 2(c)] eliminates an isopropene molecule, resulting in the formation of the $[M\text{-}CH_3\text{-}C_3H_6]^+$ OE ion (57 Da).

The significant dissociation pathway of $M^{+\cdot}$ of tertiary and quaternary alkanes is related to a complex rearrangement that generates olefin radical cations because of the loss of two radicals: alkyl and hydrogen. The appearance of a crucial pair of peaks of $[M\text{-alkyl}]^+$ and $[M\text{-alkane}]^{+\cdot}$ in the spectra of branched alkanes is a clear indication of branching in the carbon skeleton. Doublet of peaks at m/z 70 and m/z 71 in the case of 2,3,4-trimethylpentane [Fig. 2(c)] and m/z 56 and m/z 57 in the spectrum of 2,2-dimethylhexane [Fig. 2(d)] point to the location of branching at positions 3 and 2, respectively. The $C_{(3)}$-atom in a 3-methylheptane molecule is connected to methyl and two other alkyl substituents larger than methyl. Therefore, the spectrum in Fig. 2(b) displays two twin peaks at m/z 84 and m/z 85 due to the loss of an ethyl radical and ethene at branching and m/z 56 and m/z 57 due to the elimination of a butyl radical and a butene molecule at the branching point.

A typical series of ions at the 14 Da intervals ($[M\text{-}C_nH_{2n+1}]^+$, $[M\text{-}C_nH_{2n}]^{+\cdot}$, $[M\text{-}C_nH_{2n-1}]^+$, and $[M\text{-}C_nH_{2n-3}]^+$) ions and their intensity pattern reflect specific structural elements. Detailed data analysis provides information sufficient for structure elucidation; additionally, evaluation of GC retention index data guarantees a reliable structure determination of alkanes.

The EI spectrum of a fluoro-analog of alkanes—perfluorohexane—is depicted in Fig. 2(e). Contrary to alkanes, it does not show $M^{+\cdot}$, but for every 50 Da, (CF_2) reveals a series of peaks of $[C_nF_{2n+1}]^+$ cations at m/z 69, m/z 119, m/z 169, m/z 219, and m/z 269. The highest mass value peaks in the spectrum correspond to $[M\text{-}F]^+$ (319 Da) and $[M\text{-}F\text{-}F_2]^+$ (281 Da) EE ions. Unlike hydrocarbons, the carbon backbone of perfluoroalkanes is not sensitive to C–C branching; there is no significant difference in abundances of $[C_3F_7]^+$ (169 Da) cations in the spectra of perfluoro-*n*-heptane and isohexane. The same tendency is observed for the series of *n*- and isoperfluoroalkanes.

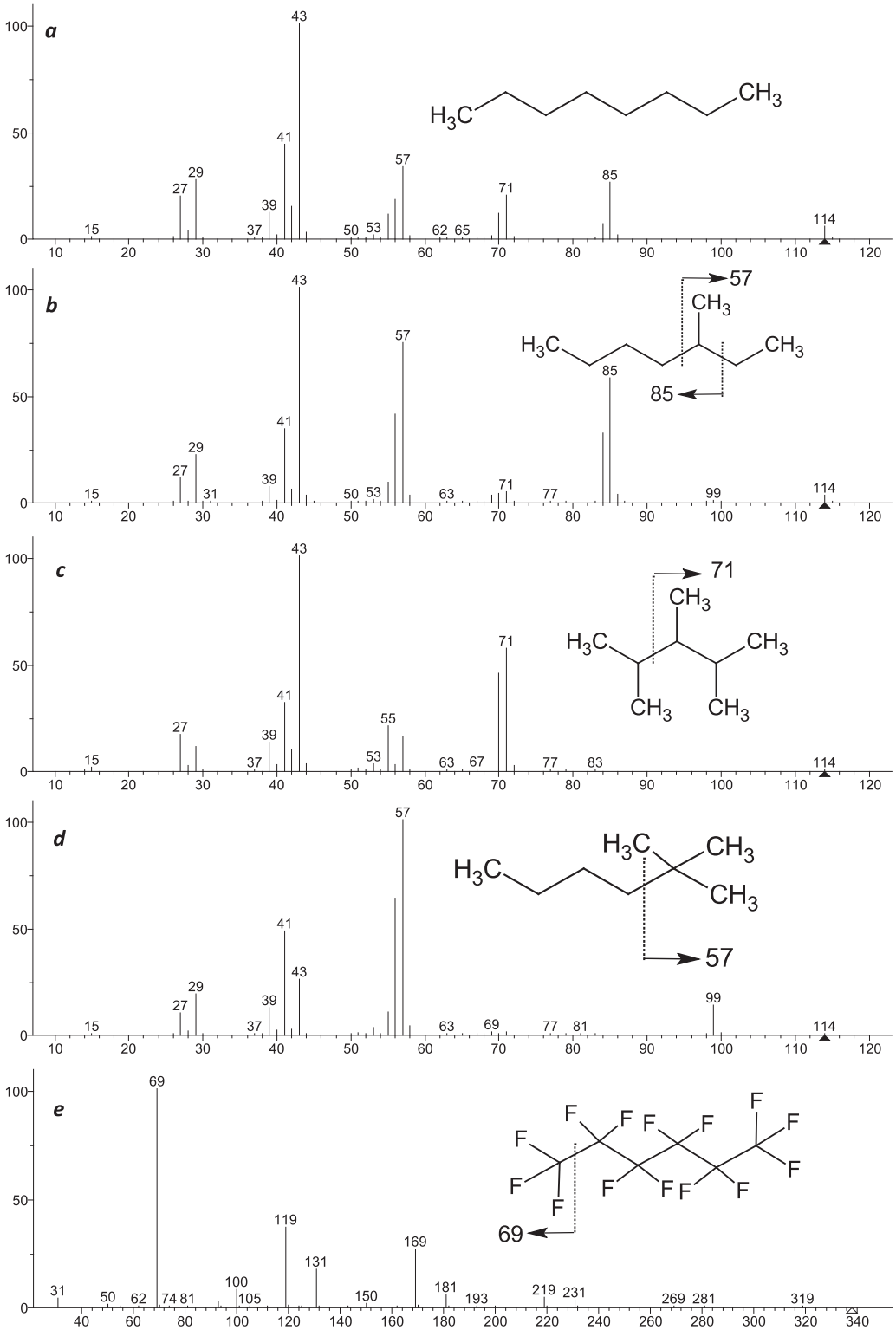

FIG. 2. Mass spectra [m/z (relative abundance, %] of isomeric octanes and 1,1,1,2,2,3,3,4,4,5,5,6,6,6-octadecafluoro-*n*-hexane.

3.2. Unsaturated hydrocarbons

Formally, dissociation of $M^{+\cdot}$ of alkenes shall be structure sensitive, and logically, the spectra shall display ions with diagnostic power because of the competency of double bond containing molecules for (a) the McLafferty rearrangement initiated by a double bond and (b) the allylic cleavage—a cleavage of σ-C–C bonds at the allylic position. In practice, EI spectra of alkenes are not as instructive as expected because $M^{+\cdot}$ of alkenes reveal a strong tendency to isomerize through migration of a double bond and to undergo skeletal rearrangements.

Two methods of preliminary derivatization of a double bond are recommended for locating unsaturation in a carbon skeleton by MS. One includes the introduction of functional groups at an unsaturation site causing specific fragmentations under EI conditions and the other uses deuteration of the double bonds. Some reactions can be carried out online during GC–MS experiments.[24]

Mass spectra of isomeric alkynes can display distinctly different abundances of product ions. However, it is difficult to reliably locate the position of a triple bond and identify each isomer. Parts of their $M^{+\cdot}$ undergo various rearrangements.

Isomerization of $M^{+\cdot}$ of aliphatic alkynes to allenes is well accepted. There are some differences in the dissociation of $M^{+\cdot}$ of allenes. Thus, the most abundant peaks in the spectra of isomeric 1,2-, 2,3-, 3,4-, and 4,5-nonadienes correspond to ions due to the McLafferty rearrangement, as shown in Scheme 14.

It is concluded that the abilities of MS for structure determination of unsaturated hydrocarbons are limited, and a comparative analysis of spectra of all isomers is required for reliable structure elucidation.

3.3. Acyclic compounds with group IV elements

Molecular ions of hydrides of group IV elements are detectable and the $M^{+\cdot}$ abundance increases in the series: $I_{[SiH4]+\cdot} > I_{[GeH4]+\cdot} > I_{[SnH4]+\cdot} > I_{[PbH4]+\cdot}$.

Their dissociation proceeds via successive loss of all hydrogens, and the most abundant peaks in the spectra correspond to ions $[M\text{-}2H]^{+\cdot}$ and $[M\text{-}3H]^{+\cdot}$.[25]

Spectra of hydrides of a general formula Met_2H_6 also (Met = Si, Ge, Sn, Pb) display $M^{+\cdot}$ and the most abundant peaks corresponding to OE ions: $[M\text{-}2H]^{+\cdot}$ and $[M\text{-}4H]^{+\cdot}$; note that the peak of an ion $[M\text{-}4H]^{+\cdot}$ (26 Da) is only about 20% in the spectrum of ethane—their carbon analog.

Similar to neopentane, in the case of (tetramethyl)silane and (tetramethyl)germane, $[M\text{-}CH_3]^+$ cations undergo a skeletal rearrangement, resulting in the formation of $[M\text{-}CH_3\text{-}C_2H_4]^{+\cdot}$ ions. However, a successive elimination of all methyl radicals is more favorable for $M^{+\cdot}$ of (tetramethyl)stannate and (tetramethyl)plumbate. The same tendency is documented for tetraethyl

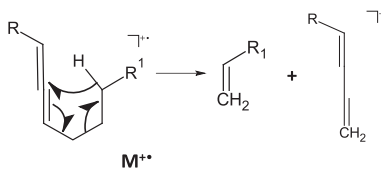

R	R¹	Dien, Da	Abundance, %
H	C_3H_7	54	100
CH_3	C_2H_5	68	100
C_2H_5	CH_3	82	72
C_3H_7	H	96	47

SCHEME 14. Loss of an alkene from $M^{+\cdot}$ of 1,2-, 2,3-, 3,4-, and 4,5-nonadienes.

compounds for group IV elements. The loss of alkyl groups heavier than methyl is preferable, as expected.

α,ω-Di(trimethylsilyl)alkanes, such as 1,2-bis[di(trimethylsilyl)]ethane and 1,3-bis[di(trimethylsilyl)]propane, show a pair of $[M\text{-}CH_3\text{-}Si(CH_3)_3]^{+\cdot}$ and $[M\text{-}CH_3\text{-}HSi(CH_3)_3]^+$ ions along with $M^{+\cdot}$, $[M\text{-}CH_3]^+$, and $[Si(CH_3)_3]^+$ ions.

These few examples demonstrate the ability of silicon- and germane-alkanes to undergo hydrogen and skeletal rearrangements. Nevertheless, EE ions of organo-tin and organo-lead compounds prefer a successive elimination of alkyl radicals and violate the "EE" rule.

These differences in the behavior of group IVa elements are explained in terms of metal–carbon, carbon–hydrogen, and metal–hydrogen bond dissociation energies relative to each other.

4. Alcohols and Their Chemical Modification Products

4.1. Alcohols

4.1.1. Saturated alkanols

Oxonium ions are the major and diagnostically important products in the EI spectra of alkanols. They are produced due to α-cleavages on either side of the carbon attached to the hydroxyl group. This process typically involves the preferable elimination of the largest alkyl group.

Another competitive dissociation pathway of $M^{+\cdot}$ of alkanols is dehydration. It mainly involves the 1,4-loss of OH/H moieties with a much smaller hydrogen contribution from $C_{(3)}$ and very little contribution from $C_{(5)}$.

$M^{+\cdot}$ of alkanols may not always display noticeable peaks because of multiple extensive fragmentation directions initiated by the ionized alcohol function. Corresponding peaks are of low intensity in the spectra of lower alkanols, and they disappear with the increase in the length of an alkyl chain. In the spectra of secondary *n*-alkanols and branched 1-alkanols, the highest mass value peaks usually correspond to $[M\text{-}H]^+$ EE ions. Nevertheless, frequently $[M\text{-}H_2O]^{+\cdot}$ OE ions are the heaviest peaks observed in the spectra, and the erroneous assumption of these peaks as $M^{+\cdot}$ should be avoided. The determination of a molecular weight via systematic evaluation of peaks in the highest mass regions along with consideration of oxonium ion peaks is standard practice. Commonly high mass peaks of the $[M\text{-}H]^+$, $[M\text{-}H_2O]^{+\cdot}$, and $[M\text{-alkyl}]^+$ ions are successfully used for the determination of molecular weight.

An even number of the heaviest $[M\text{-}H_2O]^{+\cdot}$ radical cations and the presence of $[M\text{-}H_2O\text{-}C_nH_{2n}]^{+\cdot}$ OE ions usually point to the molecular weight of an *n*-alkanol. For example, in addition to the oxonium cation at m/z 31, the spectrum of 1-nonanol in Fig. 3(a) displays a peak at m/z 126 for the $(M\text{-}18)^{+\cdot}$ OE ion and a series of peaks at m/z 98, m/z 84, and m/z 70 formally corresponding to the loss of ethene, propene, and butene from the $[M\text{-}H_2O]^{+\cdot}$ radical cation. The $[M\text{-}H_2O]^{+\cdot}$ radical cations are also accountable for the production of major peaks of other homologous hydrocarbon ions characterizing the backbone of the primary *n*-nonanol; see the cluster of peaks at m/z 55 to m/z 57, m/z 67 to m/z 71, m/z 82 to m/z 84, and m/z 97 to m/z 99 in Fig. 3(a). While the oxonium EE ion peak at m/z 31 is important from an analytical point of view, it is not

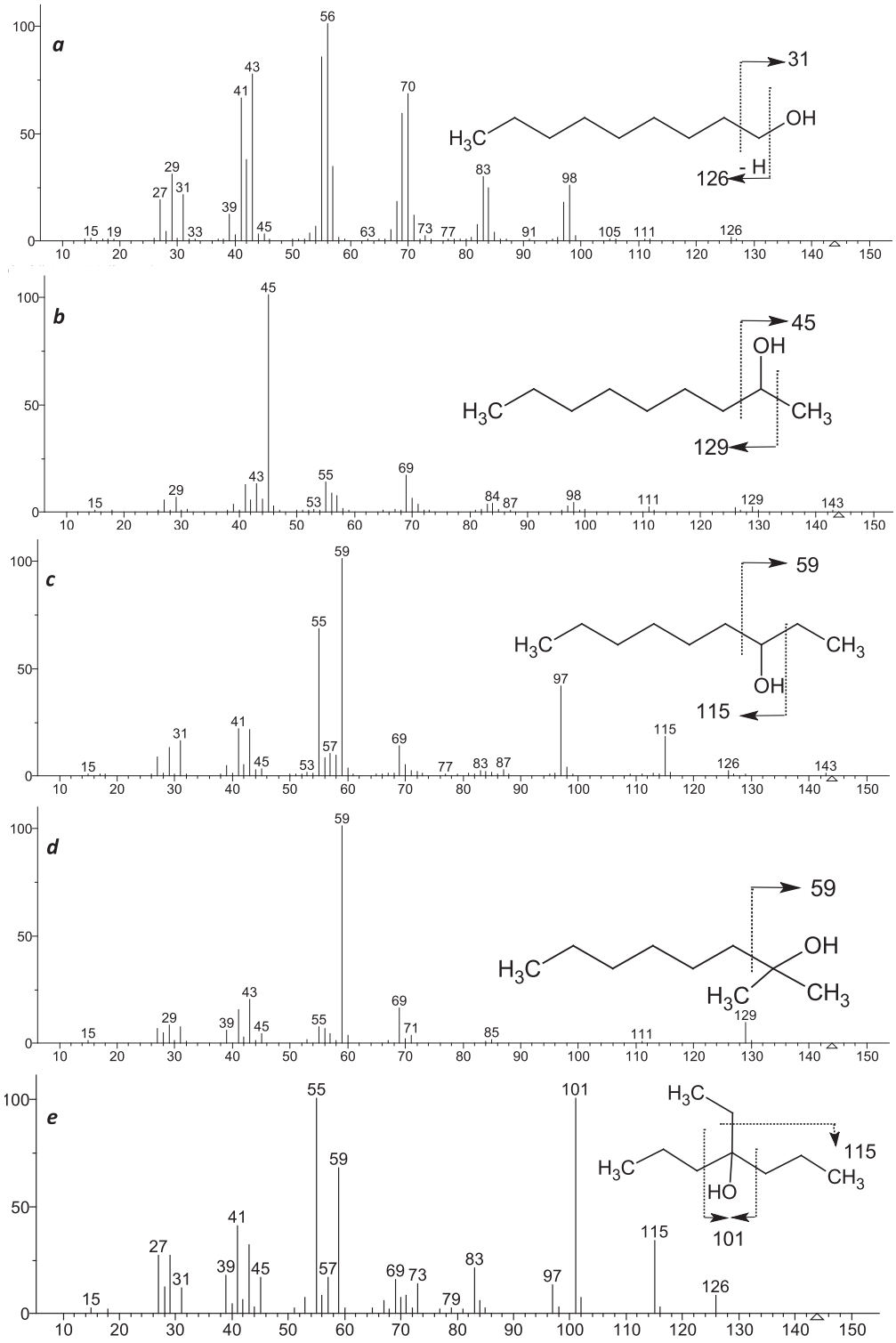

FIG. 3. Mass spectra [m/z (relative abundance, %)] of isomeric nonanols.

specifically diagnostic since in some cases it can also originate from higher oxonium cations. Note that primary alcohols yield the smallest and tertiary alcohols produce the largest quantity of oxygen containing ions.

As pointed out above, oxonium cations are the key ions when analyzing EI spectra of alkanols. One step dissociation of $M^{+\cdot}$ of primary alcohols yields only one type of oxonium ion at 31 Da, whereas $M^{+\cdot}$ of secondary alcohols generate three oxonium ions (one of which corresponds to the $[M\text{-}H]^+$ ion), and tertiary alcohols also generate three oxonium ions, all due to the loss of alkyl radicals at the tertiary carbon; some of these oxonium cations can further lose neutral alkenes and produce new oxonium EE ions. As illustrated in Fig. 3, peaks of oxonium ions display a sufficient abundance in the case of primary alcohols [m/z 31 in Fig. 3(a)], and usually, peaks of homologous ions are dominant in the spectra of secondary [m/z 45, m/z 129, and m/z 143 in Fig. 3(b) and m/z 59, m/z 115, and m/z 143 in Fig. 3(c)] and tertiary alcohols [m/z 59 and m/z 129 in Fig. 3(d) and m/z 101 and m/z 115 in Figs. 3(d) and 3(e), respectively].

EI spectra of two secondary alcohols, 2- and 3-nonanols, are depicted in Figs. 3(b) and 3(c). The main fragmentation pathways for 3-nonanol are given in Scheme 15. The spectrum interpretation includes the following: (a) $[M\text{-}H]^+$ EE ions point to the secondary substitution of the hydroxyl group (as noted above, the H radical is also eliminated from a secondary carbon), (b) $[M\text{-}C_2H_5]^+$ and $[M\text{-}C_6H_{13}]^+$ cations indicate that the hydroxyl is attached to $C_{(3)}$ that bears additional ethyl and hexyl substituents, and (c) $[M\text{-}H_2O]^{+\cdot}$ OE ions along with $[M\text{-}H]^+$ EE ions confirm the molecular weight and the structure for 3-nonanol. However, the spectrum cannot reliably confirm normal alkanes for C_4–C_9 when dealing with an unknown; additional efforts are to be made to exclude branching in this part of a molecule.

The mass spectrum of 2-methyl-2-octanol [Fig. 3(d)] easily confirms the dimethyl(hydroxy) methyl moiety of the tertiary alcohol in the presence of the $[M\text{-}CH_3]^+$ (129 Da) EE ion and the base peak at m/z 59. However, the spectrum cannot reliably confirm normal alkanes for C_3–C_8 when dealing with an unknown; additional efforts are required to exclude branching in this part of a molecule.

The structure of the other tertiary alcohol—4-ethyl-4-heptanol [see the spectrum in Fig. 3(e)]—is readily determined on the basis of mass values of $[M\text{-}H_2O]^{+\cdot}$ and the oxonium ions; the absence of $[M\text{-}CH_3]^+$ in the spectrum excludes the presence of an iso-structure in the carbon chain on either side of the molecule.

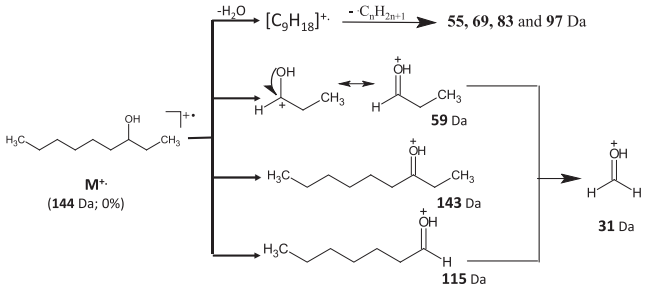

SCHEME 15. Dissociation pathways of $M^{+\cdot}$ of 3-nonanol.

The spectra given in Figs. 3(a) and 3(d) for two isomeric nonanols provide enough evidence to completely determine molecular structures of these alkanols. The spectra of nonanols depicted in Figs. 3(b)–3(d) prove the molecular structure but fail to exclude branching in alkyl chains; additional steps may be required for the entire structure elucidation.

4.1.2. Unsaturated alkanols

Mass spectra of unsaturated alkanols are more complicated because the number of competing processes of dissociation is increasing and the structural tasks to be solved are extending, such as alcohol function location, unsaturation location, and carbon skeleton structure. Unlike alkanols, molecular mass determination of unsaturated alcohols is an easy task since alkenols demonstrate noticeable $M^{+\cdot}$ peaks, and for the lower alkenols, these peaks are rather abundant; sometimes their relative intensity may reach 50%. These $M^{+\cdot}$ successively eliminate hydrogen as radicals and as neutral molecules; corresponding peaks may be higher than the $M^{+\cdot}$ peak.

The loss of a water molecule from $M^{+\cdot}$ of alkenols also proceeds readily, usually easier than for alkanols. The other characteristic dissociation pathway, formation of oxonium ions, can be enhanced or diminished depending on the unsaturation location. Thus, peaks of $[CH_3CHOH]^+$ (45 Da) oxonium cations in the spectra of 3-alken-2-ols are noticeable but of very low intensity.

Consequently, alkenol structure assignment to an unknown is not an easy task. However, the candidates presenting an alkenol structure can be suggested based on their spectra. The proposed structure of an alkenol may be subsequently verified (or rejected) after the utilization of chemical modification of a sample. Characteristic bond cleavages and rearrangement processes in $M^{+\cdot}$ of unsaturated alcohols are demonstrated below on concrete examples of lower representatives of this class: allyl alcohol, butenols, dienic alcohols, and acetylenic alcohols.

New competing processes take over in dissociation of $M^{+\cdot}$ of lower unsaturated alcohols. This is due to the absence in their molecules of C–C-bonds capable of favorable cleavages.

(a) The major dissociation pathway of $M^{+\cdot}$ of the allyl alcohol (2-propen-1-ol) proceeds via β-C–H cleavage giving rise to the formation of the dien-type $[H_2C{=}CHCH{=}OH]^+$ EE ion that displays maximum intensity in the spectrum.

(b) The β-C–C cleavage in $M^{+\cdot}$ of $C_{(1)}$-alkyl-substituted 2-methyl-3-butenols generates the two most prominent ions in the spectra: $[M\text{-}55]^+$ oxonium cations and rearrangement ions—2-butene (56 Da) OE ions (Scheme 16):

(c) Molecular ions of alcohols of diene and acetylene series undergo extensive rearrangements. 1,2-Dienes, such as $(CH_3)_2C(OH){-}CH{=}C{=}CH_2$ and the isomeric 1-acetylene analog $(CH_3)_2C(OH){-}CH_2{-}CCH$, produce similar mass spectra containing peaks of $[M\text{-}CH_3]^+$, $[(CH_3)_2C{=}OH]^+$, and $[CH_3CO]^+$ ions without noticeable peaks of $M^{+\cdot}$. By the way, isomerization of $M^{+\cdot}$ of these alcohols to α,β-unsaturated ketone $\{(CH_3)_2C{=}CH{=}C(=O)CH_3\}$ is established.

Primary alcohols of type $H_7C_3CR{=}C{=}CHCH_2OH$ produce unstable $M^{+\cdot}$ that are readily dehydrated. Competing pathways of $M^{+\cdot}$ dissociation include the loss of CH_3, C_2H_5, and C_3H_7 radicals and of neutral C_2H_4. Another major dissociation of $M^{+\cdot}$ includes the elimination of the CH_2OH radical, and the corresponding peak

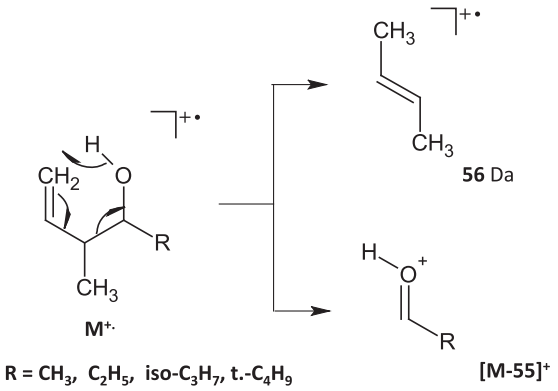

SCHEME 16. Dissociation of ionized 1-alkyl-2-methyl-3-butenols.

may be the most abundant in a spectrum. Overall EI spectra of isomeric allenic and β-acetylenic alcohols can be differentiated when reference spectra are available. However, some discretion should be exercised when suggesting them as candidates for an unknown.

4.2. Dy(alkyl) and (alkenyl)alkyl ethers

Alkanols and di-alkyl ethers have the same general formula—$C_nH_{2n+2}O$—and the competing fragmentation pathways in their $M^{+\cdot}$ are rather similar. However, $M^{+\cdot}$ of ethers, unlike alcohols, display noticeable peaks; consequently, the molecular weight and chemical formula of ether are determined readily.

(a) The formation of oxonium EE ions is a common dissociation pathway of $M^{+\cdot}$ of ethers, like alkanols. These ions in the high mass region of the spectra correspond to $[M\text{-}H]^+$ cations for methyl alkyl ethers [see Figs. 4(a), 4(c), and 4(d)] and $[M\text{-}CH_3]^+$ cations for ethyl-alkyl ethers [see Fig. 4(b)] due to σ-C–C-bond cleavage in the *O*-ethyl moiety. The peak of $[M\text{-}CH_3]^+$ ions, but of a different origin, is also observed in Fig. 4(c); in this case, the ion is produced via methyl substituent elimination at the carbon connected to the ether function. Two oxonium ions (peaks at m/z 59 and m/z 129) are produced directly from the $M^{+\cdot}$ of *n*-heptyl ethyl ether as presented in Scheme 17. As expected, the heavier alkyl radical elimination is responsible for the appearance of the base peak. These "primary product ions" further lose alkene neutrals to give rise to prominent peaks at m/z 31. This secondary fragmentation does not take place in the absence of a γ-hydrogen, such as methyl groups in Figs. 4(a) and 4(c)–4(e).

(b) Another principal characteristic dissociation pathway $M^{+\cdot}$ of alkanols is associated with the loss of a water molecule to generate an alkene-like radical cation. In the case of di-alkyl ethers, a noticeable elimination of water neutral is not detected.

However, similar alkene OE ions are produced via hydrogen rearrangement and elimination of an alkanol neutral. For example, the corresponding peaks of $[M\text{-}CH_3OH]^{+\cdot}$ (112 Da) ions are present in the spectra of alkyl methyl ethers [Figs. 4(a) and 4(c)–4(e)] and $[M\text{-}C_2H_5OH]^{+\cdot}$ (98 Da) ions in the spectrum of *n*-heptyl ethyl ester [Fig. 4(b)].

(c) Alkanol loss from $M^{+\cdot}$ of ethers is accompanied by cleavage of the carbon–oxygen bond to produce alkenyl EE ions, and the latter becomes dominant in the spectra of symmetrical ethers. Accordingly, the abundance of oxonium ions is diminished. While the abundance of oxonium ions can reach up to 13% in the case of dibutyl and dipentyl ethers, their intensities may barely reach 2% in the spectra of di-(*n*-hexyl)- to di-(*n*-decyl) ethers.

(d) There is an additional fragmentation pathway associated with C–O bond cleavage and the migration of two hydrogen atoms mainly from the $C_{(5)}$ position relative to oxygen. This process is characteristic for alkyl pentyl ethers of the general formula R-O-R^1 ($R^1 > n\text{-}C_4H_9$). Thus, peaks of $[CH_3OH_2]^+$ (33 Da) EE ions are noticeable in the spectra of methyl ethers depicted in Figs. 4(a) and 4(c)–4(e) and $[C_2H_5OH_2]^+$ (47 Da) EE ions in the case of ethyl ether [Fig. 4(b)].

All the above indicate a rather characteristic nature of mass spectra for di-alkyl ethers; identified diagnostically important dissociation pathways of these compounds provide enough evidence for suggesting candidate di-alkyl ether structures for an unknown. Other instrumental methods, such as GC and GC-RI, help the determination of the carbon skeleton.

Spectra of unsaturated aliphatic ethers are more complicated and less suitable for generating candidates for unknowns. For the purpose of correct selection of candidates, some rearrangement reactions in $M^{+\cdot}$ of unsaturated ethers are noted. For example, vinyl- and allyl-alkyl ethers (alkyl > CH_3) and their homologs, containing alkyl substituents at the unsaturation site, produce prominent peaks of OE ions of vinyl and allyl alcohols, respectively. However, starting with 3-butenyl alkyl ethers, the formation of oxonium cations takes the lead, and the identification of these EE ions is important for the structure elucidation.

4.3. Alkyl hydroperoxides, peroxides, and ozonides

Hydroperoxides lack stability and readily decompose. Similarly, alkyl hydroperoxides of the general formula R(OOH) demonstrate unstable $M^{+\cdot}$ and their stability decreases with the increase in the size of the molecule (pentyl > hexyl > heptyl hydroperoxides). The location of the peroxide group also affects the stability, and molecular ions of primary hydroperoxides (3- > 2- > 1-) are less stable. The EI mass spectra of this class of compounds are exemplified by 2-hexyl hydroperoxide [Fig. 5(a)]. Dissociation of their $M^{+\cdot}$ proceeds via loss of a water molecule and OH and O_2H radicals. The abundance of $[M\text{-}O_2H]^+$ EE ions is higher for lower hydroperoxides and decreases with the increase in the carbon chain. The majority of ions in the spectra correspond to hydrocarbon EE ions, such as $[C_nH_{2n+1}]^+$, $[C_nH_{2n-1}]^+$, and $[C_nH_{2n-3}]^+$. Alkoxy cations may also demonstrate a prominent peak at m/z 45 along with a peak at m/z 31 in Fig. 5(a).

Alkyl peroxides demonstrate more characteristic spectra. Their $M^{+\cdot}$ are rather stable only for compounds with short alkyl chains. As shown in Fig. 5(b), the $M^{+\cdot}$ abundance for a C_6 peroxide is over 10%. The corresponding alkyl cations appear in the spectra as the most intensive peaks. Elimination of one olefin from $M^{+\cdot}$ is an important dissociation process. The resulting ions further lose a hydroxyl radical. For example, in the case of dipropyl peroxide, this process gives rise to the $[CH_3CH_2CH{=}OH]^+$ (59 Da) oxonium ion [see Fig. 5(b)].

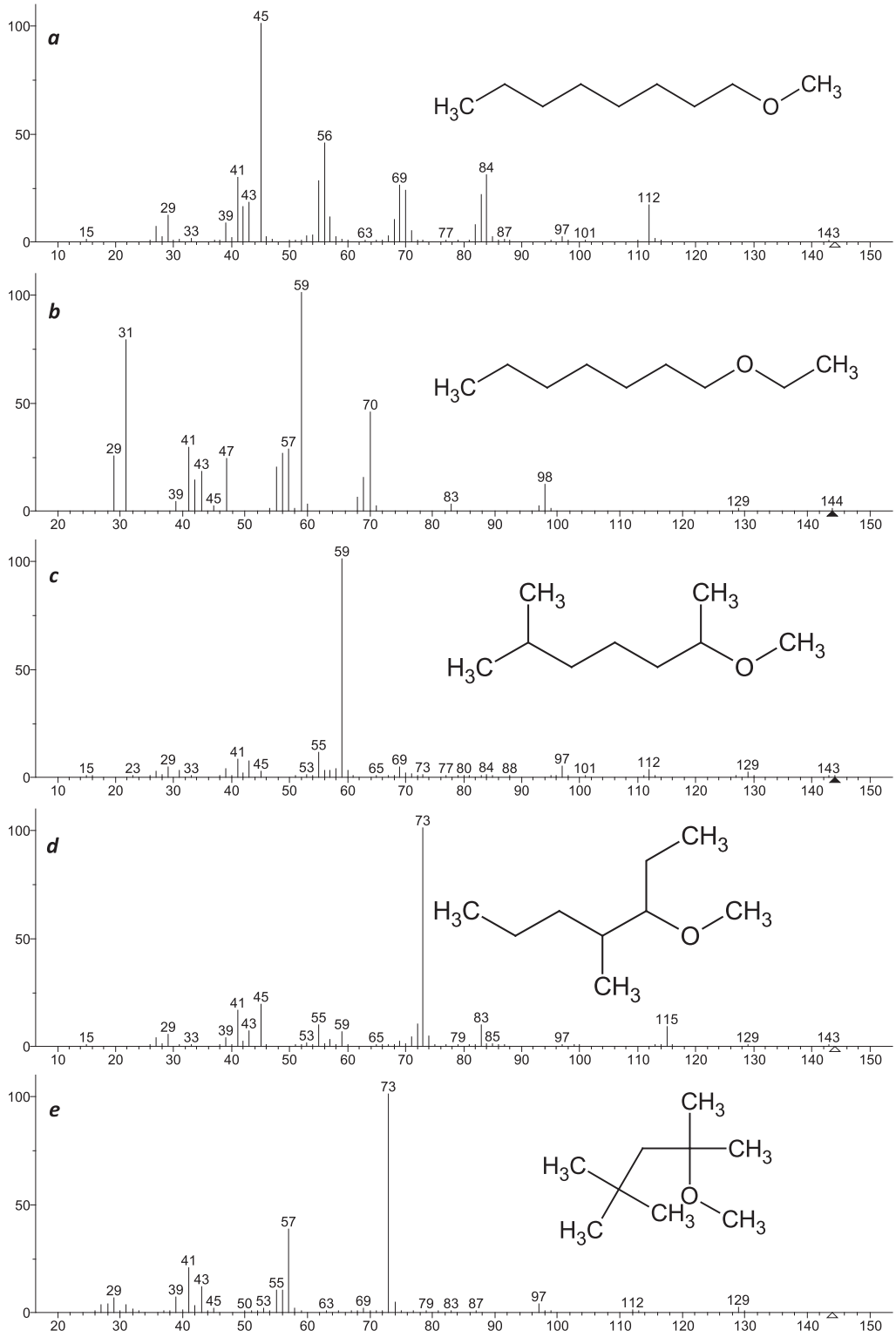

FIG. 4. Mass spectra [m/z (relative abundance, %)] of dialkyl ethers of the general formula $C_9H_{20}O$.

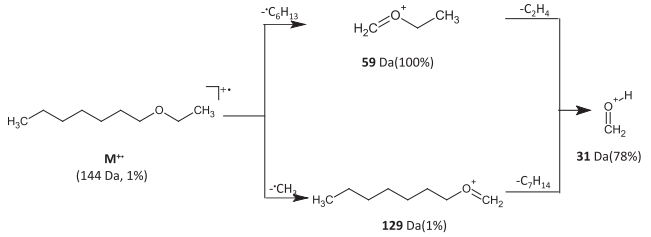

SCHEME 17. Oxonium ions in the spectrum of *n*-heptyl ethyl ether.

Molecular ions of aliphatic ozonides are unstable and their primary dissociation involves cleavage of O–O and C–C bonds. For example, the prominent peaks in EI spectra of alkyl ozonides $R^1CH{=}O_3{=}CHR^2$ correspond to alkyl ions $[R^1]^+$ and $[R^2]^+$. Concurrently, high intensity peaks of oxygen containing ions, such as $[M\text{-}O]^+$, $[R^1CHO]^+$, $[R^2CHO]^+$, $[R^1CHO_2]^+$, and $[R^2CHO_2]^+$, are observed in their spectra.

4.4. Silyl ethers

Silylation is the most convenient and effectively used technique for the modification of alcohols via blocking the polar and unstable alcohol function with a substituted silyl group. This common laboratory procedure enables an increase in the diagnostic power of MS and improves sensitivity and selectivity. Additionally, the replacement of the active alcohol hydrogen with a silyl protecting group increases volatility and reduces polarity of the initial alcohol, thereby improving the chromatographic properties of a sample. EI spectra of trimethylsilyl derivatives of alcohols are selected for discussion in this section among available several dozen types of alkyl-silyl derivatives varying from methyl to dodecyl and alkenyl substituents.[28,42] Mass spectra of flophemesyl and picolinyldimethylsilyl derivatives of alcohols are also analyzed because of their diagnostic power. Note that a preferential silylation group and a silylation reagent shall be identified in advance, and an assessment of a comparative strength of a silyl donor be considered in detail.[28]

4.4.1. Trimethylsilyl (TMS) ethers

Determination of two key structural elements, namely, the molecular weight and the branching at β-carbon, is the appealing feature of TMS ethers of alkanols. The $M^{+\cdot}$ value is easily generated by the $[M\text{-}CH_3]^+$ EE ion when the $M^{+\cdot}$ peak is not present in a spectrum. Peaks of the $[M\text{-}CH_3]^+$ ions along with $[(CH_3)_3Si]^+$ (73 Da) and at $[(CH_3)_2SiOH]^+$ (75 Da) EE ions are characteristic of the trimethylsilyloxy moiety and do not carry information on the structure of the initial alcohol. However, another major dissociation pathway of $M^{+\cdot}$ of ethers is due to β-cleavage and, as a result, trimethylsilyl substituted oxonium ions are produced (Fig. 6). In fact, the comparison of the spectra of three isomeric ethers demonstrates that the TMS ether of the primary nonanol [Fig. 6(a)] is good to determine $M^{+\cdot}$ and suggests an *n*-alkyl skeleton. *sec*-nonanol ether [Fig. 6(b)] reveals a prominent peak of $[CH_3CH{=}OSi(CH_3)_3]^+$ (117 Da) oxonium EE ions suggesting methyl branching at $C_{(2)}$. Note that several oxonium ions are produced in the case of TMS ethers of alkanols containing multiple substituents larger than methyl at carbon carrying the alcohol function [Fig. 6(c)]. For example, the formation of the oxonium ions at m/z 159 Da and m/z 103 are presented in Scheme 18.

4.4.2. tert-Butyldimethylsilyl (tBDMS) ethers

TBDMS ethers of alkanols are characterized by unstable $M^{+\cdot}$ ions that are usually absent in their EI spectra. However, the detection of $[M\text{-}CH_3]^+$ and $[M\text{-}C_4H_9]^+$ ions formed by the loss of alkyl substituents at the Si atom makes it possible to reliably establish the molecular weight. This is demonstrated by the spectrum of 2-nonanol TBDMS ether [Fig. 6(d)], which contains the corresponding peaks at m/z 243 and m/z 201, respectively. In addition, the spectrum exhibits $[M\text{-}H]^+$ (257 Da) ions due to the loss of hydrogen from the tertiary carbon. These three peaks guarantee a reliable determination of the molecular weight. Additionally, the spectrum demonstrates a prominent peak of $[CH_3CH{=}OSi(CH_3)_2C_4H_9]^+$ (159 Da) oxonium EE ion that is a homolog of the oxonium ion (117 Da) in the case of TMS derivative [Fig. 6(b)]. Note that $[M\text{-}C_4H_9]^+$ ions are well suited for the quantification of alcohols.

4.4.3. Picolinyldimethylsilyl (PicDMS) ethers

PicDMS ethers have demonstrated a powerful diagnostic ability among various silyl protection groups in structure determination of saturated and unsaturated alcohols. PicDMS ethers of primary *n*-alkanols show prominent $M^{+\cdot}$ and a series of $[M\text{-}C_nH_{2n+1}]^+$ EE ions of comparable abundance. On the other hand, $M^{+\cdot}$ is of maximum intensity in the EI spectra of PicDMS ethers of higher *n*-alkanols starting from *n*-undecanol. In addition, the peaks of $[M\text{-}C_nH_{2n}]^{+\cdot}$ OE ions start rising and they line up in ascending order of intensity.

Mass spectra of PicDMS ethers of isomeric 2- and 3-hexanols are depicted in Figs. 7(a) and 7(b). Prominent peaks of $M^{+\cdot}$, $[M\text{-}CH_3]^+$ (252 Da), $[M\text{-}C_6H_{13}]^+$ (182 Da), $[M\text{-}CH_3\text{-}C_6H_{12}]^+$ (168 Da), and $[M\text{-}OC_6H_{13}]^+$ (166 Da) confirm the molecular weight and the presence of an hexanyloxy moiety in the structure. Ions determining the hexane skeleton are associated with σ-C–C bond cleavages at the branching sites: (a) peaks of $[M\text{-}CH_3]^+$ (252 Da; 14%) and $[M\text{-}C_4H_9]^+$ (210 Da; 100%) in Fig. 7(a) verify the 2-hexanol structure for the initial alcohol and (b) prominent peaks of $[M\text{-}C_2H_5]^+$ (238 Da; 84%) and $[M\text{-}C_3H_7]^+$ (224 Da; 100%) ions in Fig. 7(b) confirm the 3-hexanol structure for the initial alcohol.

Similar to PicDMS ethers of branched alcohols, the presence or absence of peaks of $[M\text{-}C_nH_{2n+1}]^+$ EE ions and their abundance provide evidence of unsaturation location. For example, the mass spectrum of 3-hexenol-1 derivative [Fig. 7(c)] shows very low intensity peaks between peaks of ions $[M\text{-}CH_3]^+$ (250 Da) and $[M\text{-}C_4H_7]^+$ (210 Da) and a prominent peak of $[M\text{-}CH_3\text{-}C_4H_6]^+$ (196 Da) EE ion; all the above clearly determines the double bond location in the hexenol skeleton. Note that the allylic cleavages may proceed via a simple β-cleavage ($[M\text{-}C_4H_7]^+$ formation) or β-cleavage with hydrogen migration (formation of $[M\text{-}CH_3\text{-}C_4H_6]^+$).

Dienic alcohol derivatives produce more complex spectra. However, allylic cleavage produces a doublet of peaks at m/z 250 and m/z 251 [Figs. 7(d) and 7(e)] corresponding to $[M\text{-}C_5H_9]^+$ EE ions and $[M\text{-}C_5H_8]^{+\cdot}$ OE ions clearly indicate the "6-en-7-methyl" part of the structure of nerol and geraniol derivatives. These spectra of (*E*)- and (*Z*)-isomers show only qualitative differences.

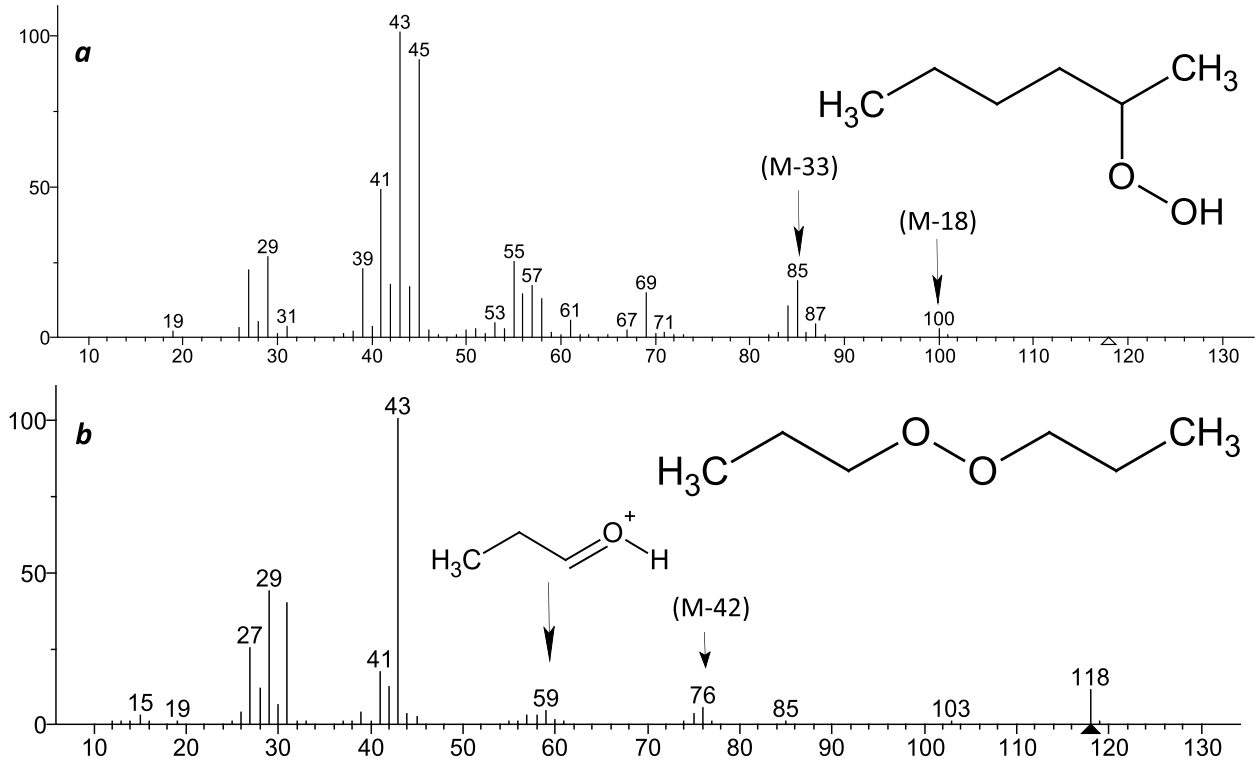

FIG. 5. Mass spectra [m/z (relative abundance, %)] of 2-*n*-hexyl hydroperoxide (a) and di-*n*-propyl peroxide (b).

4.5. Acyl derivatives

Acylation, like silylation, is a widely used derivatization method for successful chromatographic separation of mixtures and identification of components. Acylated alcohols are formally alkyl esters of acids. However, historically, derivatization of mono- and polyols to acetates, propionates, and butanoates prior to GC–MS experiments has been successfully employed. For that reason, alkyl esters of lower acids are considered in this section. At the present time, however, perfluoro-analogs of the above acid residues along with pentafluorobenzyloxycarbonyl and nicotinoyl derivatives of alkanols are in great demand because of their superiority to increase the diagnostic power.

4.5.1. Acetates of alcohols

Mass spectra of aliphatic alcohol acetates are not helpful for structure elucidation since they readily eliminate an acetic acid molecule under EI and do not show $M^{+\cdot}$ peaks. Prominent peaks in their spectra correspond to the ions $[CH_3CO]^+$ (43 Da), $[CH_3COOH_2]^+$ (61 Da), as well as $[C_nH_{2n}]^{+\cdot}$ and $[C_nH_{2n-1}]^+$ ions produced from $[M\text{-}CH_3COOH]^{+\cdot}$. However, these ions cannot be utilized for the determination of a carbon skeleton or the location of an alcohol function.

Acetates of unsaturated alcohols can be used as intermediates to obtain the corresponding adducts with dimethyldisulfide. The resulting derivatives produce characteristic mass spectra containing prominent $M^{+\cdot}$ and two diagnostically important $[CH_3S{=}CHR^1]^+$ and $[CH_3S{=}CH(CH_2)_nOCOCH_3]^+$ EE ions that are formed as a result of σ-bond cleavage between the methylthio-substituted carbons (Scheme 19). The $[CH_3S{=}CH(CH_2)_nOCOCH_3]^+$ EE ions further undergo the loss of CH_3COOH neutral; the corresponding peaks are rather abundant in the spectra. Identification of these characteristic ions enables a reliable determination of the double bond location in the initial alcohol. For example, this approach was successfully applied to the structure determination of acetates of mono-unsaturated alcohols in pheromone extracts of insects.

4.5.2. Perfluoroacyl derivatives of alcohols

Trifluoroacetates are suitable for molecular weight determination since their spectra always contain noticeable peaks of $[M\text{-}CF_3]^+$ EE and $[M\text{-}CF_3COOH]^{+\cdot}$ OE ions. However, their spectra do not contain characteristic ions to be considered as "ions of interest" in structure determination of unknowns. Nevertheless, trifluoroacetates, pentafluoropropionates, heptafluorobutyrates, and pentafluorobenzoates are still utilized for the separation of components of complex mixtures and their quantitative determination.

4.5.3. Alkyl nicotinates

Over 90% yield of alkyl nicotinates is achieved when using alkanol and nicotinoyl chloride as starting materials.[28] Alkyl nicotinates, as well as their alkenyl analogs, exhibit noticeable $M^{+\cdot}$ that is important for the dependable determination of their molecular weight. Nitrogen in the pyridine ring directs random aliphatic hydrogen

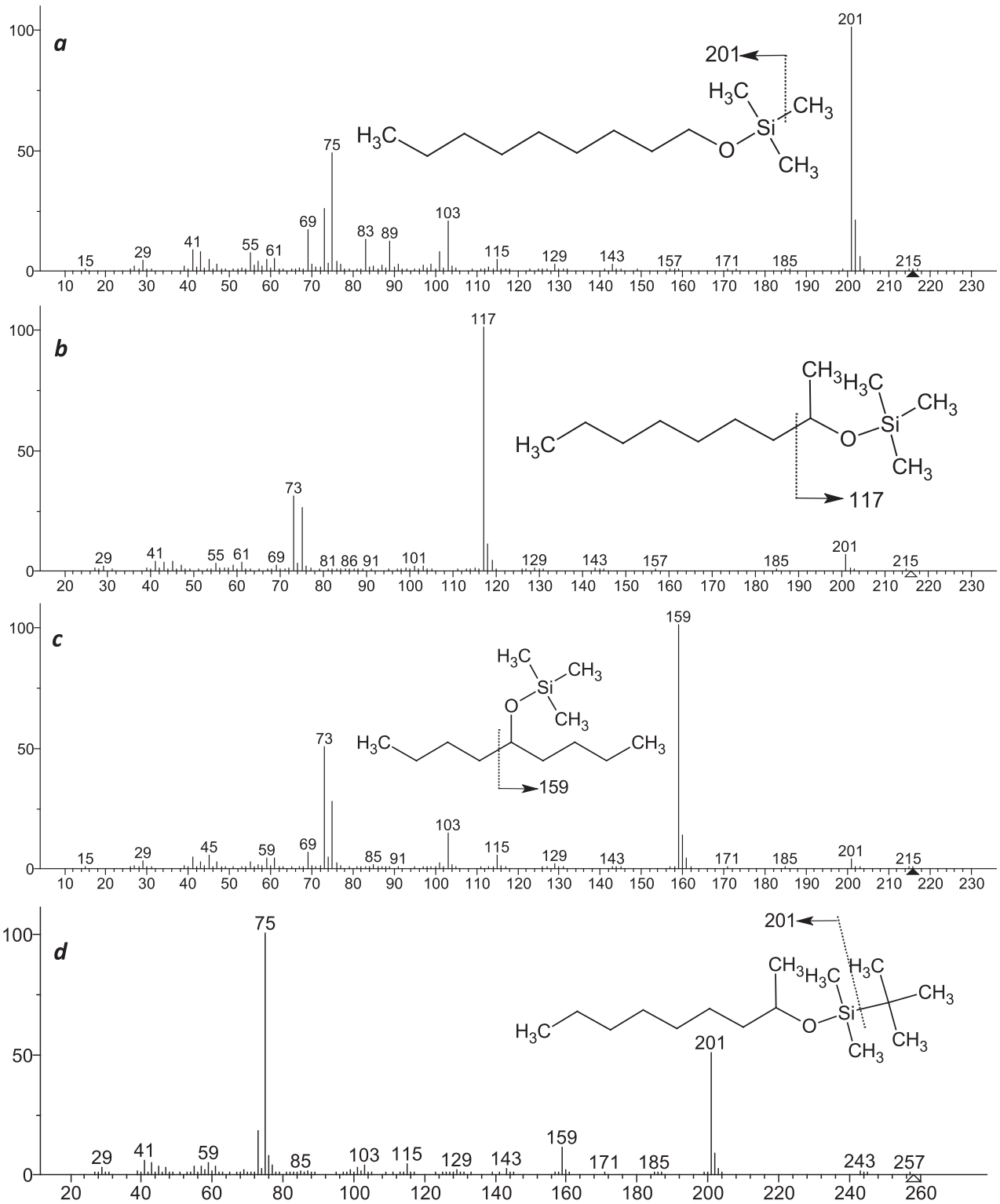

FIG. 6. Mass spectra [m/z (relative abundance, %)] of the TMS ether of *n*-nonanol-1 (a), TMS ether of *n*-nonanol-2 (b), TMS ether *n*-nonanol-3 (c), and TBDMS ether of *n*-nonanol-1 (d).

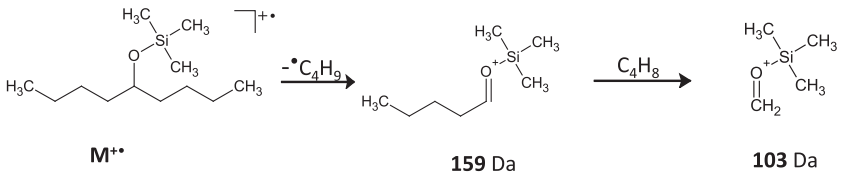

SCHEME 18. Formation of silyloxonium ions in the case of TMS ether of 5-nonanol.

abstractions in $M^{+\cdot}$ followed by cleavage of β-C–C-bonds relative to the abstraction site. As a result, a series of homologous peaks of $[M\text{-}C_nH_{2n+1}]^+$ EE ions are generated. The intensities of these EE ion peaks are of comparable abundance in the spectra of alkanol derivatives. This type of "fingerprint" spectrum is a clear and convincing proof that an unknown is a derivative of an *n*-alkanol.

An interruption to the regular series of peaks spaced by 14 Da occurs when a double bond is introduced to the alkyl chain. Consequently, a difference of 26 Da rather than 28 Da between adjacent pairs of peaks of ions arises, and these peaks point to the location of unsaturation. Note that the peaks, observed between formal allylic cleavage ion peaks, show significantly lower abundances in the spectra of alkenol derivatives. It is justifiable to state that the charged pyridine ring controls the dissociation of $M^{+\cdot}$ of the derivatives and provides a "stabilizing effect" to unsaturation sites. The similarity of the dissociation patterns for alkyl nicotinates and β-picolinyldimethylsilyl ethers of alcohols discussed in Sec. 4.4 confirms the leading role in the dissociation of nitrogen in the pyridine ring.

Branching in the carbon skeleton also affects the regularity of $[M\text{-alkyl}]^+$ cations. These irregularities in the spectra of branched alkanol derivatives provide information with regard to the character and location of branching points, as shown in Scheme 20.

4.6. α- and β-aminopyridine and pyrrolidinone-derivatives

There are two steps involved in the preparation of these derivatives from an alcohol and aminopyridines or pyrrolidone.[28] A tendency similar to alkyl nicotinates is observed in the dissociation of aminopyridine and pyrrolidone derivatives. In fact, σ-C–C cleavages leading to a series of ions at 14 Da intervals ($[M\text{-}C_nH_{2n+1}]^+$ EE ions) with monotonous intensities are interrupted when a substituent or branching is introduced. Typical σ-C–C cleavages for branched alkanol (3,7,11,15-tetramethylhexadecnol-1) derivatives are noted in Scheme 20.

It is established that the EI spectra of *N*-alkyl-2-pyrrolidones explicitly recognize the branching points and less clearly indicate double bonds in the chain. The spectra of 2-alkylaminopyridines allow successful determination of branching and double bond locations. Note that the EI spectra of 3-alkylaminopyridines exhibit almost the same diagnostic power as their 2 analogs.[28]

4.7. Chemical modifications of acyclic alcohols via hydrogenation/dehydrogenation

4.7.1. Dehydrogenation

Quantitative and selective conversion of alcohols to carbonyl compounds is suitable for the location of the alcohol function as well as for reliable differentiation of (a) secondary and tertiary alcohols and (b) primary alcohols and di-alkyl ethers. This reaction can be carried out in a solution with pyridinium chlorochromate. However, the application of catalytic dehydrogenation over copper dust at 320 °C is preferable for two reasons: (a) no by-products and (b) the reaction can be carried out online during GC–MS experiments via adding a heated unit with a catalytic bed into the inlet system of an instrument. Primary and secondary alcohols are converted to the corresponding aldehydes and ketones; tertiary alcohols remain intact under the reaction conditions (Scheme 21). Mass spectra of the resulting carbonyl compounds provide additional analytical information useful for structure elucidation. Mass spectral characteristics of aldehydes and ketones are discussed in Sec. 5.

4.7.2. Hydrogenation

Reduction of the alcohol function and saturation of double and triple bonds generate alkanes. As shown above, EI mass spectra of alkanes, produced from saturated and unsaturated alcohols, provide sufficient information on the carbon skeleton. A combined analysis of data acquired from the spectra of the initial alcohols and their transformation products provides evidence to resolve any questions with regard to the structure of the backbone in the initial alcohol. A few approaches are utilized to carry out a series of reactions. Among them, direct catalytic deoxygenation on a fused iron catalyst at 320–350 °C is suitable.

4.7.3. Conclusion

Alcohols can be identified among unknowns. It is hard to overstate the diagnostic power of multiple spectral datasets for a given compound. Identification of characteristic ions specific for selected structural elements enables the reconstruction of a molecular structure of an unknown alcohol based on a comparative analysis of the EI spectra of initial alcohols and a wide variety of their chemical modification products, such as alkanes, carbonyl compounds, ethers, acyl derivatives, and amines.

5. Carbonyl Compounds and Their Chemical Modification Products

5.1. Aldehydes and ketones

5.1.1. Aldehydes

The abundance of $M^{+\cdot}$ of alkanals is prominent for the lower aldehydes and their peak intensities fall with the rise of the size of a carbon skeleton and some degree of chain branching. Identification of $[M\text{-H}]^+$ and $[M\text{-R}]^+$ EE ions that are generated via α-cleavages in $M^{+\cdot}$ of aldehydes with the general structure of RCHO are helpful for $M^{+\cdot}$ validation. Further confirmation of $M^{+\cdot}$ is achieved by revealing prominent ions due to parallel loss of water and ethylene

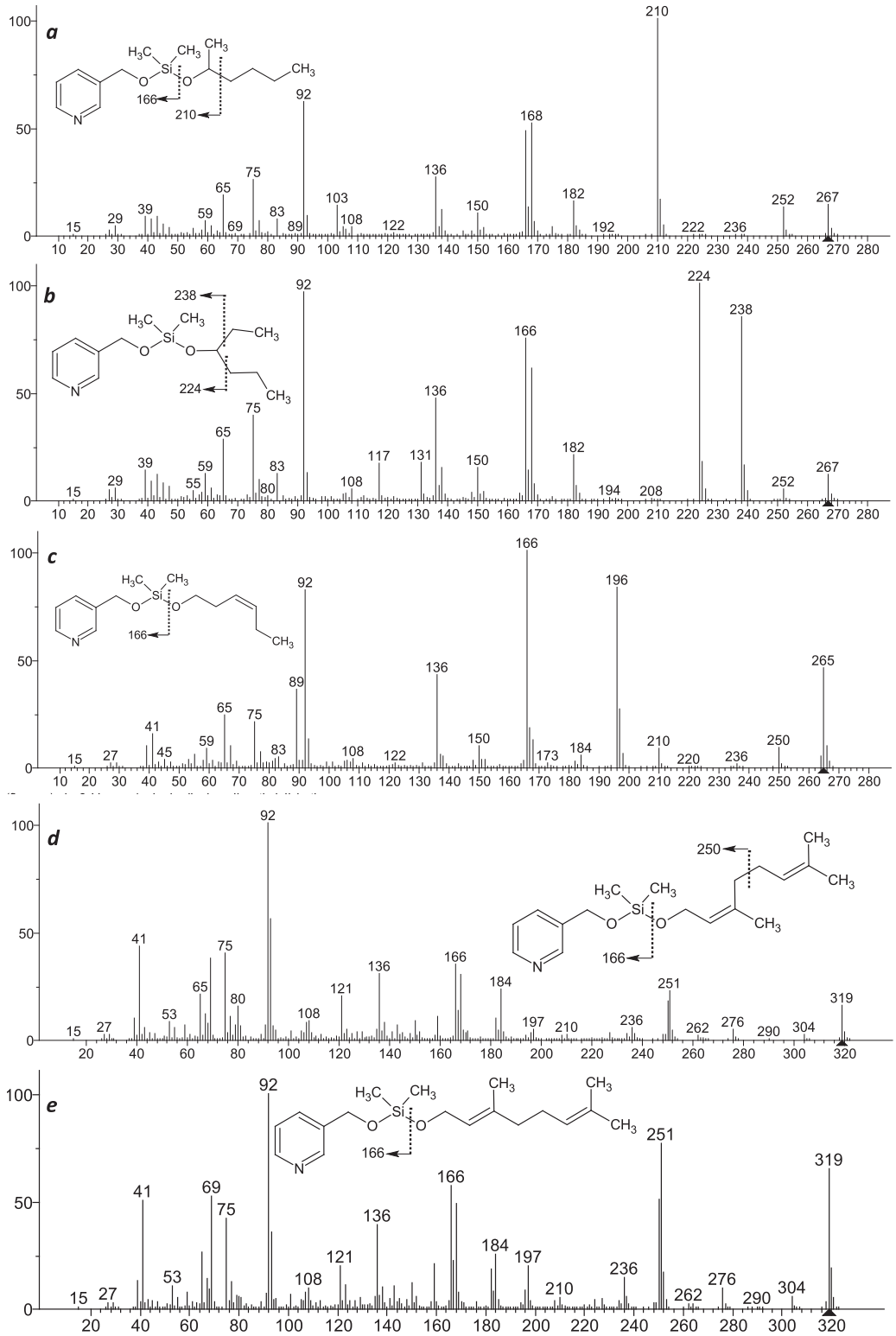

FIG. 7. Mass spectra [m/z (relative abundance, %)] of PicDMS ethers of *n*-nonanol-2 (a), *n*-nonanol-3 (b), *n*-hex-3-en-1-ol (c), nerol (d), and geraniol (e).

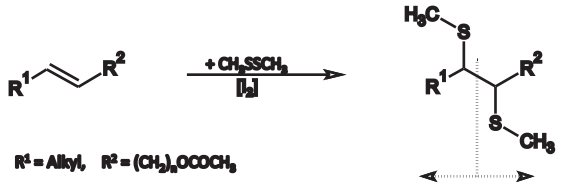

SCHEME 19. Synthesis of acetates of vicinal di(methylthio)alkanols.

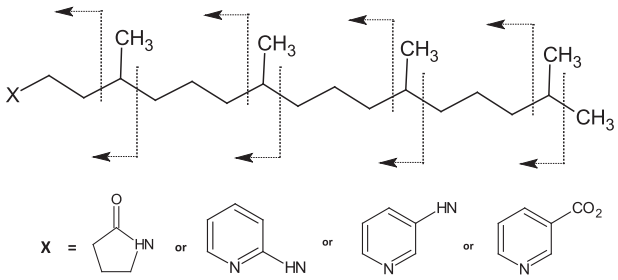

SCHEME 20. Characteristic dissociation of selected alkanol derivatives under EI.

molecules from $M^{+\cdot}$. For example, prominent peaks corresponding to $[M\text{-}H_2O]^{+\cdot}$ (110 Da) and $[M\text{-}C_2H_4]^{+\cdot}$ (100 Da) OE ions are present in the spectra of isomeric nonanals in Figs. 8(a) and 8(b). Note that the $[M\text{-}C_2H_4]^{+\cdot}$ radical cation is a product of a complex rearrangement and the elimination of ethylene neutral; this ion includes β- and γ-carbon atoms.

The above-mentioned loss of the hydrogen radical is due to α-cleavage in $M^{+\cdot}$, and it is the only fragmentation process giving rise to the base peak in the spectrum of formaldehyde (Scheme 22). With the rise of the carbon chain length, the corresponding peaks become less visible. The other product of α-cleavage around the carbonyl function is the $[HCO]^+$ (29 Da) EE ion. It is characteristic only for acetaldehyde and has no analytical value in the case of higher alkanals where this ion is superimposed on an isobaric $[C_2H_5]^+$ (29 Da) EE ion.

Dissociation of $M^{+\cdot}$ of saturated aliphatic aldehydes via McLafferty rearrangement is of a diagnostic value. This fragmentation type is accomplished in aldehydes containing γ-hydrogen atoms that can migrate to the ionized carbonyl group. For example, *n*-octanal [Fig. 8(a)] contains one γ-C atom, whereas 2-ethylhexanal [Fig. 8(b)] contains two γ-carbon atoms: one in ethyl- and the other in *n*-butyl moieties. Thus, the abundant $[CH_2{=}CH(OH)]^{+\cdot}$ (44 Da) OE ion is observed for *n*-octanal [Fig. 8(a)]. Contrastingly, the mass spectrum of 2-ethylhexanal [Fig. 8(b)] contains three product ions generated via McLafferty rearrangement: $[M\text{-}C_2H_4]^{+\cdot}$ (100 Da) due to the loss of ethylene neutral from the 2-ethyl moiety, $[M\text{-}C_4H_8]^{+\cdot}$ (72 Da), due to elimination of the butylene neutral from the *n*-butyl part of the molecule and $[M\text{-}C_2H_4\text{-}C_4H_8]^{+\cdot}$ (44 Da) as a result of sequential realization of both available γ-hydrogen migrations. The mass values of McLafferty ions point to the presence or absence of branching at α-carbon. Really, a single ion at m/z 44 in Fig. 8(a) indicates the absence of substituents at α-carbon. Note $[CH_2{=}CH{=}OH]^{+\cdot}$ (44 Da) OE ion peaks show maximum intensity in the spectra of *n*-butanal to *n*-hexanal and then gradually decrease in the intensity with elongation of the carbon chain (e.g., its intensity is only 35 rel. % in the spectrum of *n*-tetradecanal).

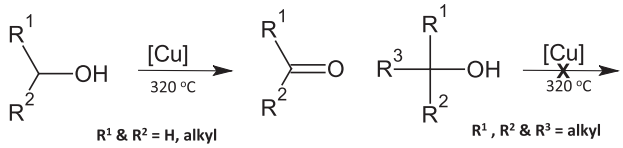

SCHEME 21. Dehydrogenation of primary and secondary alcohols.

The other dissociation pathway valuable for structural diagnosis, particularly for *n*-alkanals, includes a migration of hydrogen to the carbonyl group followed by β-C–C bond cleavage and generation of alkenyl OE ions [see the peak at 84 Da corresponding to the $[M\text{-}CH_3CHO]^{+\cdot}$ radical cation in Fig. 8(a)].

5.1.2. Ketones

Dialkylketones exhibit rather stable $M^{+\cdot}$ even for high molecular homologs. Primary determination of the carbonyl group location in a molecule is based on the identification of ions due to α-C–C bond cleavages around the keto function and due to the McLafferty rearrangement. For example, the first process gives rise to acyl ions at m/z 113 and m/z 43 in the case of 2-octanone [Fig. 8(c)] and 3,4-dimethylhexan-2-one [Fig. 8(d)]. These ions readily lose CO neutrals to generate alkyl EE ions, and the corresponding peaks at m/z 85 and m/z 15 are present in the spectrum. The acyl ion abundance rises with the increase in the weight of the eliminated alkyl group; thus, $I_{[M\text{-}CH3]+} > I_{[M\text{-}C6H13]+}$..

Similar to alkanals, ions generated via McLafferty rearrangement are successfully used for the determination of substituents at α-carbon atoms around the carbonyl group. Equally, sequential McLafferty rearrangements are realized when two or more γ-hydrogen atoms are present on either side of the carbonyl function. Because such a situation complies with the requirements for the rearrangement, there are possibilities for two or more different rearrangements.

For example, $[CH_3CH{=}C(O)CH_3]^{+\cdot}$ (72 Da) OE ions in the case of 3,4-dimethyl-2-hexanone [Fig. 8(d)] and $[CH_2{=}C(O)CH_3]^{+\cdot}$ (58 Da) in the case of n-oct-2-enone [Fig. 8(c)] are originated via McLafferty rearrangement; these ions are successfully employed for structure elucidation. Thus, these findings along with the identification of acyl cations provide evidence for "3-methyl" substructure determination in the ketone molecule depicted in Fig. 8(d). It should be stated that neither acyl cations nor OE ions generated via McLafferty rearrangement do not provide information on the carbon skeleton except substitution patterns at α- and β-carbon atoms around the keto group.

The other characteristic ion series at m/z 29, m/z 43, m/z 57, m/z 71, m/z 85, and more corresponding to alkyl ($[C_nH_{2n+1}]^+$) EE ions as well as acyl ($[C_nH_{2n+1}CO]^+$) OE ions can be observed in the spectra of saturated aliphatic alcohols and ketones, but their diagnostic value may not always be high.

5.1.3. Unsaturated carbonyl compounds

Unsaturated ketones possess more stable $M^{+\cdot}$, and the corresponding peaks are more visible. As one can see from the spectrum of α,β-unsaturated ketone [Fig. 8(e)], dissociation pathways of $M^{+\cdot}$

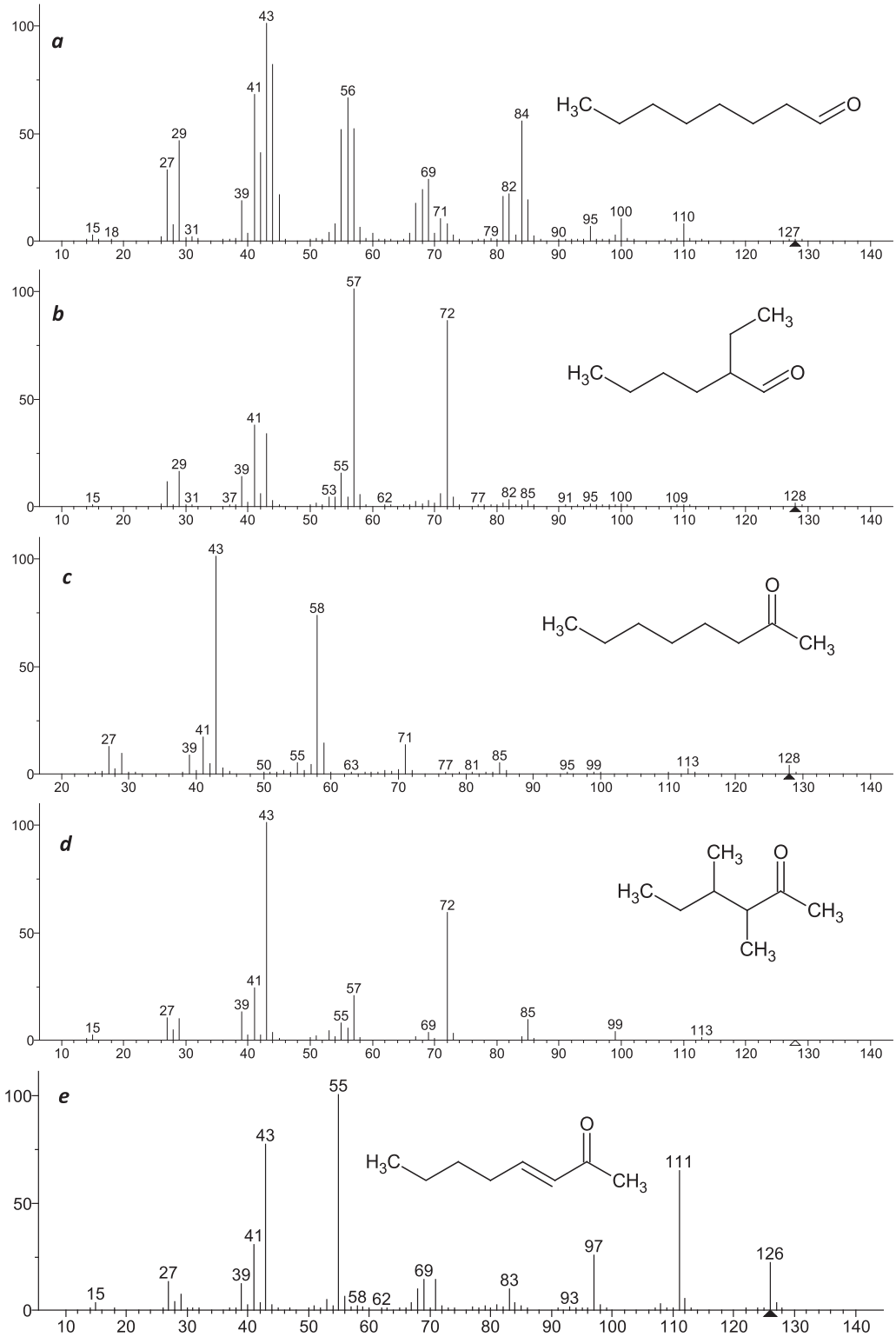

FIG. 8. Mass spectra [m/z (relative abundance, %)] of isomeric *n*-octanal (a) and 2-ethylhexanal (b), *n*-octanone-2 (c) and 3,4-dimethyl-2-hexanone (d), and 3-octen-2-one (e).

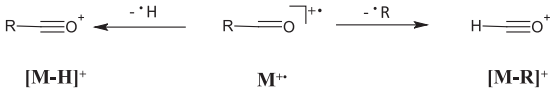

SCHEME 22. α-Cleavage in ionized alkanals.

are partly similar to saturated carbonyl compounds, including the loss of a water molecule from $M^{+\cdot}$ (108 Da) and generation of acyl cations (peaks at m/z 111 and m/z 43). At the same time, McLafferty rearrangement does not occur in similar α,β-unsaturated methyl alkenyl ketones; the double bond blocks the expected cleavage even though the molecules contain γ-hydrogens that are capable for migration. The situation changes in the case of alkyl alkenyl ketones (type C in Table 1) where McLafferty rearrangement can proceed at the expense of a saturated alkyl group.

Table 1 shows that the relative location of a carbonyl group and unsaturation in isomers and homologs of carbonyl compounds are successfully utilized for structural diagnosis. For α,β-unsaturated methyl alkyl ketones (type "A" in Table 1), a specific fragmentation pattern involves a double hydrogen transfer process with the elimination of an acetone molecule. Thus, the $[M\text{-}CH_3C(O)CH_3]^{+\cdot}$ (68 Da) OE ion is notable in the spectrum of 3-octen-2-one in Fig. 8(e). It shall be pointed out that McLafferty rearrangement that is typical for type "C" ketones (see Table 1) does not proceed in the corresponding acetylene analogs. Instead, major dissociation pathways mainly become fragmentation of the alkyl chain (the left part) of the molecule.

5.2. Acetals and ketals of carbonyl compounds

Two oxygen atoms separated by a single carbon in molecules strongly affect the stability of $M^{+\cdot}$ of acetals and ketals derived from aliphatic carbonyl compounds. Their EI spectra do not contain $M^{+\cdot}$ peaks, and only acetals of lower aldehydes contain noticeable peaks of $[M\text{-}H]^+$ EE oxonium ions in the molecular region. Note that the hydrogen at the acetal function is eliminated when generating $[M\text{-}H]^+$ ions.

Commonly, dissociation of ionized acetals and ketals proceeds similar to dialkyl ethers. Their $M^{+\cdot}$ undergo multiple competitive bond cleavages, such as C–H, C–C, and C–O at carbon of the carbonyl function in the initial carbonyl compound. As shown in Scheme 23, the generated variety of oxonium ions can easily lose alkene neutrals starting from diethyl acetal derivatives. Additionally, the alkyl group in the acetal function may undergo C_α–C_β bond

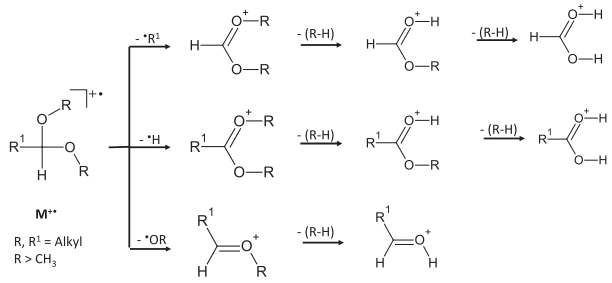

SCHEME 23. Dissociation of ionized dialkyl-acetals of alkanals.

cleavage in the "O-R" moiety, and the resulted product ions may further eliminate alkene neutrals.

5.2.1. Dimethyl-acetals

The spectra of dimethyl-acetals are simple. Their fragmentation ends after elimination of hydrogen, alkyl, or methoxy radicals from $M^{+\cdot}$. Usually, $[M\text{-}R]^+$ cations, e.g., $[CH(OCH_3)_2]^+$ (75 Da) EE ions, are the base peaks in the spectra, as depicted in Fig. 9(a). Note that only dimethyl acetals of formaldehyde and acetaldehyde show the base peaks of $[M\text{-}OCH_3]^+$ ions.

The presence of prominent peaks of $([HC(OH)_2]^+$ (47 Da), $([HC(OH)(OCH_3)]^+$ (61 Da), and $([HC(OCH_3)_2]^+$ (75 Da) EE ions is strong evidence, pointing to the presence of the dimethyl-acetal moiety in the unknown molecules. Similarly, abundant homologous $([HC(OH)(OC_2H_5)]^+$ (75 Da) and $([HC(OC_2H_5)_2]^+$ (103 Da) OE ions along with $([HC(OH)_2]^+$ (47 Da) OE ions do have the diagnostic power for the identification of the diethyl-acetal moiety in the molecule of an unknown.

5.2.2. Dimethyl ketals

The mass spectrum of dimethyl-ketal of 3-hexanone depicted in Fig. 9(b) proves the carbonyl location owing to the presence of prominent peaks of $[M\text{-}C_3H_7]^+$ (103 Da) and $[M\text{-}C_2H_5]^+$ (117 Da) EE ions. The dimethyl-ketal group is characterized by the $[M\text{-}OCH_3]^+$ (115 Da) EE ion.

Cyclic acetals and ketals that are often employed as derivatives for the characterization of carbonyl compounds will be discussed later in a review on alicyclic compounds.

TABLE 1. Competing processes of dissociation in the $M^{+\cdot}$ of α,β-unsaturated carbonyl compounds (R, R^1, R′ = alkyl)

α,β-Unsaturated ketone Dissociation process	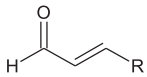 *Aldehyde*	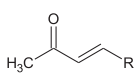 *Type "A" ketone*	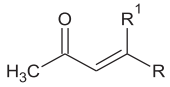 *Type "B" ketone*	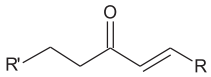 *Type "C" ketone*
Elimination of acetone neutral	No	**Yes**	No	No
McLafferty rearrangement	No	No	No	**Yes**
Formation of acyl cations	**Yes**	**Yes**	**Yes**	**Yes**

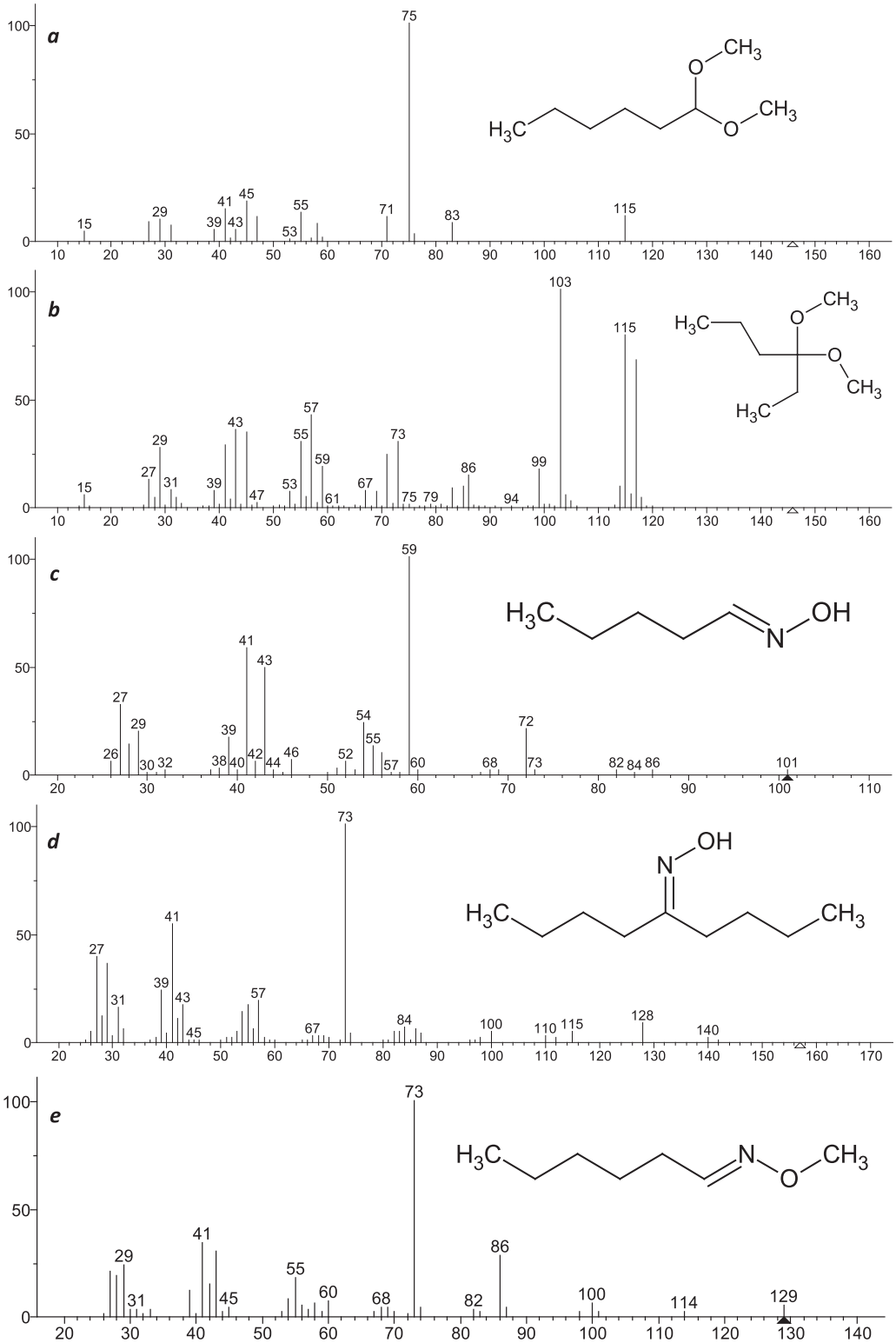

FIG. 9. Mass spectra [m/z (relative abundance, %)] of dimethyl-acetal of *n*-hexanal (a), dimethyl-ketal of 3-hexanone (b), aldoxime of *n*-pentanal (c), ketoxime of 5-nonanone (d), and *O*-methyl oxime of *n*-hexanal (e).

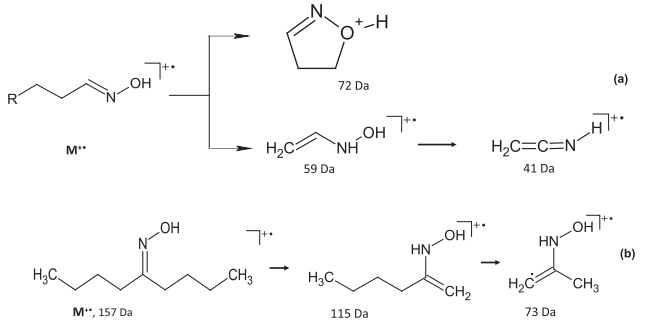

SCHEME 24. McLafferty rearrangements in *n*-alkyl aldoximes (a) and oxime of 5-nonanone (b).

5.3. Oximes of aldehydes and ketones

5.3.1. Oximes

The stability of $M^{+\cdot}$ for aliphatic oximes is low. McLafferty rearrangement and γ-cleavages are the two major fragmentation reactions typically proceeded in their molecular ions (Scheme 24). The mass spectrum of the pentanal oxime depicted in Fig. 9(c) exhibits a base peak (m/z 59) of the McLafferty rearrangement OE ion that further eliminates water neutral (peak at m/z 41). As a rule, peaks of this OE ion (59 Da) are of maximum intensity in the spectra of *n*-alkyl aldoximes. An isoxazolidinyl (m/z 72 Da) OE ion in the spectrum is due to γ-cleavage in the alkyl chain in the molecular ion (Scheme 24).

Similar dissociation processes take place in $M^{+\cdot}$ of ketoximes. However, additional McLafferty rearrangements are realized at the expense of additional alkyl chains around the oxime function. Scheme 24 demonstrates the formation of corresponding ions for the oxime of 5-nonanone [Fig. 9(d)].

5.3.2. O-Methyloximes

The above competitive fragmentation pathways typical for oximes are also characteristic for *O*-methyloximes of carbonyl compounds. Thus, the analogous (*O*-methyl analog) EE ion at $[CH_2CHNOCH_3]^{+\cdot}$ (73 Da) is expectedly present in the case of *O*-methyloxime analogs. The same ion types ($[CH_2C(CH_3)NOCH_3]^{+\cdot}$) are characteristic for methoximes of 2-alkanones; the corresponding peaks usually exhibit the highest intensities in the spectra. Consequently, abundances of these ion peaks at m/z 73 and m/z 87 are utilized for differentiation of methoximes of long chain aldehydes and isomeric 2-alkanones. In addition, the EI spectra of *O*-methyloxime of 2-alkanones contain abundant $[CH_3C{\equiv}NH]^+$ (42 Da) EE ions; the corresponding peaks show maximum intensity in the case of unbranched 2-alkanone derivatives. The initial elimination of the methoxy radical followed by γ-hydrogen shift and β-cleavage is responsible for the formation of the methylnitrilium EE ion (42 Da), as shown in Scheme 25.

Note that *O*-aryl-oximes, such as *O*-pentafluorobenzyl-oximes of carbonyl compounds, will be discussed in a review dealing with aromatic compounds.

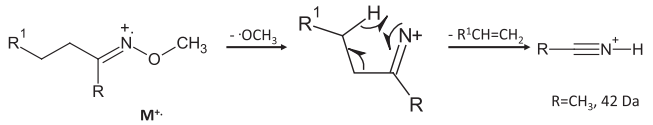

SCHEME 25. Formation of methylnitrilium ions from $M^{+\cdot}$ of methoximes of 2-alkanones.

5.4. Aldimines and ketimines

5.4.1. Methylimines

The molecular mass of *N*-methylimines, derived from aliphatic aldehydes, is easily determined because of their noticeable intensity. Breakdown of the $M^{+\cdot}$ ion is rather characteristic and gives rise to EE and OE ions. Prominent peaks in the spectra of *N*-alkylidene-methanamines are due to nitrilium cations at 42 Da; they demonstrate maximum intensities in the spectra of lower aldehyde derivatives. Other diagnostic ions for such compounds originate via the loss of alkyl radicals (beginning from CH_3) from molecular ions; the charge is localized on the imino function, as noted in Fig. 10(a). However, McLafferty-type rearrangement proceeding through a shift of the γ-hydrogen atom to the nitrogen atom of the imine group is frequently very characteristic. This decomposition reaction generates $[CH_2{=}CHN(H)CH_3]^{+\cdot}$ (57 Da) OE ions in the case of *N*-*n*-heptylidene-methylamine [Fig. 10(a)].

Similar dissociation pathways are realized in the case of methimines derived from dialkylketones. Their molecular ions are easily decomposed via McLafferty rearrangements: (a) $M^{+\cdot}$ undergoes double McLafferty rearrangements with the formation of $[M\text{-}C_3H_6]^{+\cdot}$ (113 Da) and $[M\text{-}C_3H_6\text{-}C_3H_6]^{+\cdot}$ (71 Da) OE ions and (b) the loss a butyl radical produces $[M\text{-}C_4H_9]^+$ (98 Da) EE ions; the latter further undergoes McLafferty rearrangement and generates $[M\text{-}Da\text{-}C_4H_8]^+$ (42 Da) OE ions [Scheme 26 and Fig. 10(b)].

5.4.2. N-Alkylimines

The abundance of molecular ions of higher *N*-alkylimines derived from aliphatic carbonyl compounds (Alkyl > CH_3) goes down because of easy breakdown of the *N*-alkyl chain. Additional dissociation patterns originate from the β-cleavage that is responsible for the generation of $[M\text{-}C_3H_7]^+$ (84 Da) EE ions in the case of *N*-butylidene-*n*-butylamine depicted in Fig. 10(c). Note that β-cleavage that is typical for alkylamines will be discussed in Sec. 8.1. In the case of *N*-alkylimines derived from higher ketones, additional breakdown processes occur in ions produced via α-C–C cleavage and elimination of an alkyl radical from the either side of the imino group. The generated EE ions undergo hydrogen rearrangement and readily lose alkene neutral from the *N*-alkyl moiety, as shown in Scheme 27. However, double McLafferty rearrangement in a molecular ion can frequently produce very prominent ions [see the peak at m/z 70 in Fig. 10(d)].

5.5. Hydrazones, semicarbazones, and thiosemicarbazones

5.5.1. Hydrazones

N,*N*-Dialkylhydrazones of aliphatic aldehydes and ketones show rather stable $M^{+\cdot}$. Simple β-C–C bond cleavages as well as simultaneous hydrogen migrations and β-cleavages (McLafferty

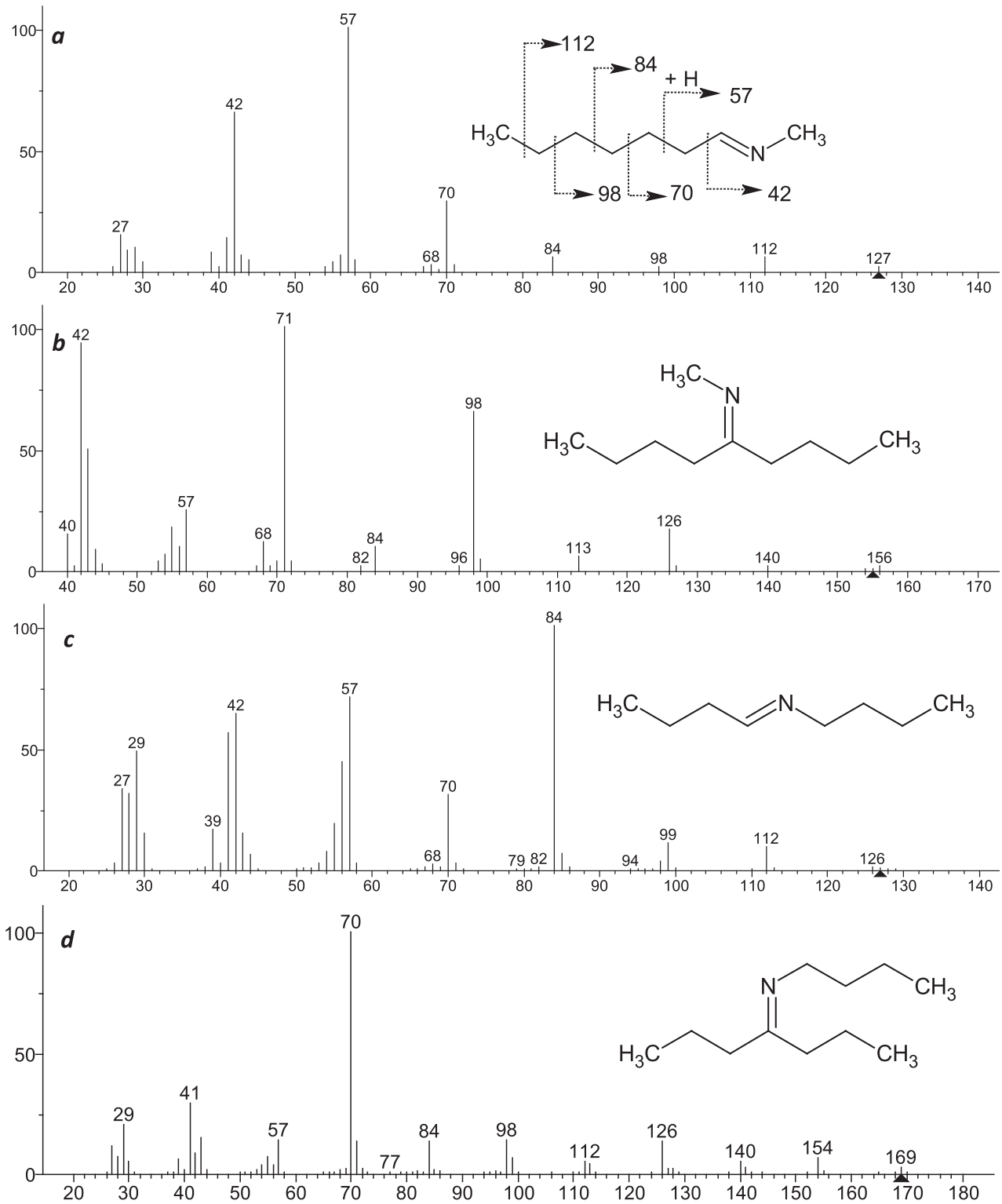

FIG. 10. Mass spectra [m/z (relative abundance, %)] of *N*-*n*-heptylidene-methylamine (a) and *N*-(5-*n*-nonilidene)methylamine (b), *N*-butylidene-1-butanamine (c) and *N*-(4-*n*-heptylidene)-1-butanamine (d).

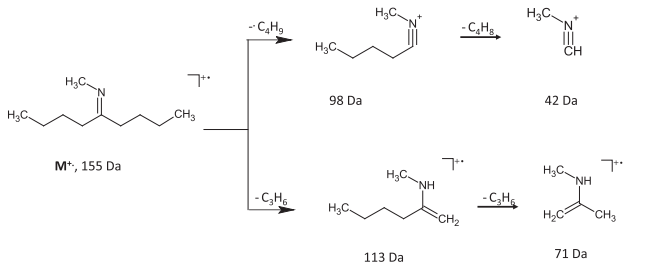

SCHEME 26. Major dissociation pathways of $M^{+\cdot}$ of *N*-methylimine of 5-nonanone.

rearrangement) are characteristic for this type of alkanal derivatives. For example, $[M\text{-}C_5H_{11}]^+$ (85 Da) and $[M\text{-}C_5H_{10}]^{+\cdot}$ (86 Da) ions are due to these processes in the case of dimethylhydrazone of heptanal [Fig. 11(a) and Scheme 28]. The following group of ions $[(CH_3)_2NH]^{+\cdot}$ (45 Da), $[CH_2N(H)CH_3]^+$ (44 Da), $[CH_2NCH_3]^+$ (43 Da), and $[CH_3NCH]^+$ (42 Da) appearing in the low mass region of the spectra characterize the hydrazine function, and they are not utilized for structure elucidation of the initial carbonyl compounds.

β-C–C Cleavages do not occur in $M^{+\cdot}$ of *N*,*N*-dimethylhydrazones of alkanones. Instead, hydrogen rearrangements, including single and double Mclafferty rearrangements, take place [Fig. 11(b)]. However, the abundant ions, such as $[(CH_3)_2N]^+$ (44 Da) EE and $[(CH_3)_2NH]^{+\cdot}$ (45 Da) OE ions, in the spectra are due to the dimethylhydrazone moiety, and they do not have an analytical value for the structure determination of an alkanone.

Higher *N*,*N*-dialkylhydrazones (alkyl > methyl) show similar fragmentation patterns. However, a new decomposition pathway associated with β-C–C-cleavages in *N*,*N*-dialkyl moieties takes place, and the generated ions can be the most abundant.

Along with *N*,*N*-dialkylaminohydrazones, many *N*-arylhydrazones, such as *N*-2-methyl-, *N*-2-nitro-, *N*-2-chloro-, *N*-4-methoxy- and *N*-2,4-dinitrophenyl-, *N*-phenyl-, *N*-2-naphthyl-, *N*-4-biphenyl-, *N*-2-pyrimidinyl-hydrazones, are used for the characterization of carbonyl compounds. Their aromatic moieties are usually responsible for the formation of the most characteristic ions. This is why the EI-induced dissociation of such compounds will be discussed in a review on aromatic compounds.

5.5.2. Semicarbazones

The mass spectra of semicarbazones of aliphatic aldehydes and ketones show observable $M^{+\cdot}$ peaks. Primary dissociation

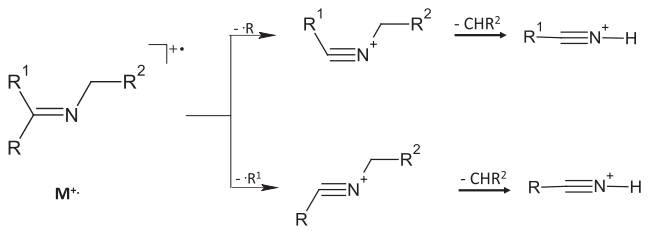

SCHEME 27. α-Cleavage followed by McLafferty rearrangement in the case of *N*-alkylimines of ketones (alkyl > CH_3).

of molecular ions proceeds via McLafferty rearrangements with the preferable formation of $[M\text{-}RCH{=}CH_2]^{+\cdot}$ OE ions along with $[M\text{-}HNCO]^{+\cdot}$ radical cations, as shown in Scheme 29. The very abundant $[H_3CCH_2N{=}NH]^{+\cdot}$ (58 Da) OE ions are formed from $[M\text{-}RCH{=}CH_2]^{+\cdot}$ ions through a subsequent McLafferty rearrangement.

As can be seen in Fig. 11(c), other characteristic ions in the spectra of semicarbazones of alkanals are two nitrilium $[CH_3CH_2CH_2CH_2CNH]^+$ (84 Da) and $[HCNNHCONH_2]^+$ (86 Da) EE ions and an iminium ion at $[HNC(NH_2)OH]^{+\cdot}$(60 Da). The $[M\text{-}C_2H_5]^+$ (114 Da) EE ion is a product of γ-C–C-bond cleavage that is typical for semicarbazones of alkanals. The latter can further elimination of the HNCO neutral.

The major decomposition pathway typical for semicarbazones of dialkylketones is a double McLafferty rearrangement. Thus, the derivatives of the general formula $(RCH_2)_2C{=}NNHCONH_2$ readily eliminate two (R-H) molecules and generate $[M\text{-}(R\text{-}H)]^{+\cdot}$ and $[M\text{-}(R\text{-}H)\text{-}(R\text{-}H)]^{+\cdot}$ OE ions. These product ions further lose an isocyanic acid (HNCO) molecule.

The competing fragmentation of $M^{+\cdot}$ of these derivatives may start from the loss of $HNCONH_2$ or RCH_2 and continue via the elimination of molecules RCH or HNCO and NH_3 accordingly. Similar to alkanals, β-C–C-bond cleavages are also characteristic for semicarbazones of dialkylketones; the generated ions further may lose HNCO or (NH_3 and HNCO) neutrals.

5.5.3. Thiosemicarbazones

The mass spectra of thiosemicarbazones of aliphatic aldehydes have little in common with those produced by their semicarbazone analogs. First, they show more stable $M^{+\cdot}$. The dominant fragmentation pathway of the molecular ions leads to $[M\text{-}C_4H_9]^+$ (112 Da) EE ions; the corresponding peaks are usually the base peaks in the spectra [Scheme 30(a), Fig. 11(d)]. The McLafferty rearrangement, characteristic of semicarbazones of alkanals, is negligible for the corresponding thiosemicarbazones (elimination of RCH and/or HNCS from $M^{+\cdot}$).

The same is true for thiosemicarazones of aliphatic ketones. Their $M^{+\cdot}$ do not dissociate via McLafferty rearrangement and do not lose alkene molecules. Instead, α-C–C cleavage around the imine nitrogen followed by the loss of a thiondiaziridine molecule becomes characteristic; this fragmentation pattern produces ions at 158 and 84 Da in the case of thiosemicarbazones 5-nonanone, as shown in Scheme 30(b) and Fig. 11(e).

Careful spectral correlation of carbonyl compounds and their derivatization products provide valuable structural information on such compounds, and the acquired evidence can be utilized for the identification of unknowns.

6. Acids and Their Modification Products

6.1. Carboxylic acids

6.1.1. Saturated acids

Aliphatic carboxylic acids show noticeable $M^{+\cdot}$ and these ions are of maximum intensity in the spectrum of formic acid. The $M^{+\cdot}$ intensity goes down to 45% and 27% in the spectra of acetic and propionic acids, and starting from butanoic acids, it does not exceed 10%.

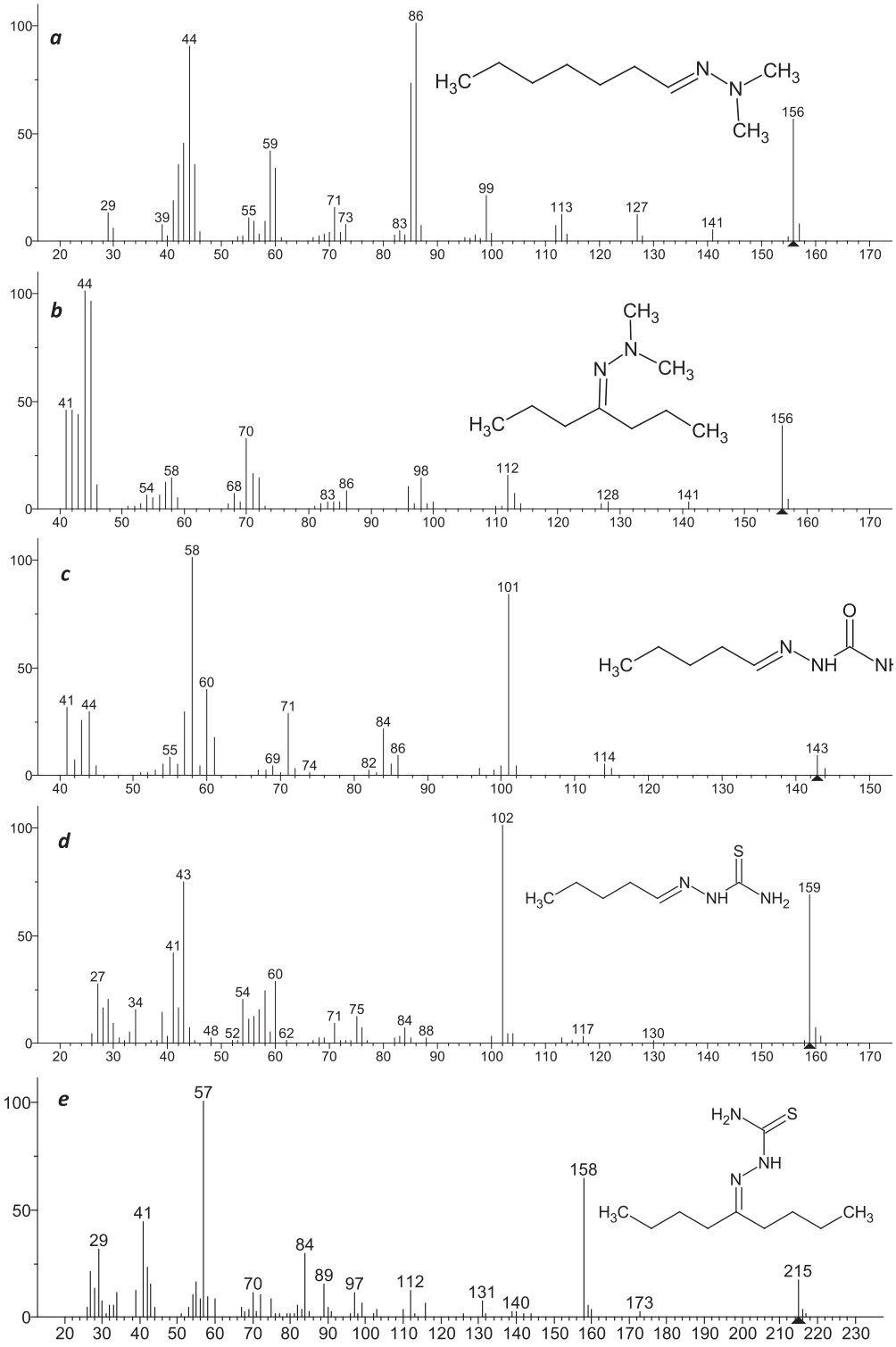

FIG. 11. Mass spectra [m/z (relative abundance, %)] of dimethylhydrazones of *n*-heptanal (a) and 4-heptanone (b), semicarbazone of *n*-pentanal (c), and thiosemicarbazones of *n*-pentanal (d) and 5-nonanone (e).

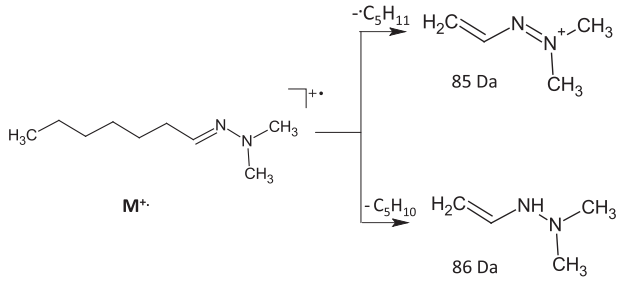

SCHEME 28. Typical β-cleavages in molecular ions of *n*-heptanal dimethylhydrazone.

Molecular ions of the simplest alkanoic acids dissociate similar to ketones. Their $M^{+\cdot}$ mainly undergo *α*-cleavages such as (a) loss of OH and/or H in the case of formic acid, (b) elimination of methyl and/or hydroxyl in the case of acetic acid, and (c) removal of methyl, ethyl, and/or OH in the case of propanoic acid. The elimination of OH and COOH radicals becomes less probable with the increase in the size of a carbon skeleton.

McLafferty rearrangement becomes one of the major dissociation pathways of alkanoic acids beginning from butyric acids. This pathway generates $[CH_2{=}C(OH)_2]^{+\cdot}$ (60 Da) OE ions when there are no substituents at *α*-carbon in the alkyl chain, as shown in Scheme 31. The other $[CH_2CH_2COOH]^+$ (73 Da) EE ion with diagnostic power is a product of β-cleavage in alkanoic acids with no substituents at C_α and C_β atoms (Scheme 31). This pair of ions becomes "fingerprints" of nonbranched *n*-alkanoic acids and of acids substituted at remote positions. In fact, the EI mass spectrum of *n*-nonanoic acid [Fig. 12(a)] shows the most abundant $[CH_2{=}C(OH)_2]^{+\cdot}$ (60 Da) OE and $[CH_2CH_2COOH]^+$ (73 Da) EE ions. Peaks of these diagnostic ions are shifted by 14 Da (increment of the methyl group) or 28 Da (increment of the ethyl group) with the introduction of the methyl or ethyl group to the C_α position [Fig. 12(b)]; the $[CH_2CH(C_2H_5)COOH]^+$ (101 Da) OE further undergoes McLafferty rearrangement, yielding $[CH_2CH(C_2H_5)COOH{-}C_2H_4]^+$ (73 Da) EE ions at the expense of the C_α-C_2H_5 moiety.

The introduction of the ethyl group to C_β does not affect the $[CH_2{=}C(OH)_2]^{+\cdot}$ (60 Da) OE ions [Fig. 12(c)]. However, β-cleavage produces the $[(C_2H_5)CHCH_2COOH]^+$ (101 Da) EE ion that constitutes 28 Da mass shift. Examples of spectra of three isomeric nonanoic acids in Figs. 12(a)–12(c) well illustrate the analytical power of the above pair of ions for structure determination of alkanoic acids, particularly the substitutions at *α*- and β-carbon atoms. Note that the spectra of *n*-alkanoic acids demonstrate an unusual periodicity in the series of ions with the general formula $[(CH_2)_mCHCHC(OH)_2]^+$ at m/z 87, m/z 101, m/z 115, and more. This periodicity significantly changes with the introduction of branching. The characteristic changes may point to the location and the nature of branching in carbon chains.

Another analytically useful dissociation route in this series gives rise to protonated 1,1-dihydroxy-6-heptene (129 Da) EE ions in the case of *n*-alkanoic acids having nine or more carbon atoms in the

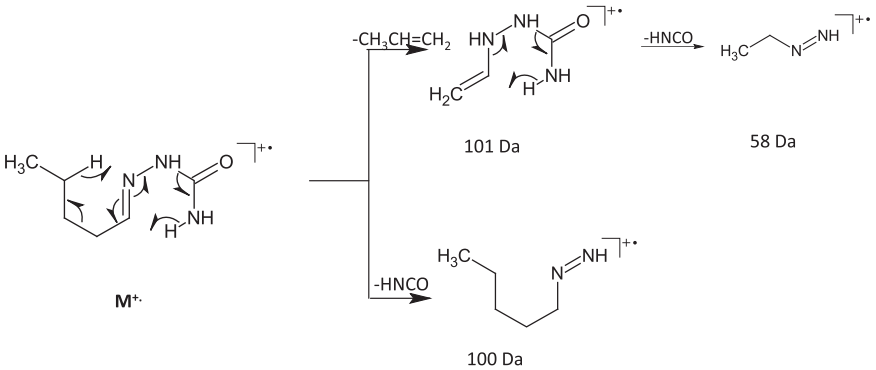

SCHEME 29. McLafferty rearrangements in an ionized valeraldehyde semicarbazone [Fig. 11(c)].

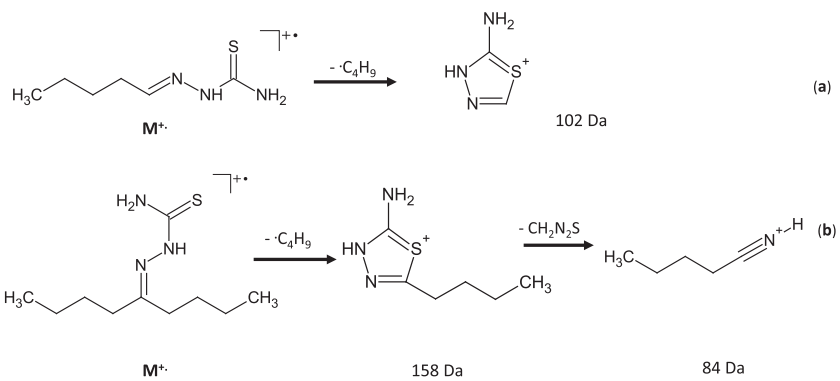

SCHEME 30. Major fragmentation pathways of $M^{+\cdot}$ of thiosemicarbazones of *n*-pentanal (a) and 5-nonanone (b).

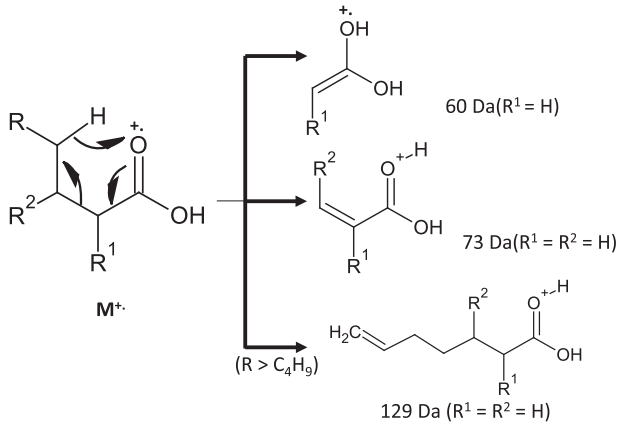

SCHEME 31. Major fragmentation pathways of $M^{+\cdot}$ of saturated aliphatic acids.

chains [Fig. 12(a)]. Therefore, a group of three ions (60, 73, and 129 Da) is diagnostically important for the structure determination of higher straight chain alkanoic acids.

Methyl substituted at $C_{(4)}$-position alkanoic acids demonstrate an additional unusual dissociation pathway. Technically, $M^{+\cdot}$ of these acids undergo "pseudo-McLafferty rearrangement," which involves δ-hydrogen migration followed by γ-C–C-bond cleavage (in this case, note that the γ-carbon atom carries the methyl substituent). The preference of "δ-hydrogen migration and γ-cleavage" over "γ-hydrogen migration and β-cleavage" is well realized for 4-methylpentanoic and -hexanoic acids, and it is noticeable right up to 4-methylnonanoic acid (Table 2). However, this process does not occur in the case of 4-methyloctadecanoic acid. A similar tendency is observed in the spectra of methyl esters of 4-methypentanoate and -hexanoate.

6.1.2. Unsaturated acids

Generation of rearrangement $[CH_2{=}C(OH)_2]^{+\cdot}$ (60 Da) OE ions and $[CH_2CH_2COOH]^+$ (73 Da) EE ions due to "β-cleavage" is also reasonable for unsaturated acids when a double bond is far enough from the carboxyl function. These dissociation pathways are justifiable for δ,ε-alkenoic acids, starting from 5-hexenoic acid and higher, since they possess a mobile hydrogen atom at γ-carbon and the β-C–C bond cleavage in the molecules is allowed. In fact, the EI mass spectrum of 5-hexenoic acid reveals strong peaks at m/z 60 Da and m/z 73 [Fig. 12(d)]. The named requirement is not met in the case of 3-hexenoic acid whose mass spectrum should not display this pair of peaks. However, relative intensities of the correspondent peaks are rather intense, as shown in Fig. 12(e). This fact can be explained by the isomerization of $M^{+\cdot}$ via a "double bond migration" into a remote position when the disposition of participating groups fulfills the requirements for the generation of this ion pair. The same reason is accountable for the presence of these ions in the spectra of higher 2-, 3-, and 4-alkenoic acids.

For the lower aliphatic unsaturated acids, such as acrylic, methacrylic, crotonic and isocrotonic, angelic and tiglic, and pentenoic acids, the loss of H, CH_3, OH, and H_2O is typical; the sequence of their elimination may be different. As a result, prominent multiplets of ions at m/z 27–29 (n = 2), m/z 39–41 (n = 3), and m/z 53–55 (n = 4) are observed in the spectra of these acids ($C_nH_{2n-1}COOH$).

Dissociation of carboxylic acids containing a triple bond in the β,γ-position of the carbon chain and conjugated double or cumulated double bonds proceeds like monounsaturated acids. However, some of them demonstrate unexpected fragmentation pathways that may be unique for a specific class. For that reason, a careful consideration of all details is required when selecting and proposing a candidate structure. Note, for example, rather specific fragmentation of the ionized 2,2-dimethylpenta-3,4-dienoic acid involves elimination of dimethylketene neutral and generates abundant propargyl alcohol (56 Da) OE ions (Scheme 32).

6.2. Carboxylic acid derivatives

Generally, mass spectra of fatty acids do not provide sufficient information on chain branching, the position of unsaturation, and other structural features. Several chemical modification methods are developed to solve the structural problems. Characteristic dissociation pathways of some of the widely utilized chemical modification products are discussed below. Note, however, that in addition to analytical derivatives prepared for MS purposes, various acid derivatives are produced in the industry and by lower micro-organisms in nature.

6.2.1. Alkyl esters

6.2.1.1. Alkyl formates. Dissociation of rather stable methyl, ethyl, and propyl esters of formic acid differs from the decomposition of long chain alkyl esters. For example, major dissociation pathways of C_1–C_3-alkyl formates lead to the most abundant hydroxy methylene (31 Da) EE ion (Scheme 33), whereas isopropyl formate produces a hydroxy ethylidene (45 Da) EE ion (Scheme 33). Other ions observed in the spectra of all formates are $[HCO]^+$ (29 Da)EE ions that are due to α-cleavage.

6.2.1.2. Methyl esters. Dissociation of methyl esters of fatty acids is similar to that of corresponding carboxylic acids. Thus, $[CH_2{=}C(OH)(OCH_3)]^{+\cdot}$ (74 Da) OE, $[CH_2CH_2COOCH_3]^+$ (87 Da) EE, and $[C_6H_{12}COOCH_3]^+$ (143 Da) EE ions [see Fig. 13(a)] are of diagnostic power in the spectra of methyl *n*-alkanoates. They are produced via the same mechanisms described above for *n*-alkanoic acids. Likewise, mass values of the first pair of ions provide evidence on the substitution at $C_{(2)}$ and $C_{(3)}$ atoms in the alkyl chain of methyl esters, and the shift of the peak at m/z 143 Da indicates total substituents in the $C_{(4)}$–$C_{(7)}$ region of the carbon skeleton.

The formation of other $[(CH_2)_nCOOCH_3]^+$ type of ions becomes easy with the appearance of branching. For example, α-C–C cleavages at branching points lead to prominent peaks at m/z 185 and m/z 213 in the spectrum of methyl 11-methylnonadecanoate [Fig. 13(b)] and peaks at m/z 171 and m/z 199 in the case of ethyl 9-methyloctadecanoate [Fig. 13(c)].

The high mass region of the spectra of methylalkanoates contains prominent $M^{+\cdot}$ and observable peaks of $[M\text{-}OCH_3]^+$ EE ions due to α-cleavage. The $[CH_3OCO]^+$ cation is also produced via α-cleavage. It is rather abundant in the spectra of lower methylalkanoates and the relative intensities of these ions in the spectra of higher esters are up to 10% [Figs. 13(a) and 13(b)].

6.2.1.3. Alkyl alkanoates. Increase in the size of the alcoholic chain in ester molecules complicates the spectra. However,

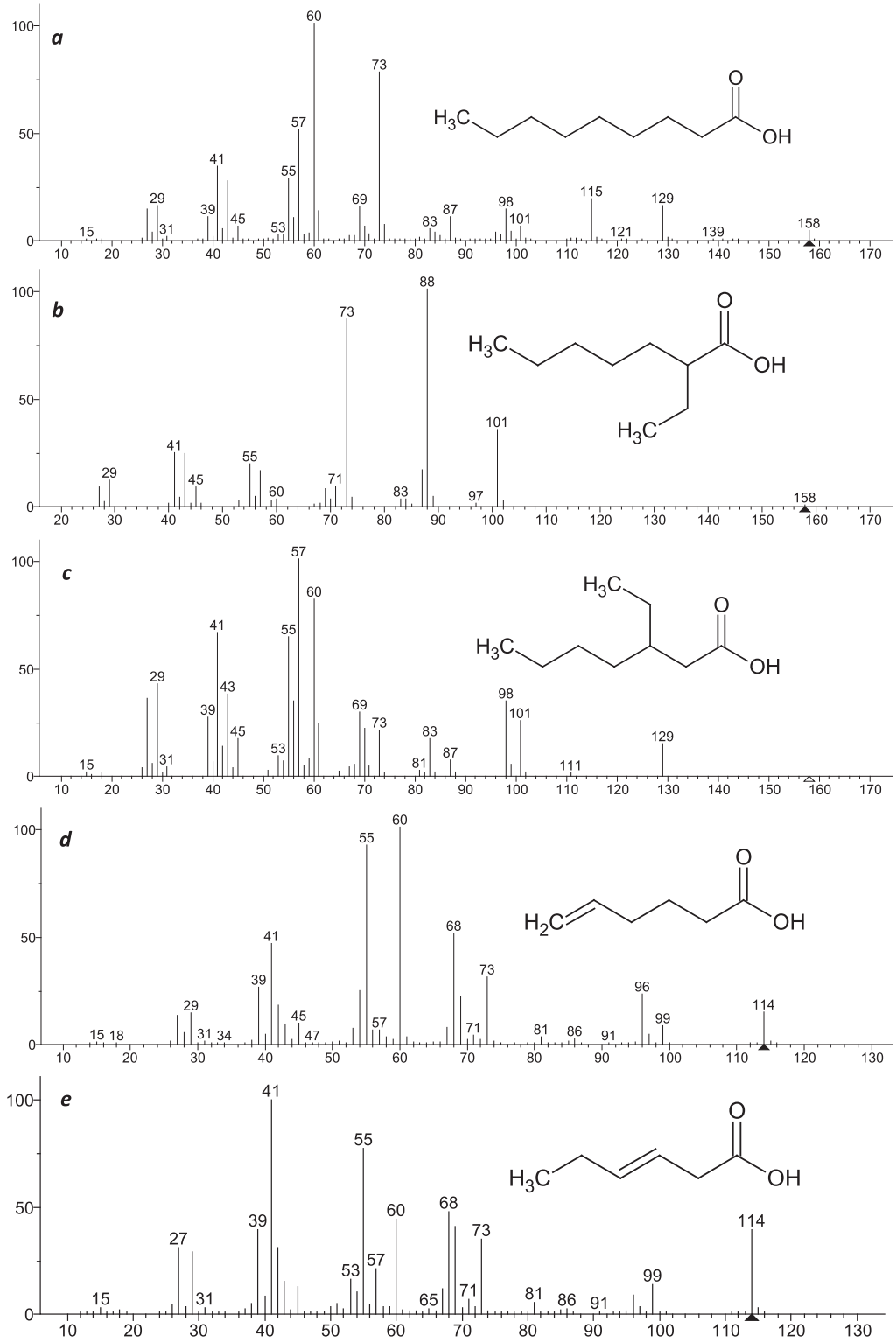

FIG. 12. Mass spectra [m/z (relative abundance, %)] of *n*-nonanoic (a), 2-ethylheptanoic, (b) 3-ethylheptanoic (c), 5-hexenoic (d), and 3-hexenoic acids (e).

TABLE 2. Relative intensities of selected ions in the spectra of 4-methylalkanoic acids

Acid	Relative intensities of ions (structure, Da)		
	$[CH_2{=}C(OH)_2]^{+\cdot}$, 60 Da (%)	$[CH_3CH{=}C(OH)_2]^{+\cdot}$, 74 Da (%)	$[CH_2CH_2COOH]^+$, 73 Da (%)
4-Methylpentanoic	41	63	58
4-Methylhexanoic	40	52	75
4-Methyloctanoic	35	19	68
4-Methylnonanoic	26	15	68
4-Methyloctadecanoic	29	<1	100

ions typical for methyl esters are present in the spectra. Thus, the mass spectrum of ethyl 9-methyloctadecanoate depicted in Fig. 13(c) demonstrates abundant $[CH_2{=}C(OH)(OC_2H_5)]^{+\cdot}$ (88 Da) OE, $[CH_2CH_2COOC_2H_5]^+$ (101 Da) EE, and $[C_6H_{12}COOC_2H_5]^+$ (157 Da), and the spectrum of pentyl decanoate [Fig. 13(d)] shows noticeable peaks of $[CH_2{=}C(OH)(OC_5H_{11})]^{+\cdot}$ (130 Da) OE, $[CH_2CH_2COOC_5H_{11}]^+$ (143 Da) EE, and $[C_6H_{12}COOC_5H_{11}]^+$ (199 Da) EE ions.

Additional dissociation pathways of $M^{+\cdot}$ of alkyl alkanoates of the general formula $RCOOR^1$ include generation of $[RCOOH]^{+\cdot}$ OE ions and EE ions corresponding to the protonated acid $[RCOOH_2]^+$. As one can see in the spectrum of pentyl decanoate [Fig. 13(d)], the peak of the latter $[C_9H_{19}COOH_2]^+$ (173 Da) EE ion is rather intense (48%), while the peak corresponding to the acid (172 Da) OE ion is small (about 6% relative intensity).

α-Cleavages relative to the carbonyl group generate abundant acyl cations ($[RCO]^+$) in the spectra of alkyl alkanoates with long alkyl chains. For example, a peak of the $[C_9H_{19}CO]^+$ (155 Da) EE ion in the spectrum of pentyl decanoate is rather intense [Fig. 13(d)]. The other abundant ions in the spectra are due to the loss of carboxylic acid neutrals from $M^{+\cdot}$ with formation of olefinic OE ions. For example, the base peak of the $[M\text{-}C_{10}H_{21}COOH]^{+\cdot}$ (70 Da) EE ion in the spectrum of pentyl decanoate [Fig. 13(d)] has a pentene structure. As demonstrated in Table 3, the analytical importance of this pair of ions depends on the size of the acid chain backbone.

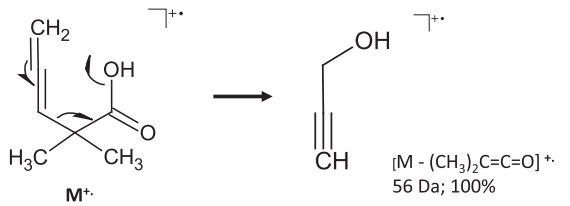

SCHEME 32. Generation of the propargyl alcohol OE ion from $M^{+\cdot}$ of 2,2-dimethylpenta-3,4-dienoic acid.

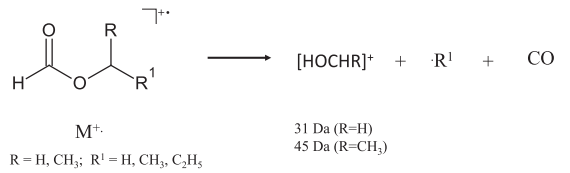

SCHEME 33. Dissociation of $M^{+\cdot}$ of methyl, ethyl, and *n*- and isopropyl formates.

6.2.1.4. Alkyl acetates. Acetates represent a special group of esters because of their wide use as analytical derivatives to improve volatility and stability of alcohols. For that reason, the basic fragmentation tendencies of their $M^{+\cdot}$ are discussed in Sec. 4.5. Molecular ions of aliphatic acetates readily eliminate acetic acid neutral, and usually, $M^{+\cdot}$ peaks are not observed in the spectra. The origin of product ions is similar to that discussed above for alkyl alkanoates. The mass spectrum of heptyl acetate [Fig. 13(e)], for example, reveals peaks of $[CH_3CO]^+$ (43 Da) EE and $[CH_3COOH_2]^+$ (61 Da) EE ions along with $[M\text{-}CH_3COOH]^{+\cdot}$ OE ions. The latter is responsible for the generation of a major set of hydrocarbon ions in the total ion current.

6.2.1.5. Alkyl alkenoates. Esters of unsaturated acids have more stable $M^{+\cdot}$ than their saturated analogs. The direct determination of unsaturation location in their molecules is unattainable by MS. However, there are cases where double bonds are easily determined. For example, unsaturation may be determined in methyl α,β-alkenoates. Their spectra contain peaks of $[M\text{-}CH_3]^+$, $[M\text{-}OCH_3]^+$, $[M\text{-}COOCH_3]^+$, $[COOCH_3]^+$ EE, and $[M\text{-}CH_3OH]^{+\cdot}$ OE ions along with abundant $M^{+\cdot}$. In addition, molecular ions of methyl and ethyl acrylates and methacrylates can readily lose H, H_2O, CO, and CO_2. The diagnostically important dissociation pathway of $M^{+\cdot}$ of methyl esters of fatty α,β-alkenoic acids includes C_β-C_γ-bond cleavage relative to the double bond and generation of oxonium $[C_5H_6O(OCH_3)]^+$ (113 Da) EE ions [Scheme 34(a)]. Another specific dissociation can be of analytical importance for structure determination of alkyl esters of fatty γ,δ-alkenoic acids; their $M^{+\cdot}$ undergo a skeletal rearrangement depicted in Scheme 34(b).

6.2.1.6. Alkyl alkynoates and alkadienoates. Molecular ions of alkyl 2-alkynoates containing triple bond at the α,β-position generally eliminate an alkyloxy radical, and the peaks of the corresponding acyl EE ions are dominant in the spectra. For the 3- and 4-alkynoate analogs, the loss of a carboalkyloxy group from $M^{+\cdot}$ becomes favorable, and the peaks of generated alkynyl cations demonstrate maximum intensities in their spectra.

Some specific dissociation pathways useful for structure elucidation are recognized for alkyl esters of alkadienoic acids. For

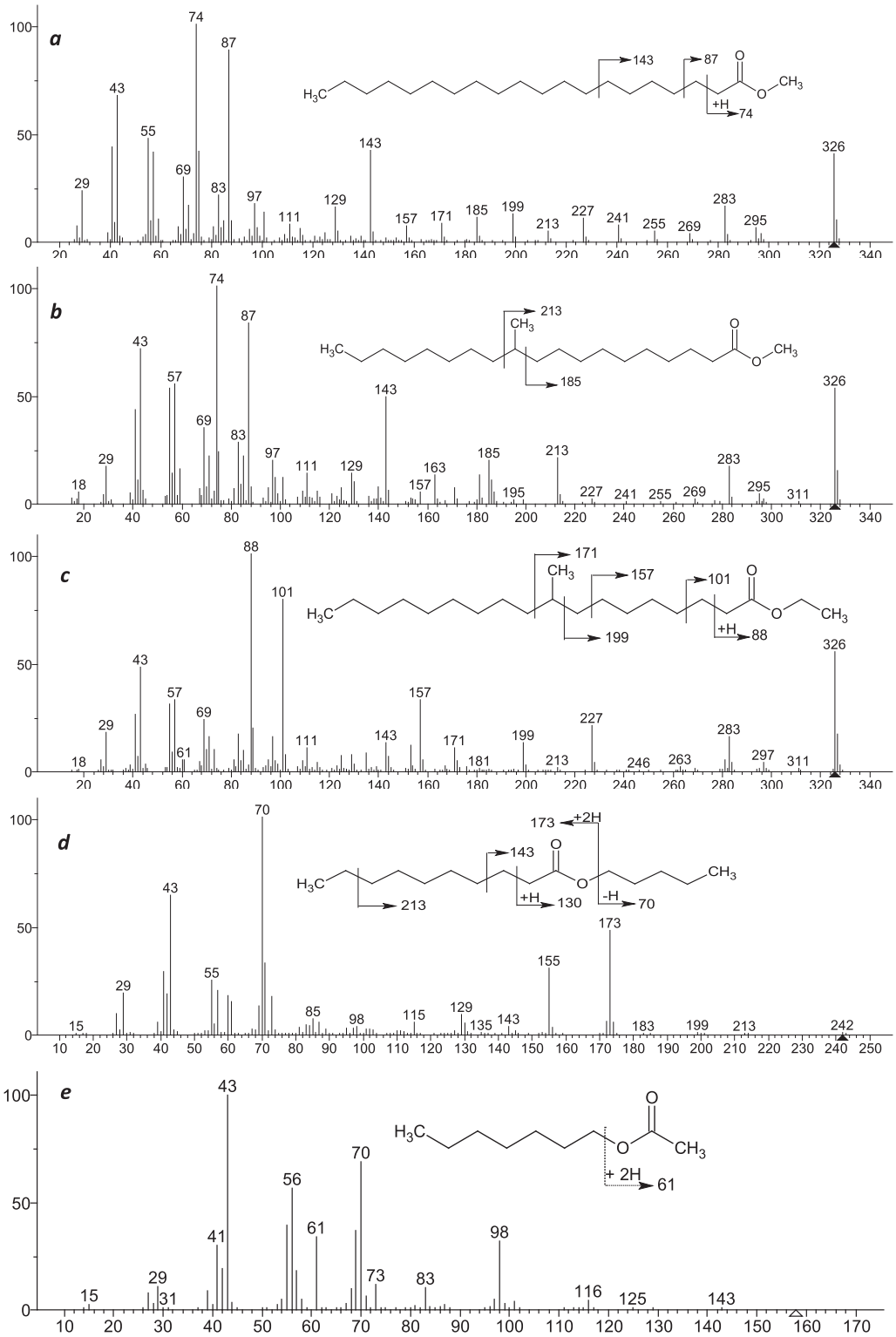

FIG. 13. Mass spectra [m/z (relative abundance, %)] of methyl eicosanoate (a) 11-methylnonadecanoate (b), ethyl 9-methyloctadecanoate (c), *n*-pentyl decanoate (d), and *n*-heptyl acetate (e).

TABLE 3. Relative intensities of pentene OE ions and acyl cations in the spectra of *n*-pentyl *n*-alkanoates of the general formula $C_nH_{2n+1}COOC_5H_{11}$

Ions	n = 1–4	n = 5–8	n = 9–13	n = 14–17
$[C_5H_{10}]^{+\cdot}$, 70 Da (%)	47–90	100	100	100
$[C_nH_{2n+1}CO]^+$ (%)	100	50–75	19–31	12–18

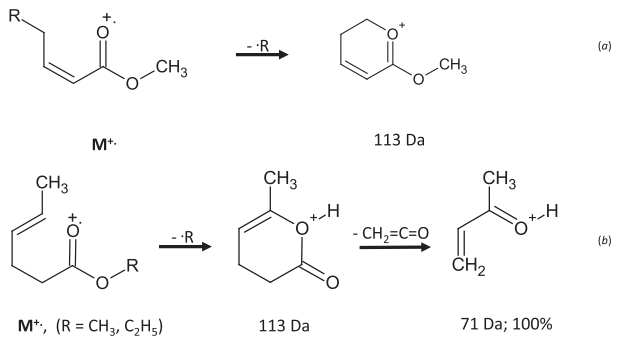

SCHEME 34. Typical dissociation of ionized alkyl α,β- (a) and γ,δ-alkenoates (b).

example, molecular ions of methyl and ethyl 3,7,11-trimethyl-2.4-dodecadienoates generate pyrylium $[M\text{-}C_8H_{17}]^+$ EE ions (Scheme 35).

6.2.2. Double bond derivatization in esters

As was noted above, generally the determination of the double bond position in alkenoic acids and their esters is almost impossible even though a correlation between the location of double bonds and relative abundances of selected ions for a limited range of acids and esters can be sometimes established. For that reason, several derivatization methods are developed to solve the problem, such as (a) selective deuterium reduction of unsaturation with tetradeuterohydrazine or Wilkinson's catalyst [chloridotris(triphenylphosphine)rhodium], (b) oxidation to polyhydroxy acid esters with permanganate or osmium tetroxide followed by further derivatization of hydroxyl functions, (c) methylthiolation via iodine-catalyzed reaction with dimethyl disulfide, and more.

Spectra of selected methyl esters of monoenic and dienoic acids and their "double bond derivatives" can be compared in Fig. 14. While the spectrum of methyl oleate [Fig. 14(a)] fails to provide any structural information on the $C_{(4)}$–$C_{(18)}$ part of the alkyl chain, the

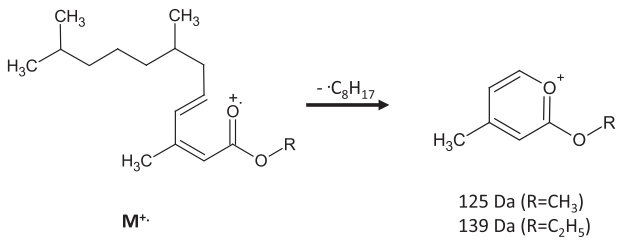

SCHEME 35. Formation of pyrylium EE ions from ionized alkyl 3,7,11-trimethyl-2,4-dodecadienoates.

spectrum of vicinal di(trimethylsilyloxy) methyl stearate [Fig. 14(b)] prepared by successive double bond hydroxylation and silylation reveals the peaks of two major oxonium ions at 215 and 259 Da. Both these ions originate from the bond cleavage between C-atoms bearing silyloxy groups of the stearate residue and prove the double bond location at $C_{(9)}$ of the initial oleate. More even number of trimethylsilyloxy groups are formed in polyenic acids and interpretation of the spectra of resulting poly(TMS) compounds becomes increasingly more difficult.

α-C–C bond cleavage between vicinal methylthio substituents in di(methylthio) derivatives, prepared by methylthiolation, generates analytically important ions with charge localization on both sides of the chain, and the ions associated with this cleavage are dominant in the spectra. Thus, the spectrum of methyl 9,10-di(methylthio)octadecenoate depicted in Fig. 14(c) demonstrates the most abundant thionium $[C_8H_{17}CHOSi(CH_3)_3]^+$ (215 Da) EE and $[(CH_3)_3SiOCHC_7H_{14}COOCH_3]^+$ (259 Da) EE ions. These key ions along with $[CH_2{=}C(OH)(OCH_3)]^{+\cdot}$ (74 Da) OE and $[CH_2CH_2COOCH_3]^+$ (87 Da) EE ions, which characterize the methoxycarbonyl group, have diagnostical power. The high intensity peak of $[CH_2{=}SCH_3]^+$ (61 Da) EE ions in the spectrum does not possess a diagnostic value.

The spectrum of methyl linoleate [Fig. 14(d)], like its monoenic analog, provides information on the composition of a molecule (molecular weight and chemical formula), confirms the presence of a carbomethoxy moiety and the absence of branching at $C_{(2)}$–$C_{(3)}$. At the same time, the spectrum of the tetra(methoxy) derivative depicted in Fig. 14(e) provides additional information. Dissociation of $M^{+\cdot}$ is dominated by α-cleavages with respect to the methoxy groups, and oxonium ions at m/z 115, m/z 159, m/z 201, m/z 217, m/z 245, and m/z 303 are generated These ions further lose methanol neutrals. A comparative analysis of the spectra of methyl linoleate and its tetra(methoxy) derivative [Figs. 14(d) and 14(e)] allows elucidation of the dienic structure of the methyl ester.

6.2.3. Silyl esters

Molecular ions of trimethylsilyl esters are usually of low abundance. However, the $[M\text{-}CH_3]^+$ EE ions allow a reliable determination of the molecular weight. Note that the charge in the $[M\text{-}CH_3]^+$ cation may be localized on oxygen as well as on the silicon atom. In addition to $[M\text{-}CH_3]^+$, $[(CH_3)_3Si]^+$ (73 Da), and $[(CH_3)_2SiOH]^+$ (75 Da) ions, the spectra of saturated long-chain fatty acids (Fig. 15) contain groups of analytically important ions.

The mass spectra of TMS esters of linear and polymethyl-substituted alkanoic acids depicted in Figs. 15(a) and 15(c) exhibit the $[CH_2{=}C(OH)(OSi(CH_3)_3)]^{+\cdot}$ (132 Da) OE ion that is produced via McLafferty rearrangement. This ion further eliminates a methyl radical and generates $[CH_2{=}C(OH)(OSi(CH_3)_2)]^+$ (117 Da) EE ions (Scheme 36). The other ion of diagnostic power is a result of a classic cleavage between β- and γ-carbon atoms; this process in the case of TMS decanoate [Fig. 15(a)] yields a $[CH_2CH_2COOSi(CH_3)_3]^+$ (145 Da) EE ion (Scheme 36).

Homologous ions in the case of TMS 3,7,11,15-tetramethylhexadecanoate include the 3-methyl group, and the mass of the latter ion is shifted by 14 Da and the $[CH(CH_3)CH_2COOSi(CH_3)_3]^+$ (159 Da) EE ion is generated [Fig. 15(c), Scheme 36].

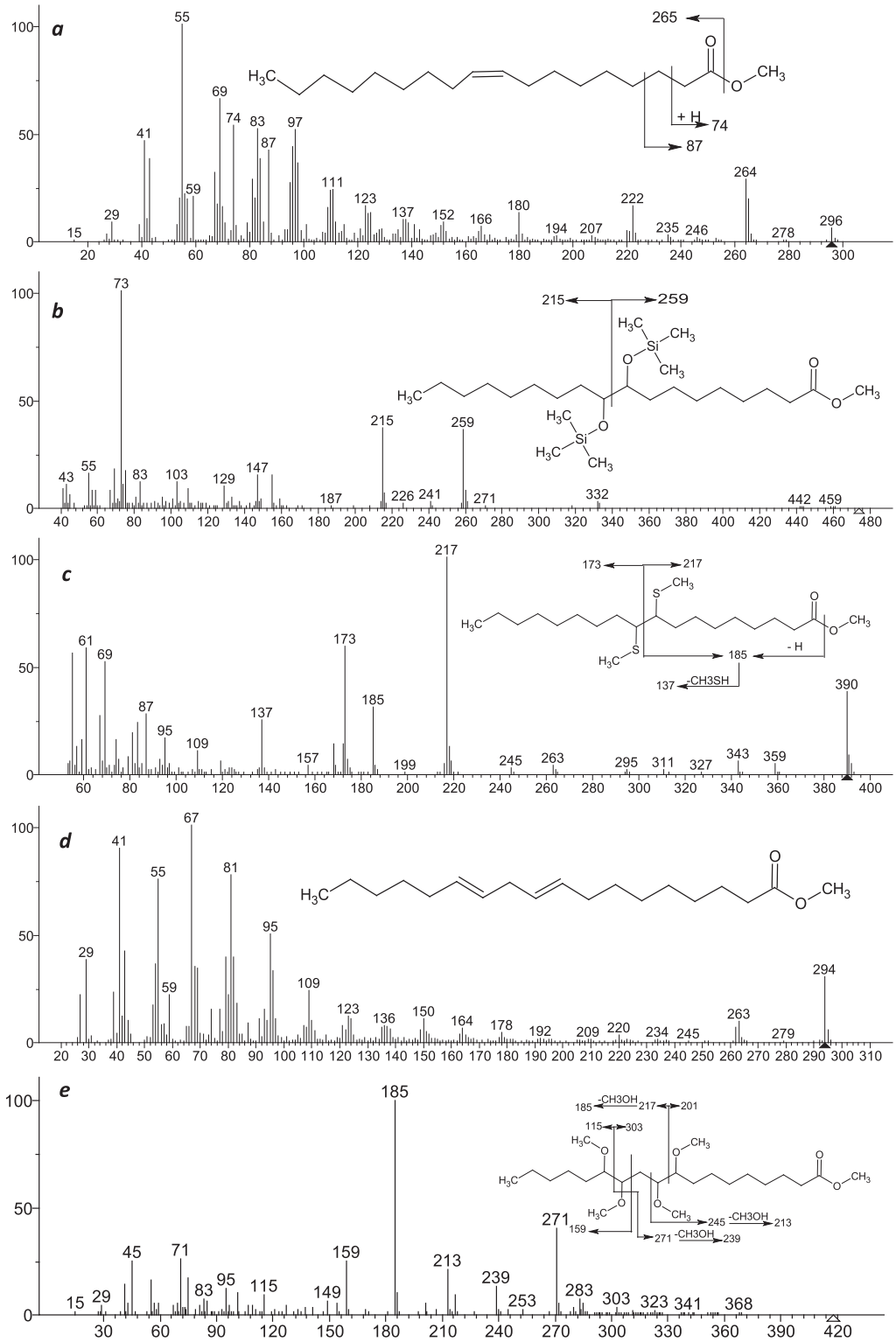

FIG. 14. Mass spectra [m/z (relative abundance, %)] of methyl oleate (a), methyl 9,10-di(trimethylsilyloxy)stearate (b), methyl 9,10-di(methylthio)stearate (c), methyl 9*E*,12*E*-octadecadienoate (d), and methyl 9,10,12,13-tetra(methoxy)stearate (e).

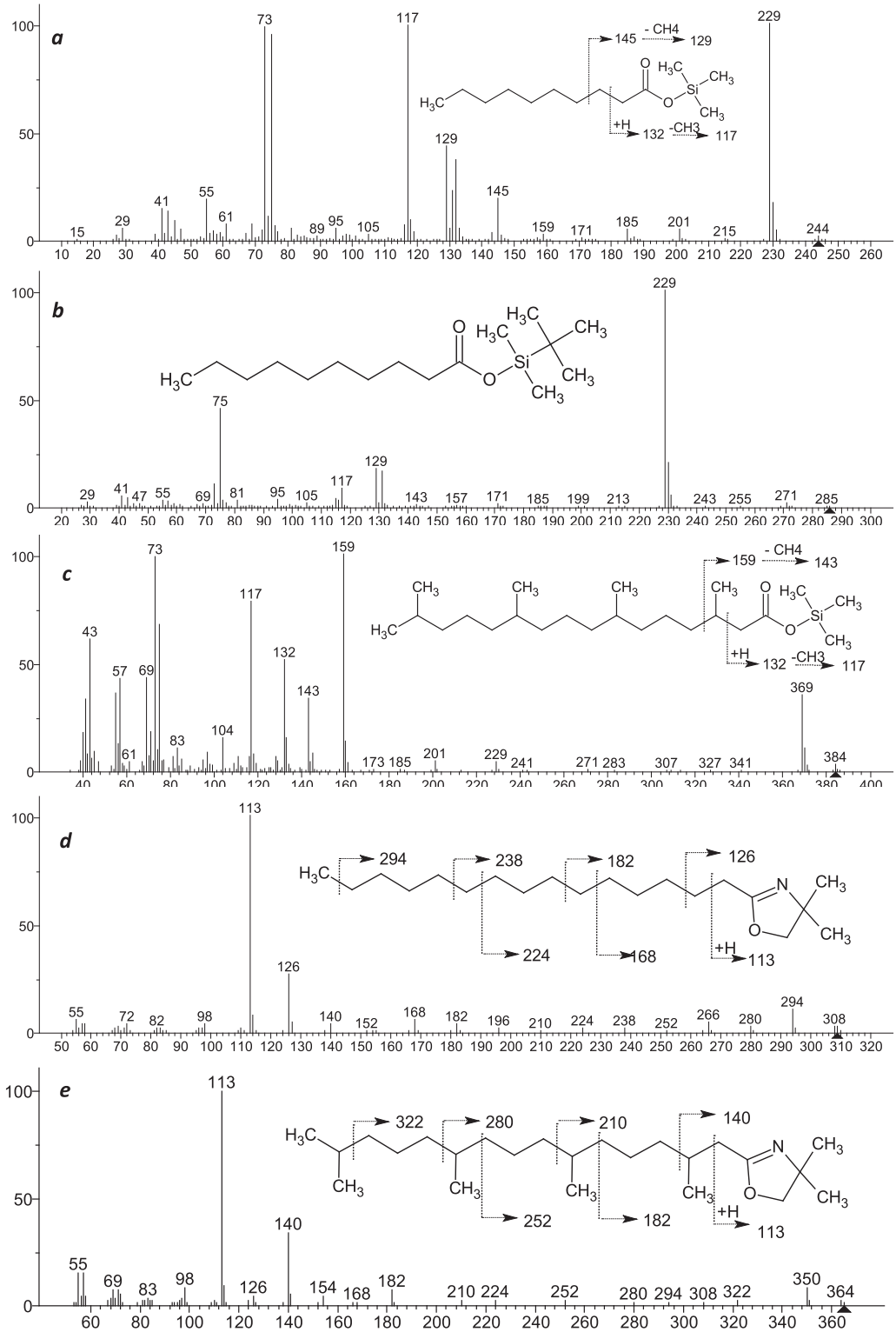

FIG. 15. Mass spectra [m/z (relative abundance, %)] of trimethylsilyl (a) and *tert*-butyldimethylsilyl-*n*-decanoates (b), trimethylsilyl-3,7,11,15-tetramethylhexadecanoate (c), 4,4-dimethyloxazoline derivatives of *n*-hexadecanoic (d) and 3,7,11,15-tetramethylhexadecanoic acids (e).

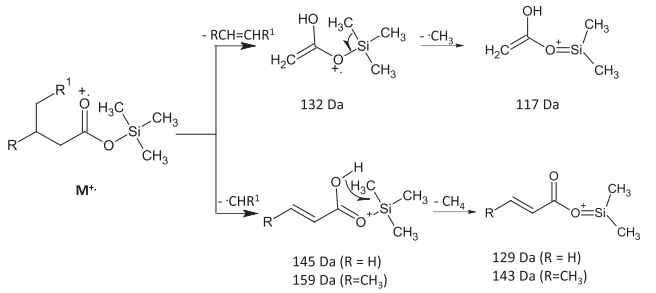

SCHEME 36. Major fragmentation pathways of molecular ions of trimethylsilyl esters of alkanoates.

Note that peaks at m/z 117 and m/z 129 are present in the spectra of both TMS alkanoates and TMS ethers of alkanols; they have different compositions and correspond to isobaric ions. Mass spectra of tBDMS alkanoates provide less structural information when compared to TMS derivatives. The spectrum of tBDMS decanoate that is depicted in Fig. 15(b) is typical for analogous alkanoates; the spectrum is dominated by the $[M\text{-}C_4H_9]^+$ EE ion that is successfully used for a reliable determination of molecular weight and in quantitative analysis.

Similar dissociation processes are observed in the case of trimethylsilyl esters of unsaturated carboxylic acids. The positions of unsaturation cannot be determined directly from the spectra due to the migration of double bonds during ionization/fragmentation.

6.2.4. 4,4-Dimethyloxazoline (DMOX) derivatives

DMOX derivatives can be prepared from acids but better from their methyl esters via the reaction with 2-amino-2-methyl-1-propanol. They are suitable for the determination of molecular weight of alkanoic acids because these derivatives produce noticeable $M^{+\cdot}$ and $[M\text{-}H]^+$ ions as well as $[M\text{-}CH_3]^+$ and $[M\text{-}C_3H_7]^+$ EE ions. The $[M\text{-}CH_3]^+$ ion arises solely from the gem-dimethyl moiety of the DMOX ring, and the latter is also responsible for the formation of $[M\text{-}C_3H_7]^+$ ions. Accordingly, the $[M\text{-}CH_3]^+$ and $[M\text{-}C_3H_7]^+$ EE ions at 294 and 266 Da in the case of the DMOX derivative of hexadecanoic acid [Fig. 15(d)] cannot be used for structure determination of the acid residue.

The doublets of abundant $[C_5H_9NOCH_2]^{+\cdot}$ (113 Da) OE and $[C_5H_8NOC_2H_4]^+$ (126 Da) EE ion peaks in the spectrum given in Fig. 15(d) as well as $[C_5H_9NOCH_2]^{+\cdot}$ (113 Da) OE and $[C_5H_8NOC_3H_6]^+$ (140 Da) EE ions in Fig. 15(e) are due to McLafferty-like rearrangement and β-cleavage, respectively. Like linear aliphatic acids, the peak at 126 Da in the spectrum of the DMOX derivative [Fig. 15(d)] is followed up by an ion series of small peaks with [126 + (n × 14)] Da. However, the intensities of these ion peaks are varied, and these variations are employed for the determination of branching. For example, three pairs of peaks at m/z 182 and m/z 210, m/z 252 and m/z 280, and m/z 322 and m/z 350 [Fig. 15(e)] provide sufficient information on the positions of branching in the 3,7,11,15-teramethylhexadecanoic acid derivative.

DMOX derivatives are also useful for MS determination of unsaturation in aliphatic acids. For example, mass differences between neighboring peak clusters reflect the double bond position in monoenoic aliphatic acids. The same principle applies to poly-unsaturated aliphatic acids. However, their spectra are more complicated, and several spectra interpretation approaches should be employed for the determination of the unsaturation location.

6.2.5. Acyl pyrrolidines

Pyrrolidide and oxazolidine derivatives coincidentally have the same chemical formula for a given acid, and pyrrolidides also exhibit noticeable $M^{+\cdot}$. The typical mass spectrum of pyrrolidide of polymethylsubstituted alkanoic acid is presented in Fig. 16(a). It illustrates fragmentation pathway similarities between pyrrolidide and oxazolidine derivatives; the mass values of diagnostically important ions appear to be the same. Pyrrolidides are successfully employed for the unsaturation location by analyzing peaks in 12 mass intervals between prominent peaks. Thus, in the spectrum of pyrrolidide of eicosatrienoic acid [Fig. 16(b)], the triplet of peaks at m/z 152 to m/z 154 and at m/z 232 to m/z 234 are used for the location of double bonds. The listed peaks formally correspond to ions generated via the cleavage of a C=C bond accompanied by protonation and deprotonation.

6.2.6. β-Pycolinyl esters

The mass spectrum of picolinyl eicosanate typical for straight-chain saturated acid derivatives is depicted in Fig. 16(c). It exhibits a stable $M^{+\cdot}$ and prominent peaks of $[C_5H_4NCH_2]^+$ (92 Da) EE and $[C_5H_4NCH_2O]^+$ (108 Da) EE ions characterizing the picolinyl moiety. The other outstanding peaks in the spectrum reveal typical dissociations for acids: the $[CH_2{=}C(OH)(OCH_2NC_5H_4)]^{+\cdot}$ (151 Da) OE ion is a result of McLafferty rearrangement, while β-cleavage is responsible for the formation of the $[CH_2CH_2C(O)(OCH_2NC_5H_4)]^{+\cdot}$ (164 Da) EE ion. These ions along with the ion series at m/z [164 + (n × 14)] with a comparable relative intensity distribution can be used for elucidation of structural elements [Fig. 16(c)]. Note that all ion peaks at m/z [164 + (n × 14)] separated by 14 mass units are present in the case of picolinyl alkanoates with branched alkyl chains. Ions generated via C–C-bond cleavage at branching exhibit enhanced relative abundance.

The location and confirmation of the double bond position in picolinyl alkenoates is not a difficult task. For example, the mass spectrum of the 9-eicosenoate derivative [Fig. 16(d)] contains (a) a triplet of peaks at m/z 246–248 formally corresponding to C=C cleavage at C_9 accompanied by deprotonation and protonation, (b) a separation of 13 mass units in the ion series: m/z 234–247–260, and (c) β- and γ-cleavages relative to the double bond are responsible for the prominent peaks at m/z 274 and m/z 288 in the spectra.

Similar behavior is characteristic for picolinyl alkadienoates containing double bonds that are separated by more than three carbon atoms. Analogous fragmentation is typical for picolinyl esters with triple bonds as well. However, spacing between ions neighboring to the triple bond is 24 Da instead of 26 Da for ions adjacent to a double bond. For example, a spectrum of picolinyl *n*-eicosanoate containing triple and double bonds at C_{11} and C_{13} is depicted in Fig. 16(e). Here, $M^{+\cdot}$ dissociation proceeds according to the general rule stating that only the unsaturated bonds distal to the (picolinyloxy)carbonyl group produce diagnostic ions: (1) triplet peaks at m/z 298–300 due to formal cleavage of C_{13}–C_{14} and neighboring

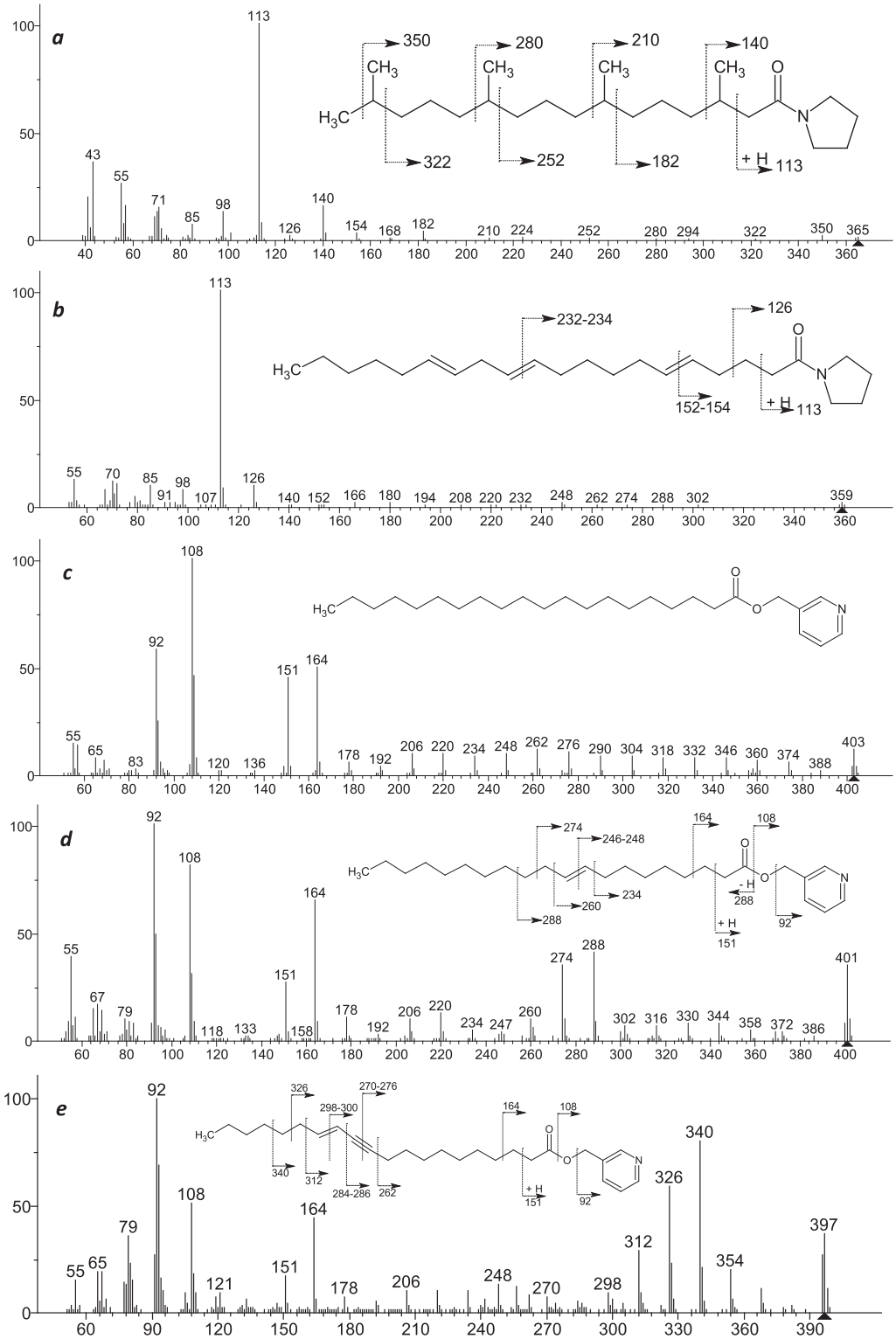

FIG. 16. Mass spectra [m/z (relative abundance, %)] of 3,7,11,15-tetramethylhexadecanoyl pyrrolidide (a), 15,11,14-*E*-eicosatrienoyl pyrrolidide (b), picolinyl *n*-eicosanoate (c), picolinyl 9-eicosenoate (d), and picolinyl eicosa-11-yn-(13*E*)-enoate (e).

ions at m/z 312 (299 + 13) and m/z 286 (299 − 13) and (b) prominent peaks of $[M\text{-}C_4H_9]^+$ (340 Da) EE and $[M\text{-}C_5H_{11}]^+$ (326 Da) EE ions corresponding to γ- and β-cleavages relative to the double bond at C_{13}.

6.3. Anhydrides

Molecular ions of the majority of anhydrides are unstable, and the corresponding peaks are absent in the spectra of alkanoic anhydrides. For example, the spectrum of *n*-butyric anhydride does not show $M^{+\cdot}$, and the base peak corresponds to the acylium $[C_3H_7CO]^+$ (71 Da) EE ion [Fig. 17(a)]. Successive loss of carbon monoxide and hydrogen from the acylium ion gives rise to $[C_3H_7]^+$ (43 Da) EE, $[C_3H_6]^{+\cdot}$ (42 Da) OE, and $[C_3H_5]^+$ (41 Da) EE ions.

Like anhydrides, acyl chlorides do not demonstrate $M^{+\cdot}$, and acyl ions are used for their determination. For instance, the molecular mass of octanoyl chloride [Fig. 17(b)] is determined by using the $[M\text{-}Cl]^+$ (127 Da) EE ion. Most of the ions appearing in the spectra are produced via decomposition of this product ion. Peaks of ions generated via McLafferty rearrangement (78/80 Da) and β-cleavage relative to the functional group (91/93 Da) are of moderate intensities—up to 13% rel. [Fig. 17(b)].

6.4. Amides, hydrazides, and imides

Fragmentation pathways of classic amides, including primary, secondary, and tertiary amides, are discussed in this section. Behavior of acyl pyrrolidines under MS conditions are presented in Sec. 6.2.4 since the pyrrolidine derivatives are widely utilized for structure determination of aliphatic acids.

6.4.1. Amides

Alkyl amides demonstrate rather stable molecular ions [Figs. 17(c)–17(e)]. Cleavages at both sides of the amidic carbonyl are characteristic dissociation pathways for lower amides of C_1–C_3-acids. As a result, the corresponding spectra contain noticeable $[M\text{-}NH_2]^+$ EE ions and base peaks of $[OCNH_2]^+$ (44 Da) cations; in the latter ion, the charge may be localized at oxygen as well as at the nitrogen atom.

Starting from butyramide, major fragmentation of primary and secondary amides of alkanoic acids [Figs. 17(c) and 17(d)] proceeds via McLafferty rearrangement and β-cleavage relative to the amido function. These dissociation processes resemble that of corresponding alkanoic acids. Thus, the two most abundant ions in the spectrum of *n*-octanamide [Fig. 17(c)] correspond to the rearrangement $[CH_2{=}C(OH)NH_2]^{+\cdot}$ (59 Da) OE ion and to the $[CH_2CH_2C(O)NH_2]^{+\cdot}$ (72 Da) ion that is generated via the β-cleavage; peaks of $[C(O)NH_2]^{+\cdot}$ (44 Da) have also a noticeable intensity.

The introduction of an *n*-butyl substituent to amidic nitrogen provides grounds for additional fragmentation pathways [Fig. 17(d)]. However, the ions resulting from McLafferty rearrangement and the β-cleavage still remain the most prominent with the diagnostic power: the outstanding peaks of $[CH_2{=}C(OH)N(H)C_4H_9]^{+\cdot}$ (115 Da) OE and $[C_2H_4C(O)N(H)C_4H_9]^+$ (128 Da) EE ions are present in the spectrum of *N*-butyloctanamide [Fig. 17(d)]. Furthermore, the $[CH_2{=}C(OH)N(H)C_4H_9]^{+\cdot}$ (115 Da) OE ion undergoes β-cleavage accompanied with the hydrogen shift and eliminates propylene neutral. In the spectrum, a noticeable $[H_2N{=}CH_2]^+$ ion is also observed, which is originated from the *N*-alkyl moiety and includes hydrogen from the acyl residue. Thus, ions produced as a result of β-cleavage and McLafferty rearrangement are the key ions for successful determination of primary and secondary amides. Note that a simple amidic C–N bond cleavage with the charge localization at the acyl moiety and formation of octanoyl (127 Da) EE ions is reduced as compared with that of esters: the relative intensity of the $[C_7H_{15}CO]^+$ EE ion in *N*-butyloctanamide is up to 22% against the intensity of the same ion (46%) in the case of butyl octanoate. Note that small amounts of the protonated acetamide (60 Da) EE ion peak are present in the spectrum.

The competing fragmentation pathways typical for *N*-alkyl compounds become dominant for tertiary amides due to powerful fragmentation reactions directed by nitrogen. McLafferty rearrangement and β-cleavage become less important for them. In fact, the intensity of the rearrangement $[CH_2{=}C(OH)N(C_3H_7)C_4H_9]^{+\cdot}$ (157 Da) OE ion does not exceed 8% rel. in the spectrum of *N*-propyl-*N*-butyloctanamide [Fig. 17(e)]. Instead, competing processes of amide CO–N bond cleavage followed by bond dissociations characteristic for amines become dominant (Scheme 37). Note that the latter process is unavailable for *N*′,*N*-dimethyl amides.

6.4.1.1. N-TMS derivatives of amides. Similar to alkanamides, molecular ions of their *N*-TMS derivatives decompose through McLafferty rearrangement and β-cleavage. The resulting ions as well as the $M^{+\cdot}$ eliminate methyl radicals at the expense of the TMS moiety. Ions arising due to loss of a methyl radical from $M^{+\cdot}$ and from the products of McLafferty rearrangement are prominent in the spectrum of *N*-TMS-hexanamide [Fig. 18(a)]. The TMS moiety is also well represented by trimethylsilyl (73 Da) and dimethylhydroxysilyl (75 Da) EE ions. The $[C_2H_4C(O)N(H)Si(CH_3)_3]^+$ (144 Da) EE ion that is produced via β-cleavage further eliminates a methane molecule giving rise to the noticeable peak $[C_2H_4C(O)N{=}Si(CH_3)_2]^+$ (128 Da) EE ion.

N-TMS derivatives of polyunsaturated amides decompose under EI similarly to fragmentation of the corresponding TMS esters. As demonstrated in Fig. 18(b), ions arising due to McLafferty rearrangement and β-cleavage can be generated during the dissociation of TMS unsaturated amides. The conditions for proceeding these reactions remain the same: the nearest double bond shall be located at least three methylene groups apart from the amide function.

6.4.2. Acyl hydrazines

Acyl hydrazines demonstrate rather stable molecular ions. The major dissociation of their $M^{+\cdot}$ proceeds with the cleavage of the C–N bond. This process generates two most prominent ions in the spectra: (a) rearrangement $[NH_2NH_2]^{+\cdot}$ OE hydrazine ions and (b) $[C_nH_{2n+1}CO]^+$ acyl cations. Hydrazine (32 Da) OE ions are usually the base peaks in the spectra [Figs. 18(c) and 18(d)]. In the case of hydrazine 2,2-dimethylpropionamidate, the *tert*-butyl (57 Da) EE ion becomes expectedly dominant, and the hydrazine OE ions are second in relative intensity (72%) [Fig. 18(e)].

Starting from hydrazine acetamidate, the acyl EE ions, $[C_nH_{2n+1}CO]^+$, can further eliminate carbon monoxide, giving rise to alkyl cations. The expected ions corresponding to McLafferty rearrangement in the spectra of hydrazine derivatives are also

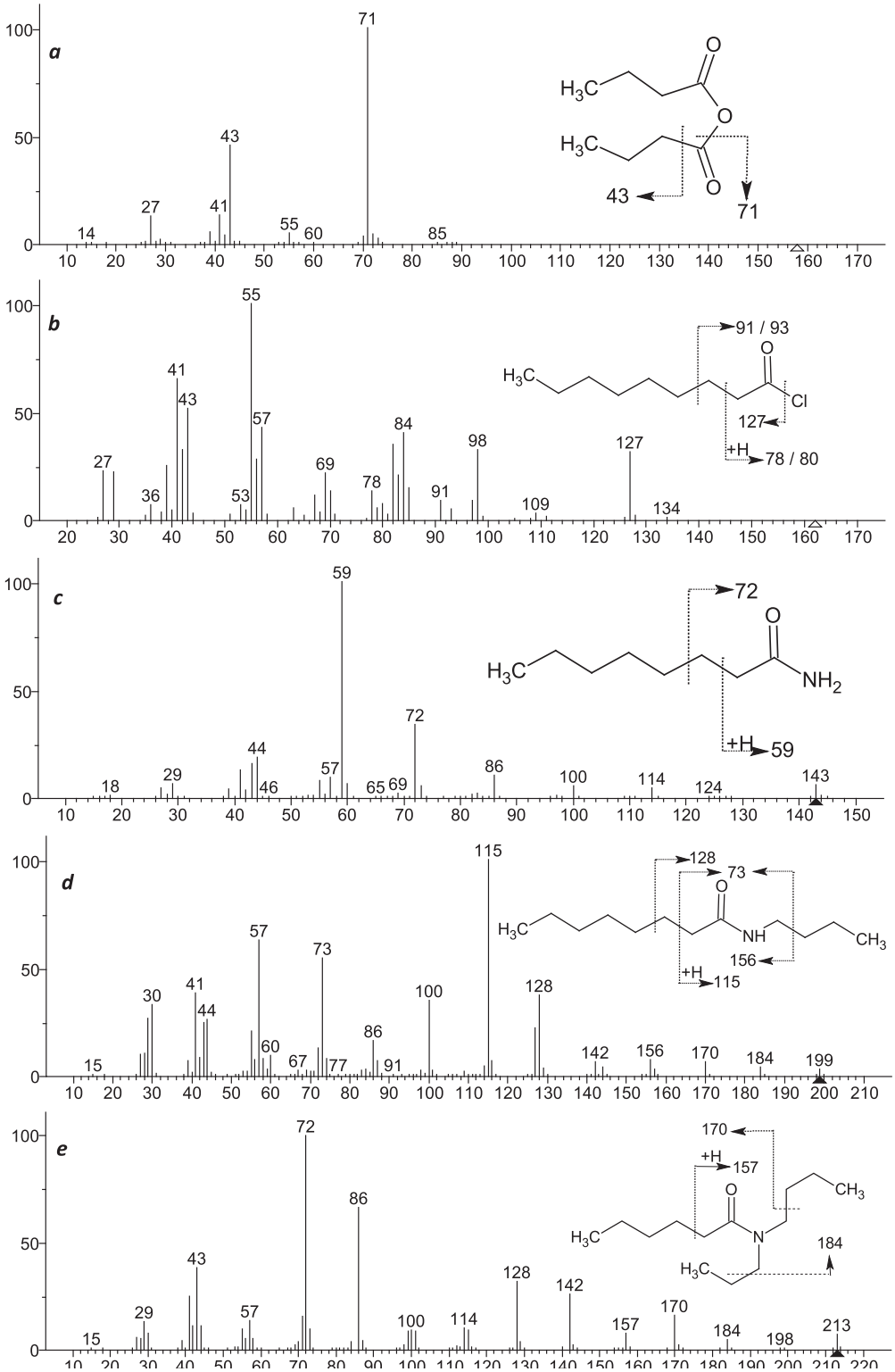

FIG. 17. Mass spectra [m/z (relative abundance, %)] of *n*-butyric anhydride (a), *n*-octanoyl chloride (b), *n*-octanamide (c), and *N*-(*n*-butyl)- (d) and *N*-(*n*-propyl)-*N*-(*n*-butyl)octanamides (e).

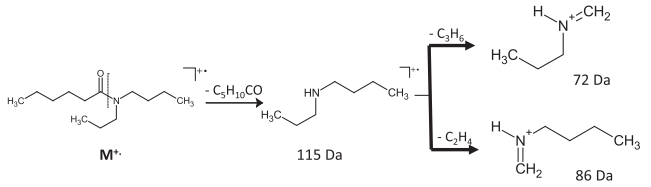

SCHEME 37. Dissociation of *N*,*N*-dialkylamino moiety in the case of *N*-propyl-*N*-butylhexanamide [Fig. 17(e)].

present, starting from hydrazine butyrate. These ions are not of high intensity, but the intensities increase with the rise of the size of the alkyl chain. For example, the peak intensity of the corresponding $[CH_2=C(OH)NHNH_2]^{+\cdot}$ (74 Da) OE ion reaches 42% in the spectrum of hydrazine decanamidate [Fig. 18(c)]. The spectra of hydrazine alkanamidates also contain peaks of homologous hydrocarbon ions of the following composition: $[C_nH_{2n+1}]^+$, $[C_nH_{2n}]^{+\cdot}$, $[C_nH_{2n-1}]^+$, $[C_nH_{2n-2}]^{+\cdot}$, and $[C_nH_{2n-3}]^+$.

6.4.3. Imides

Symmetric imides [Figs. 19(a) and 19(b)] derived from one alkanoic acid and asymmetric imides [Fig. 19(c)] containing two different acyl residues are discussed in this section along with *N*-alkyl substituted imides. Other imides containing various N-substitutions will be considered in the following review articles.

Mass spectra of imides of alkanoic acids demonstrate noticeable $M^{+\cdot}$ and prominent peaks of acyl cations. Thus, $[CH_3CO]^+$ (43 Da) EE ions demonstrate maximum intensities in the spectra of di-(acetyl)imides [Figs. 19(a), 19(d), and 19(e)]; peaks of $[C_3H_7CO]^+$ (71 Da) EE ions are one of the most outstanding peaks in the case of di(butyryl)imide [Fig. 19(b)] and propionyl(butyryl)imide [Fig. 19(c)] containing a butyryl moiety. The propionyl(butyryl)imide containing both propionyl and butyryl moieties generates two acyl $[C_2H_5CO]^+$ (57 Da; 100%) and $[C_3H_7CO]^+$ (71 Da; 54%) EE ions. Expectedly, the acyl cations readily eliminate carbon monoxide and produce alkyl EE ions [Fig. 19(c)].

Imides of alkanoic acids undergo numerous hydrogen and skeletal rearrangements under EI: (1) molecular ions of di(acyl)imides lose carbon monoxide as a result of a skeletal rearrangement, and the corresponding ions are outstanding in the molecular region of the spectra [Figs. 19(a)–19(c)]. (2) Cleavage of imidic C–N bonds accompanied with mono and two hydrogen migrations generate $[C_nH_{2n+1}CONH_3]^+$ EE and $[C_nH_{2n+1}CONH_2]^{+\cdot}$ OE ions in the spectra of di(acyl)imides [Figs. 19(a)–19(c)]. In the case of di(butyryl)imide, a peak corresponding to the protonated butyrylamide (88 Da) EE ion ($[C_3H_7CONH_3]^+$) is the base peak in the spectrum. Propionyl(butyryl)imide, consisting of two different acyl residues, generates two pairs of ions corresponding to propionamide (73 Da) OE and butyrylamide (87 Da) OE ions and their protonated analogs (74 and 88 Da) [Fig. 19(c)]. Ion pairs of the same origin demonstrate peaks at m/z 59 and m/z 60 in the spectra of diacetylmides [Figs. 20(a), 20(d), and 20(e)].

Introduction of an alkyl substituent to nitrogen in the imide molecule brings additional dissociation routes [Figs. 19(d) and 19(e)]. For example, cleavage of the $N–C_{(alkyl)}$ bond accompanied with migration of two hydrogen atoms from an alkyl substituent generates $[M-C_4H_7]^+$ (102 Da) EE ions in the case of *N*-alkyldiacylimides. The latter ion further undergoes parallel decomposition reactions via (a) skeletal rearrangement and generation of $[M-C_4H_7-H_2O]^+$ (84 Da) ions and (b) hydrogen migration and elimination of a ketene molecule to yield $[M-C_4H_7-CH_2CO]^+$ (60 Da) EE ions. The spectra of *N*-alkyl imides [Figs. 19(d) and 19(e)] also contain prominent peaks of $[CH_2=NH_2]^+$ cations characteristic for *N*-alkylamines. The origin of this type of ions will be discussed in Sec. 8.

6.5. Carbonic acid derivatives

In this section, mass spectral characteristics having diagnostic power are discussed for the following derivatives of carbonic acids:(1) dialkyl esters of carbonic acid (carbonates, $R^1O–CO–OR^2$), (2) alkyl esters of alkyl (*N*,*N*′-dialkyl) monoamides of carbonic acid (carbamates, $R^1R^2N–CO–OR^3$), and (3) *N*,*N*′-alkyl(poly-alkyl)diamides of carbonic acid (carbamides, urea, $R^1R^2N–CO–NR^3R^4$).

6.5.1. Carbonates

Commonly, di(alkyl)-carbonates under EI produce $M^{+\cdot}$ of low stability, and corresponding peaks are often absent in the spectra. Dimethyl carbonate, the first member of this homologous series, shows a noticeable molecular ion and the base peak of the methyl (15 Da) EE ion. The abundant peaks of $M-CH_3]^+$ (75 Da) EE, $[M-OCH_3]^+$ (59 Da) EE, and $[OCH_3]^+$ (31 Da) EE ions in the spectrum are due to simple cleavages [Fig. 20(a)]. Skeletal rearrangements in molecular ions of dimethyl-carbonate generate (a) $[M-CO]^{+\cdot}$ (62 Da) OE and $[M-COH]^+$ (61 Da) EE ions and $[M-H-CO_2]^+$ (45 Da) EE ions. Hydrogen rearrangement in the $[M-OCH_3]^+$ EE ion followed by the loss of ketene neutral produces $[HCO]^+$ (29 Da) EE ions.

New dissociation routes emerge with the increase in the alkyl chain length. Thus, the spectrum of ethyl butyl carbonate [Fig. 20(b)] contains peaks of the $[C_2H_5OCOOH]^{+\cdot}$ (90 Da) OE and $[C_4H_9OCOOH]^{+\cdot}$ (118 Da) OE ions along with EE ions of their deprotonated (89 and 117 Da) and protonated (91 and 119 Da) analogs. The protonated ions (91 and 119 Da) further eliminate the other alkyl group as an alkene molecule, and both ions generate $[HOC(OH)OH]^{+\cdot}$ (63 Da) EE ions that have a structure of the protonated carbonic acid cation. The corresponding peak shows maximum intensity in the spectrum [Fig. 20(b)]. However, the abundance of this ion decreases with the increase in the size of alkyl chains, and the intensity of the protonated carbonic acid becomes just about 2% rel. in the spectrum of decyl octadecyl carbonate.

Other typical ions in the spectra of higher dialkyl carbonates $[(RO)_2CO]$ correspond to $[R]^+$, $[OR]^+$, and $[M-OR]^+$ EE ions and to products of their further decomposition. Branching of the alkyl chain at α-carbon may also initiate dissociation of $M^{+\cdot}$ followed by skeletal and hydrogen rearrangements, such as sequential loss of carbon dioxide and an alkene molecule.

6.5.2. Carbamates

Methylcarbamate produces rather stable $M^{+\cdot}$ that can decompose in two ways. The major route includes cleavage of the $C_{amidic}–O_{ether}$ bond with the charge localization on both parts of a molecule to yield $[NH_2CO]^+$ (44 Da) EE and $[OCH_3]^+$ (31 Da) EE ions. The minor fragmentation path produces $[M-NH_2]^+$ (59 Da) EE

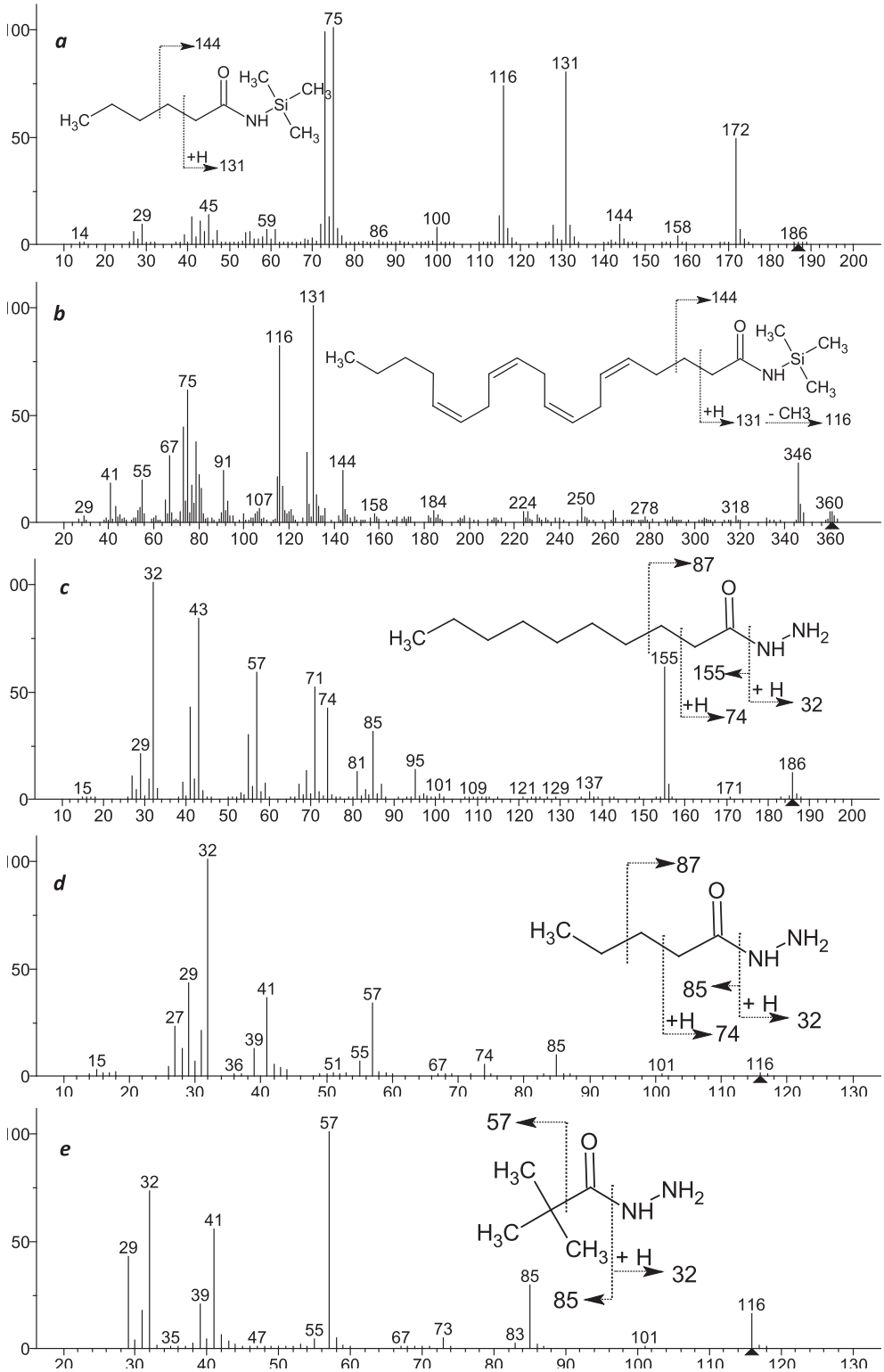

FIG. 18. Mass spectra [m/z (relative abundance, %)] of *N*-trimethylsilyl-*n*-hexanamide (a), *N*-trimethylsilyl-5,8,11,14 (all *Z*)-nonadecatetraenamide (b), and hydrazides of *n*-decanoic (c), *n*-pentanoic (d), and 2,2-dimethylpropanoic acids (e).

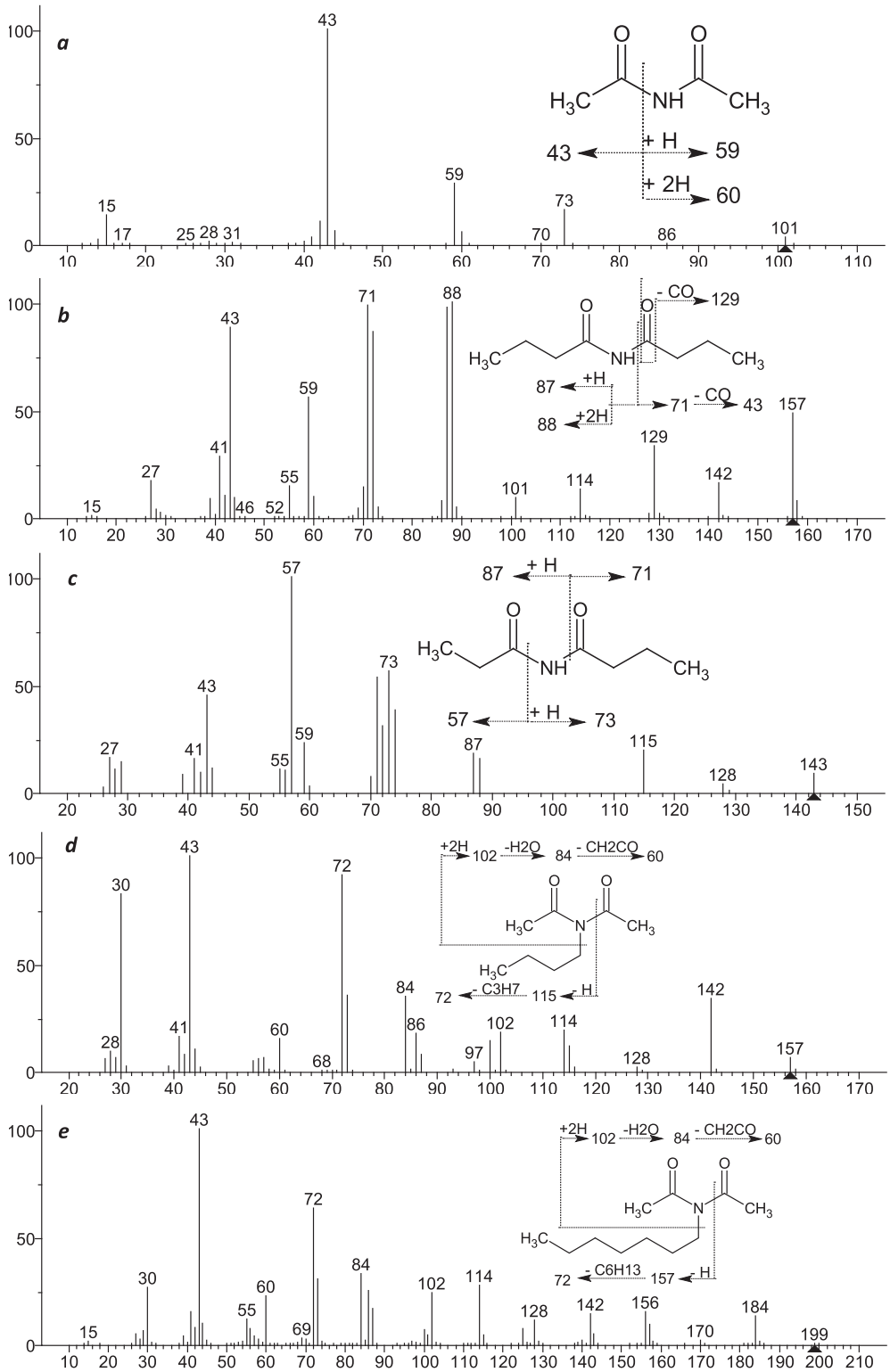

FIG. 19. Mass spectra [m/z (relative abundance, %)] of di(acetyl)amine (a), di(*n*-butyryl)amine (b), *n*-propionyl(butyryl)amine (c), *N*-(*n*-butyl)-*N*-acetyl acetamide (d), and *N*-*n*-heptyl-*N*-acetyl acetamide (e).

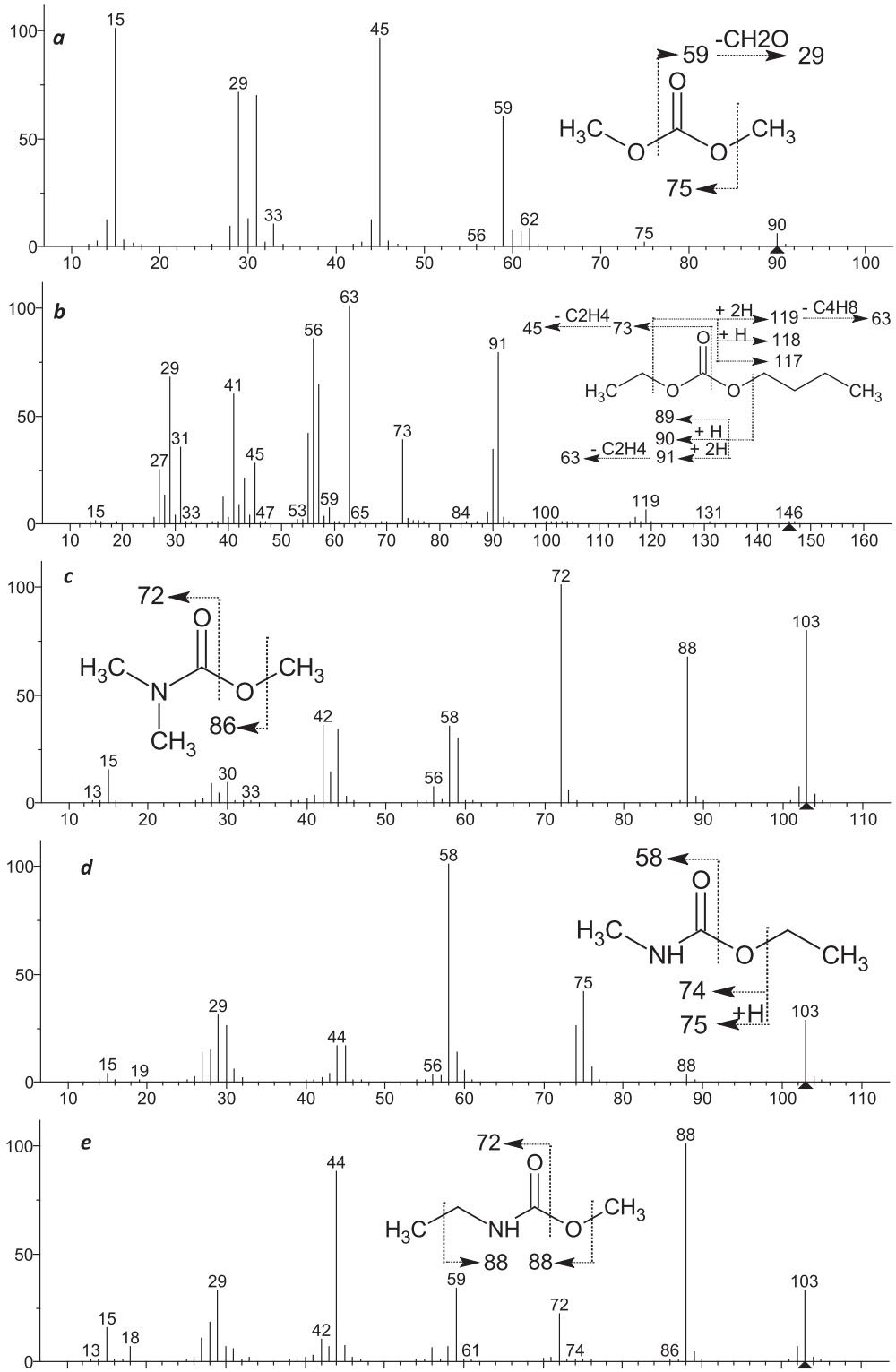

FIG. 20. Mass spectra [m/z (relative abundance, %)] of dimethyl (a) and ethyl-*n*-butyl esters of carbonic acid (b), methyl *N*,*N*-dimethyl- (c), ethyl *N*-methyl- (d), and methyl *N*-ethylcarbamates (e).

TABLE 4. Characteristic ions in the spectra of lower alkyl carbamates ($NH_2COOC_nH_{2n+1}$)

Ion	Alkyl carbamate [m/z (relative intensity, %)]				
	O–CH_3	O–C_2H_5	O-n-C_3H_7	O-i-C_3H_7	O-n-C_4H_9
$M^{+\cdot}$	75(25)	89(5)	103(0)	103(0)	117(0.2)
$[M-(R-2H)]^+$	⋯	62(84)	62(46)	62(44)	62(100)
$[M-OR]^+$	44(100)	44(100)	44(59)	44(17)	44(75)

ions. In addition to the C_{amidic}–O_{ether} bond cleavage, molecular ions of higher alkyl carbamates (alkyl > CH_3) undergo fragmentations similar to those for alkyl alkanoates. Thus, $M^{+\cdot}$ of ethyl, propyl, isopropyl, and butyl carbamates readily undergo O–C-alkyl bond cleavage accompanied with the migration of two hydrogen atoms to the amidic part. As a result, ions of the protonated carbamic acid (62 Da) EE ion are generated, and the corresponding peak is abundant in the spectra (Table 4).

Introduction of alkyl substituents to the amidic N atom instigates diversion of fragmentation patterns of $M^{+\cdot}$ of alkyl carbamates. Thus, $M^{+\cdot}$ of ethyl *N*-methylcarbamate eliminates mostly ethylene molecules and produces a $[CH_3NHCOOH]^{+\cdot}$ (75 Da) OE ion [Fig. 20(d)] instead of a C_2H_3 radical, which is the major dissociation route in the case of ethylcarbamate and generates abundant (84%) protonated carbamic acid $[NH_2COOH_2]^+$ (62 Da) EE ions (Table 4). This specific fragmentation reaction at the expense of the *O*-alkyl (alkyl > CH_3) group and β-cleavage at *N*-alkyl (alkyl > CH_3) in the molecule is successfully employed for the differentiation of isomers. In fact, while distinctive dissociation of $M^{+\cdot}$ of ethyl *N*-methylcarbamate generates $[CH_3NHCOO]^+$ (74 Da) EE, $[CH_3NHCOOH]^{+\cdot}$ (75 Da) OE, and $[CH_3NHCOOH_2]^+$ (76 Da) EE ions at the expense of the *O*-ethyl group [Fig. 20(d)], the molecular ion of *O*-methyl *N*-ethylcarbamate produces $[M-CH_3]^+$ (88 Da) EE ions at the expense of the *N*-ethyl group [Fig. 20(e)]; the latter shows maximum intensity in the spectrum. It is a good example of utilization of competing fragmentation processes for structure elucidation.

Introduction of an additional alkyl to the amidic nitrogen and an increase in the size of alkyl substituents does not change the dissociation pathways. However, the spectra become more complex, and more time is required for the identification of competing fragmentation patterns and structure elucidation. The competing fragmentation pathway is well demonstrated in Scheme 38 for the case of ethyl *N*-propyl-*N*-butyl carbamate.

6.5.3. Carbamides (urea)

Unsubstituted urea shows very stable $M^{+\cdot}$ and prominent peaks of $[M-NH_2]^+$ EE and $[NH_3]^{+\cdot}$ OE ions in its spectrum. Alkylcarbamides also produce distinct molecular ions. $M^{+\cdot}$ of the simplest representative of this class— tetramethylurea—undergoes a simple cleavage of the amidic C–N bond with the distribution of the charge on both parts of the molecule; as a result, $[N(CH_3)_2]^+$ (44 Da) EE and $[C(O)N(CH_3)]^+$ (72 Da) EE ions are generated [Fig. 21(a)]. In addition, this process can be accompanied by a hydrogen shift. The intensities of the above ions vary in the spectra of mono-, di-, and trimethyl substituted urea (Table 5). A comparative analysis of these types of cleavages with and without hydrogen migration and examination of ions arose from either part of a molecule is useful when defining a structure. Consideration of relative stabilities of the following ions is also effective: $(CH_3)_2N^+ > CH_3(H)N^+ > H_2N^+$ and $(CH_3)_2(CO)N^+ > CH_3(H)(CO)N^+ > H_2(CO)N^+$.

More dissociation patterns emerge in the case of alkylurea with alkyls longer than methyl. Thus, the spectra of ethyl urea [Figs. 21(b)–21(d)] contain a variety of iminium ions resulting from

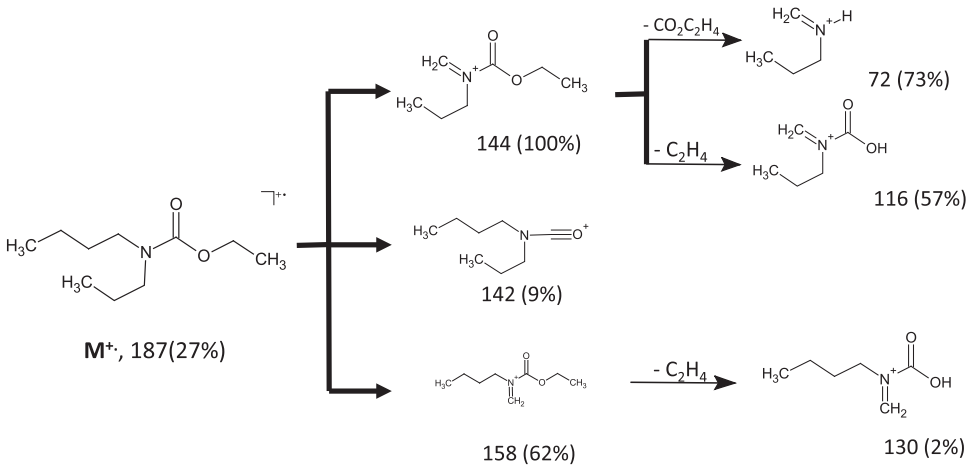

SCHEME 38. Major fragmentation pathways of $M^{+\cdot}$ of ethyl *N*-(*n*-propyl)-*N*-(*n*-butyl) carbamate.

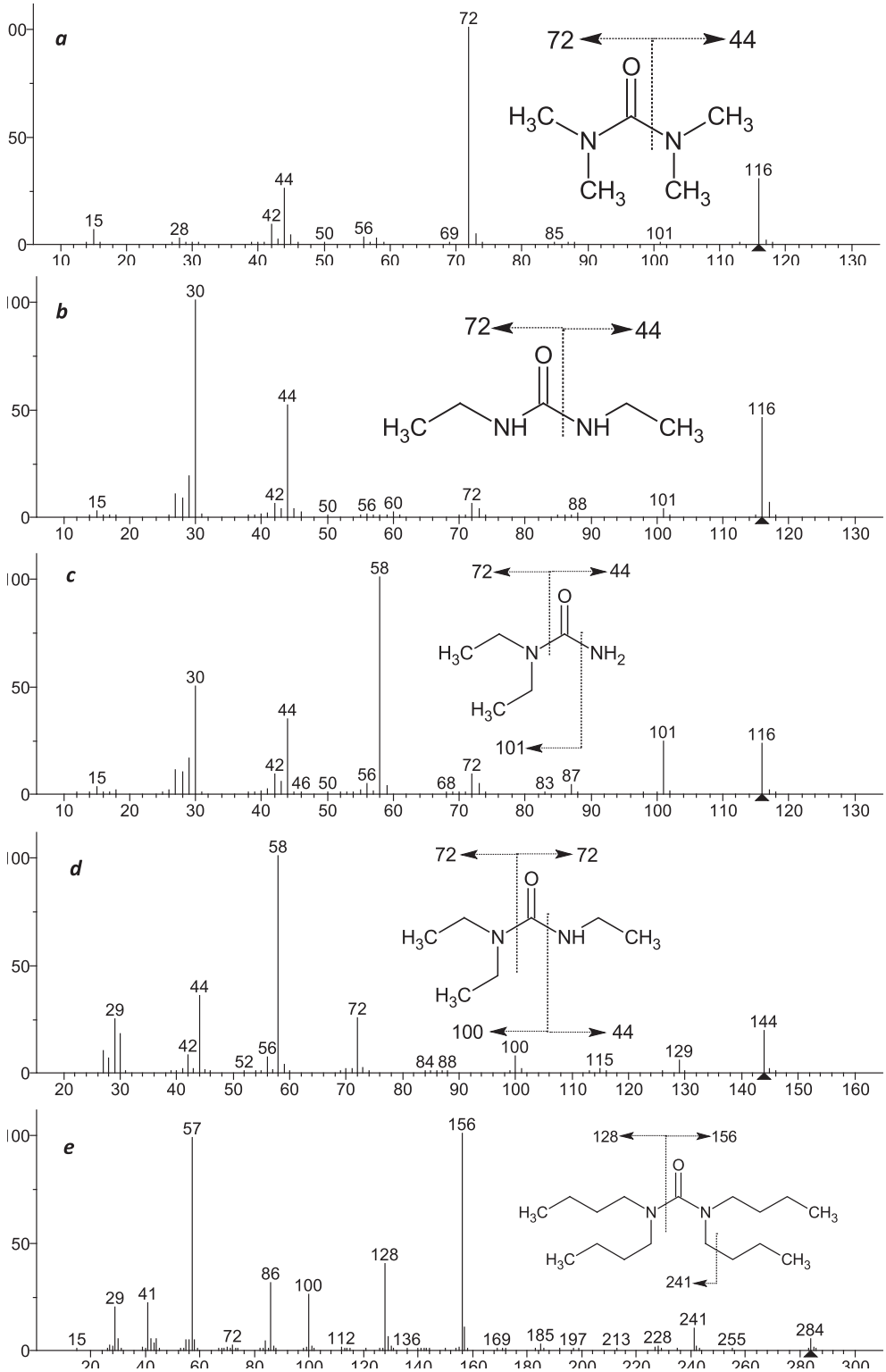

FIG. 21. Mass spectra [m/z (relative abundance, %)] of tetramethylurea (a) *N*,*N*′- (b) and *N*,*N*-diethylurea (c), *N*,*N*,*N*′-triethylurea (d), and tetra(*n*-butyl)urea (e).

TABLE 5. Relative intensities of ions in the spectra of ureas of the general formula $R^1R^2NC(O)N'R^3R^4$

Urea	m/z (rel. intensity, %) of ions			
	$[R^1R^2N]^+$	$[R^1R^2NH]^+$	$[R^1R^2NCO]^+$	$[R^1R^2NCOH]^{+\cdot}$
Unsubstituted	16(17)	17(100)	44(81)	45(2)
N-methyl	30(100)	31(55)	58(8)	59(0.3)
N,*N*′-dimethyl	30(100)	31(42)	58(44)	59(3)
N,*N*-dimethyl	44(100)	45(43)	72(6)	73(1)
N,*N*,*N*′-trimethyl	44(100)	45(18)	72(16)	73(1)
N,*N*,*N*′,*N*′-tetramethyl	44(26)	45(4)	72(100)	73(4)

β-cleavage of the *N*-alkyl chain. Scheme 39 demonstrates the origins of major iminium ions in the spectra of isomeric *N*,*N*- and *N*,*N*′-diethylcarbamides. The spectra of these isomers are quite different [Figs. 21(b) and 21(c)], and structure elucidation of isomers appears an easy task. The spectrum of triethylurea [Fig. 21(d)] contains all ions characteristic for *N*,*N*- and *N*,*N*′-substituted homologs.

A further increase in the *N*-alkyl carbon chain adds a competing process for generation of alkyl cations. Thus, the mass spectrum of tetrabutylurea [Fig. 21(e)] produces abundant alkyl and alkenyl EE ions: $[C_2H_5]^+$ (29 Da) EE, $[C_3H_5]^+$ (41 Da) EE, and $[C_4H_9]^+$ (57 Da) EE ions.

Note that the mass spectra of mono *N*-trimethylsilyl derivatives of urea and alkyl ureas will be discussed in another review devoted to polyfunctional compounds.

7. Compounds with a Sulfur Containing Functional Group

Sulfur is the next element to oxygen in the main VI group, and similar behavior of compounds containing both these elements is not surprising. However, (a) sulfur is less electronegative than oxygen [χ = 2.58 (S) vs 3.44(O)], (b) the ionization energy of sulfur is higher than that of oxygen (Table 8), and (c) sulfur assumes oxidation states ranging from −2 to +6 while oxygen is found mainly in −2 oxidation state (−1 in peroxides) in their organic compounds. The similarities and the differences in fragmentation patterns of alcohols and thiols, ethers and sulfides, as well as ketones and thiones will be considered when revealing diagnostically important dissociation pathways of aliphatic sulfur containing compounds.

7.1. Aliphatic thiols

Alkanethiols produce rather stable $M^{+\cdot}$ under EI. Unlike alkanols, the corresponding peaks are much more visible and can be identified easily. The considerable intensity of the $M^{+\cdot}$ peak and its characteristic isotope profile (owing to the increased content of S^{34}) are of particular value for the recognition of sulfur presence and the establishment of the elemental composition of an unknown [Figs. 22(a) and 22(b)].

Molecular ions of primary thiols solely eliminate mercapto (sulfanyl) radicals with the formation of $[M\text{-}HS]^+$ (126 Da) EE ions [Fig. 22(a)], secondary thiols evenly lose both the sulfanyl radical and hydrogen sulfide neutral, giving rise to $[M\text{-}HS]^+$ (126 Da) EE and $[M\text{-}H_2S]^{+\cdot}$ (127 Da) OE ions, and tertiary analogs mainly generate $[M\text{-}H_2S]^{+\cdot}$ (127 Da) OE ions [Fig. 22(b)]. Another rearrangement $[M\text{-}CH_3CH_2SH]^{+\cdot}$ (98 Da) OE ion is diagnostically important for primary alkanethiols. The corresponding peak shows a maximum intensity in the spectrum of *n*-hexanethi-1-ol and decreases in intensity in the case of *n*-heptanethi-1-ol (76%) and *n*-octanethi-1-ol (47%); the spectrum of *n*-nonanethi-1-ol peak demonstrates just 17% rel. intensity [Fig. 22(a)]. Noticeable peaks of $[C_nH_{2n}SH]^+$ EE

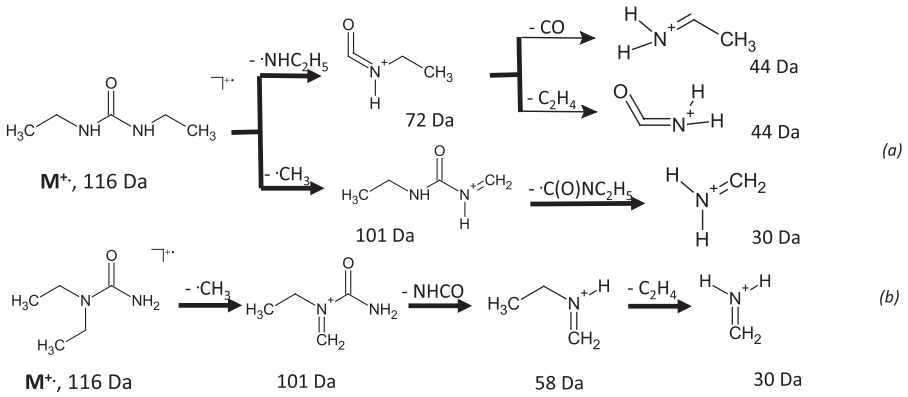

SCHEME 39. Generation of iminium ions in the case of isomeric *N*,*N*′- (a) and *N*,*N*-diethylurea (b).

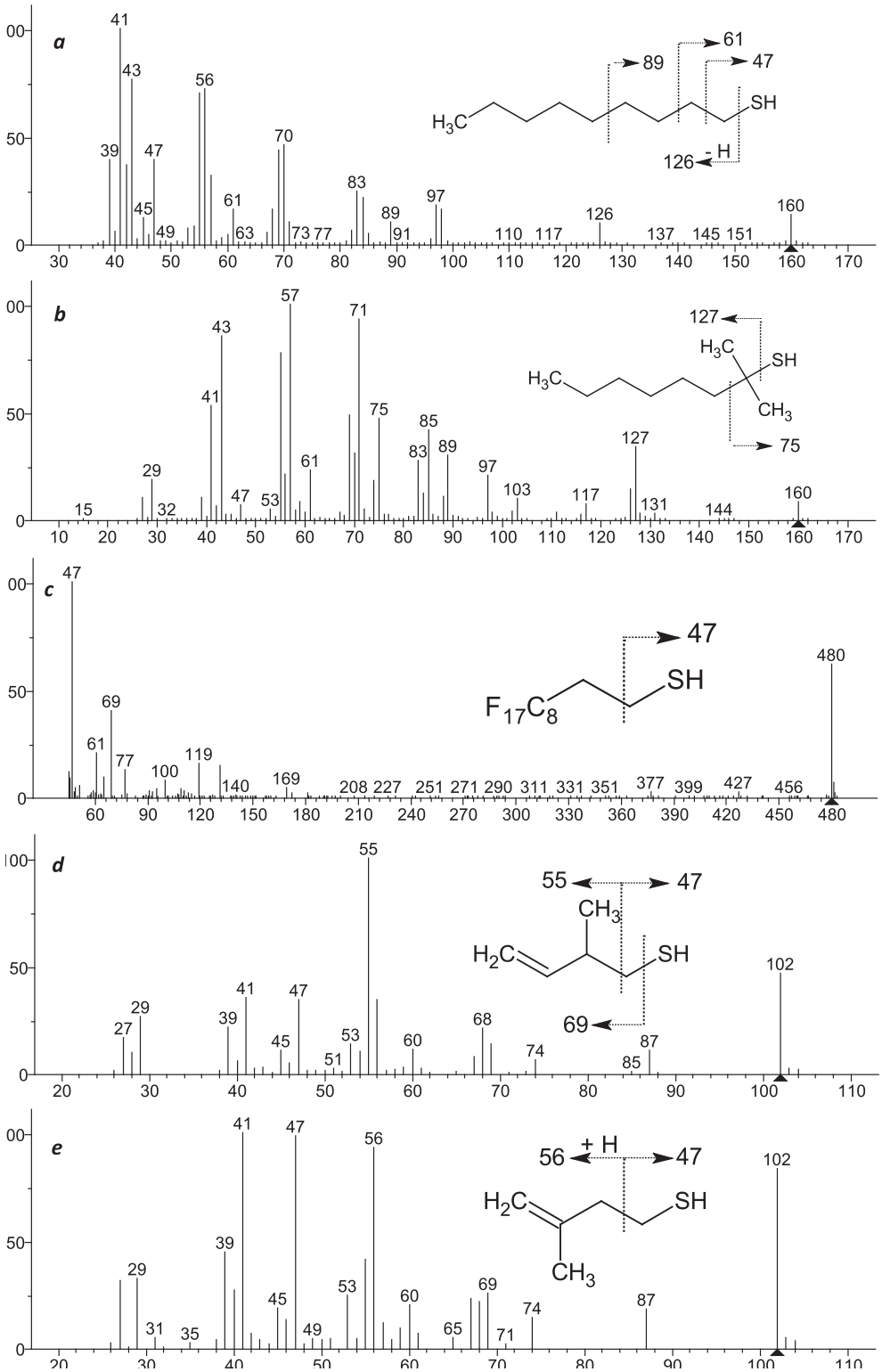

FIG. 22. Mass spectra [m/z (relative abundance, %)] of *n*-nonanethiol (a), *tert*-nonanethiol (b), 2-*n*-perfluorooctylethanethiol (c), 2-methyl-3-butenethiol (d), and 3-methyl -3-butenethiol (e).

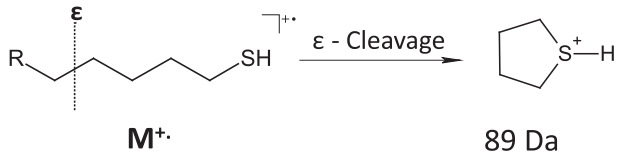

SCHEME 40. Generation of the protonated thiolane cation from molecular ions of alkanethiols.

ions at m/z 47, m/z 61, m/z 75, and m/z 89 Da are originated due to α-, β-, γ-, and δ-cleavages of C–C bonds and provide additional evidence of sulfur presence in molecules under study. Among them, protonated thiolane (89 Da) EE ions (Scheme 40) that are generated via ε-C–C bond cleavage are the strongest ones. The corresponding $[C_4H_9S]^+$ (89 Da) EE and $[C_6H_{13}S]^+$ (117 Da) EE ions are present in the spectra of *n*-nonanethi-1-ol [Fig. 22(a)] and *tert*-nonanethiol [Fig. 22(b)], respectively.

However, the $[C_nH_{2n}SH]^+$ EE ions may not be always successfully utilized for structure confirmation since they can be products of both primary and secondary fragmentation process(es). In the case of tertiary thiols, the loss of the largest alkyl groups from α-carbon is the most intense in the series. For instance, the intensity of the $[M\text{-}C_6H_{13}]^+$ (75 Da) ion peak is over 50 times more than that of $[M\text{-}CH_3]^+$ (145 Da) ions in the spectrum of *tert*-nonanethiol [Fig. 22(b)]. The homologous series of $[C_nH_{2n-1}]^+$ alkenyl cations with higher abundance of lower members is also characteristic for alkanethiols. Ethanethiols containing long-chain 2-perfluoroalkyl substituents reveal very stable $M^{+\cdot}$ and abundant $[CH_2{=}SH]^+$ (47 Da) EE ions corresponding to α-cleavage. The other peaks in the spectra are due to $[C_nF_{2n+1}]^+$ ions with higher abundance of lower "n" numbers [Fig. 22(c)].

Unlike alcohols, branching and unsaturation instigate selectivity in the dissociation of aliphatic thiols. Thus, β-cleavage relative to the double bond that is additionally stimulated by branching at $C_{(2)}$ produces the $[M\text{-}CH_2SH]^+$ (55 Da) EE ion that is the base peak in the spectrum of 2-methyl-3-butenethiol [Fig. 22(d)], and formation of a rearrangement $[M\text{-}CH_2S]^{+\cdot}$ (56 Da) OE ion is not favorable. However, hydrogen rearrangement becomes competitive in the absence of branching in the case of 3-methyl-3-butenethiol, and the corresponding ion peak is one of the strongest in the spectrum [Fig. 22(e)]. Branching at a place more remote from the sulfhydryl group has almost no effect on the fragmentation pathways.

7.1.1. Sulfides

Similar to thiols, di(alkyl)sulfides demonstrate significant molecular ion peaks. The absence of the peaks of $[M\text{-}HS]^+$ and $[M\text{-}H_2S]^{+\cdot}$ ions in their spectra makes it possible to clearly distinguish sulfides from thiols. Cleavage of β-C–C bonds in $M^{+\cdot}$ with preferable elimination of the largest alkyl group is characteristic for di(alkyl)sulfides; this behavior is common for ethers and sulfides. Accordingly, the differences in peak intensities are observed for the following ion pairs: (a) $[M\text{-}CH_3]^+$ (145 Da) and $[M\text{-}C_8H_{17}]^+$ (47 Da) in the case of methyl octyl sulfide [Fig. 23(a)] and (b) $[M\text{-}C_3H_7]^+$ (117 Da) and $[M\text{-}C_6H_{13}]^+$ (75 Da) in the case of isopropyl hexyl sulfide [Fig. 23(b)]. While the loss of methyl and isopropyl groups proceeds via a simple α-cleavage of the S–C bond, the elimination of octyl and hexyl radicals involves hydrogen rearrangements. For example, peaks of $[M\text{-}C_8H_{17}]^+$ EE ions are accompanied by peaks of $[M\text{-}C_8H_{16}]^{+\cdot}$ (48 Da) OE and $[M\text{-}C_8H_{15}]^+$ (49 Da) EE ions in the spectrum of methyl *n*-octyl sulfide, as shown in Fig. 23(a). The triplet of peaks at m/z 75, m/z 76, and m/z 77 correspond to ions due to the loss of the hexyl moiety in the case of isopropyl hexyl sulfide [Fig. 23(b)]. Hydrogen rearrangement in di(alkyl) sulfides is characteristic when hydrogens at γ-carbons become available, starting from *n*-propyl. This diagnostically important fragmentation pathway is well illustrated in the case of *n*-propyl *n*-butyl sulfide by two sets of triplets at m/z 75–77 (C_4 loss) and m/z 89–91 (C_3 loss) [Fig. 23(c)]. Here, the base peak represents the $[CH_2{=}S{-}CH_3]^+$ (61 Da) EE ion that is due to a secondary fragmentation: alkene neutral elimination from the ions produced via β-cleavage of C–C-bond in $M^{+\cdot}$.

As demonstrated above, C–C bond scissions along a lengthy alkyl chain are not significant, and the corresponding peaks in the spectra have monotonous abundance. However, the introduction of substituents at carbons neighboring to sulfur initiates dissociations at the branching, and the generated ions possess diagnostic power. For illustration, compare the spectra of di(sec-butyl) and di(isobutyl) sulfides [Figs. 23(d) and 23(e)]. The former reveals outstanding peaks for the EE ion pair $[M\text{-}CH_3]^+$ and $[M\text{-}C_2H_5]^+$, whereas the latter exhibits an abundant $[M\text{-}C_3H_7]^+$ EE ion peak.

Mass spectra of unsaturated sulfides demonstrate stable $M^{+\cdot}$. Their dissociation pathways strongly depend on the nature of unsaturation, the number of unsaturated substituents, and the location of unsaturation relative to the sulfide function (Fig. 24). Sulfides containing a $C_\alpha C_\beta$-double bond, such as vinyl alkyl sulfides, undergo scission of the C–S bond accompanied by a hydrogen shift and generation of $[HSCH{=}CH_2]^{+\cdot}$ (60 Da) OE ions [Fig. 24(a)]. A similar fragmentation reaction takes place in the case of sulfides containing a C_β-C_γ-double bond, such as allyl alkyl sulfides, and a rather abundant homologous $[HSCH_2CH{=}CH_2]^{+\cdot}$ (74 Da) OE ion is produced [Fig. 24(b)]. This fragmentation pathway is diminished with the migration of the double bond, and starting with 3-butenyl alkyl sulfides, the peaks of analogous ions ($[HS(CH_2)_n\ CH{=}CH_2]^{+\cdot}$, $n > 1$) become negligible. Note that in the case of allyl alkyl sulfides, the most prominent peaks correspond to allyl (41 Da) and $[M\text{-}C_3H_5]^+$ (117 Da) EE ions [Fig. 24(b)].

Various competing decomposition reactions take over in sulfides with unsaturation in both substituents. For example, dissociation of an ionized symmetrical di(allyl) sulfide [Fig. 24(c)] proceeds via a cleavage of the S–C bond with the formation of significant $[M\text{-}C_3H_5]^+$ (73 Da) EE, $[M\text{-}C_3H_6]^{+\cdot}$ (72 Da) OE and $[M\text{-}C_3H_7]^+$ (71 Da) EE ions. The other peaks in the molecular region corresponds to rearrangements ions, such as $[M\text{-}CH_3]^+$, $[M\text{-}HS]^+$, and $[M\text{-}H_2S]^{+\cdot}$; the base peak in the spectrum corresponds to $[CHS]^+$ (45 Da) EE ions.

The behavior of vinyl 3-butenyl sulfide [Fig. 24(d)] under EI is close to fragmentation of viny alkyl sulfides owing to the remote location of unsaturation relative to the sulfide function. As a result, the base peak in the spectrum corresponds to $[CH_2{=}SCHCH_2]^+$ (73 Da) EE ions. Note that a $[M\text{-}H_2S]^{+\cdot}$ (80 Da) rearrangement OE ion is observed in the spectrum.

Sulfides containing double and triple bonds behave similarly under EI. Thus, the mass spectrum of vinyl 1-propynyl sulfide exhibits the most prominent peaks of $M^{+\cdot}$ and $[M\text{-}H]^+$ ions.

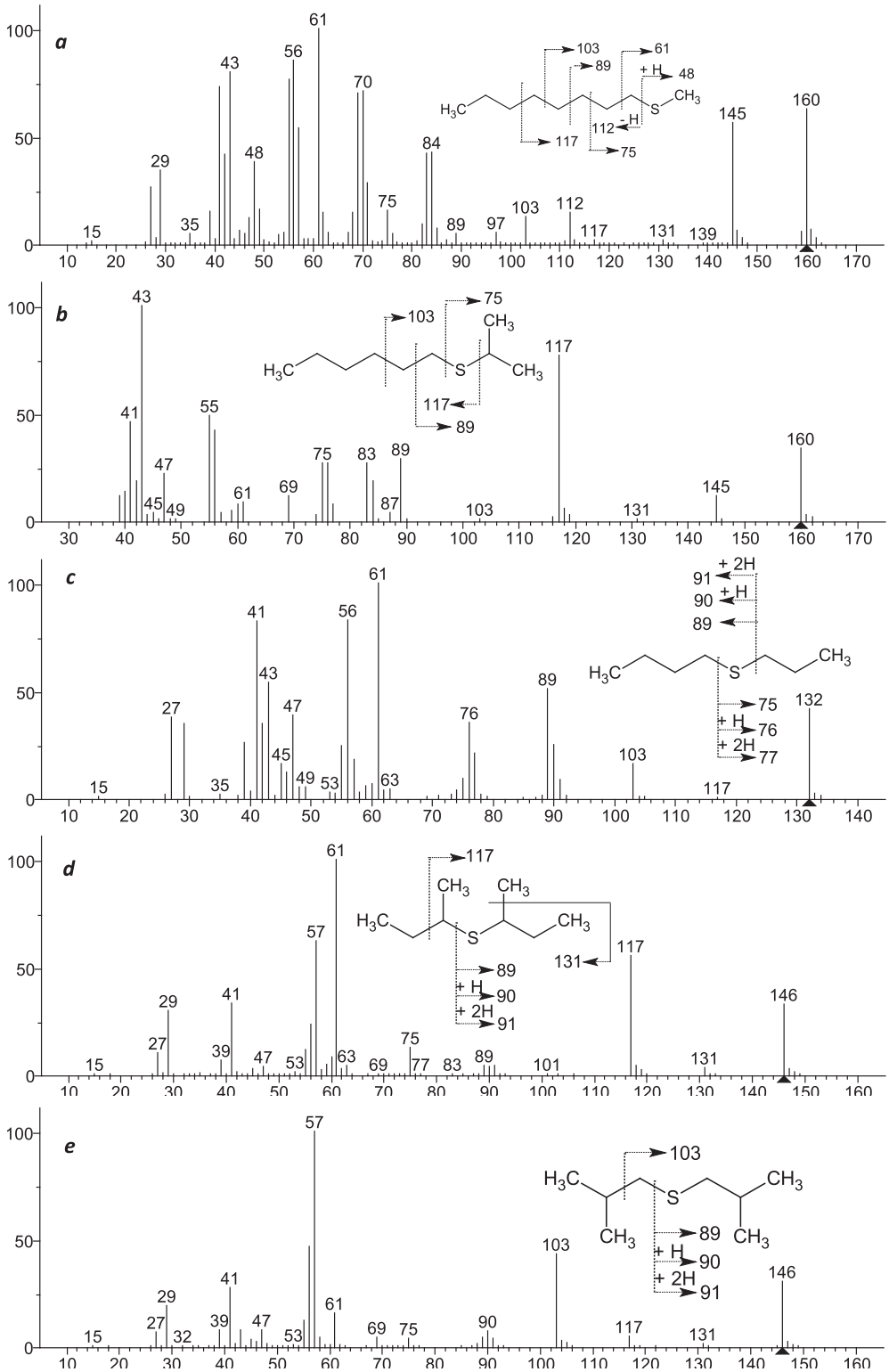

FIG. 23. Mass spectra [m/z (relative abundance, %)] of methyl *n*-octyl sulfide (a), isopropyl *n*-hexyl sulfide (b), *n*-propyl *n*-butyl sulfide (c), di(sec-butyl) sulfide (d), and di(isobutyl) sulfide (e).

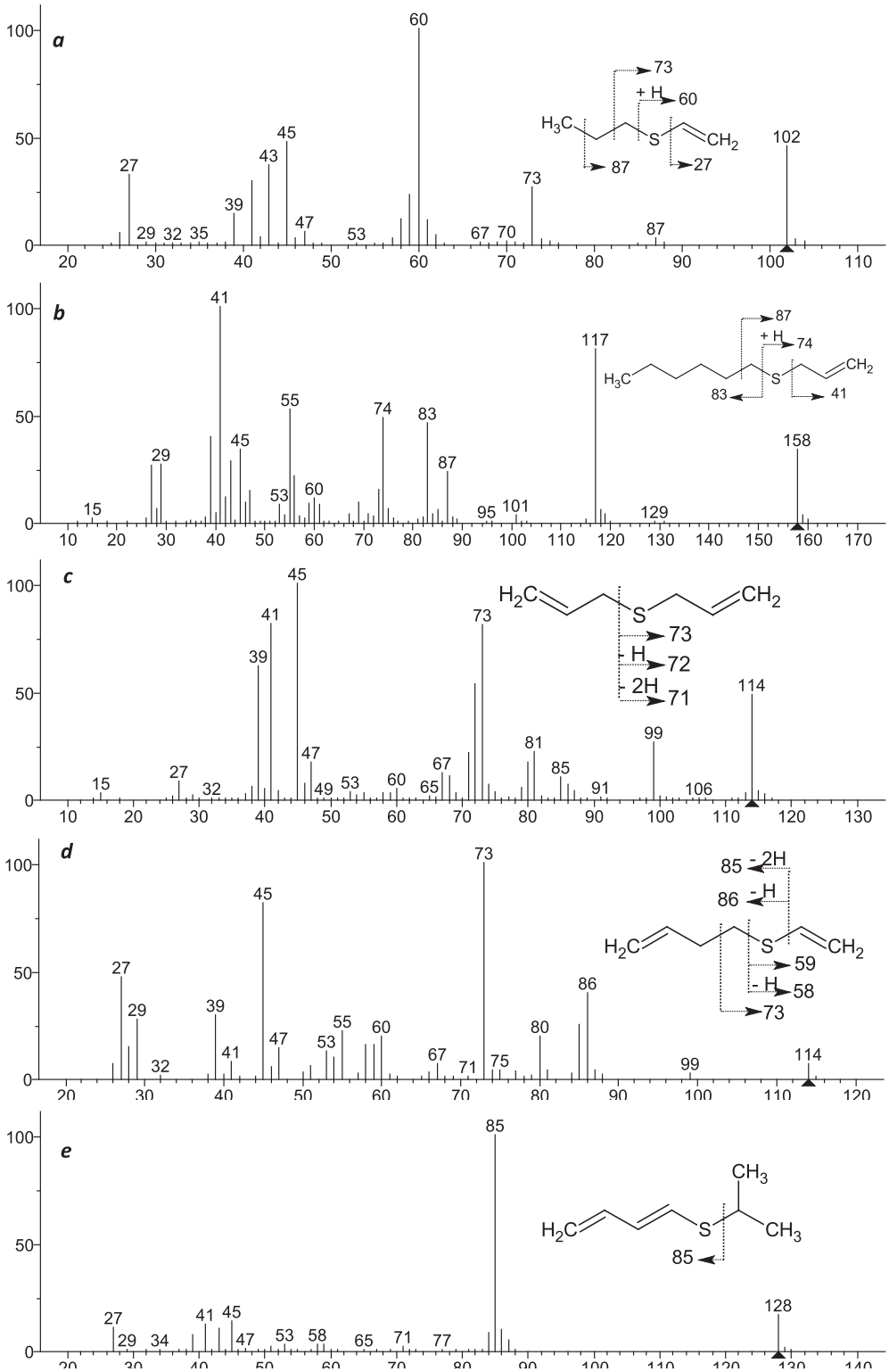

FIG. 24. Mass spectra [m/z (relative abundance, %)] of vinyl *n*-propyl sulfide (a), allyl *n*-hexyl sulfide (b), di(allyl) sulfide (c), vinyl 3-butenyl sulfide (d), and isopropyl 1,3-butadienyl sulfide (e).

Other abundant ions correspond to $[M\text{-}C_2H_3]^+$, $[M\text{-}H\text{-}C_2H_4]^+$, $[M\text{-}H\text{-}C_3H_3]^+$, $[C_2H_3]^+$, and $[C_3H_3]^+$ ions.

In the case of isopropyl butadienyl sulfide, the dissociation proceeds at the expense of the saturated part of the molecule, and the base peak corresponds to the loss of an isopropyl radical: formation of the $[M\text{-}C_3H_7]^+$ (85 Da) EE ion [Fig. 24(e)].

7.1.2. Di- and polysulfides

Unlike hydroperoxides, alkyl hydro disulfides produce stable molecular ions under EI. The base peak of $M^{+\cdot}$ in the spectrum of propyl disulfane well demonstrates this phenomenon [Fig. 25(a)]. The mass spectra of di(alkyl) di-, tri-, and tetra-sulfides also show stable molecular ions [Figs. 25(b)–25(e)]. As for di(alkyl) sulfides, fragmentation at the expense of the dissociation of S–C bonds occurs in di(alkyl) polysulfides. While the charge can be evenly localized on the alkyl part and the sulfur-containing moieties in the case of di(*n*-hexyl) disulfide [Fig. 25(b)], hydrocarbon cations are formed preferentially when sulfur is bonded to the tertiary carbon. The fission of S–S bonds may proceed via a simple cleavage, or it can be accompanied by hydrogen rearrangements to produce $[C_3H_7S]^+$ (75 Da) EE, $[C_3H_8S_2]^{+\cdot}$ (108 Da) OE, $[C_3H_7S_3]^+$ (139 Da) EE, and $[C_3H_8S_3]^{+\cdot}$ (140 Da) OE ions in the case of di(*n*-propyl) tetra-sulfide. Skeletal rearrangements leading to the loss of $S^{\cdot}$ or $HS_2^{\cdot}$ produce $[M\text{-}S]^+$ (150 Da) EE and $[M\text{-}S_2H]^+$ (117 Da) EE ions in the case of trisulfide [Fig. 25(d)]. Analogous rearrangement ions are present in the spectrum of tetra-sulfide depicted in Fig. 25(e): $[M\text{-}S]^{+\cdot}$ (182 Da), $[M\text{-}S_2]^{+\cdot}$ (150 Da), $[M\text{-}S_2H]^+$ (149 Da), and $[M\text{-}S_3]^{+\cdot}$ (118 Da). Note that the intensity of $[S_2]^{+\cdot}$ OE ions at 64 Da grows with the increase in the number of sulfur atoms in the chain. Branching as well as methylene moieties between sulfur in the skeleton may diminish these dissociation pathways. Thus, the mass spectrum of 3,6-dimethyl-2,4,5,7-tetrathiaoctane is dominated by the $[C_3H_7S]^+$ (75 Da) EE ion, and intensities of the rest of the ion peaks do not exceed 14% rel.

The major peaks observed in the spectra of di(alkenyl) polysulfides are the result of the same types of cleavages observed for their saturated analogs. The feasible dissociations among other competing fragmentation directions can be illustrated on the example of di(allyl) disulfide [Fig. 26(a)]. The spectrum reveals abundant molecular ions and $[M\text{-}C_3H_{6-x}]^{+\cdot}$ (103–105 Da) ions along with $[C_3H_5]^+$ (41 Da) and $[C_3H_3]^+$ (39 Da) EE ions characterizing the propenyl moieties. The other major fragmentation processes are due to skeletal rearrangements giving rise to high abundant $[M\text{-}SH]^+$ (113 Da), $[M\text{-}S_2H]^+$ (81 Da), $[SC_2H_5]^+$ (61 Da), and $[CHS]^+$ (45 Da) ions.

The introduction of additional sulfur atoms into the chain, as in the case of di(propenyl) tetra-sulfide, increases the chance for skeletal rearrangements. As a result, the peaks for $[M\text{-}S_2]^{+\cdot}$ (146 Da) and $[M\text{-}S_3H]^+$ (113 Da) ions are pronounced in its spectrum [Fig. 26(b)].

7.1.3. Acyl and silyl derivatives of thiols

The high stability of thiols under EI and specific fragmentation of their molecular ions provide sufficient information concerning selected structural elements of a molecule. Sadly, most of the common derivatives of thiols do not provide additional structural information. For example, the mass spectrum of the *S*-acetyl derivative depicted in Fig. 26(c) exhibits $M^{+\cdot}$ and $[M\text{-}CH_3CO]^+$ ion peaks that characterize the thiol-acetate moiety, whereas the origins of other ions in the spectrum are similar to those of the original thiol. The spectrum of the *S*-trifluoroacetyl derivative [Fig. 26(d)] mainly contains peaks of the ions resulting from the dissociation of the trifluoroacetyl moiety of the molecule, such as $[CF_3]^+$, $[M\text{-}CF_3]^+$, $[COCF_3]^+$, and $[M\text{-}COCF_3]^+$.

Main fragmentation pathways of *S*-silyl derivatives of aliphatic thiols are due to the presence of the silyl group. In fact, the outstanding peaks in the spectrum of *S*-trimethylsilyl butanethiol [Fig. 26(e)] correspond to $[M\text{-}CH_3]^+$ (147 Da), $[M\text{-}CH_3\text{-}C_4H_8]^+$(91 Da), $[M\text{-}CH_3\text{-}C_4H_8\text{-}CH_4]^+$ (75 Da), and $[Si(CH_3)_3]^+$ (73 Da) ions. While acyl and silyl derivatives do not provide much structural information, they are widely used to improve the GC properties for the identification of thiols in complex mixtures.

7.2. Aliphatic sulfoxides and sulfones

S-Oxides and *S*,*S*-dioxides are oxidized derivatives of sulfides. While the hexavalent sulfur in sulfones is double bonded to oxygens, the bond between S and O in sulfoxides is considered as an intermediate between a dipolar and a polarized double bond, and the positive charge is being shifted to sulfur and negative to oxygen. However, for simplicity, the double bond structures are utilized to depict sulfoxides.

7.2.1. Sulfoxides

Under EI, propanethial *S*-oxide [Fig. 27(a)] produces rather stable $M^{+\cdot}$ that dissociates primarily via the elimination of hydrogen, hydroxyl, and methyl radicals. The base peak of the $[C_3H_5]^+$ (41 Da) EE ion in the spectrum is a product of a double bond rearrangement followed by C–S bond scission.

Rather stable molecular ions of di(alkyl) sulfoxides lose oxygen from sulfur in the form of oxygen or hydroxyl radicals yielding the $[M\text{-}O]^{+\cdot}$ (132 Da) OE and $[M\text{-}OH]^+$ (131 Da) EE ions [Figs. 27(b)–27(c)]. Alkyl substituents at sulfur are eliminated from $M^{+\cdot}$ as corresponding alkenes via migration of hydrogen to oxygen. Expectedly, the loss of a heavier substituent is favorable. For example, the intensity of the $[M\text{-}C_4H_8]^{+\cdot}$ (92 Da) OE ion is 8 times higher than that of the $[M\text{-}C_3H_6]^{+\cdot}$ (106 Da) OE ion in the spectrum of propyl butyl sulfoxide [Fig. 27(b)]. However, the introduction of branching at α-carbon facilitates this process, and S–C cleavage at the branching site becomes more favorable. In fact, in the case of isomeric isopropyl butyl sulfoxide, the peak of the $[M\text{-}C_3H_6]^{+\cdot}$ (106 Da) OE ion is 9 times as high as the peak of the $[M\text{-}C_4H_8]^{+\cdot}$ (92 Da) OE ion. The generated $[M\text{-}C_nH_{2n}]^+$ ions further undergo β-C–C bond cleavage at the expense of the second alkyl substituent to produce $[HOS{=}CH_2]^+$ (63 Da) EE ions (Scheme 41). These ions are characteristic for di(alkyl) sulfoxides; they are always present in their spectra and can be utilized for structure elucidation of unknowns.

In addition, the $[M\text{-}C_nH_{2n}]^+$ OE ions readily lose hydroxyl radicals when they contain long alkyl groups starting from butyl (Scheme 41). For example, the $[M\text{-}C_3H_6]^{+\cdot}$ (106 Da) OE ion generates rather abundant $[M\text{-}C_3H_6\text{-}OH]^+$ (89 Da) EE ions in the case of *n*- and isopropyl butyl sulfoxides [Figs. 27(b) and 27(c)]. At the same time, the peak of the $[M\text{-}C_3H_6\text{-}OH]^+$ (75 Da) EE ions is negligible in the spectrum of di-*n*-propyl sulfoxide [Fig. 27(d)].

The mass spectrum of methyl vinyl sulfoxide is more complicated. The outstanding peaks in its spectrum correspond to $M^{+\cdot}$ (90 Da, 66%), $[CH_3SOH]^{+\cdot}$ (64 Da, 55%) $[C_2H_5S]^+$ (61 Da, 100%),

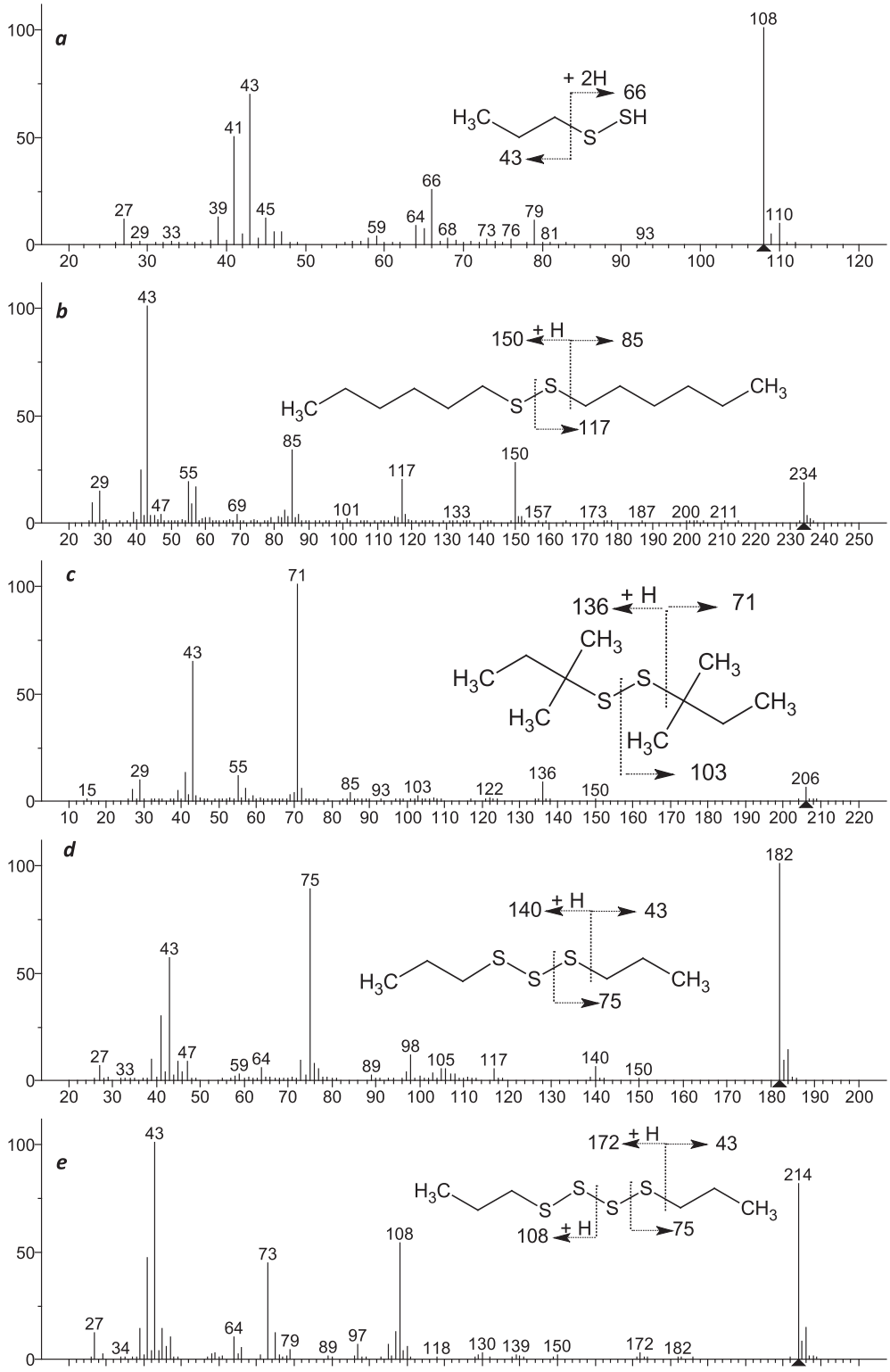

FIG. 25. Mass spectra [m/z (relative abundance, %)] of *n*-propyl hydrodisulfide (a), di(*n*-hexyl) disulfide (b), di(1,1-dimethylpropyl) disulfide (c), di(*n*-propyl) trisulfide (d), and di(*n*-propyl) tetrasulfide (d).

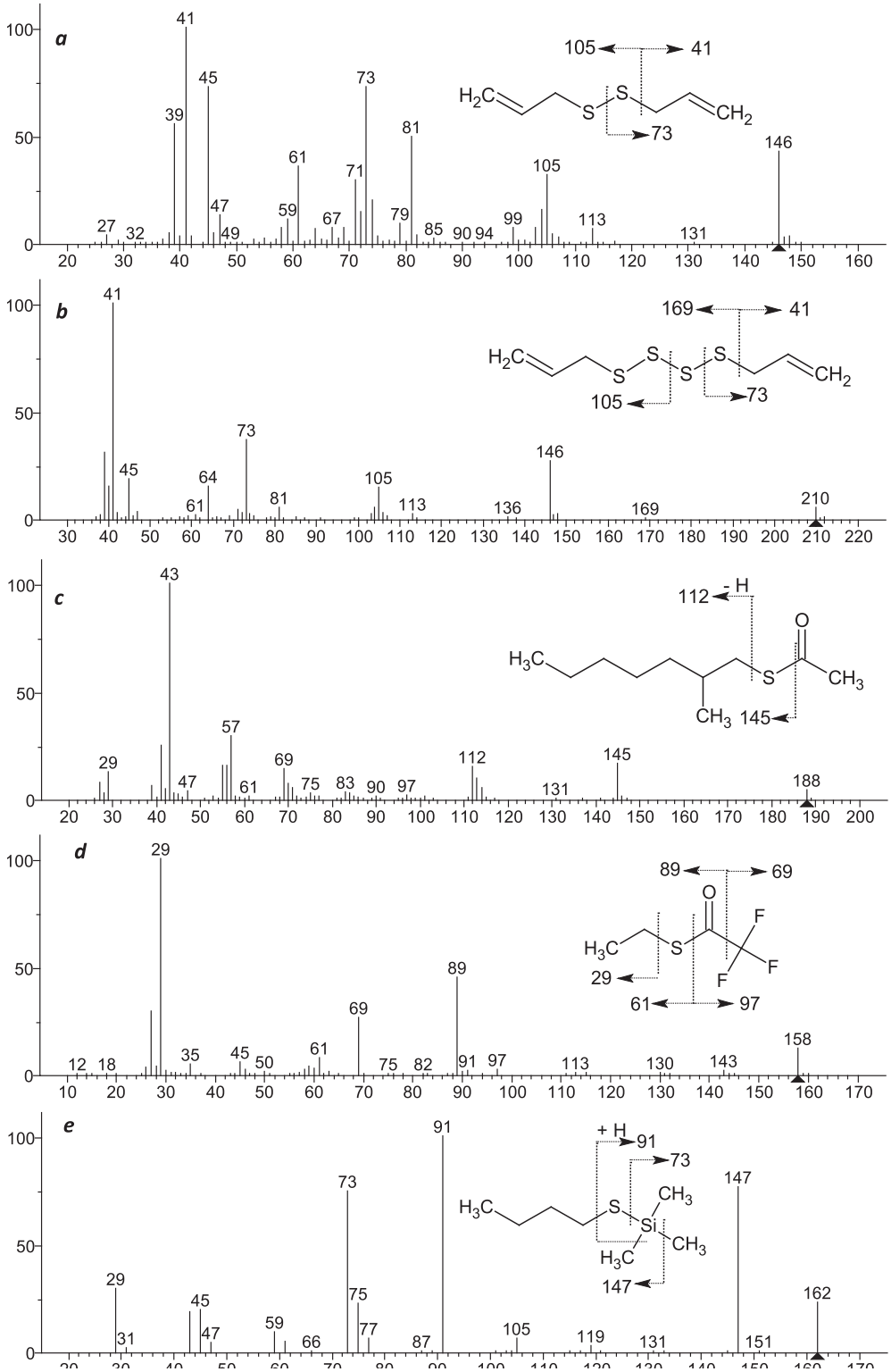

FIG. 26. Mass spectra [m/z (relative abundance, %)] of diallyl disulfide (a), diallyl tetrasulfide (b), *S*-acetyl 2-methylheptanethiol (c), *S*-trifluoroacetyl ethanethiol (d), and *n*-butyl *S*-trimethylsilyl *n*-butanethiol (e).

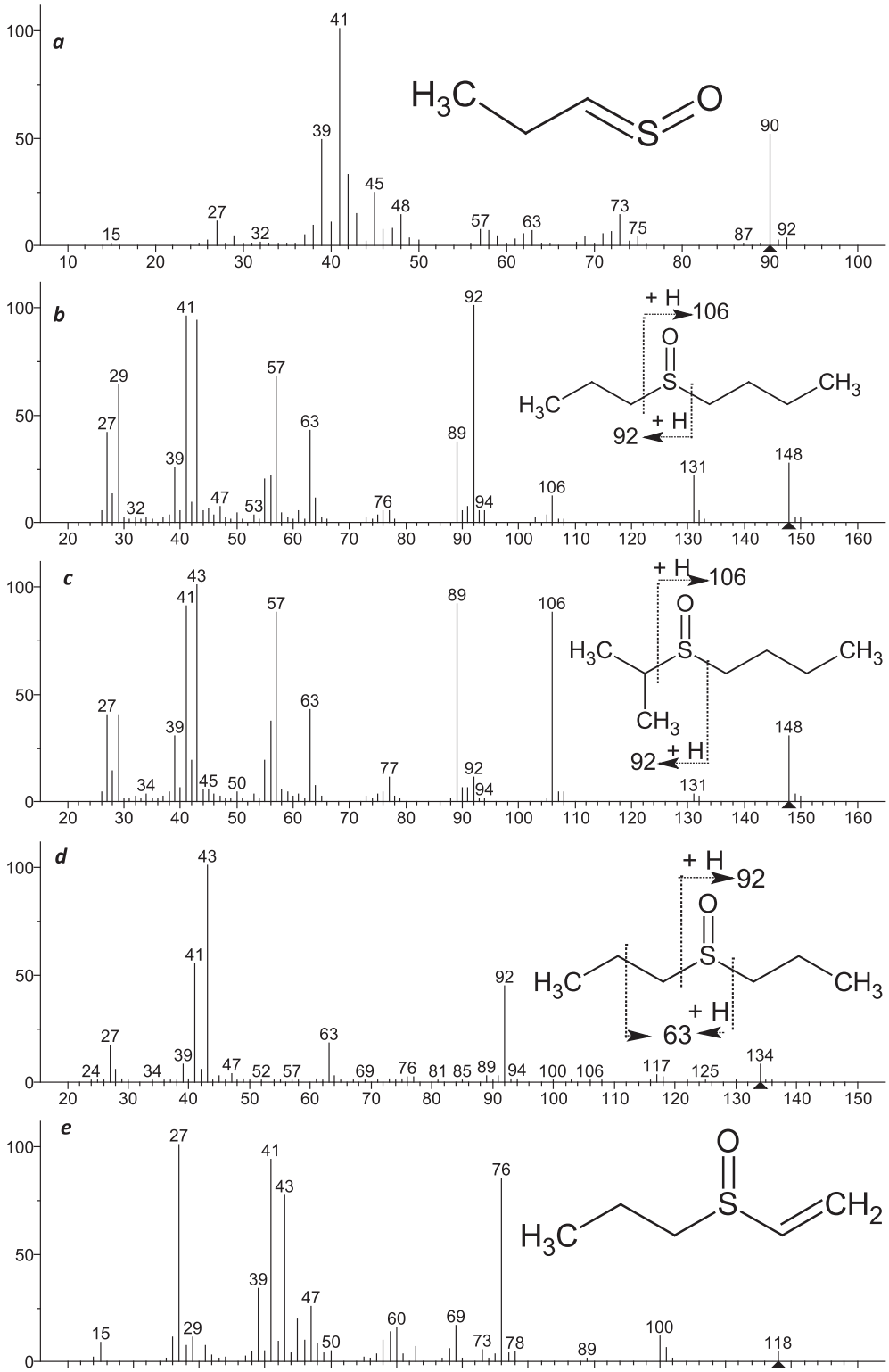

FIG. 27. Mass spectra [m/z (relative abundance, %)] of *n*-propanethial *S*-oxide (a), *n*-butyl *n*-propyl sulfoxide (b), *n*-butyl isopropyl sulfoxide (c), di(*n*-propyl) sulfoxide (d), and *n*-propyl vinyl sulfoxide (e).

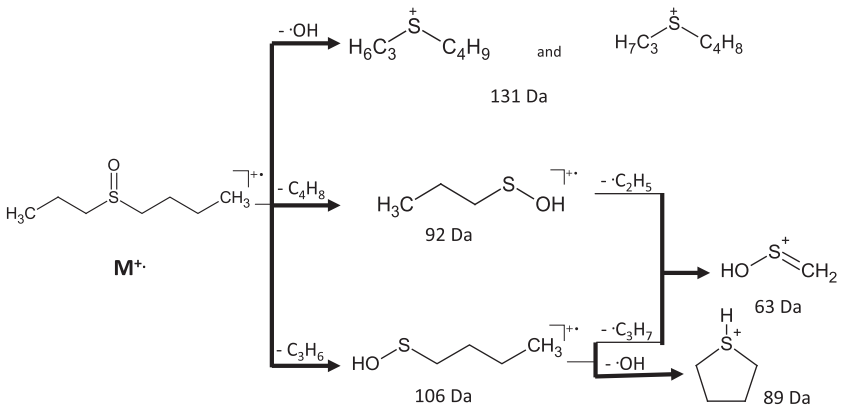

SCHEME 41. Major fragmentation routes of ionized *n*-propyl *n*-butyl sulfoxide.

$[CH_3S]^+$ (47 Da, 67%), and $[C_2H_3]^+$ (27 Da, 84%) ions. However, the growth of an alkyl chain in the saturated substituent leads to a fragmentation that is characteristic for di(alkyl) sulfoxides. For example, one of the highest intensity peaks in the high mass region of the spectrum of *n*-propyl vinyl sulfoxide corresponds to the $[M\text{-}C_3H_6]^{+\cdot}$ (76 Da) OE ion [Fig. 27(e)]. Note that noticeable peaks corresponding to the $[M\text{-}H_2O]^+$ ions are observed in the spectra of alkenyl alkyl sulfoxides.

7.2.2 Sulfones

Intensities of molecular ion peaks in the spectra of di(alkyl) sulfones are low. The decomposition of the simplest di(alkyl) sulfones does not involve much of hydrogen rearrangements. Thus, the spectrum of methyl ethyl sulfone contains noticeable peaks of $M^{+\cdot}$ and ions due to the loss of methyl radicals and ethylene neutrals. Sequential elimination of these two species leads to the formation of the $[M\text{-}CH_3\text{-}C_2H_4]^+$ (65 Da) EE ion [Fig. 28(a)]. Ions due to migration of two hydrogens are not observed in the spectra of lower di(alkyl) sulfones.

The dissociation of the *S*-propyl group in the case of ethyl *n*-propyl sulfone proceeds via rearrangement of one and two hydrogen atoms, giving rise to $[M\text{-}C_3H_6]^{+\cdot}$ (94 Da) OE ions and $[M\text{-}C_3H_5]^+$ (95 Da) EE ions [Fig. 28(b)]. Formation of ions due to migration of two hydrogen atoms becomes dominant with the increase in the size of alkyl chains in a molecule; at the same time, the $[M\text{-}C_nH_{2n}]^{+\cdot}$ ions become negligible. Thus, $[M\text{-}C_5H_9]^+$ ions are the most abundant among the ions originating due to the loss of other hydrocarbon species from $M^{+\cdot}$ of di(pentyl) sulfone [Fig. 28(c)]. A loss of a heavier alkyl substituent as a radical from $M^{+\cdot}$ is more favorable for asymmetric sulfones. Sulfones containing *n*- and isoalkyl substituents mainly eliminate the branched alkyl radical. The loss of small alkyl radicals (C_nH_{2n+1}) from $M^{+\cdot}$ is characteristic for di(alkyl) sulfones as well.

Molecular ion peaks are negligible or absent in the spectra of alkenyl sulfones. Their molecular ions mainly decompose via (a) a simple S–C bond cleavage and elimination of alkenyl radical and (b) a skeletal rearrangement of $M^{+\cdot}$ of di(alkenyl) sulfone to alkenyl alkenylsulfinate followed by a simple S–O bond cleavage and the loss of oxoalkenyl radical (Scheme 42). In fact, the mass spectra of di(vinyl) and di(allyl) sulfones show prominent peaks of $[M\text{-}C_2H_3]^+$ (91 Da) EE [Fig. 28(d)] and $[M\text{-}C_3H_5]^+$ (105 Da) EE ions [Fig. 28(e)] along with the peaks of $[M\text{-}OC_2H_3]^+$ (75 Da) EE [Fig. 28(d)] and $[M\text{-}OC_3H_5]^+$ (89 Da) EE ions [Fig. 28(e)].

7.3. Thiocarboxylic acid derivatives

Carbothionic and carbothiolic acids undergo skeletal rearrangements under EI and molecular ions of both thione (*O*-acid) and thiol (*S*-acid) forms are produced. For example, the spectrum of neopentathionic acid [Fig. 29(a)] shows noticeable $[M\text{-}OH]^+$ (101 Da) EE and $[M\text{-}SH]^+$ (85 Da) EE ion peaks, indicating that the spectrum is due to the dissociation of molecular ions of both tautomeric forms of the parent compound. Usually, ionized thionecarboxylic acids are easily isomerized into thiolcarboxylic acids than conversely.

Molecular ions of alkyl thiocarboxylates appear as the most pronounced peaks in the spectra. However, their intensities decrease with the increase in the size of alkyl groups. As in the case of free thioacids, thiol–thione tautomerization under EI is also common for the corresponding alkyl esters. A comparison of EI mass spectra of isomeric ethyl thioacetates clearly shows that *S*-ethyl thioacetate [Fig. 29(c)] produces only an acetyl (43 Da) EE ion, whereas the same ion along with a thioacetyl (59 Da) EE ion is formed in the case of *O*-ethyl thioacetate [Fig. 29(b)]. This fact clearly proves that $M^{+\cdot}$ of the latter compound can exist in two tautomeric forms (Scheme 43).

7.3.1. S-Alkyl alkanethioates

Unlike alkyl carboxylates that generate characteristic $(C_nH_{2n+1}COOH_2)^+$ EE ions due to the shift of two hydrogens to the carboxyl moiety, the thiol analogs do not undergo this type of rearrangement. Instead, their $M^{+\cdot}$ eliminates alkyl from the thioester moiety as an alkene neutral and/or alkyl radical. In addition, McLafferty rearrangement, which generates diagnostically important ions in the case of alkyl alkanoates, does not take place during EI-promoted dissociation of *S*-alkyl thiocarboxylates. The most abundant ions in their spectra correspond to $[C_nH_{2n+1}CO]^+$ and $(C_nH_{2n+1})^+$ cations. The mass values of these ions provide information on the nature of the acid residue (Scheme 43).

Starting from *n*-butyl ester, $RCOSC_nH_{2n+1}$ ($n > 3$) esters exhibit a characteristic skeletal rearrangement that is associated with the loss of thiirane neutral (or its substituted analog) (Scheme 44).

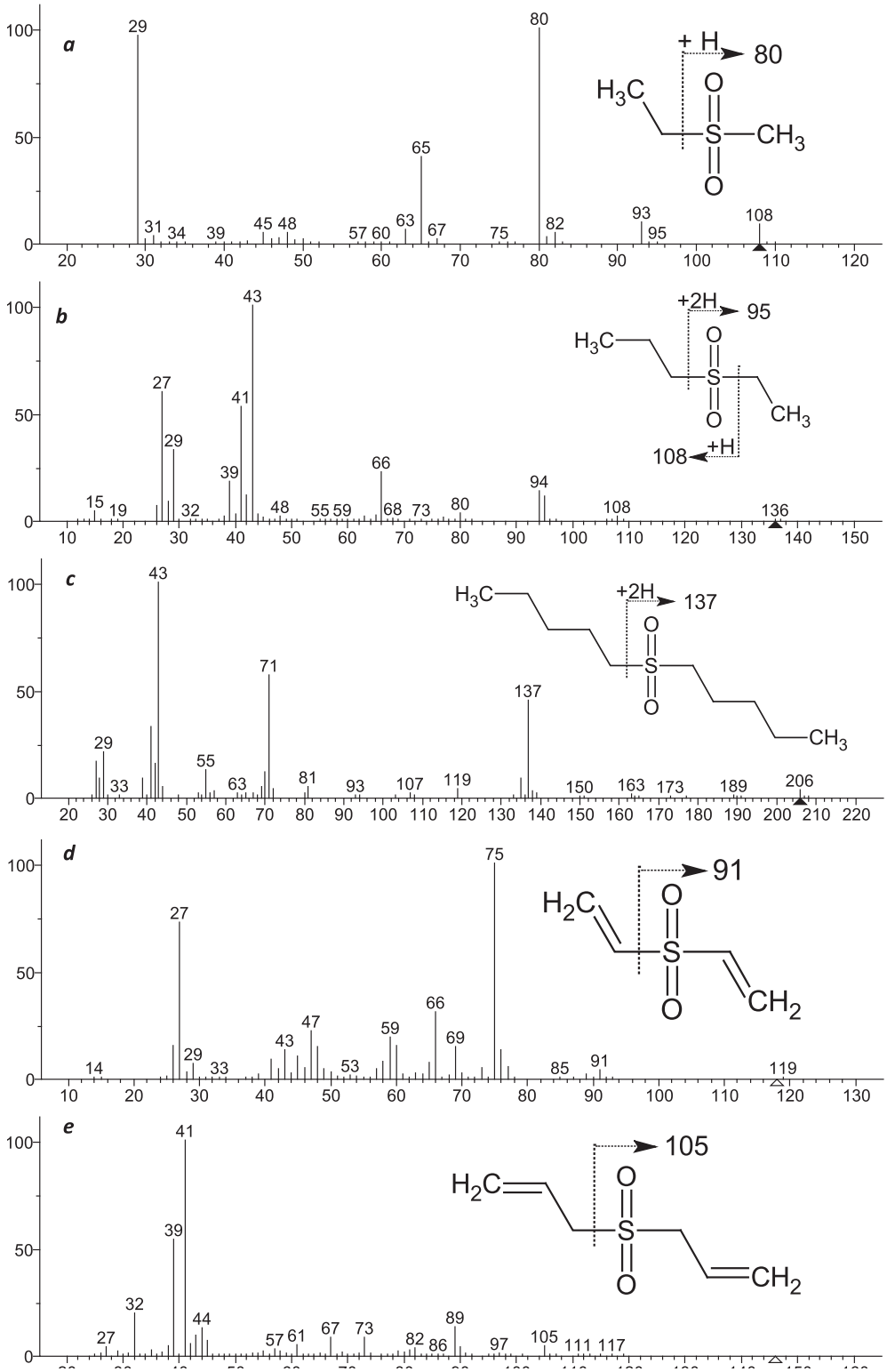

FIG. 28. Mass spectra [m/z (relative abundance, %)] of methyl ethyl sulfone (a), ethyl *n*-propyl sulfone (b), di(*n*-pentyl) sulfone (c), di(vinyl) sulfone (d), and di(allyl) sulfone (e).

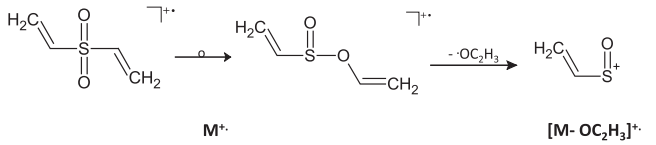

SCHEME 42. EI-induced skeletal rearrangement of divinyl sulfone into vinyl vinylsulfinate followed by the loss of vinyloxy radicals.

7.3.2. O-Alkyl alkanethioates

As mentioned above, molecular ions of such compounds are readily isomerized into corresponding *S*-alkyl esters. Usually, their mass spectra reveal more pronounced acetyl ion peaks as compared to the expected thioacetyl analogs. For example, the peak intensity ratio $I_{[CH3CO]+}/I_{[CH3CS]+}$ in the spectrum of *O*-ethyl thioacetate [Fig. 29(b)] is almost 2. In addition to the possible isomerization of molecular ions, the $[CH_3CO]^+$ EE ion can be formed via a shift of γ-hydrogen and the loss of ethylene neutral [route (a), Scheme 45] followed by the elimination of a sulfanyl radical. The parallel dissociation process involves the formation of a four-centered transition state and the shift of an ethyl radical from oxygen to sulfur, giving rise to the formation of the *S*-ethyl tautomer; further elimination of an ethylthio radical produces an acetyl cation [route (b), Scheme 45].

Unlike *S*-alkyl thiocarboxylates and similarly to alkyl alkanecarboxylates, *O*-alkyl esters of alkanethioic acids containing γ-hydrogen relative to the acidic function undergo McLafferty rearrangement, resulting in the formation of $[CHR{=}C(SH)OC_mH_{2m+1}]^{+\cdot}$ OE ions at the expense of the acid residue. Thus, part of $[M\text{-}C_2H_4]^{+\cdot}$ (120 Da) EE ions in the case of ethyl dithiobutanoate [Fig. 29(e)] is due to γ-hydrogen migration followed by the cleavage of the β-C–C bond. McLafferty rearrangement is responsible for generation of the $[M\text{-}C_3H_6]^{+\cdot}$ OE ion with maximum intensity in the case of methyl thiovalerate [n-$C_4H_9C(S)OCH_3$].

7.3.3. Alkyl alkane(dithio)ates

Both heteroatoms in the acetic function are occupied by sulfur in the case of ethyl dithioacetic acid. Accordingly, the base peak in its spectrum corresponds to the $[CH_3CS]^+$ (59 Da) EE ion [Fig. 29(d)]. This peak is shifted by 28 Da, and the $[C_3H_7CS]^+$ (87 Da) EE ion is generated in the case of dithiobutanoate homolog [Fig. 29(e)].

Molecular ions of alkenyl esters (R′ = C_3H_7, C_4H_7) of alkanedithioic acids RCSSR′ (R = CH_3, C_2H_5, i-C_3H_7) also undergo C(S)–S bond cleavage, yielding the most abundant $[RCS]^+$ ions. The other characteristic peaks in the spectra for this type of esters are due to $[M\text{-}CH_3]^+$, $[M\text{-}SH]^+$, $[M\text{-}R]^+$, $[R'SH]^+$, and $[CS_2]^+$ ions.

7.4. Thioamides and hydrazides

Molecular ion peaks are usually rather abundant in the spectra of thioamides. The main pathways of their dissociation involve (a) a simple cleavage of $C_{alkyl}\text{-}C_{(S)}$ bond and generation of $[M\text{-alkyl}]^+$ EE ions, (b) hydrogen shift to thionic sulfur followed by the loss of sulfanyl radical, and (c) fission of $C_{(S)}$–N bond and elimination of NH_2 radical and/or ammonia neutral. Peaks corresponding to these ions are present in the spectra of thioacetamide and thiopropionamide [Figs. 30(b) and 30(c)], and they are used for the identification of structural elements. In fact, the qualitative view of the spectra of isomeric *N*-methylthioformamide [Fig. 30(a)] and thioacetamide [Fig. 30(b)] is almost similar. However, the following quantitative differences may be successfully utilized for their differentiation: (a) the $[M\text{-}H]^+$ ion peak is pronounced in the thioformamide spectrum and the peak of the $[M\text{-}CH_3]^+$ ion is higher in the case of thioacetamide, and (b) the $[NHCH_3]^+$ (30 Da) EE ion peak is outstanding in the spectrum of (*N*-methyl)thioformamide and the same peak has an average intensity in the spectrum of thioacetamide.

New fragmentation patterns become dominant with the increase in the size of an acidic residue. Thus, McLafferty rearrangement is responsible for the generation of the $t[CH_2{=}C(SH)N(C_2H_5)_2]^{+\cdot}$ (131 Da) OE ion in the case of *N*,*N*-di(ethyl)dodecanethioamide, and a simple β-C–C fission relative to the thionyl group is responsible for the formation of the $[M\text{-}C_9H_{19}]^+$ (144 Da) EE ion [Fig. 30(d)]. It should be noted that the loss of a sulfanyl radical (SH) remains the important dissociation pathway.

The mass spectrum of thioacetyl hydrazide, depicted in Fig. 30(e), demonstrates preferable fission of the C(S)–N bond, which generates $[N(CH_3)_2]^+$ (45 Da) EE, $[HN(CH_3)_2]^{+\cdot}$ (46 Da) OE, and $[CH_3C{\equiv}S]^+$ (59 Da) EE ions. The loss of a sulfanyl radical becomes irrelevant.

7.5. Thiocarbonic acid derivatives

7.5.1. Thiocarbonates

Dissociation of thiocarbonates strongly depends on (a) the number of sulfur atoms in a molecule, such as mono-, di-, and trithiocarbonates; (b) the number of alkyl substituents, such as mono and di-alkyl derivatives; and (c) the nature and the size of alkyl substituents. The mass spectra of dimethyl analogs of mono-, di-, and trithiocarbonates depicted in Figs. 31(a)–31(c) demonstrate a shift in their fragmentation patterns. Note that dialkyl esters and isomeric mono-alkyl thiocarbonates are easily differentiated because the spectra of the latter do not contain the $M^{+\cdot}$ peak [Fig. 31(d)].

Three major dissociation directions are observed in the case of O,O′-dimethyl thiocarbonate, such as (a) loss of a methyl radical that is a minor process, (b) elimination of methoxy radical, and (c) hydrogen shift via a four centered transition state followed by the loss of formaldehyde neutral and generation of the $[M\text{-}CH_2O]^{+\cdot}$ (76 Da) OE ion. The latter further eliminates a methyl radical.

Fragmentation of ionized O,S-dimethyl esters of di(thio)carbonates produces $[M\text{-}OCH_3]^+$ and $[M\text{-}SCH_3]^+$ EE ions along with $[CH_3O]^+$ and $[CH_3S]^+$ cations [Fig. 31(b)]. Molecular ions of di(ethyl) and di(propyl) carbonodithioates undergo hydrogen shifts and generate $[M\text{-}OC_nH_{2n}]^{+\cdot}$ and $[M\text{-}SC_nH_{2n}]^{+\cdot}$ OE ions.

Mass spectra of mono-alkyl tri(thio)carbonates show rather unstable molecular ions that may be absent in a spectrum. The dissociation of their $M^{+\cdot}$ is very specific, and the major path of their dissociation proceeds via elimination of an alkanethiol molecule and generation of $[CS_2]^{+\cdot}$ (76 Da) OE ions [Fig. 31(d)].

Di-alkyl tri(thio)carbonates demonstrate distinct $M^{+\cdot}$. Their fragmentation proceeds via the loss of alkene neutral and alkanethiol radical; the latter is also eliminated from the $[M\text{-}C_nH_{2n}]^{+\cdot}$ OE ion. Peaks of $[C_nH_{2n+1}SH]^{+\cdot}$ ions show significant intensities in

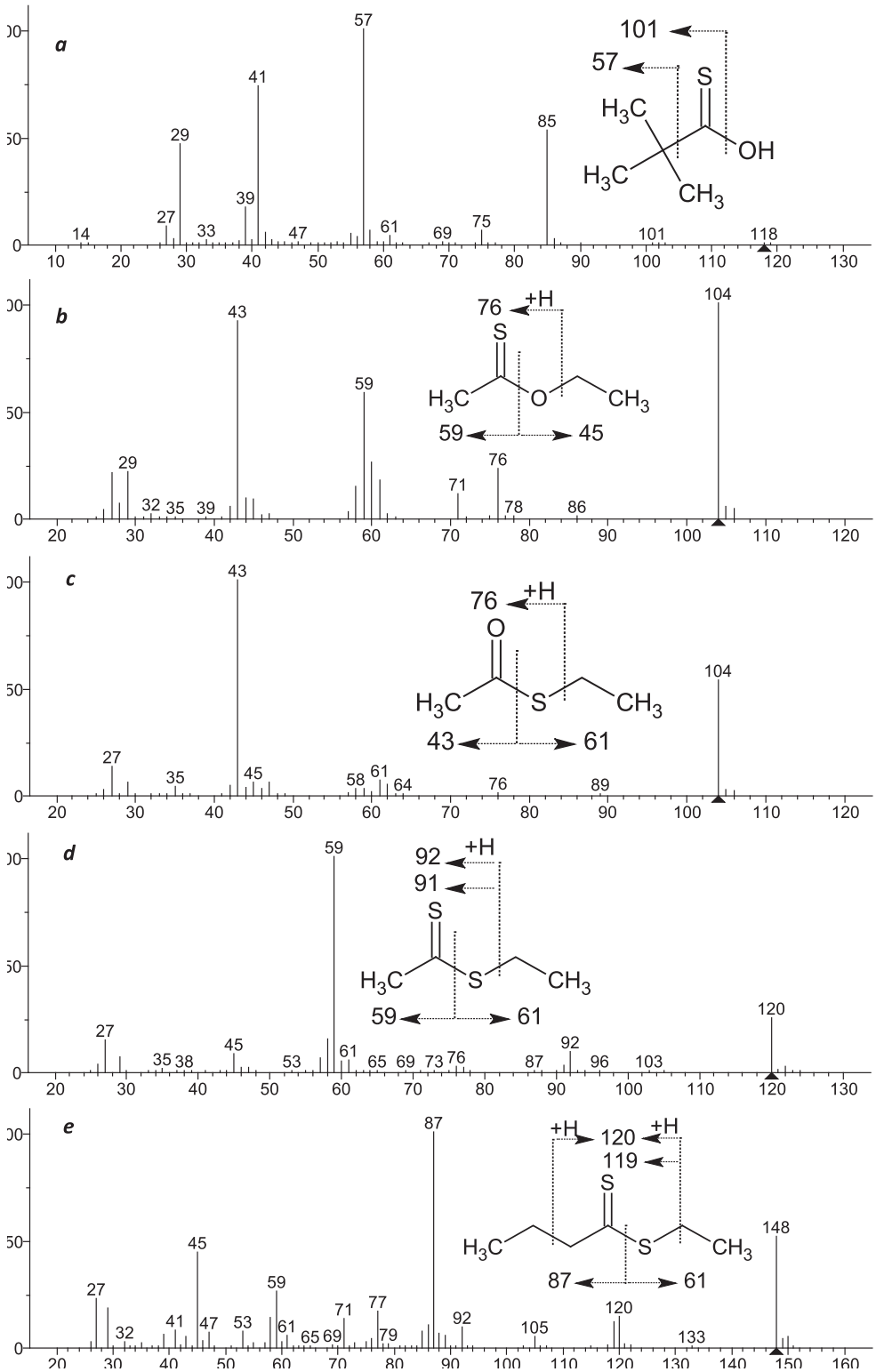

FIG. 29. Mass spectra [m/z (relative abundance, %)] of thiopivalic acid (a), *O*-ethyl thioacetate (b), *S*-ethyl thioacetate (c), ethyl dithioacetate (d), and ethyl dithiobutanoate (e).

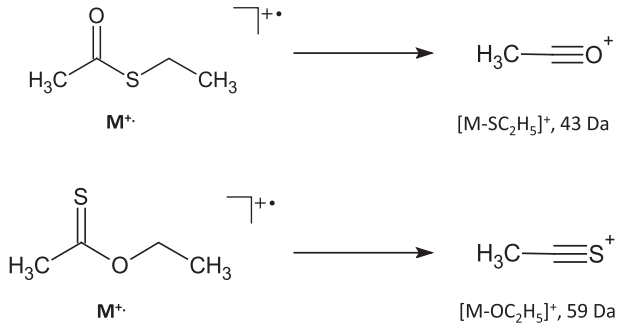

SCHEME 43. Origin of ions at acetyl and thioacetyl EE ions in the case of *O*-ethyl thioacetate [Fig. 29(b)].

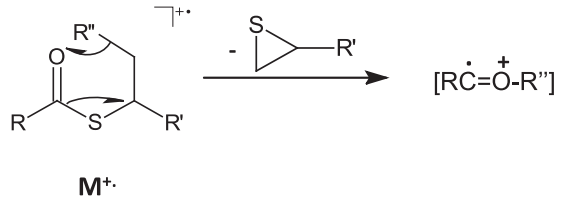

SCHEME 44. Elimination of substituted thiiranes from $M^{+\cdot}$ of *S*-alkyl thioalkanoic acids (alkyl > propyl).

the spectra. Hydrocarbon ions derived from the alkyl moieties are also pronounced [Fig. 31(c)].

7.5.2. Thiocarbamates

Mono-alkyl carbamodithioates, unlike their thiocarbonate analogs, demonstrate noticeable molecular ions that readily lose hydrogens. The other dissociation direction in the case of *N*,*N*-diethylamino-carbamodithioic acid [Fig. 32(a)] involves migration of sulfanyl hydrogen to nitrogen followed by $C_{(S)}$–N bond fission and generation of $[CS_2]^{+\cdot}$ (76 Da) OE ions. The most abundant ions in the spectrum correspond to $[M\text{-}SH]^+$, $[M\text{-}SH\text{-}C_2H_4]^+$, and $[M\text{-}SH\text{-}C_2H_4\text{-}C_2H_4]^+$ EE ions. The latter corresponds to the thioamide $[H_2NCS]^+$ (60 Da) EE ion that is a diagnostically important ion for structure determination of carbamodithioic acids and their esters.

Typical spectra of esters of *N*,*N*-disubstituted mono- and dithio-carbamic acids are depicted in Figs. 32(b) and 32(c). Major dissociation pathways of these molecules are due to the cleavages at both sides of the C(=S) function and fragmentation of alkyl substituents at the *N*- and *S* terminal positions. A diagnostically important $[H_2NCS]^+$ (60 Da) EE ion for *N*-alkyl and *N*,*N*-dialkyl carbamodithioates (alkyl > methyl) is shifted to the $[CH_3NHCS]^+$ (74 Da) EE ion and the $[(CH_3)_2NCS]^+$ (88 Da) EE ion in the case of alkyl *N*-methyl and *N*,*N*-dimethylcarbamodithioates accordingly.

7.5.3. Thioureas

Thioureas are characterized by rather stable molecular ions that demonstrate specific fragmentation patterns due to the dissociation C–N bonds on both sides of the C=S function. These patterns provide sufficient information for the differentiation of two isomeric thioureas: *N*,*N*-dimethyl and *N*,*N*′-dimethyl. While *N*,*N*-dimethylthiourea undergoes simple cleavages and generates $[M\text{-}NH_2]^+$ and $[M\text{-}N(CH_3)_2]^+$ EE ions, its *N*,*N*′-analog mainly undergoes rearrangements and produces $[M\text{-}CH_3NH]^+$ (74 Da) and $[M\text{-}SH]^+$ (71 Da) EE ions (Scheme 46). Note that sufficient quantitative differences are observed, which can be used for the differentiation of these dimethyl isomers and their mono-ethyl analog.

Dissociation of molecular ions of long-chain alkyl thioureas proceeds in the same way, including generation of $[M\text{-}SH]^+$ EE ions. However, fragmentation of *N*-alkyl moieties produces majority of peaks in the spectra.

Decomposition of *N*-alkenyl thioureas is very different [Fig. 32(d)]. The cleavage of $C_{(S)}$–N bonds becomes insignificant, and ions generated via a preliminary rearrangement of their $M^{+\cdot}$ become dominant. For example, the mass spectrum of diallyl thiourea reveals the base peak of $M^{+\cdot}$ and prominent peaks of $[M\text{-}CH_3]^+$, $[C_3H_5NH]^+$, and $[C_3H_5]^+$ EE ions; the intensities of peaks of $[M\text{-}C_3H_5NH]^+$ (100 Da) and $[M\text{-}C_3H_5N]^{+\cdot}$ (101 Da) ions are insignificant [Fig. 32(d)].

7.6. Sulfonic acids and derivatives

7.6.1. Alkanesulfonic acids

Sulfonic acids possess a predisposition to low volatility and decomposition. As a result, their spectra can exhibit strong quantitative differences depending on the experimental conditions. Common ions generated by sulfonic acids are exemplified by the spectrum of methanesulfonic acid [Fig. 33(a)], which reveals the following peaks: $M^{+\cdot}$ (96 Da), $[M\text{-alkyl}]^+$ (81 Da), $[M\text{-}OH]^+$ (79 Da), $[M\text{-}OH\text{-}H]^{+\cdot}$ (78 Da), $[SO_2]^{+\cdot}$ (64 Da), $[SO_2H]^+$ (65 Da), and $[OCH_3]^+$ (31 Da).

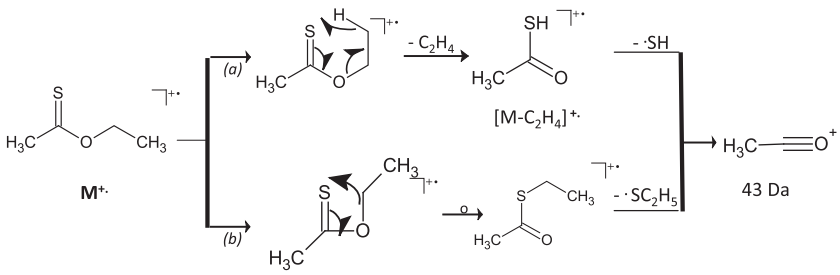

SCHEME 45. Generation of acetyl cations in the case of *O*-ethyl thioacetate.

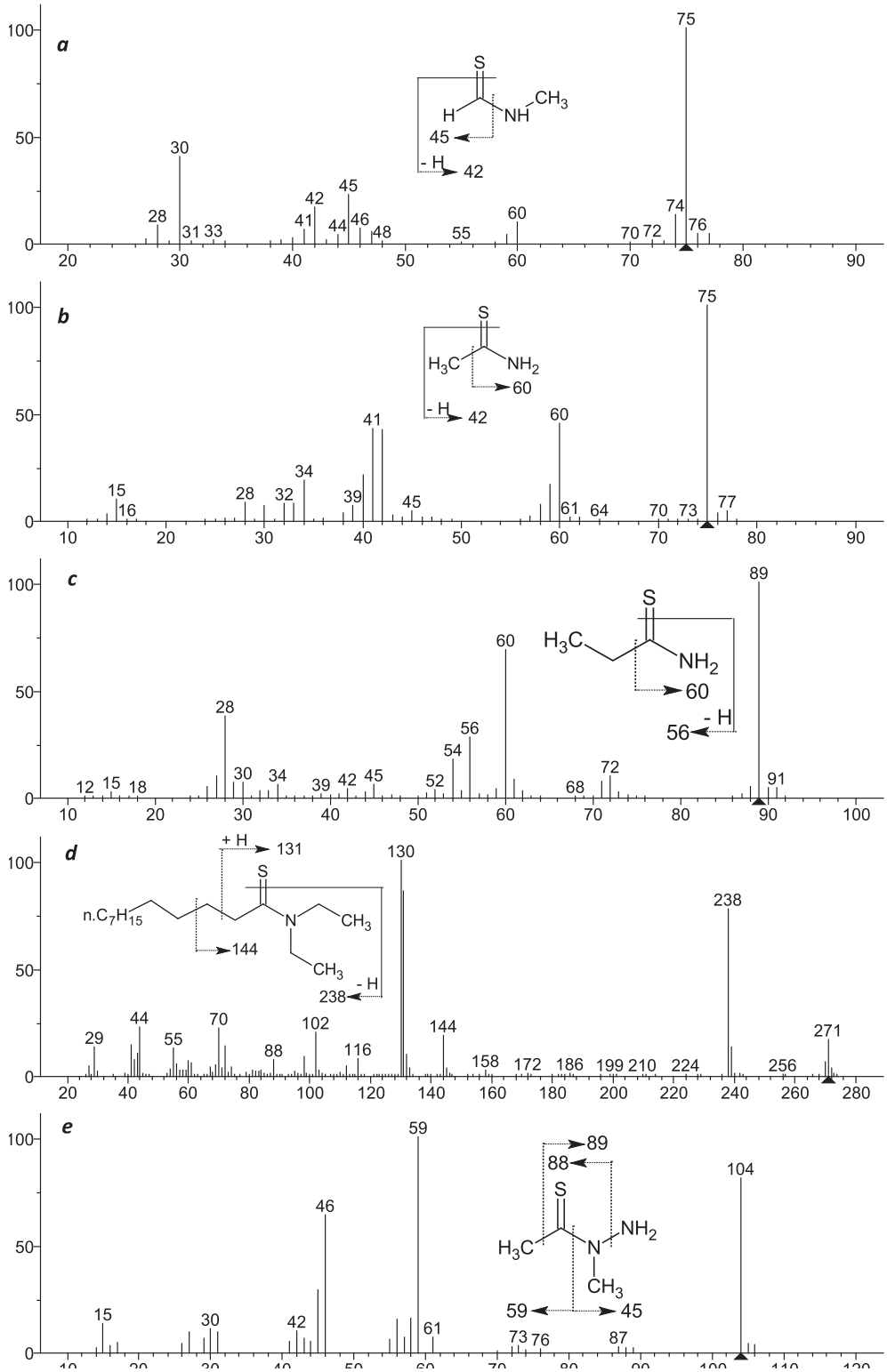

FIG. 30. Mass spectra [m/z (relative abundance, %)] of *N*-methylthioformamide (a), thioacetamide (b), *n*-propanthioamide (c), *N*,*N*-di(ethyl)-*n*-dodecanethioamide (d), and thioacetyl *N*,*N*-dimethylamide (e).

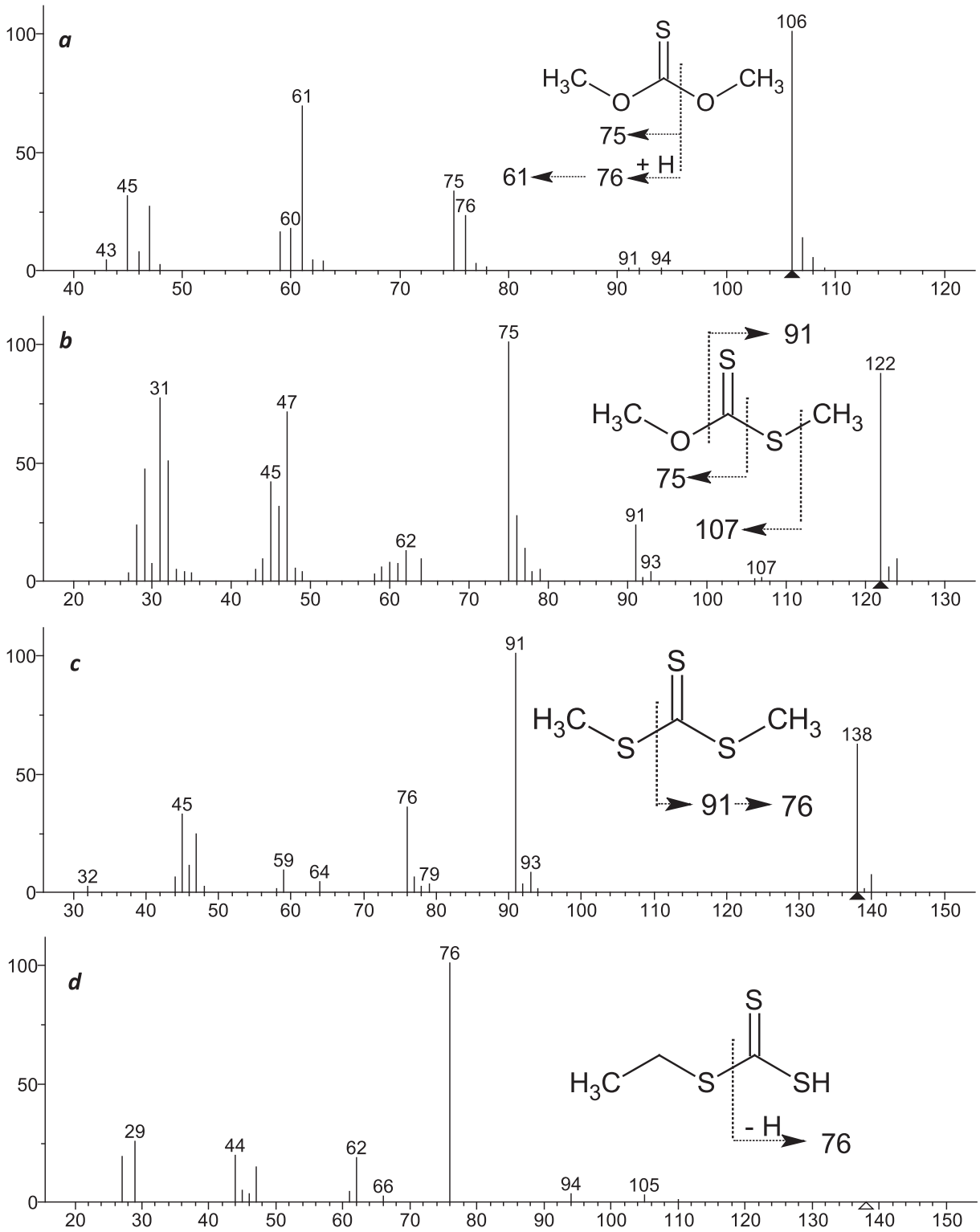

FIG. 31. Mass spectra [m/z (relative abundance, %)] of *O*,*O*′-dimethyl carbonothioate (a), *O*,*S*-dimethyl carbonodithioate (b), *S*,*S*-dimethyl carbonotrithioate (c), and monoethyl carbonotrithioate (d).

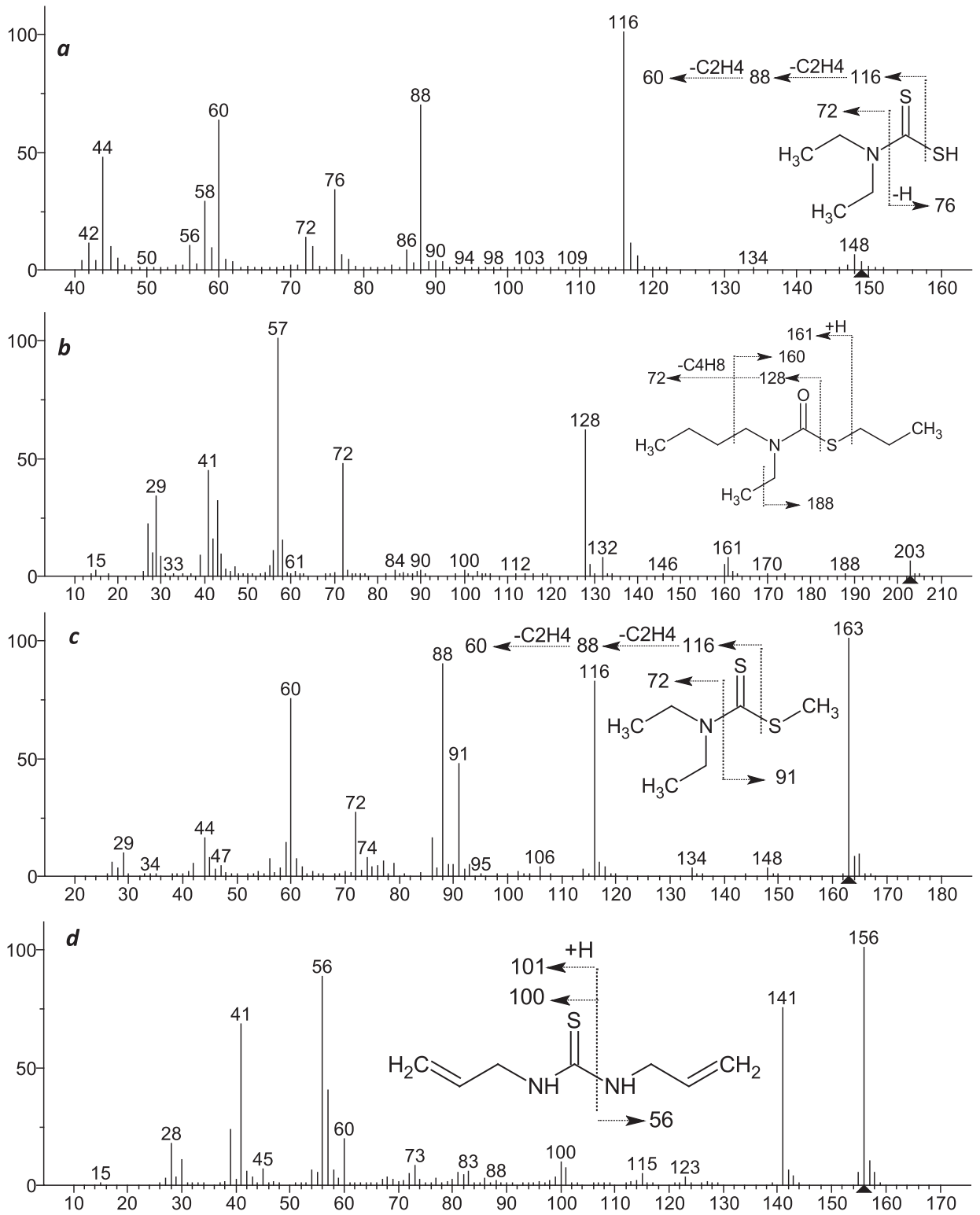

FIG. 32. Mass spectra [m/z (relative abundance, %)] of *N*,*N*-di(ethyl)carbamodithioic acid (a), *n*-propyl *N*-ethyl-*N*-(*n*-butyl)carbamodithioate (b), methyl *N*,*N*-di(ethyl)carbamodithioate (c), and di(allyl) thiourea (d).

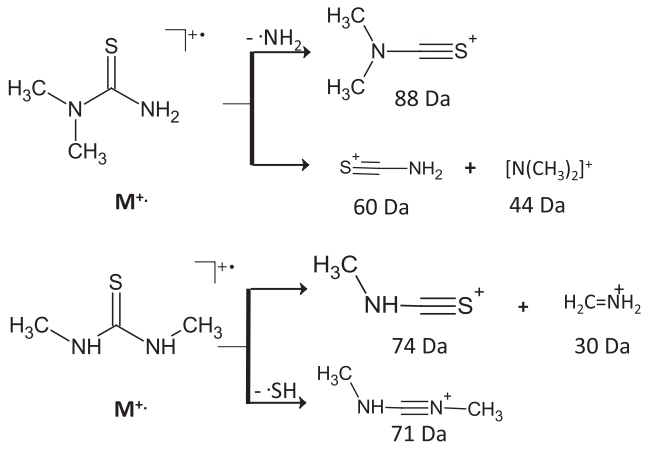

SCHEME 46. Major fragmentation pathways of isomeric dimethylthioureas.

7.6.2. Alkyl alkanesulfonates

Alkyl esters of alkanesulfonic acids show low abundance or no $M^{+\cdot}$. Two major dissociation pathways of $M^{+\cdot}$ are used for the determination of selected structural elements, such as (a) β-carbon–carbon bond cleavage relative to oxygen in the *O*-alkyl chain that leads to the $[M\text{-}C_2H_5)]^+$ (109 Da) EE ion in the case of propyl methanesulfonate [Scheme 47, Fig. 33(b)] and (b) two hydrogen shifts accompanied by elimination of an alkenyl radical and generating $[M\text{-}C_3H_5]^+$ (97 Da) EE ion. The latter further eliminates a water molecule.

Long-chain sulfonic acids (alkyl > methyl) dissociate differently. Their molecular ions undergo McLafferty rearrangement followed by the loss of an alkene molecule. Thus, the corresponding $[M\text{-}C_2H_4]^{+\cdot}$ (96 Da) OE ion is present in the spectrum of methyl ethanesulfonate [Fig. 33(c)].

Alkyl alkanesulfonates containing long chain alkyls at S- and O-atoms undergo both types of decomposition reactions. The competitive ability of each reaction determines the intensities of characteristic peaks in their spectra.

7.6.3. Sulfonyl halides

Among other halides, sulfonyl chlorides are among the most widely used in industry. In general, $M^{+\cdot}$ of alkanesulfonyl chlorides stepwise eliminate chlorine and sulfur dioxide in various order. The spectrum of butanesulfonyl chloride is depicted in Fig. 33(d) for illustration. It reveals small peaks of $[M+H]^+$, $[M\text{-}Cl]^+$ (121 Da), $[M\text{-}HSO_2]^+$ (91/93 Da), and $[M\text{-}C_nH_{2n+1}]^+$ ions. The major peaks in the spectrum correspond to alkyl and alkenyl EE ions.

7.6.4. Sulfonamides

MS cannot be much of help for the determination of structural elements of alkanesulfonamides. As demonstrated by the spectrum of hexadecanesulfonamide [Fig. 33(e)], the mass spectrum allows the determination of molecular weight and elemental composition of a compound. In addition, abundant peaks of $[M\text{-}SO_2H]^+$ (240 Da) EE, $[M\text{-}HSO_2NH_2]^{+\cdot}$ (224 Da) OE, and $[(OH)_2SNH_2]^+$ (82 Da) EE ions confirm the presence of the sulfonamido function. The majority of peaks in the spectra correspond to alkyl and alkenyl cations that do not provide much information on the structure of the carbon skeleton.

7.7. Alkanesulfinates

Methyl esters of alkanesulfinic acids $RSOOCH_3$ (R = ethyl, *n*- and isopropyl, *n*-, *sec*- and *tert*-butyl) produce detectable molecular ions that easily lose a methoxy moiety as a radical. The prominent peak of the $[HS(O)OCH_3]^{+\cdot}$ (80 Da) OE ion in the case of the above methyl esters is a result of hydrogen shift from alkyl to sulfur.

Peaks of $[HSO_2]^+$, $[C_nH_{2n+1}]^+$, and $[C_nH_{2n-1}]^+$ ions are also of high intensity in the spectra. In the case of isopropyl isopropanesulfinate, the doublet of $[M\text{-}C_3H_6]^{+\cdot}$ and $[M\text{-}C_3H_7]^+$ ion peaks is characteristic. Similar fragmentation patterns are typical for *S*-esters of methane- and propanesulfinothioic acids.

7.8. Sulfurous acid derivatives

Only dimethyl and diethyl sulfites generate detectable $M^{+\cdot}$, and this peak is essentially absent from the spectra of higher sulfites. Molecular ions of di(alkyl) sulfites ($C_nH_{2n+1} > CH_3$) undergo β-C–C cleavage, similar to alkanols, resulting in the formation of $[M\text{-}C_{n-1}H_{2n-1}]^+$ EE ions and S–O bond scission to form $[C_nH_{2n+1}O]^+$ EE ions.

However, the diagnostically important ions for the identification of di(alkyl) sulfites is the protonated sulfurous acid $[S(OH)_3]^+$ (83 Da) EE ion. Its formation involves migration of two hydrogen atoms and the loss of the heavier alkyl substituent as an alkenyl radical followed by McLafferty rearrangement and elimination of the second alkyl substituent as a neutral alkene molecule (Scheme 48).

7.9. Sulfuric acid derivatives

Dissociation of detectable $M^{+\cdot}$ of dimethyl sulfite proceeds in several directions, including two α- and one β-cleavages relative to sulfur [Fig. 34(a)]. One of the α-cleavages is associated with a four centered transition state followed by hydrogen migration and formation of $[M\text{-}CH_2O]^{+\cdot}$ (96 Da) OE ions. The other α-cleavage is a simple scission of the S–O bond that produces the $[M\text{-}OCH_3]^+$ EE ion. The β-cleavage generates the $[M\text{-}H]^+$ EE ion that has a substituted oxonium type structure. Di(alkyl) sulfates (alkyl > CH_3) also undergo cleavages of β-C–H and β-C–C bonds, resulting in the formation of $[M\text{-}H]^+$ and $[M\text{-alkyl}]^+$ EE ions. A new dissociation pathway involves two hydrogen shifts and elimination of an alkyl substituent as an alkenyl radical. Each of the above three ions further eliminate the second alkyl as an alkene molecule. These fragmentation pathways are presented in Scheme 49 and Fig. 34(b) for di(ethyl) sulfate.

The unstable molecular ion of trimethylsilyl ethyl sulfate also eliminates ethylene neutral from the $[M\text{-}CH_3]^+$ EE ion [Fig. 34(c)]. The mass spectrum of symmetrical dimethyl sulfamide contains prominent peaks of $M^{+\cdot}$ and $[M\text{-}NHCH_3]^+$ ions [Fig. 34(d)]. Other outstanding peaks in the spectrum correspond to the $[NHCH_3]^+$ (30 Da) EE, $[SO]^{+\cdot}$ (48 Da) OE, and $[SO_2]^{+\cdot}$ (64 Da) OE ions.

Substitution of all hydrogens in the sulfamide molecule by alkyl groups leads to a change in fragmentation patterns. For example, in the case of tetra(ethyl) sulfamide, rearrangement processes do not take place [Fig. 34(e)]. Instead, simple S–N and β-C–C cleavages are observed.

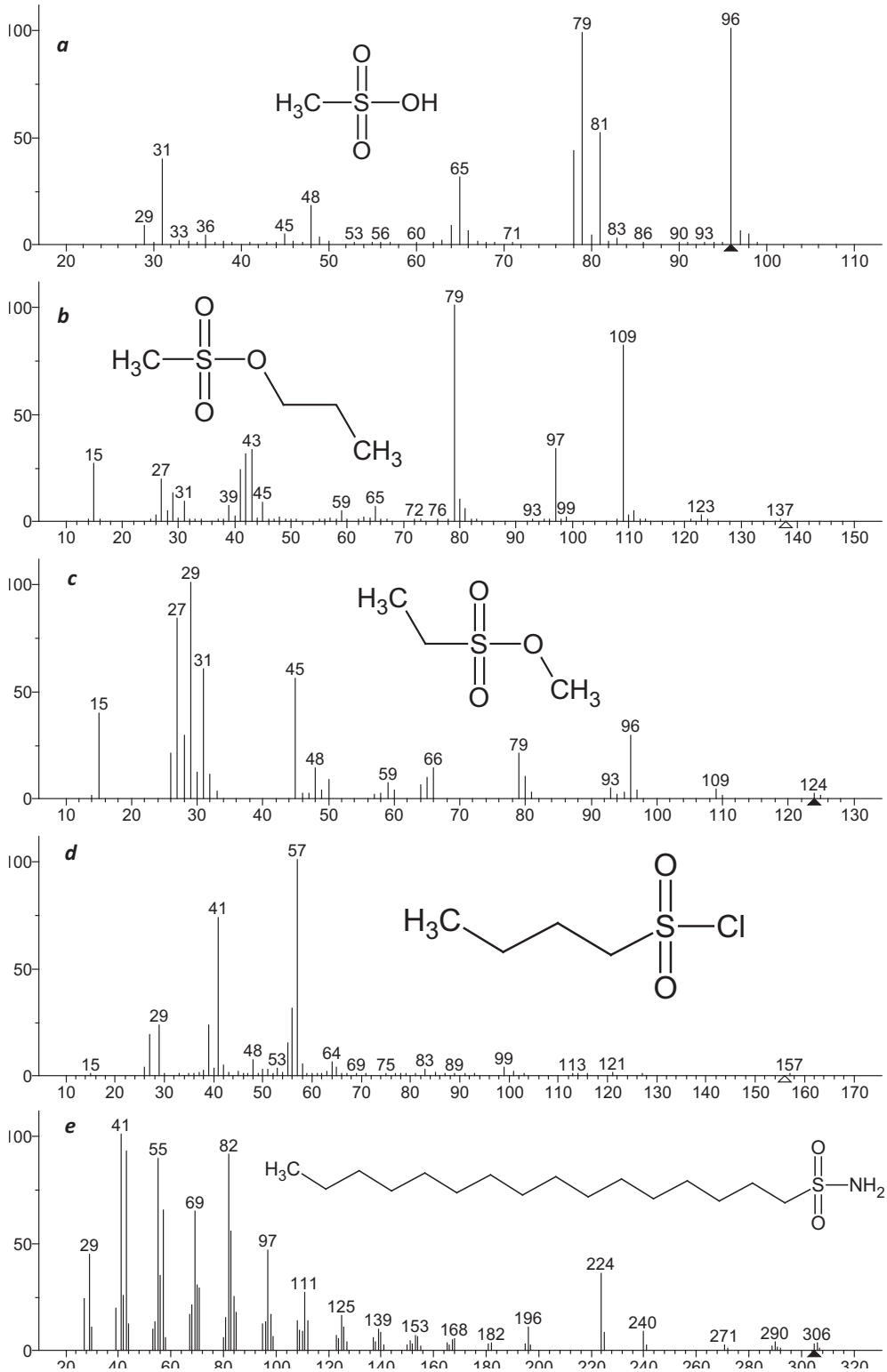

FIG. 33. Mass spectra [m/z (relative abundance, %)] of methanesulfonic acid (a), *n*-propyl methanesulfonate (b), methyl ethanesulfonate (c), *n*-butanesulfonyl chloride (d), and *n*-hexadecanesulfonamide (e).

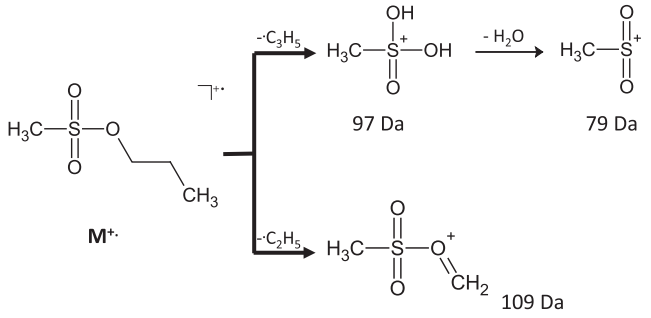

SCHEME 47. Two major dissociation pathways in the case of *n*-propyl methanesulfonate.

8. Compounds with a Nitrogen Containing Functional Group

8.1. Amines and their derivatives

8.1.1. Amines

Currently, there are two major viewpoints on the dissociation of nitrogen containing compounds stating that (a) localization of the charge on nitrogen initiates scissions of β-carbon–carbon bonds, resulting in the formation of stable ammonium ions; and (b) high stability of generated ammonium ions is the driving force for the decomposition, taking into consideration that the electron is removed from a delocalized molecular orbital, and this removal is not associated with a single nitrogen atom. Both perspectives complement each other.

Simple cleavages of the C_α–C_β bond and elimination of alkyl radical(s) from $M^{+\cdot}$ generate ammonium ions. It is the characteristic dissociation direction of alkylamines and successfully utilized for structure elucidation. This fragmentation pathway is presented in Scheme 50, and the mass values of generated ions are given for two isomeric primary amines—octylamine and 1-ethylhexylamine [Figs. 35(a) and 35(b)].

Easiness of these reactions destabilizes ionized molecules and, consequently, corresponding $M^{+\cdot}$ peaks are noticeable only in the spectra of lower amines. Their intensities are decreased and then disappear with the increase in the molecular weight of an amine and/or introduction of branching at α-carbon.

The base peak in the spectra of 1-*n*-alkylamines always corresponds to the $[CH_2{=}NH_2]^+$ (30 Da) EE ions [Fig. 35(a)]. The loss of hydrogen is responsible for the formation of this ion in the case of methylamine; other primary *n*-alkylamines produce this ion via elimination of alkyl radicals. The mass value of this ion is of a diagnostic power. The Mass shift of this ion from m/z 30 to m/z 58 (28 Da difference) in the spectrum of 1-ethylhexylamine indicates that two more methylene moieties are present in this ion [Fig. 35(b), Scheme 50]. The abundant $[M\text{-}C_2H_5]^+$ (100 Da) EE ion confirms that it is the ethyl group that is attached to $C_{(\alpha)}$, not two methyl substituents. In the case of isomeric *N*,α-dimethylhexylamine, having a tertiary amine structure, only a single $[CH(CH_3){=}NH(CH_3)]^+$ (58 Da) ammonium ion is observed; there are no traces of $[M\text{-}C_2H_5]^+$ ions in the spectrum [Fig. 35(c)].

Dissociation of $M^{+\cdot}$ of secondary amines proceeds via the loss of either of the alkyl substituents, preferably the largest one. Thus, the mass spectrum of *N*-propyl-hexylamine [Fig. 35(d)] reveals the base peak of the $[M\text{-}C_5H_{11}]^+$ (72 Da) EE ion and peak of the $[M\text{-}C_2H_5]^+$ (114 Da) EE ion with 22% relative intensity. Both ions further undergo hydrogen rearrangement followed by N–C bond cleavage and the loss of an alkene neutral, resulting in the formation of the $[CH_2{=}NH_2]^+$ (30 Da) EE ion.

Branching at α-carbon provides opportunities for multiple β-C–C bond scissions. Thus, the spectrum of (α-propyl-α-pentyl-α-heptyl)methyl-*N*-ethylamine that represents secondary amine series and containing tertiary α-carbon mainly dissociates via the elimination of alkyl radicals at $C_{(\alpha)}$. Its spectrum [Fig. 35(e)] exhibits three outstanding peaks of $[M\text{-}C_7H_{15}]^+$ (170 Da) EE, $[M\text{-}C_5H_{11}]^+$ (198 Da) EE, and $[M\text{-}C_3H_7]^+$ (226 Da) EE ions; the intensities of these peaks correlate with the size of the leaving radicals from the α-carbon atom. The *N*-ethyl moiety is not represented by the $[M\text{-}CH_3]^+$ (254 Da) EE ion.

Each alkyl substituent undergoes β-C–C bond cleavage in the case of $M^{+\cdot}$ of tertiary tri(alkyl)amines and, predictably, elimination of the heavier alkyl group is preferable. Further dissociation of $[M\text{-alkyl}]^+$ EE ions via hydrogen shift to nitrogen and N–C bond scission is less characteristic. Instead, peaks of ions due to McLafferty-like rearrangement are outstanding in the spectra (Scheme 51).

Amines containing α,β-unsaturated alkyl substituents produce more stable $M^{+\cdot}$. Consequently, the probability of β-cleavages in these compounds shall be low. However, corresponding ammonium ions are generated after the double bond migration as it can be observed in the spectrum of *N*,*N*-dimethyl-1-butenylamine revealing the base peak of the $[CH_2N(CH_3)_2]^+$ (58 Da) EE ion [Fig. 36(a)]. At the same time, β-cleavage next to unsaturation is diminished due to the appearance of additional pathways for the generation of ammonium ions, such as fragmentation at the expense of substitution at α-carbon in alkenylamines. In fact, the $[M\text{-}CH_3]^+$ (140 Da) EE ion peak shows maximum intensity, whereas the peak corresponding to the $[CH(CH_3){=}N(CH_3)_2]^+$ (72 Da) EE ion is just about 40% of relative intensity in the spectrum of α-methyl-*N*,*N*-dimethyl-2-heptenylamine [Fig. 36(b)]. Furthermore, polyenic amines demonstrate stable molecular ions. For example, the mass

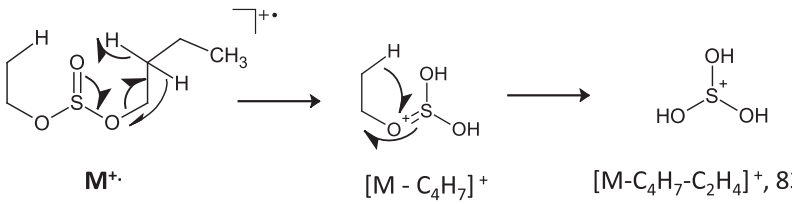

SCHEME 48. Formation of protonated sulfurous acid from $M^{+\cdot}$ of sulfite.

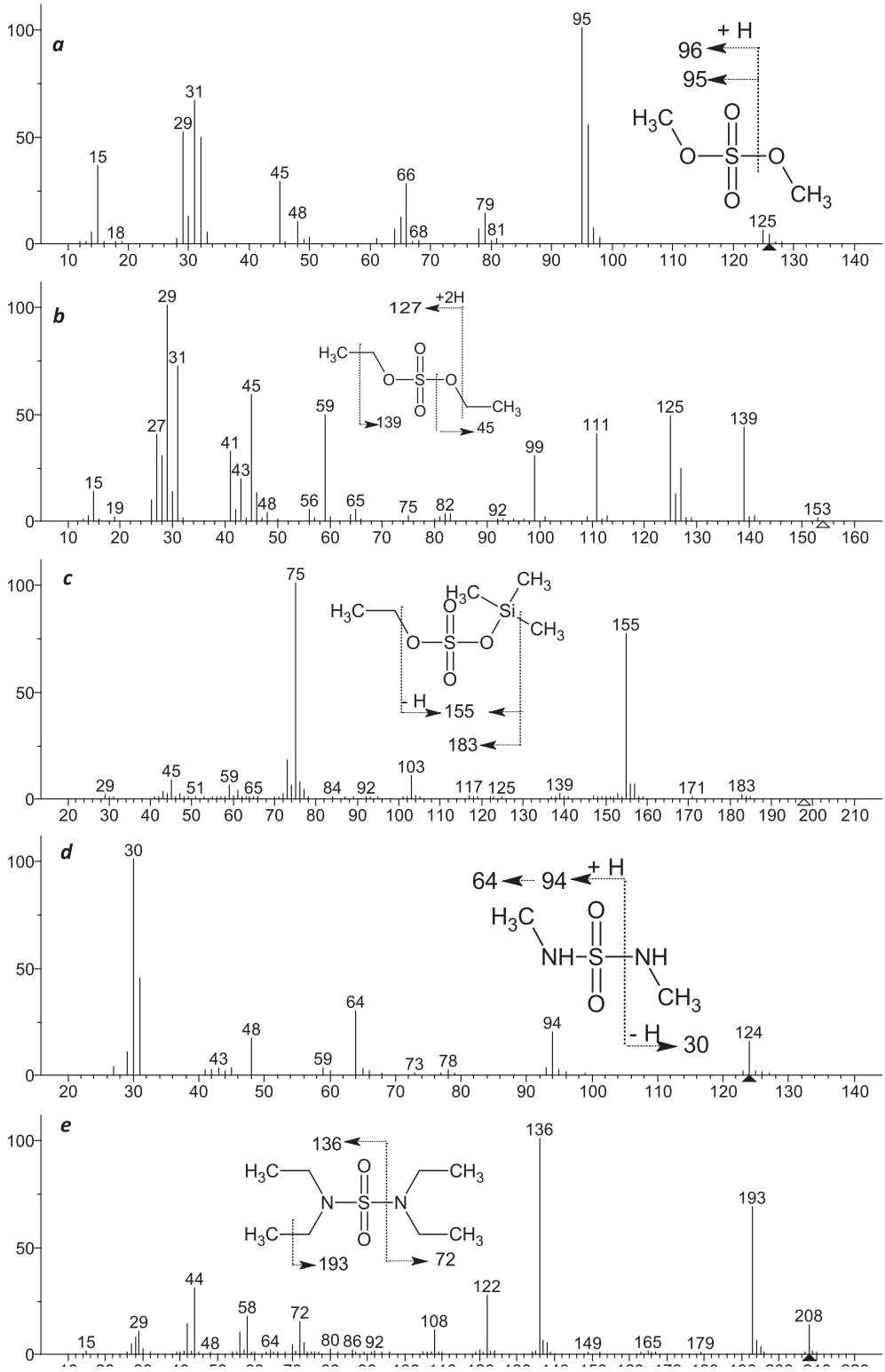

FIG. 34. Mass spectra [m/z (relative abundance, %)] of dimethyl sulfate (a), diethyl sulfate (b), ethyl trimethylsilyl sulfate (c), *N*,*N*′-dimethylsulfamide (d), and tetramethylsulfamide (e).

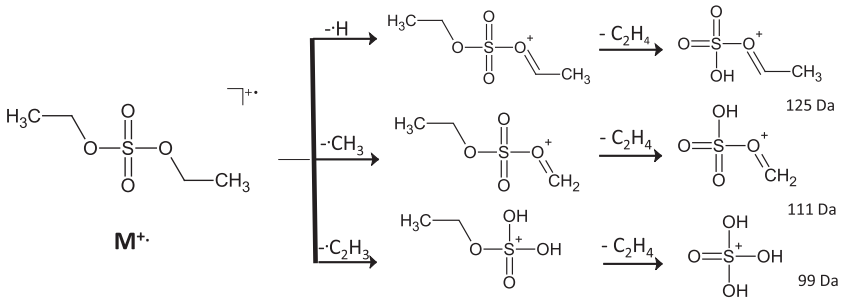

SCHEME 49. Major fragmentation pathways for $M^{+\cdot}$ of di(ethyl) sulfate.

spectrum of the *N*,*N*-diethyl derivative of hepta-1,3,5-trienylamine reveals the base peak of $M^{+\cdot}$; outstanding peaks of ions resulted from fragmentation of polyunsaturated alkyl substituent are not observed in the spectrum[(Fig. 36(c)].

8.1.2. Amine derivatives

8.1.2.1. Ammonium salts. In the case of quaternary ammonium salts, the common utilized anions are chlorides, bromides, iodides, perchlorates, hexafluorophosphates, alkylphosphites, boronhydrides, tetrafluoroborates, benzoates, p-toluenesulfonates, and more. The intact ammonium salts are not analyzed by EI-MS. They undergo thermal decomposition in the sample inlet system of an instrument, and the generated products are vaporized in a free amine form, which are then ionized in the ion source. In the case of alkylammonium salts, the dequaternization reaction yields amine and alkyl derivatives (such as alkyl chloride) or corresponding acids, such as hydrochloride, hydrobromide, hexafluorophosphoric acid, tetrafluoroboric acid, p-toluenesulfonic acid, and more (Scheme 52). As a result, a spectrum of a mixture is usually registered using a direct inlet system; unique spectra of decomposition products are being registered during GC–MS analysis.

The EI mass spectrum of tetraethylammonium bromide, recorded via a direct sample inlet, is presented in Fig. 36(d) as an example. It contains the $M^{+\cdot}$ (101 Da) peak of the expected triethylamine and its dissociation products, such as $[M\text{-}H]^+$ (100 Da), $[M\text{-}CH_3]^+$ (86 Da), $[M\text{-}CH_3\text{-}C_2H_4]^+$ (58 Da), $[M\text{-}CH_3\text{-}C_2H_4\text{-}C_2H_4]^+$ (30 Da), and more. On the other hand, the spectrum also reveals the $M^{+\cdot}$ (108/110 Da) peak of ethyl bromide along with its product ions: $[M\text{-}CH_3]^+$ (93/95 Da), $[Br]^+$ (79/81 Da), and more. Peaks at m/z 26–29 in the spectrum may be due to the fragmentation of both triethylamine and ethyl bromide.

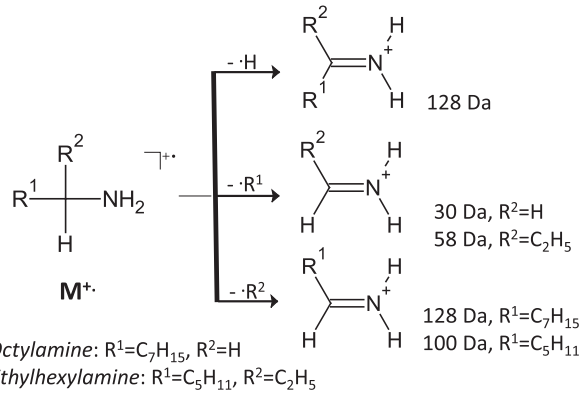

SCHEME 50. Generation of ammonium ions from $M^{+\cdot}$ of *n*-octylamine and 1-ethylhexylamine.

8.1.2.2. Hydroxylamines and N-oxides. The mass spectrum of unsubstituted hydroxylamine demonstrates the base peak of $M^{+\cdot}$ and expected ions resulting from the loss of hydrogen and hydroxyl radicals. *N*,*N*-Dimethylhydroxylamine is also characterized by stable $M^{+\cdot}$ and the substituted ammonium $[HO\text{–}N(CH_3)\text{=}CH_2]^+$ (60 Da) EE ion that is generated via the loss of a hydrogen radical from $M^{+\cdot}$. An ion with the same composition and structure shows maximum intensity in the spectrum of *N*-methyl-*N*-hexadecylhydoxylamine [Fig. 36(e)]. The $[HO\text{–}N(CH_3)\text{=}CH_2]^+$ (60 Da) EE ion has diagnostic power for the identification of *N*-alkyl-*N*-methylhydroxylamines not containing branching at *α*-carbon.

Expectedly, *N*-ethyl substituted *N*-*n*-alkyl-hydroxylamines generate homologous $[HO\text{–}N(C_2H_5)\text{=}CH_2]^+$ (74 Da) EE ions (Scheme 53). However, this ion further undergoes a four-centered hydrogen shift accompanied by the elimination of the remaining alkyl as an alkene neutral when alkyl > CH_3. Thus, starting from *N*-ethyl, two ions, namely, alkyl(hydroxyl)ammonium and (hydroxyl)ammonium ions, possess a high diagnostic power for *N*,*N*-dialkylhydroxylamines (Scheme 53).

The outstanding peaks of $M^{+\cdot}$ are also characteristic for *O*-alkoxyamines. Their dissociation proceeds in three main directions, such as β-cleavage relative to oxygen and scission of O–C and O–N bonds (Scheme 54). Each dissociation pathway may be accompanied with hydrogen shifts. Abundant ions of hydrocarbon OE and EE are characteristic for the spectra of alkoxyamines. Hydroxylamine OE ions at m/z 33 are of diagnostic power for their identification.

Note that *N*,*O*-di(methyl)hydroxylamine containing alkyls at both hetero-atoms shows the base peak of $M^{+\cdot}$ and peaks of $[M\text{-}CH_3]^+$, $[NH_2OH]^{+\cdot}$, $[OCH_3]^+$, $[CH_2NH_2]^+$, $[CHO]^+$, and $[CO]^{+\cdot}$ ions. *N*-oxide of trimethylamine demonstrates the base $M^{+\cdot}$ peak that allows a successful determination of elemental composition. The spectrum reveals also $[M\text{-}CH_3]^+$ and $[M\text{-}O]^+$ EE ion peaks.

8.1.2.3. Nitrosamines. Dialkylnitrosamines reveal well detectable molecular ions that along with the $[M\text{-}OH]^+$ EE ions enables reliable determination of the elemental composition of the molecule. The formation of $[M\text{-}OH]^+$ ions involves the removal of

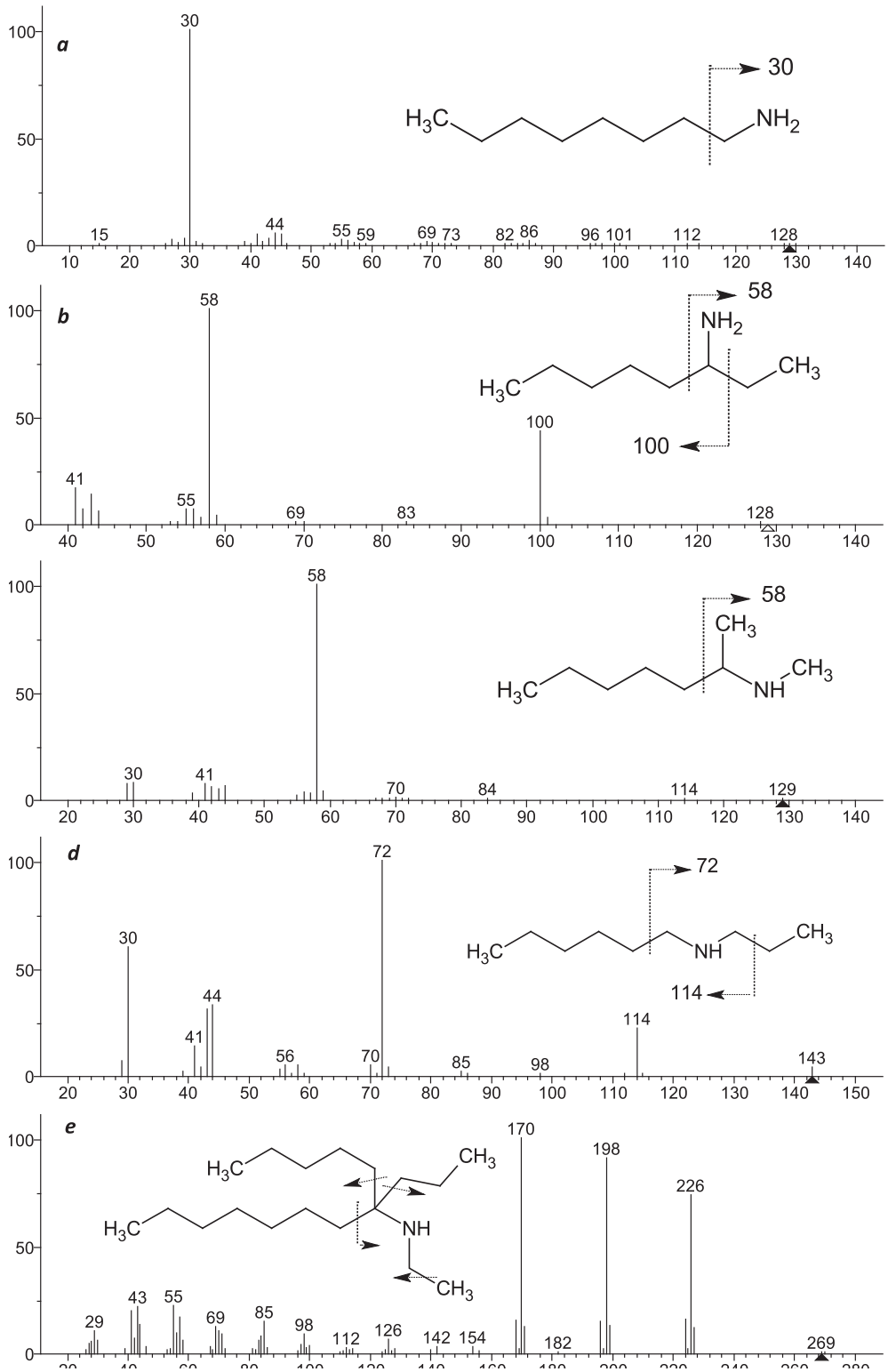

FIG. 35. Mass spectra [m/z (relative abundance, %)] of *n*-octylamine (a), 1-ethyl-*N*-(*n*-hexyl)amine (b), *N*,α-di(methyl)(*n*-hexyl)amine (c), *N*-(*n*-propyl)-*N*-(*n*-hexyl)amine (d), and *N*-ethyl-*N*-(1-*n*-pentyl-1-*n*-propyloctyl)amine (e).

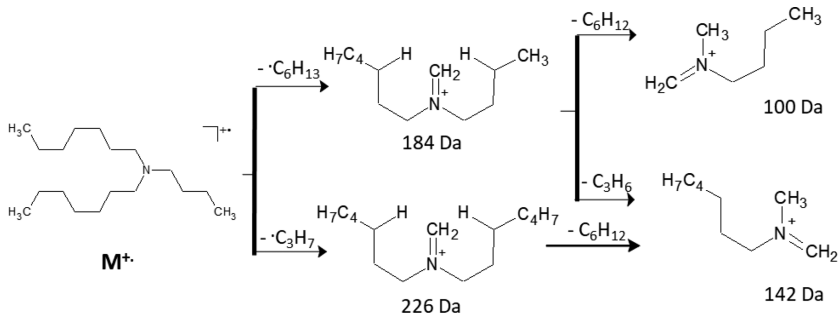

SCHEME 51. McLafferty-like rearrangement in ammonium ions generated from $M^{+\cdot}$ of *n*-butyl(di-*n*-heptyl)amine.

hydrogen atom from either alkyl substituents. Peaks of the expected $[C_3H_7N(CH_2)NO]^+$ (101 Da) EE and $[C_5H_{11}N(CH_2)NO]^+$ (129 Da) EE ions that are generated via β-cleavages in alkyl chains show noticeable intensities in the case of *N*-*n*-propyl-*N*-*n*-pentylnitrosamine [Fig. 37(a), Scheme 55]. The corresponding ions further eliminate nitroxyl groups, giving rise to prominent $[C_3H_5N(CH_2)H]^+$ (70 Da) EE and $[C_5H_9N(CH_2)H]^+$ (98 Da) EE ions. Highly abundant hydrocarbon ions are common to the spectra of alkylnitrosamines.

8.1.2.4. Nitroamines. Nitramide is the parent inorganic compound for nitroamines, the known explosives, which can be thermally labile. These compounds demonstrate noticeable $M^{+\cdot}$ that can easily lose oxygen and undergo β-cleavages in alkyl chains. Elimination of nitrogen dioxide occurs at various stages of dissociation of a molecule. One of the most abundant ions in the spectra is due to di(methylene)ammonium $[N(CH_2)_2]^+$ (42 Da) EE ions. As an example, typical fragmentation pathways are presented for di(*n*-propyl)nitramine in Scheme 56. It indicates preferable β-cleavage (formation of $[M\text{-}C_2H_5]^+$ (117 Da) EE ions) followed by the loss of nitrogen dioxide or nitrous acid and generation of $[M\text{-}C_2H_5\text{-}NO_2]^{+\cdot}$ (71 Da) OE and $[M\text{-}C_2H_5\text{-}HNO_2]^+$ (70 Da) EE ions; further elimination of the remaining alkyl radicals as alkene neutrals produces $[N(CH_2)_2]^+$ (42 Da) EE and $[HN(CH_2)_2]^{+\cdot}$ (43 Da) OE ions (Scheme 56). These very specific dissociation patterns of dialkylnitramines are diagnostically important for structure elucidation.

8.1.2.5. N-Trialkylsilyl amines. The use of silyl derivatives for blocking the amino function is a common practice to increase volatility and, hence, improve the GC properties of amines. On the other hand, from an analytical point of view, the mass spectra of trimethylsilyl derivatives allow reliable determination of molecular weight via mass values of $M^{+\cdot}$ and/or $[M\text{-}CH_3]^+$ ions [Figs. 37(b) and 37(c)]. Additionally, ions generated via the β-cleavage provide information on branching at carbon connected to nitrogen. Thus, the $[CH_2{=}NHSi(CH_3)_3]^+$ (102 Da) EE ion is the most abundant in the case of 2-ethylbutylamine [Fig. 37(b)], while the peak of the homologous $[CH(CH_3){=}NHSi(CH_3)_3]^+$ EE ion at 116 is the base peak in the spectrum of *N*-TMS-2-octylamine that contains methyl substituent at α-carbon.

8.1.2.6. N-Acyl amines. Acylation is another approach for improving the GC properties of amines and reliable determination of their molecular formula. Mass spectra of *N*-acetyl and *N*-trifluoroacetyl derivatives of *n*-butyl and sec-butyl amines, which are depicted in Figs. 37(d) and 37(e), are informative. They demonstrate $M^{+\cdot}$ and peaks of ions due to simple carbon–carbon bond cleavages. Similar to alkanes, the peaks of ions generated by alkyl chain scissions at branching are outstanding in the spectra. The relative intensities of these ions can be successfully used for the determination of the alkyl chain, as shown in Table 6. Thus, the most outstanding $[M\text{-}C_2H_5]^+$ (140 Da) EE ion in the case of *N*-trifluoroacetylbutylamine [Fig. 37(e)] is generated via β-cleavage in $M^{+\cdot}$; *N*-acetylbutylamine [Fig. 37(d)] produces two ammonium $[M\text{-}C_3H_7]^+$ (71 Da) EE and $[M\text{-}C_3H_7\text{-}CH_2CO]^+$ (30 Da) EE ions. The first decomposition reaction involves β-cleavage in the alkyl group, whereas the formation of the second ion encompasses the β-cleavage and loss a ketene neutral from the *N*-acetyl moiety. Note that the loss of the trifluoroacetyl moiety is not observed for trifluoroacetyl derivatives.

8.2. Hydrazines, diazenes, and azoxyalkanes

8.2.1. Hydrazines

Alkylhydrazines can be grouped depending on the degree of substitution, such as mono-substituted, symmetrically disubstituted, asymmetrically disubstituted, and tri- and tetra-substituted aliphatic hydrazines. All of them produce rather stable molecular ions due to charge delocalization at the hydrazine function that contains a lone electron pair on each nitrogen. The scission of the weakened N–N single bond is not observed in the spectra of alkylhydrazines, and the dissociation of their $M^{+\cdot}$ proceeds similar to amines along with some disparities. As shown in Scheme 57, α- (route *b*) and β-cleavages (route *a*) relative to the hydrazine function are two major fragmentation directions leading to the most abundant ions. Cleavage of the N–N-bond (route *c*) is characteristic for symmetrical dialkylhydrazines. This type of cleavage in the case of 1,2-di(*n*-butyl)hydrazine and 1,2-di(sec-butyl)hydrazine generates detectable $[M\text{-}N(H)C_4H_9]^+$ (72 Da) EE ions [Figs. 38(b) and 38(c)]. Route *b* is characteristic for mono-substituted and symmetrically and asymmetrically disubstituted hydrazines, and often, the peaks of the generated $[M\text{-}R^1]^+$ ammonium-type EE ions (Scheme 57) are of maximum intensity in the spectra. This type of cleavage produces $[M\text{-}C_3H_7]^+$ (101 Da) EE ions in the case of 1,1- and 1,2-dibutylhydrazines [Figs. 38(a) and 38(b)] and $[M\text{-}C_2H_5]^+$ (115 Da) EE ions for di(sec-butyl)hydrazine [Fig. 38(c)] containing a methyl substituent at α-carbon. These ($[M\text{-}R^1]^+$) ions further eliminate ammonia neutral in the case of mono(alkyl) and 1,1-dialkylhydrazines [route *a*(1) in Scheme 57],

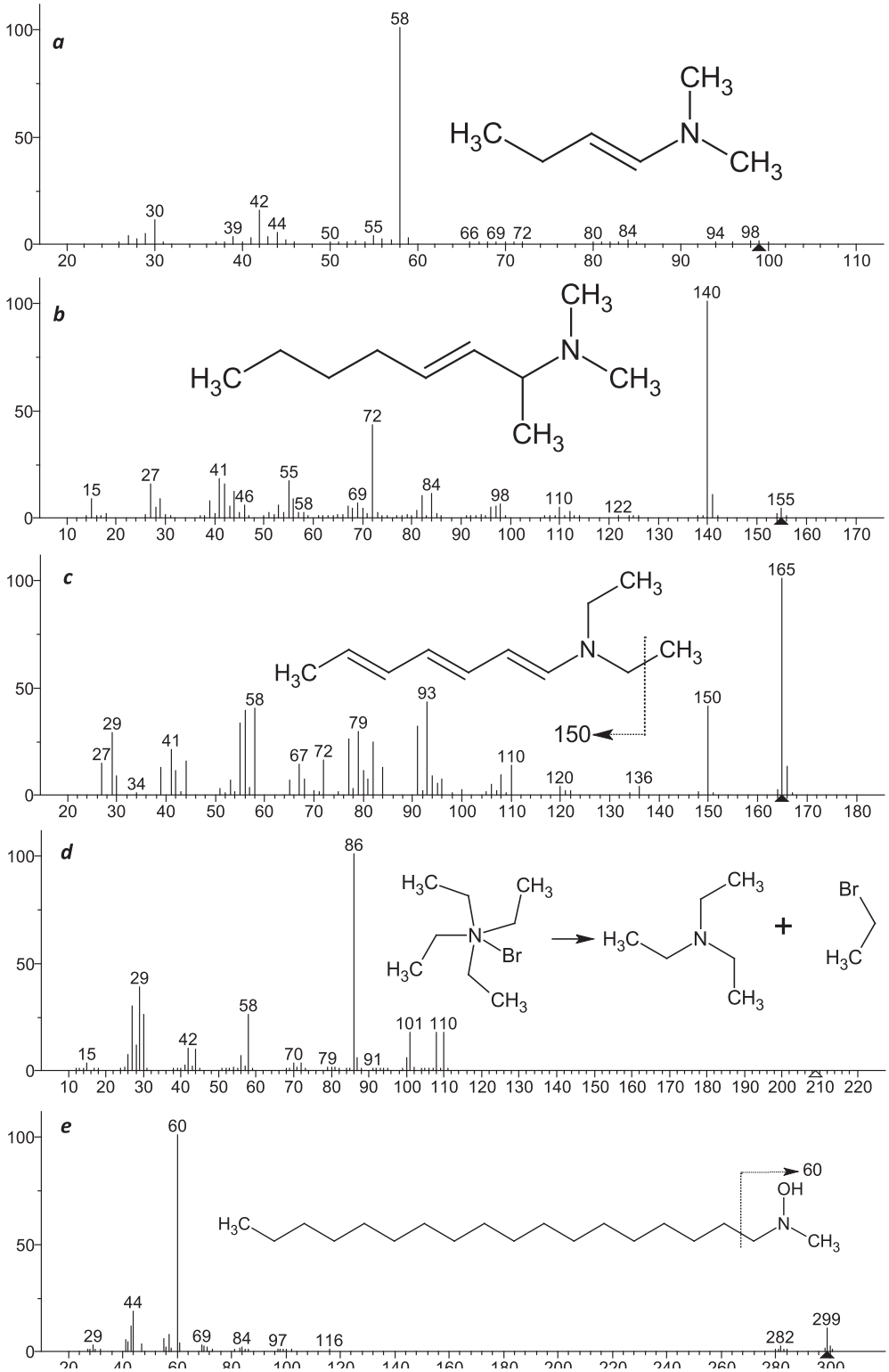

FIG. 36. Mass spectra [m/z (relative abundance, %)] of *N*,*N*-dimethyl-1-butenylamine (a), α,*N*,*N*-trimethyl-2-heptenylamine (b), *N*,*N*-diethyl(hept-1,3,5-trienyl)amine (c), products of dequaternization of tetraethylammonium bromide (d), and *N*-methyl-*N*-(*n*-octadecyl)hydroxylamine (e).

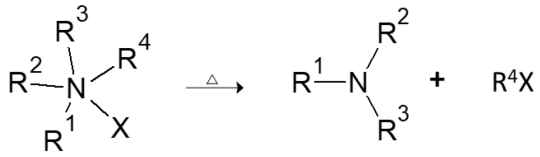

R^1, R^2, R^3, R^4 = H, C_nH_{2n+1}
X = Cl, Br, I, ClO_4, PF_6, $HPO_3C_nH_{2n+1}$, BF_4

SCHEME 52. Thermal decomposition of quaternary ammonium salts.

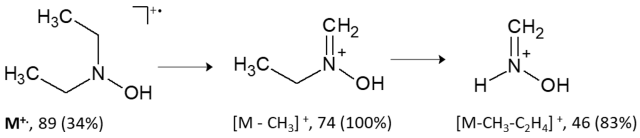

$M^{+\cdot}$, 89 (34%) [M - CH_3]$^+$, 74 (100%) [M-CH_3-C_2H_4]$^+$, 46 (83%)

SCHEME 53. Major dissociation pathway of *N*,*N*-di(ethyl)hydroxylamine.

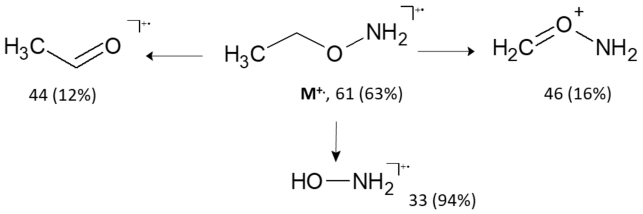

44 (12%) $M^{+\cdot}$, 61 (63%) 46 (16%) 33 (94%)

SCHEME 54. Major dissociation pathways of ionized *O*-ethoxyamine.

as demonstrated by the spectrum of 1,1-dibutylhydrazine: formation of the [M-C_3H_7-NH_3]$^+$ (84 Da) EE ion [Fig. 38(a)]. Both 1,1- and 1,2-dialkylhydrazines expel the remaining alkyl as an alkene neutral from [M-R^1]$^+$ ions [route *a*(2) in Scheme 57]; the corresponding [M-C_3H_7-C_4H_8]$^+$ (45 Da) EE ion peaks are prominent in the spectra of 1,1- and 1,2-dibutylhydrazines [Fig. 38(a) and 38(b)], and the [M-C_2H_5-C_4H_8]$^+$ (59 Da) EE ion is rather abundant in the case of 1,2-di(sec-butyl)hydrazine [Fig. 38(c)]. These differences can be utilized for unambiguous differentiation of isomers.

The probability of α-cleavage (route *b* in Scheme 57) becomes higher with the increase in the degree of substitution; the introduction of substituents at α-carbon also increases this probability. For instance, in the case of dimethylheptylhydrazine [Fig. 38(d)], the base peak corresponds to the [HNN(CH_3)$_2$]$^+$ (59 Da) EE ion (route *b* in Scheme 57). The same type [HNN(H)C_4H_9]$^+$ (87 Da) EE ion shows 16% intensity in the spectrum of di(sec-butyl)hydrazine [Fig. 38(c)] and does not exceed 1% relative in the spectra of di(*n*-butyl)hydrazine [Fig. 38(b)].

Similarly, the degree of substitution, the position of substituents, and the nature of alkenyl substituents determine the selection of the fragmentation direction among available competing pathways for alkenyl hydrazines. For example, allylhydrazine demonstrates multiple dissociation pathways under EI, such as generation of [M-H]$^+$, [M-NH_2]$^+$, [M-NH_3]$^{+\cdot}$, [M-C_2H_3]$^+$, and [C_3H_5]$^+$ ions, and the spectrum displays the base peak of the hydrazine [NH_2NH]$^+$ (31 Da) EE ion. The mass spectrum of di(allyl)hydrazine is less complicated and contains [M-C_2H_3]$^+$, [M-C_3H_5]$^+$, and [M-C_2H_3-C_2H_5]$^+$ ion peaks together with the base [C_3H_5]$^+$ (41 Da) EE ion peak. Finally, the spectrum of tri(allyl)hydrazine is very simple; it demonstrates rather stable ions of $M^{+\cdot}$ and [M-C_3H_5]$^+$ and the base peak of the [C_3H_5]$^+$ (41 Da) EE ion [Fig. 38(e)].

8.2.2. Diazenes and azoxyalkanes

Under EI, dimethyldiazene produces a predictable spectrum. It shows $M^{+\cdot}$, [M-H]$^+$, [M-CH_3]$^+$, [M-2CH_3]$^{+\cdot}$, and [CH_3]$^+$ ion peaks [Fig. 39(a)]. This dissociation tendency remains the same for homologs with a larger alkyl chain or the presence of branching. However, molecular ions sometimes may not be present. For example, the peak of the heaviest ion in the spectrum of di(*tert*-butyl)diazene corresponds to [M-CH_3]$^+$ EE ions.

The *N*-oxide of dimethyldiazene demonstrates a spectrum that can be utilized for structure confirmation. Its rather stable $M^{+\cdot}$ undergoes simple bond cleavages and generates noticeable [M-H]$^+$ and prominent [M-CH_3]$^+$ ions [Fig. 39(b)]. Hydrogen shift is involved in the formation of [M-OH]$^+$ (57 Da) EE ions, which is the base peak in the spectrum. Abundant [NO]$^+$ ions can be a product of a rearrangement reaction as well as of a deep fragmentation process.

8.3. Diazoalkanes and azides

8.3.1. Diazoalkanes

The primary loss of the nitrogen molecule is characteristic for all known diazo compounds. For example, this reaction gives rise to the base peaks of [CH_2]$^{+\cdot}$ (14 Da) OE ions in the spectrum of diazomethane(CH_2N_2). Its homolog—[C_2H_4]$^{+\cdot}$ OE ion—shows maximum intensity at m/z 28 in the spectrum of diazoethane [Fig. 39(c)]; in the latter, noticeable peaks of [M-H]$^+$ and [M-CH_3]$^+$ EE ions are also observed.

8.3.2. Azides

Only azides of lower alkanes produce noticeable $M^{+\cdot}$. No $M^{+\cdot}$ are observed in the spectra of higher azides starting from 1-azidooctane. The main characteristic dissociation pathway for alkyl azides generates [M-N_2H]$^+$ ions that may be used for the identification of molecular weight of alkyl and alkenyl azides; see [M-N_2H]$^+$ (112 Da) EE ions in the case of 4-azidoheptane [Fig. 39(d)] and [M-N_2H]$^+$ (54 Da) EE ions in the case of 3-azidopropene [Fig. 39(e)]. The spectra also contain a number of [M-C_nH_{2n+1}]$^+$, [C_nH_{2n+1}]$^+$, and [C_nH_{2n-1}]$^+$ ions. However, detection of these ions may not provide reliable information regarding the structure of alkyl chains.

8.4. Cyanides and isocyanides

Alkylcyanides and isocyanides reveal noticeable $M^{+\cdot}$ peaks only for lower representatives. In the spectra of long chain alkylcyanides and isocyanides, this peak may not be present. The presence of peaks of [M-H]$^+$ and [M+H]$^+$ EE ions in the spectra are helpful for the determination of molecular ions.

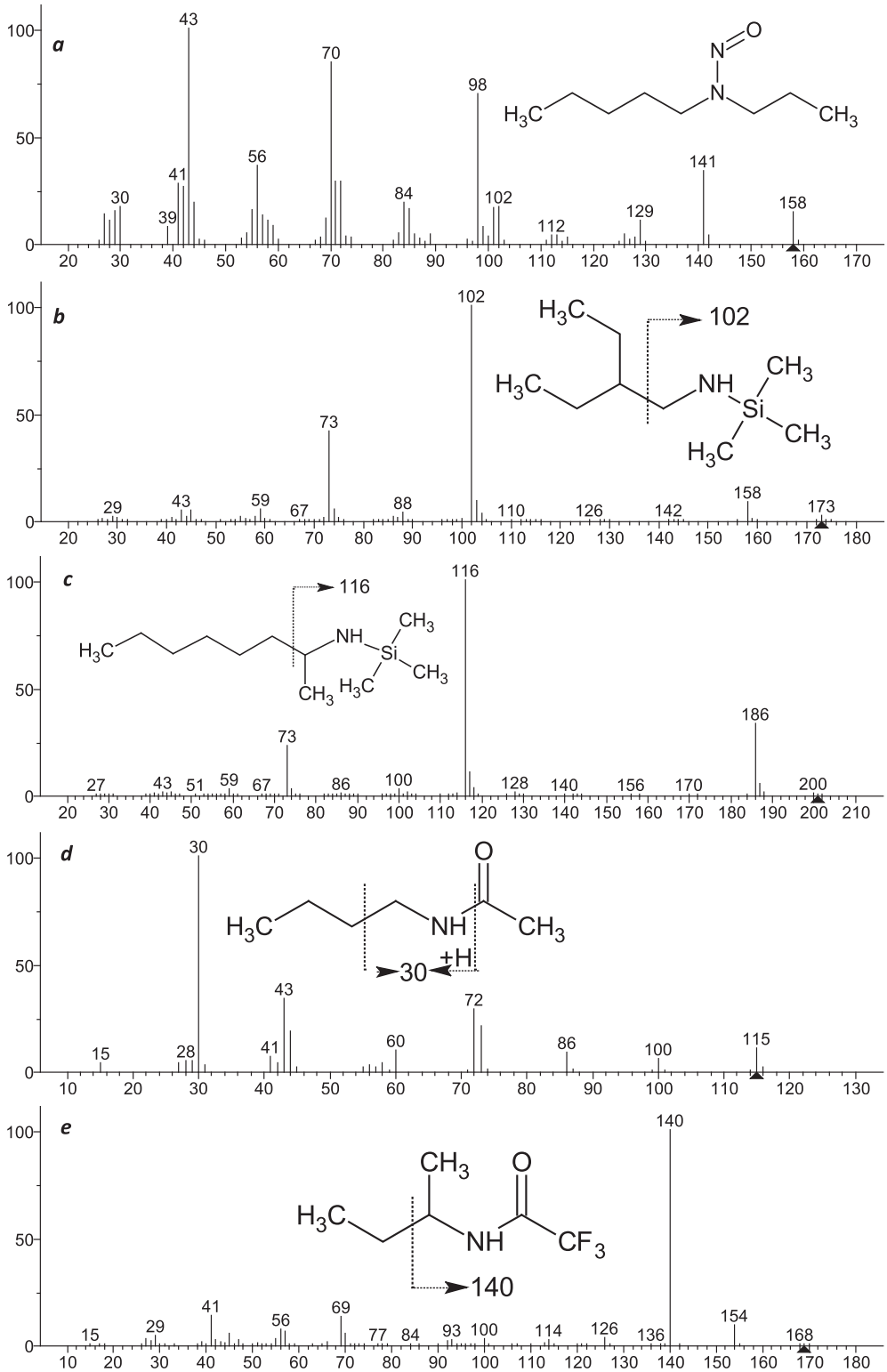

FIG. 37. Mass spectra [m/z (relative abundance, %)] of *N*-nitroso-*N*-(*n*-propyl)-*N*-(*n*-pentyl)amine (a), *N*-TMS 2-ethylbutylamine (b), *N*-TMS, 1-methylheptylamine (c), *N*-acetylbutylamine (d), and *N*-trifluoroacetyl-*sec*-butylamine (e).

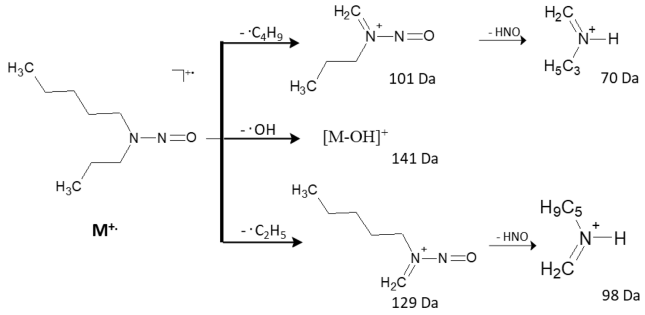

SCHEME 55. Major fragmentation pathways of the ionized *N*-*n*-propyl-*N*-*n*-pentylnitrosamine.

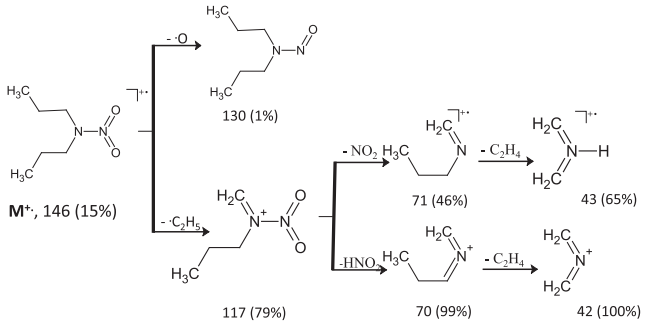

SCHEME 56. Dissociation of molecular ions of di(*n*-propyl)nitramine.

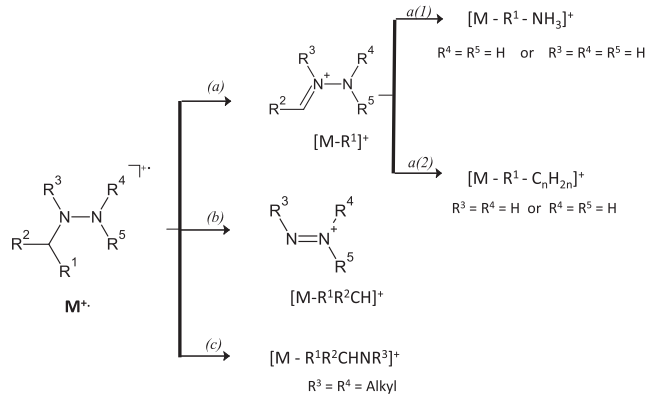

SCHEME 57. Characteristic fragmentation pathways of molecular ions of symmetrically and asymmetrically substituted mono-, di-, tri-, and tetra(alkyl) hydrazines.

8.4.1. Alkylcyanides

Major fragmentation of alkylcyanides may be considered using an example of *n*-dodecylnitrile [Fig. 40(a)]. The lower mass region (m/z 12–71) of the spectrum is mostly populated by $[C_mH_{2m-2}]^{+\cdot}$, $[C_mH_{2m-1}]^+$, and $[C_mH_{2m+1}]^+$ hydrocarbon ions; the first two are isobaric with the ion series $[C_nH_{2n-2}N]^+$ and $[C_nH_{2n-1}N]^{+\cdot}$ that are principal for alkyl cyanides. Among others, the mass spectrum of *n*-dodecylnitrile [Fig. 40(a)] shows a noticeable peak of the $[C_2H_4CN]^+$ (54 Da) EE ion that is the principal ion with diagnostic power. This ion peak can be found in the spectra of *n*-hexanenitrile to *n*-nonadecanenitrile with 15%–80% rel. peak intensities.

Most of the ions in the high (m/z 78–182) mass region correspond to the $[C_mH_{2m}CN]^+$ EE ions originating from simple carbon–carbon bond cleavages in the alkyl chain. However, elevated intensities are observed for peaks with odd mass numbers at m/z 83, m/z 97, and m/z 111, which are generated via hydrogen rearrangements. The same triplet of peaks with similar intensity ratios is present in the spectra of higher alkanenitriles. In many cases, starting from dodecanenitrile, the peak at m/z 97 becomes the base peak in the spectra.

The lowest alkanenitriles display simple mass spectra. For example, acetonitrile produces stable $M^{+\cdot}$ and ions due to consecutive loss of hydrogens. $M^{+\cdot}$ of propionitrile generates abundant ethylene OE ions along with $[CN]^+$, $[HCN]^{+\cdot}$, and $[M\text{-}H_n]^+$ (n = 1–5) ions.

Starting from butanenitrile [Fig. 40(b)], $[CH_2{=}C{=}NH]^+$ (41 Da) EE ions become characteristic with diagnostic power. These ions are represented by the base peaks in the spectra of homologous C_4H_7N–$C_{11}H_{21}N$ *n*-alkanenitriles. McLafferty-type rearrangement is responsible for the formation of the $[CH_2{=}C{=}NH]^+$ EE ions (Scheme 58).

TABLE 6. Elimination of alkyl radicals from $M^{+\cdot}$ of acetyl and trifluoroacetyl derivatives of isomeric butylamines $[C_nH_{2n+1}CH(R)NC(O)CX_3$, R = H, CH_3; X = H, F]

Derivative of butylamines		m/z (%, relative intensity)				
		$M^{+\cdot}$	$[M\text{-}CH_3]^+$	$[M\text{-}C_2H_5]^+$	$[M\text{-}C_3H_7]^+$	$[CHR{=}NH_2]^+$
Acetate	*n*-butyl	115(11)	100(6)	86(9)	72(29)	30(100)
	sec-butyl	115(6)	100(1)	86(30)	72(3)	44(100)
	isobutyl	115(11)	100(12)	86(0.6)	72(31)	30(100)
Trifluoroacetate	*n*-butyl	169(0.1)	154(2)	140(12)	126(100)	30(Trace)
	sec-butyl	169(0.3)	154(10)	140(100)	126(3)	44(Trace)
	isobutyl	169(0.5)	154(9)	140(0.4)	126(61)	30(Trace)

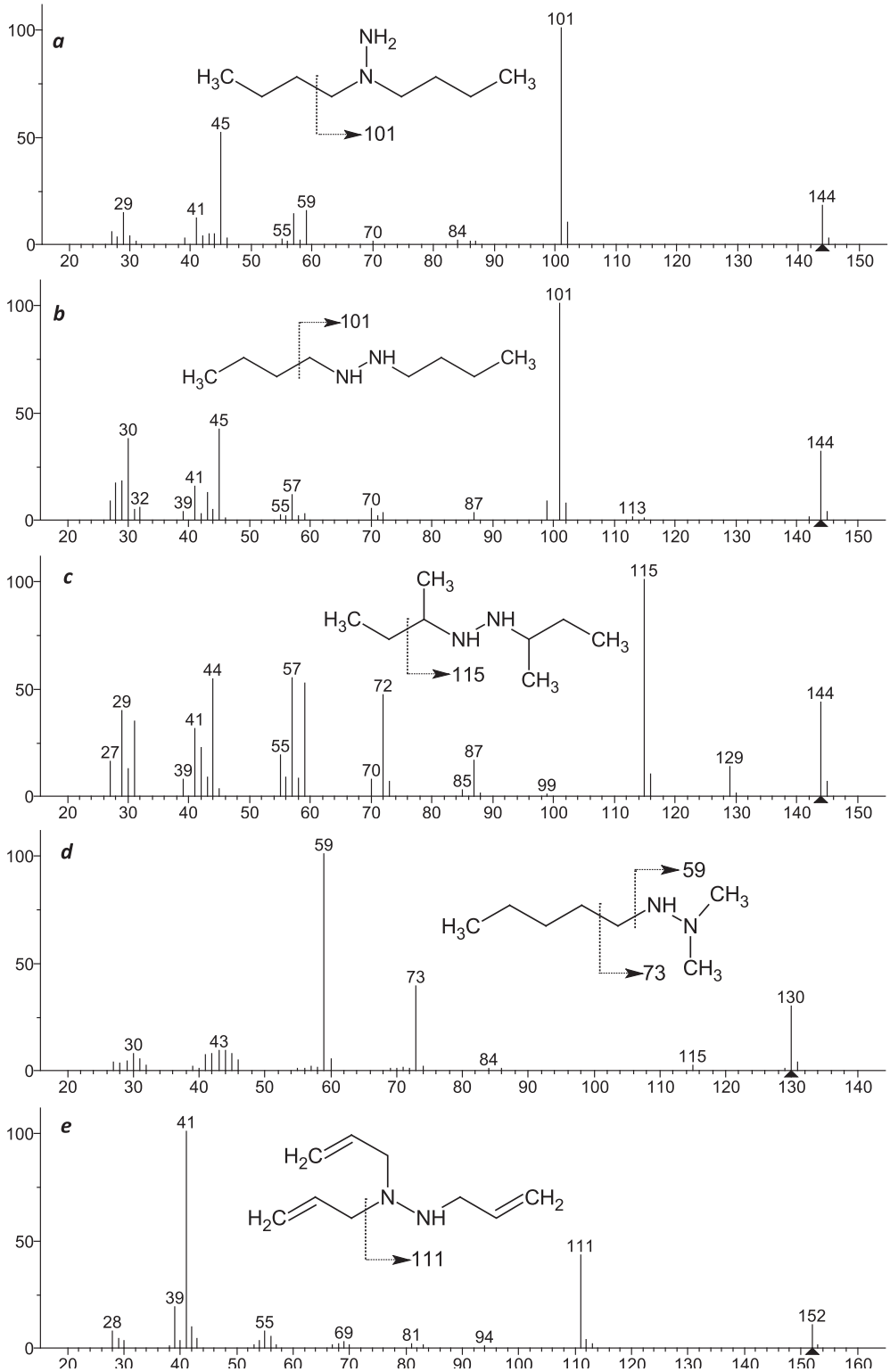

FIG. 38. Mass spectra [m/z (relative abundance, %)] of 1,1-di(*n*-butyl)hydrazine (a), 1,2-di(*n*-butyl)hydrazine, 1,2-di(sec-butyl)hydrazine (c), 1,1-dimethyl-2-(*n*-pentyl) hydrazine (d), and tri(allyl)hydrazine (e).

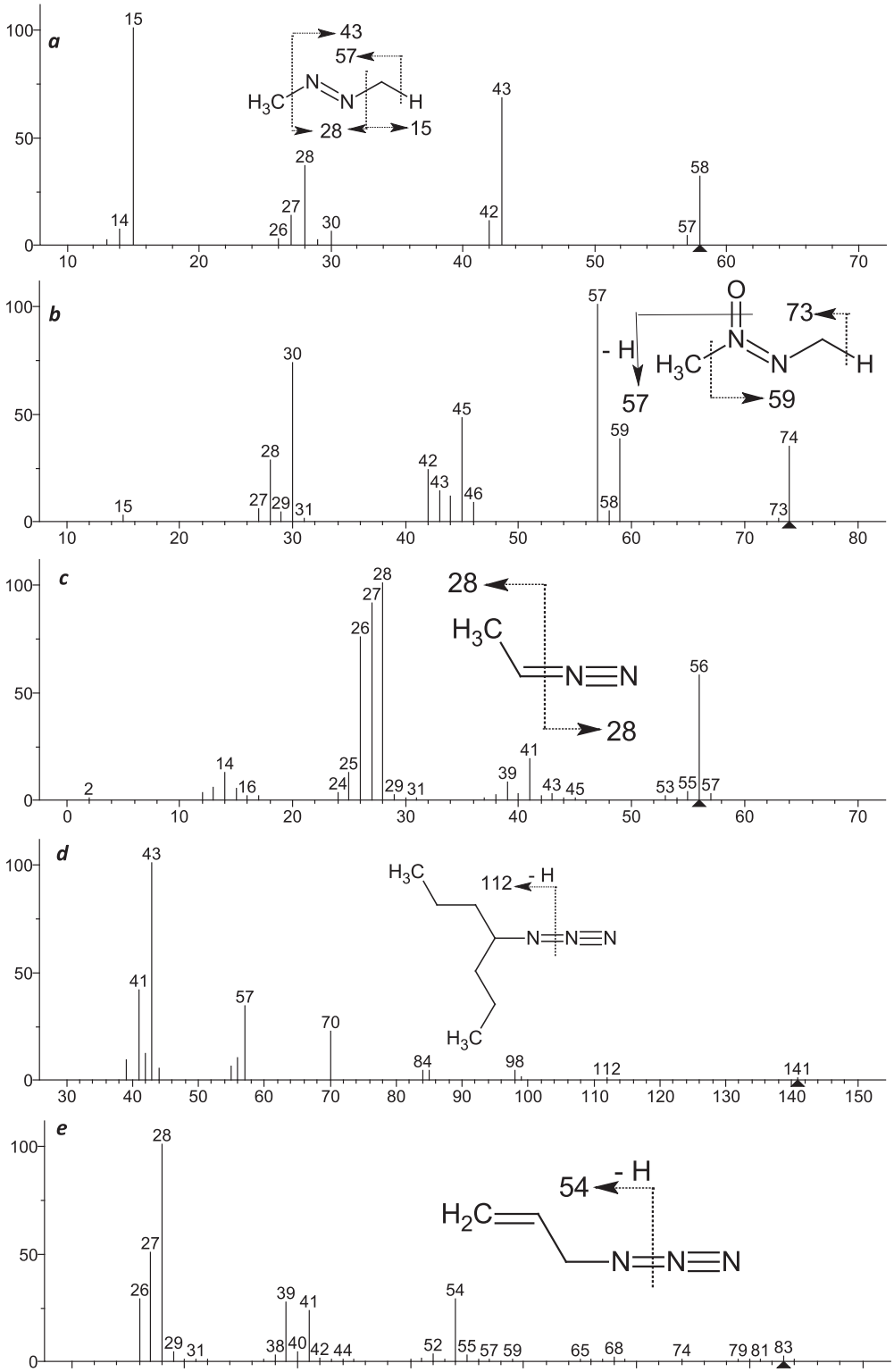

FIG. 39. Mass spectra [m/z (relative abundance, %)] of dimethyl diazine (a), dimethyl diazine-*N*-oxide (b), diazoethane (c), 4-azidoheptane (d), and 3-azidopropene (e).

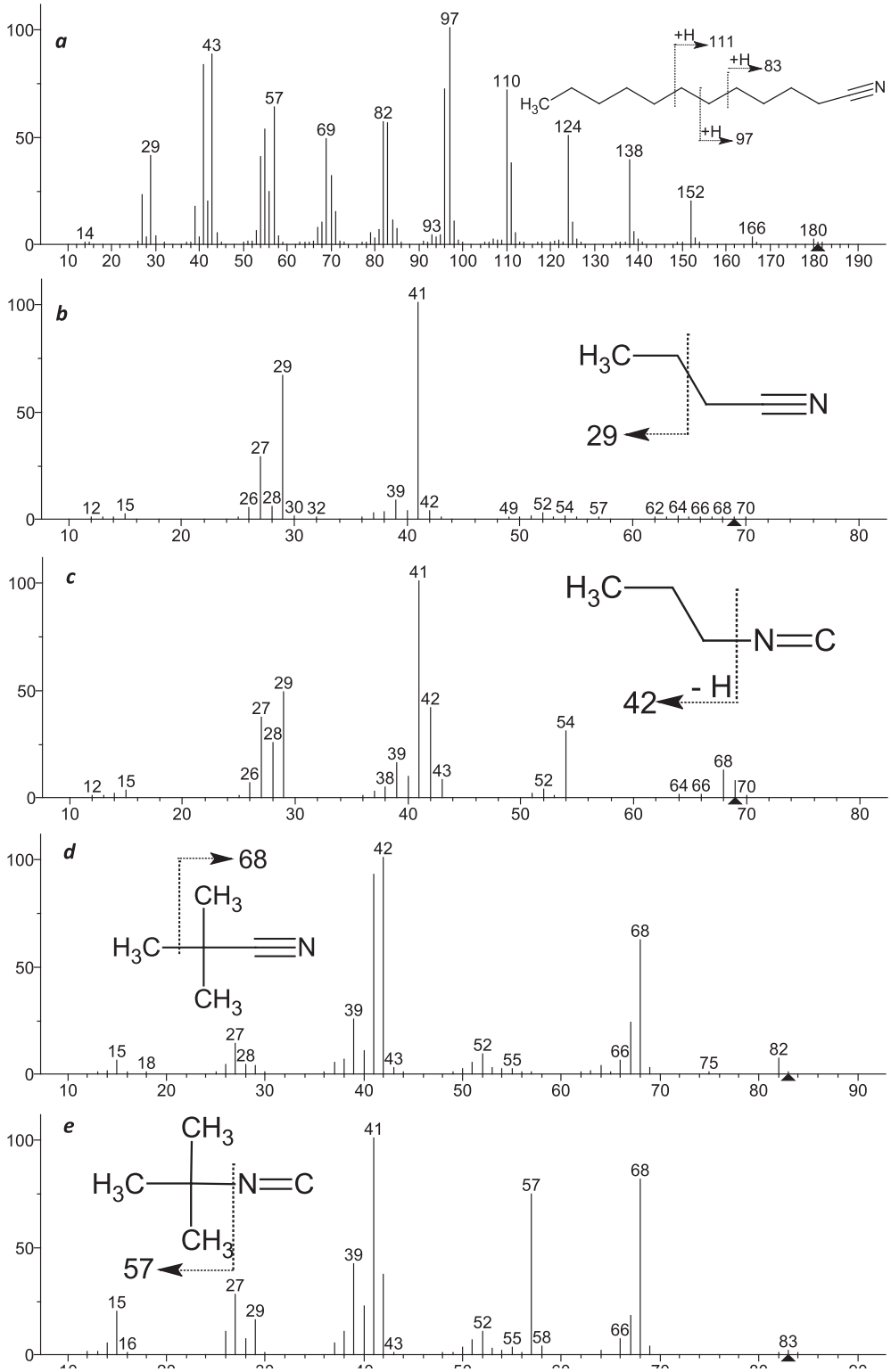

FIG. 40. Mass spectra [m/z (relative abundance, %)] of *n*-dodecaneniitrile (a), *n*-butanenitrile (b), 1-isocyanopropane (c), 2,2-dimethylpropanenitrile (d), and 2-isocyano-2-methylpropane (e).

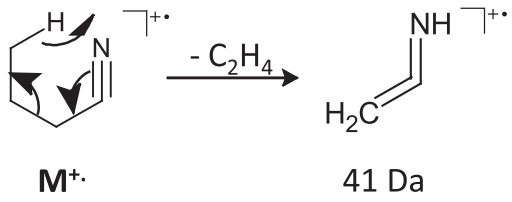

SCHEME 58. McLafferty rearrangement in $M^{+\cdot}$ of butanenitrile.

8.4.2. Alkaneisocyanides

Generally, the dissociation patterns observed for alkaneisocyanides are close to those of isomeric alkanecyanides. There are qualitative, sometimes strong, differences in the spectra that is explained by the differences in bond energies for $C_{(alkyl)}$–$C_{(\equiv N)}$ and $C_{(alkyl)}$–$N_{(\equiv C)}$ bonds.

Unlike higher alkanenitriles and isonitriles, the mass spectra of lower representatives of this class of isomers may display characteristic spectra that can be used for structure determination and differentiation of cyanides and isocyanides. Thus, mass spectra of butanenitrile [Fig. 40(b)] and isocyanopropane [Fig. 40(c)] show similar spectra. However, the spectrum of isocyanide [Fig. 40(c)] reveals a prominent $[M\text{-}CH_3]^+$ (54 Da) ion along with $[C_3H_5]^+$ (41 Da) EE and $[C_3H_6]^{+\cdot}$ (42 Da) OE ions. These ions are generated via migration of one and two hydrogens, followed by the loss of HCN and H_2CN moieties from $M^{+\cdot}$ of alkyl isocyanides. They have diagnostic power for differentiation of aliphatic cyanides and isocyanides since this type of C–N bond fission is typical for isocyanides, and it is of minor importance in cyano-isomers.

Scission of $C_{(alkyl)}$–$N_{(\equiv C)}$ bonds is made easier with the introduction of a substituent(s) at α-carbon. Thus, ionized *tert*-butyl isocyanide eliminates an isocyano radical [Fig. 40(e)], whereas ionized isocyanide with a longer 1,1-disubstituted alkyl group (such as 1,1,3,3-tetramethylbutyl) mainly expels HCN neutral. Mass spectra of *tert*-butyl cyanide [Fig. 40(d)] and isocyanide [Fig. (40e)] can be used for the estimation of the strength and dissociation of single bonds next to C≡N on N=C. Thus, *tert*-butyl isocyanide readily eliminates an isocyanide radical and generates $[M\text{-}NC]^+$ (57 Da) ions, while the cyanide isomer is unable to remove the cyanide group from the *tert*-butyl moiety.

8.4.3. Alkenecyanides

The location of unsaturation defines the behavior of unsaturated aliphatic cyanides under EI. Lower *N*-alkanenitriles produce stable molecular ions, the intensities of which go down starting from 6-hexanenitrile. At the same time, $[M\text{-}H]^+$ ions become important for the determination of the elemental composition. 2-Alkenenitriles always show much stronger $M^{+\cdot}$, and their abundance is one of the indicators of the β-position of a double bond. Note that alkenecyanides containing substituents at $C_{(2)}$ produce rather stable molecular ions. The spectrum of 2-methyl-5-hexenenitrile in Fig. 41(e) demonstrates this detail well.

The double bond location far enough from the cyano group, such as δ,ε-unsaturation, does not significantly affect major dissociation pathways discussed above for saturated aliphatic cyanides. However, drastic changes are observed for 2-alkenenitriles, and a scission of a single $C_{(alkyl)}$–$C_{(\equiv N)}$ bond between the cyano function and the double bond becomes dominant. This simple cleavage in the case of 2-butenenitrile [Fig. 41(a)] produces the $[M\text{-}CN]^+$ (41 Da) EE ion. In the case of longer alkenyl chains, $[M\text{-}HCN]^{+\cdot}$ (54 Da) OE ions are generated in the case of 2-pentenenitrile [Fig. 41(b)] and 82 Da in the spectrum of its 4,4-dimethyl-analog [Fig. 41(c)].

Note that ionized 3-methyl-2-methylenebutanenitrile containing a methylene group at $C_{(2)}$ demonstrates dissociation patterns that are typical for both alkane cyanide (formation of $[M\text{-}C_3H_6]^+$ (53 Da)) OE ions and 2-alkenecyanide (formation of $[M\text{-}HCN]^{+\cdot}$ (68 Da)) OE ions [Fig. 41(d)].

8.5. Cyanates, isocyanates, thiocyanates, and isothiocyanates

Along with some differences, there are many common features in dissociation pathways of alkyl cyanates (R-OCN), isocyanates (R-N=C=O), thiocyanates (R-SCN), and isothiocyanates (R-N=C=S). The intensities of molecular ions of these compounds are rather high only for the lower homologs; they vary from 100% rel. for methyl isocyanate to trace values in the case of hexyl isocyanate.

8.5.1. Isocyanates and isothiocyanates

Simple β-cleavage in the alkyl chain is a common dissociation pathway for ionized *n*-alkyl isocyanates and isothiocyanates. This process gives rise to $[CH_2NCO]^+$ (56 Da) EE ions [Fig. 42(b)] for isocyanates. The S-analog—$[CH_2NCS]^+$ (72 Da)—EE ions are typical for isothiocyanates [Fig. 42(e) and Scheme 59]. Moreover, γ-, δ-, ε-, and ω-cleavages deliver homologous $[(CH_2)_nNCO]^+$ (70, 84, 98, and 112 Da) EE ions in the case of alkyl isocyanates; usually, peaks at m/z 98 and m/z 112, corresponding to ions generated via δ- and ω-scissions, are the prominent ones in this group. Starting from isocyanates and isothiocyanates with the $C_{(6)}$ *n*-alkyl chain, strong substituted tetrahydropyridine $[C_5H_9NO]^{+\cdot}$ (99 Da) OE and $[C_5H_9NS]^{+\cdot}$ (115 Da) OE ions are generated, respectively [Figs. 42(c) and 42(e); Scheme 59].

The other diagnostically important ions are $[M\text{-}SH]^+$ EE ions for isothiocyanates containing at least five carbons in a contiguous chain; the peak of the corresponding ion ($[M\text{-}SH]^+$, 166 Da) is among the five most prominent peaks in the spectrum of *n*-decyl isothiocyanate [Fig. 42(e)]. A loss of hydroxyl radical from $M^{+\cdot}$ of isocyanates of any type is not observed.

C–N bond cleavage accompanied with hydrogen shift is observed only for ethyl isothiocyanate. As a result, one of the two most abundant $[M\text{-}C_2H_4]^{+\cdot}$ OE ions is produced. This dissociation pathway is unimportant for higher homologs.

Dissociation of ionized unsaturated isothiocyanates strongly depends on the location of a double bond in the alkyl chain. Like alkyl cyanides and isocyanides [Sec. 8.4, Figs. 40(a)–40(e)], unsaturated isothiocyanates may undergo $C_{(alkyl)}$–N bond cleavage with charge localization on the hydrocarbon moiety or the functional group.

For example, ionized 2-butenylisothiocyanate generates $[M\text{-}NCS]^+$ (55 Da) EE butenyl ions appearing as the base peak in the spectrum. The molecular ion of the 3-butenyl isomer produces the $[CH_2NCS]^+$ 72 Da EE ion (100%) due to allylic cleavage, and the $[M\text{-}NCS]^+$ ion peak shows just 24% rel. intensity in the spectrum.

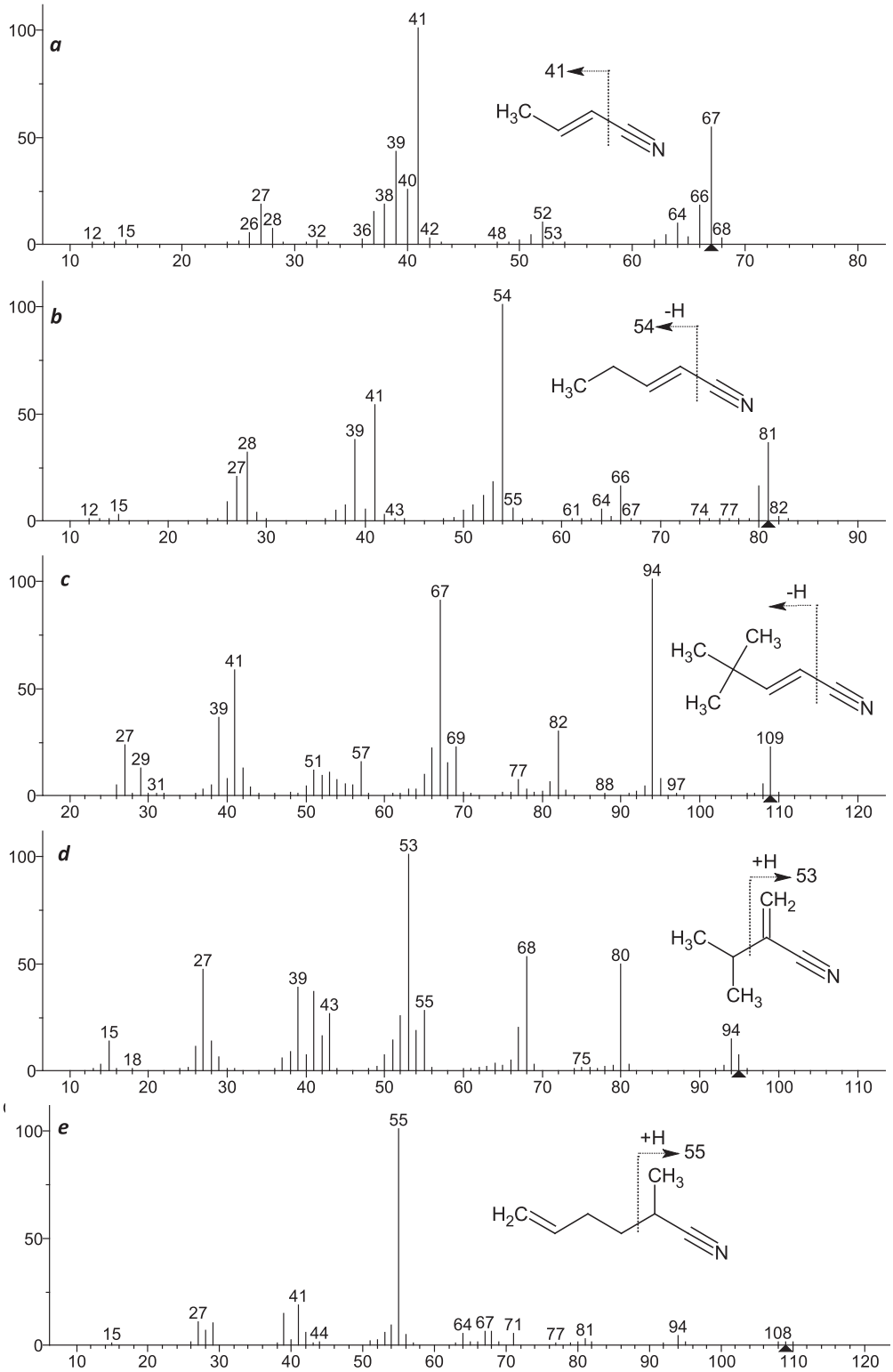

FIG. 41. Mass spectra [m/z (relative abundance, %)] of 2-butenenitrile (a), 2-pentenenitrile (b), 4,4-dimethyl-2-pentenenitrile (c), 3-methyl-2-methylenebutanenitrile (d), and 2-methyl-5-hexenenitrile (e).

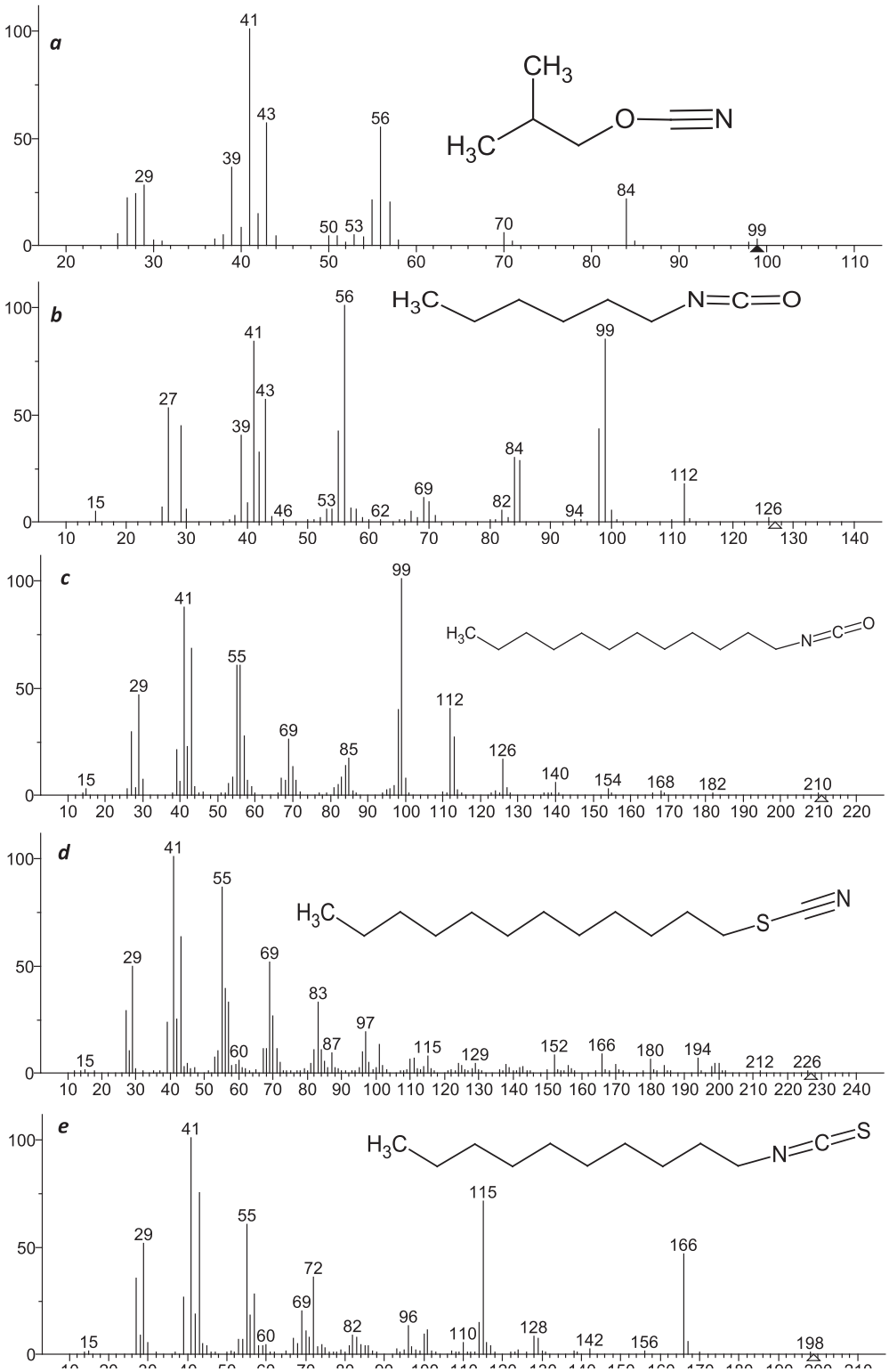

FIG. 42. Mass spectra [m/z (relative abundance, %)] of 2-methylpropyl cyanate (a), *n*-hexyl isocyanate (b), *n*-dodecyl isocyanate (c), *n*-dodecyl thiocyanate (d), and *n*-decyl isothiocyanate (e).

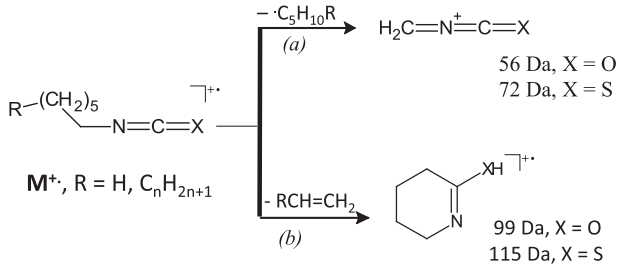

SCHEME 59. Major fragmentation pathways of ionized *n*-alkyl isocyanates and isothiocyanates.

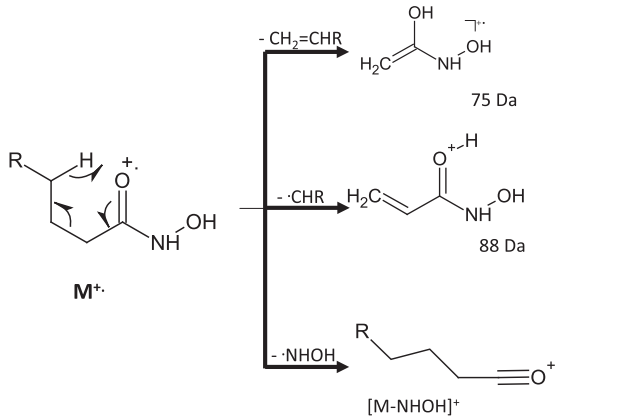

SCHEME 60. Major fragmentation pathways of ionized *O*-alkyl hydroxamic acids.

8.5.2. Cyanates and thiocyanates

The behavior of isomeric alkyl cyanates and isocyanates under EI is quite similar, and the recorded spectra mainly differ quantitively. Only thiocyanates demonstrate the ability to lose hydrogen cyanide from molecular ions. Thus, a peak of the $[M\text{-}HCN]^{+\cdot}$ (99 Da) OE ion in the spectrum of dodecyl thiocyanate shows 4% rel. intensity. The outstanding peaks corresponding to hydrocarbon fragments are present only in the lower mass range, and they are not of interest from an analytical point of view. Abundance of these ions is higher for thiocyanates when compared to isomeric isothiocyanates. Generally, EI spectra of the alkyl thiocyanate are less informative than their isothiocyanate analogs.

8.6. Aliphatic hydroxamic acids

Aliphatic hydroxamic acids produce noticeable molecular ions along with $[M\text{-}H]^+$ and $[M+H]^+$ ions. The loss of a hydroxylamine radical from $M^{+\cdot}$ is common for all of them; $[M\text{-}NHOH]^+$ EE ions are successfully utilized for the final determination of elemental composition of the intact sample. Acids containing γ-hydrogen undergo typical McLafferty rearrangement and β-cleavage and generate $[CH_2{=}C(OH)NHOH]^{+\cdot}$ (75 Da) OE and $[CH_2CHC(OH)NHOH]^{+\cdot}$ (88 Da) EE ions for *O*-*n*-alkyl hydroxamic acids, as shown in Scheme 60.

Peaks of this pair of ions with detectable intensities are present in the spectrum of hexanehydroxamic acid [Fig. 43(a)] as well as in the spectrum of undecenehydroxamic acid containing unsaturation remote from γ-carbon [Fig. 43(b)]. The $[CH_2{=}C(OH)NHOH]^{+\cdot}$ (75 Da) OE ions may further lose an oxygen radical giving rise to $[CH_2{=}C(OH)NH_2]^{+\cdot}$ (59 Da) OE ions. Elimination of a water molecule from $[M\text{-}NHOH]^+$ EE ions is also characteristic for all alkyl hydroxamic acids. However, the abundance of $[M\text{-}NHOH\text{-}H_2O]^+$ sharply increases with the introduction of unsaturation. For example, in the spectrum of undecenehydroxamic acid [Fig. 43(b)], the $[M\text{-}NHOH]^+$ (167 Da) EE and $[M\text{-}NHOH\text{-}H_2O]^+$ (149 Da) EE ions demonstrate similar abundance. Hydrocarbon ions in the spectra of these compounds cannot be used for the determination of the alkyl chain structure.

8.7. Aliphatic nitro compounds

The nitro function cannot afford charge stabilization in aliphatic compounds, and the mass spectra of nitroalkanes are mostly populated by hydrocarbon product ions. Identification of these compounds by MS is difficult because their $M^{+\cdot}$ are non-detectable or absent in most cases with the exception of nitromethane that produces an abundant molecular ion (over 50% rel.). However, some specifics of their dissociation can be successfully used for the determination of selected structural elements.

Elimination of nitrogen dioxide from $M^{+\cdot}$ of nitroalkanes followed by the dissociation of the generated hydrocarbon ions is an important decomposition pathway. The minor fragmentation mode includes sequential loss of hydroxyl radicals and water neutrals from $M^{+\cdot}$ (Scheme 61). Thus, noticeable peaks of $[M\text{-}OH]^+$ (100 Da) EE and $[M\text{-}OH\text{-}H_2O]^+$ (82 Da) EE ions are present in the spectrum of 1-nitropentane [Fig. 43(c)].

McLafferty rearrangement is not typical for nitropropanes. In fact, only a negligible (1%) peak of corresponding $[CH_2{=}N(O)OH]^{+\cdot}$ (61 Da) OE ions is detected in the spectrum of *n*-nitropropane.

Starting from 1-nitrobutane, another rearrangement reaction associated with the shift of two hydrogens becomes prevalent (Scheme 61). The corresponding $[CH_2{=}N(OH)_2]^{+\cdot}$ (62 Da) OE ion is noticeable in the case of 1-nitropentane [Fig. 43(c)].

Unlike primary and secondary nitroalkanes, $M^{+\cdot}$ of tertiary analogs do not lose nitrogen dioxide with the notable exception of nitro-*tert*-butane. Elimination of the elements of nitrous acid from $M^{+\cdot}$ becomes characteristic, and the peak intensities of $[M\text{-}HNO_2]^{+\cdot}$ OE ions in the range of 13%–24% are typical for C_6–C_8 nitroalkanes.

Introduction of unsaturation at α-carbon allows charge delocalization. As a result, primary and secondary nitro alkenes (alkenyl = C_4H_7–$C_{11}H_{21}$) exhibit rather stable molecular ions and a dominant fragmentation mode leading to $[M\text{-}OH]^+$ EE ions [Fig. 43(d)]. However, distancing the nitro function and the unsaturation from each other zeroes out this effect, and the $M^{+\cdot}$ peaks become undetectable or absent in the spectra. At the same time, the $[M\text{-}HNO_2]^+$ ions become more important than $[M\text{-}NO_2]^+$ ions.

It is important to remember that aliphatic nitro compounds under EI do not undergo nitro–nitrito isomerization.

8.8. Alkyl esters of nitrous and nitric acids

8.8.1. Alkyl nitrites

Mass spectra of alkyl esters of nitrous acid usually do not contain $M^{+\cdot}$ peaks except methyl nitrite. Dissociation of ionized nitrite

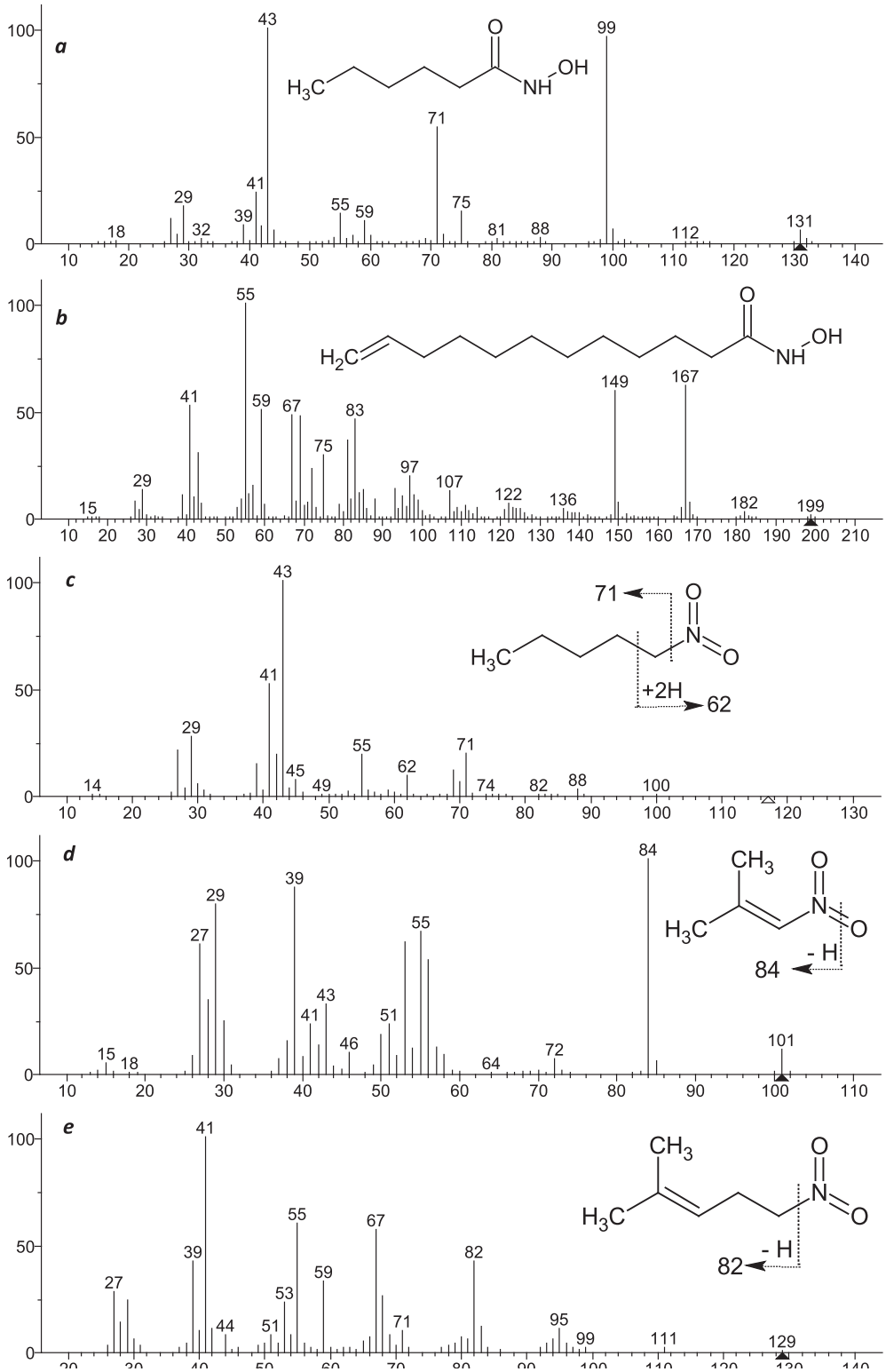

FIG. 43. Mass spectra [m/z (relative abundance, %)] of *n*-hexanehydroxamic acid (a), 10-undecenehydroxamic acid (b), 1-nitro-*n*-pentane (c), 1-nitro-2-methylpropene (d), and 1-nitro-4-methyl-3-pentene.

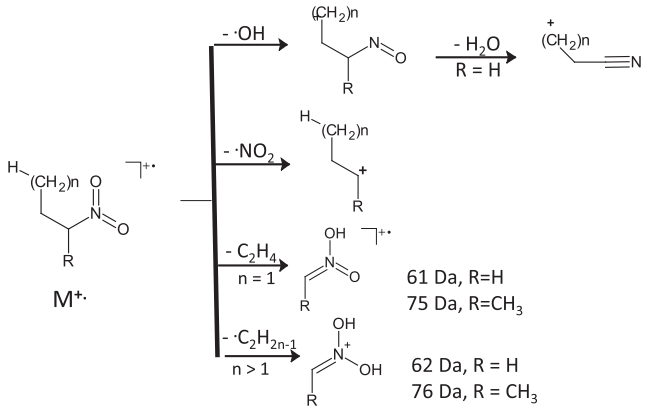

SCHEME 61. Major dissociation pathways of nitroalkanes.

proceeds via parallel cleavages of C–O and C_α–C_β bonds. The simple scission of the ester C–O bond generates alkyl cations, such as the $[C_5H_{11}]^+$ (71 Da) EE ion in the case of isopentyl nitrite [Fig. 44(a)]. The charge can be localized on both parts of nitrite molecules after C_α–C_β bond dissociation: the hydrocarbon part ($[C_4H_9]^+$ ion at 57 Da in Fig. 44(a)) and the acidic function $[CH_2{=}ONO]^+$ (60 Da) EE ion. The latter ion has diagnostic power and its mass value is increased by 14 Da intervals for C_α branched alkyl residues. The other ions with diagnostic power are the ones in the highest mass region of the spectra and correspond to ions $[M\text{-}NO]^+$ and ions due to further loss of hydrogen radicals/molecules. Additionally, a prominent $[NO]^+$ (30 Da) ion peak is present in the spectra; they may be generated by both molecular and product ions.

8.8.2. Alkyl nitrates

Ionized esters of nitric acids readily decompose, and for that reason, $M^{+\cdot}$ peaks in their spectra are usually too small to be detected. Similar to nitrites, C_α–C_β bond dissociation in alkyl esters of nitric acid becomes the major fragmentation mode and yields $[RCH{=}ONO_2]^+$ EE ions. In the case of primary *n*-alkylnitrates, $[CH_2{=}ONO_2]^+$ (76 Da) EE ions are detected [see Figs. 44(b) and 44(d)] and $[CH(CH_3){=}ONO_2]^+$ (90 Da) EE ions in the case of *sec*-pentyl nitrate (secondary nitrate) [R = CH_3; see Fig. 44(c)] (Scheme 62). These ions are always accompanied by the $[NO_2]^+$ (46 Da) EE ion. This pair of ions has diagnostic power for the identification of alkylnitrates among unknowns. Additionally, the composition of alkyl cations generated during C_α–C_β bond cleavage allows the determination of the molecular weight of the initial compound. For example, the sum of masses of (57 + 76 = 133) and (43 + 90 = 133) successfully determines the molecular weight of pentyl nitrates [Figs. 44(b) and 44(d)]. Ions produced at the expense of the $C_{(alkyl)}$–O bond cleavage can provide additional evidence on the structure of alkyl chains in a molecule.

9. Compounds Containing the Main Group VII Elements

9.1. Aliphatic monohalides

The abundance of molecular ions in the spectra of *n*-alkyl halides increases in the series: F < Cl < Br < I. This tendency is explained by the decrease in electronegativity (χ) of these elements in a raw state: F(3.98) > Cl(3.16) > Br(2.96) > I(2.66). $M^{+\cdot}$ abundance also decreases as branching is introduced and as the size of the alkyl is increased. Dissociation of *n*-alkyl halides under EI involves various patterns, including the elimination of halogen and hydrogen halide, alkyl C_α-C_β-, C_δ-C_ε-, and C_ε-C_ζ-bond scissions along with other C–C bond cleavages (Scheme 63). All these pathways are not universal for all halogenated alkanes, but they occur in selected cases. The major dissociation patterns of ionized fluoro-, chloro-, bromo-, and iodo-alkanes largely depend on the nature of the halogen atom, its location in the alkyl chain, and the structure of the carbon skeleton.

9.1.1. Fluoroalkanes

Isotope distribution in ions present in the spectra of monofluoroalkanes is similar to hydrocarbon ions since fluorine is a monoisotopic element and its input is limited. For example, a prediction of the elemental composition of the $[C_3H_6F]^+$ (61 Da) EE ion is impossible just by examination of isotope distribution in a cluster at m/z 61–62 if the structure of the sample is unknown. Preliminary knowledge allows its identification as the $[M\text{-}CH_3]^+$ EE ion with $[C_3H_6F]^+$ composition in the case of 1-fluoro-*tert*-butane [Fig. 45(b)].

Carbon–carbon bond scissions in fluoroalkanes may start from both sides of a carbon skeleton and generate pairs of $[C_nH_{2n+1}]^+$ and $[C_nH_{2n}F]^+$ EE ions. In the case of fluorotetradecane, for example, these pair are $[CH_3]^+$ (15 Da) and $[CH_2F]^+$ (33 Da), $[C_2H_5]^+$ (29 Da) and $[C_2H_4F]^+$ (47 Da), $[C_3H_7]^+$ (43 Da) and $[C_3H_7F]^+$ (61 Da), $[C_4H_9]^+$ (57 Da) and $[C_4H_8F]^+$ (75 Da), $[C_5H_{11}]^+$ (71 Da) and $[C_5H_{10}F]^+$ (89 Da), $[C_6H_{13}]^+$ (85 Da) and $[C_6H_{12}F]^+$ (103 Da), and more [Fig. 45(c)].

Dissociation routes (1)–(4) presented in Scheme 63 are characteristic for fluoroalkanes. However, the preference of each of them depends on the nature of the alkyl chain and on the presence of a substitution at the carbon atom bearing fluorine. For example, the outstanding $[M\text{-}HF]^{+\cdot}$ ion peak is characteristic for 1-fluorobutane [Fig. 45(a)] that contains a short alkyl chain. The abundance of the corresponding ions drastically decreases with the size increase of a carbon skeleton. The $[M\text{-}HF]^{+\cdot}$ (196 Da) OE ion is detectable in the case of 1-fluorotetradecane [Fig. 45(c)]. However, the loss of a fluorine radical rather than hydrogen fluoride becomes more favorable for ionized secondary and tertiary fluorides, such as isopropyl fluoride and *tert*-butyl fluoride. In fact, the abundance of the $[M\text{-}F]^+$ (57 Da) EE ion peak is higher than that of the $[M\text{-}HF]^{+\cdot}$ (56 Da) OE ion in the spectrum of *tert*-butyl fluoride [Fig. 45(b)]. The loss of an alkyl radical at α-carbon becomes the major dissociation pattern for secondary and tertiary fluorides. Thus, $[M\text{-}CH_3]^+$ ion peaks are the most abundant in the spectra of isopropyl and *tert*-butyl fluorides; further elimination of hydrogen fluoride from these ions gives rise to the $[M\text{-}CH_3\text{-}HF]^+$ (41 Da) EE ion in the case of *tert*-butyl fluoride [Fig. 45(b)].

9.1.2. Chloroalkanes

Chlorine-containing ions appear in the spectra as doublet peaks with 2 Da difference and intensity ratios of about 3 to 1 due to the ratio of the natural distribution of ^{35}Cl and ^{37}Cl isotopes (Appendix, Table 7). Lower alkyl chlorides usually produce noticeable molecular ions. In the absence of the $M^{+\cdot}$ peak, the molecular weight of

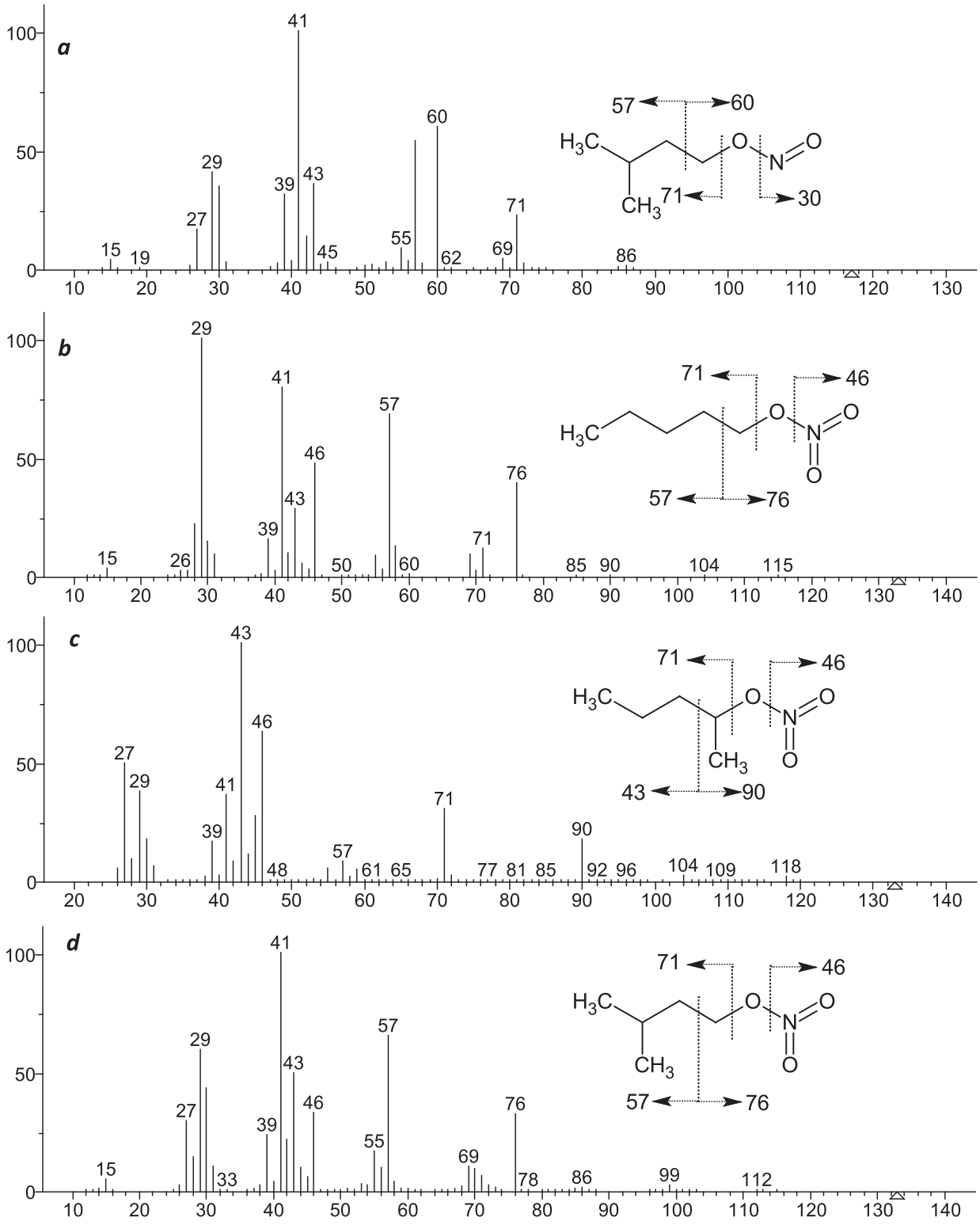

FIG. 44. Mass spectra [m/z (relative abundance, %)] of isopentyl nitrite (a), *n*-pentyl nitrate (b), *sec*-pentyl nitrate (c), and isopentyl nitrate (d).

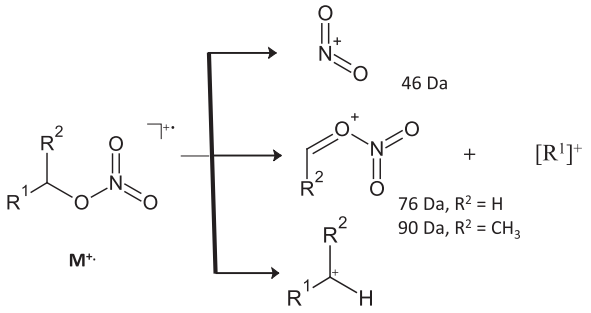

SCHEME 62. General fragmentation patterns of alkyl nitrates.

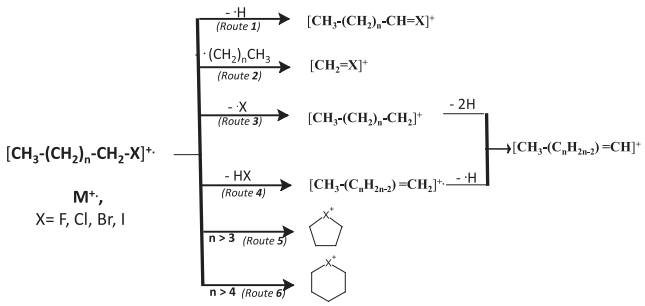

SCHEME 63. Characteristic fragmentation patterns for selected mono-halogenated alkanes.

alkyl chlorides can be determined via mass values of the heaviest $[M\text{-}HCl]^{+\cdot}$ OE ions that typically originate via dehydrochlorination of any ionized 1-chloro-*n*-alkanes (Scheme 63, route 4). The exception is only methyl chloride and partially ethyl chloride that contain both $[M\text{-}Cl]^+$ and $[M\text{-}HCl]^{+\cdot}$ ions in their EI spectra. The erroneous identification of the $[M\text{-}HCl]^{+\cdot}$ OE ion as a molecular ion of an alkene must be avoided since the chloride and the corresponding alkene produce similar mass spectra. In fact, the $[M\text{-}HCl]^{+\cdot}$ ions, which are generated via dehydrochlorination of 1-chloro-*n*-alkanes, further undergo fragmentation giving rise to abundant hydrocarbon ions: $[C_nH_{2n-1}]^+$, $[C_nH_{2n}]^{+\cdot}$, and $[C_nH_{2n+1}]^+$ (mainly n = 3, 4, and 5), which are characteristic of *n*-alkenes. For example, these ions appear as outstanding cluster peaks at m/z 41–43, m/z 55–57, and m/z 69–71 in the spectrum of 1-chlorodecane [Fig. 45(d)]. It should be noted that relative intensities of hydrocarbon ions in the m/z 41–71 mass region reflect the structure of the carbon skeleton as demonstrated by the mass spectrum of 2-chloro-2-methylnonane [Fig. 45(e)].

The closeness of the general picture of the mass spectra of 1-chloroalkanes and corresponding alkenes requires careful analysis of the former in order to detect chlorine-containing fragment ions appearing in the spectra as characteristic doublets.

Chlorolanium (Scheme 63, route 5) and chlorane (Scheme 63, route 6) EE ions are of diagnostic importance for structure determination of any 1-chloro-*n*-alkanes. The chlorolanium $[C_4H_8Cl]^+$ (91/93 Da) EE ion shows prominent peaks in the spectra of chlorides starting from *n*-hexyl chloride, and the chloraan $[C_5H_{10}Cl]^+$ (105/107 Da) EE ion demonstrates noticeable peaks in the spectra starting from *n*-heptyl chloride. These ions are typical for *n*-alkyl chlorides, and they are untraceable in the case of branched alkyl chlorides.

9.1.3. Bromoalkanes

The natural distribution of ^{79}Br and ^{81}Br isotopes in the ratio of about 1:1 is the foundation for the discovery of bromine containing ions because they appear as equal intensity doublet peaks with a mass difference of 2 Da. While the primary alkyl bromides produce noticeable $M^{+\cdot}$, the secondary bromides fail in producing noticeable molecular ions starting from 2-bromoheptane, and no traces of $M^{+\cdot}$ are usually observed in the spectra of tertiary bromides.

Ionized 1-bromo-*n*-alkanes, similar to primary chlorides, generate bromo analogs of chlorolanium and chloraane EE ions starting from 1-bromo-*n*-hexane and *n*-heptane, respectively (Scheme 63, routes 5 and 6). These five-membered ($[C_4H_8Br]^+$ (135/137 Da)) and six-membered ($[C_5H_{10}Br]^+$ (149/151 Da)) EE ions are prominent for 1-bromooctane [Fig. 46(a)]. This fragmentation pattern does not take place in the case of branched 1-bromoalkanes [Fig. 46(c)] and secondary alkyl bromides [Fig. 46(b)].

The loss of a bromine radical from $M^{+\cdot}$ is characteristic for primary 1-bromides of branched alkanes and secondary bromides of alkanes. The $[M\text{-}Br]^+$ EE ion is used for the determination of the elemental composition of a sample and the alkyl residue of a compound under study. Other prominent peaks in the spectra correspond to ions generated via the C–C bond cleavages at branching sites [Figs. 46(b) and 46(c)].

9.1.4. Iodoalkanes

Iodine, like fluorine, is among the 26 mono-isotopic natural elements. All alkyl iodides usually produce noticeable molecular ions that immediately confirms the elemental composition of a sample.

Generation of iodine (127 Da) cations and $[HI]^{+\cdot}$ (128 Da) OE ions is characteristic for lower 1-iodo-*n*-alkanes, and starting from 1-iodo-*n*-hexane, the corresponding peak may gain equal intensity. The formation of $[I]^+$ (127 Da) EE and $[HI]^{+\cdot}$ (128 Da) OE ions is also observed in the case of secondary and tertiary iodides; the corresponding peaks are detectable in the spectrum of a tertiary iodide—2-iodo-2,3-dimethylbutane [Fig. 46(e)]. Molecular ions of primary, secondary, and tertiary lose iodine as a radical from $M^{+\cdot}$ and do not produce $[M\text{-}HI]^{+\cdot}$ OE ions. However, hydrogen iodide can be readily eliminated from $[M\text{-alkyl}]^+$ EE ions generated in the case secondary and tertiary alkyl iodides with *n*- and branched-alkyl chains. For example, the mass spectrum of 2-iodo-2,3-dimethylbutane contains a prominent $[M\text{-}I]^+$ (85 Da) EE ion peak along with the peaks of $[C_5H_9]^+$ (69 Da) EE and $[C_3H_5]^+$ (41 Da) EE ions [Fig. 46(e)]. The latter ions originate from $[M\text{-}CH_3]^+$ and $[M\text{-}C_3H_7]^+$ via the loss of hydrogen iodide (Scheme 64).

9.1.5. Unsaturated alkyl halides

Monoenic, dienic, and acetylenic halides produce detectable molecular ions. General fragmentation patterns of these compounds resemble dissociation of ionized saturated halides. However, the center of unsaturation may direct the dissociation. Some spectra of isomeric chlorohexenes and chlorohexadienes along with chlorohexyne are presented in Fig. 47. Common dissociation of these

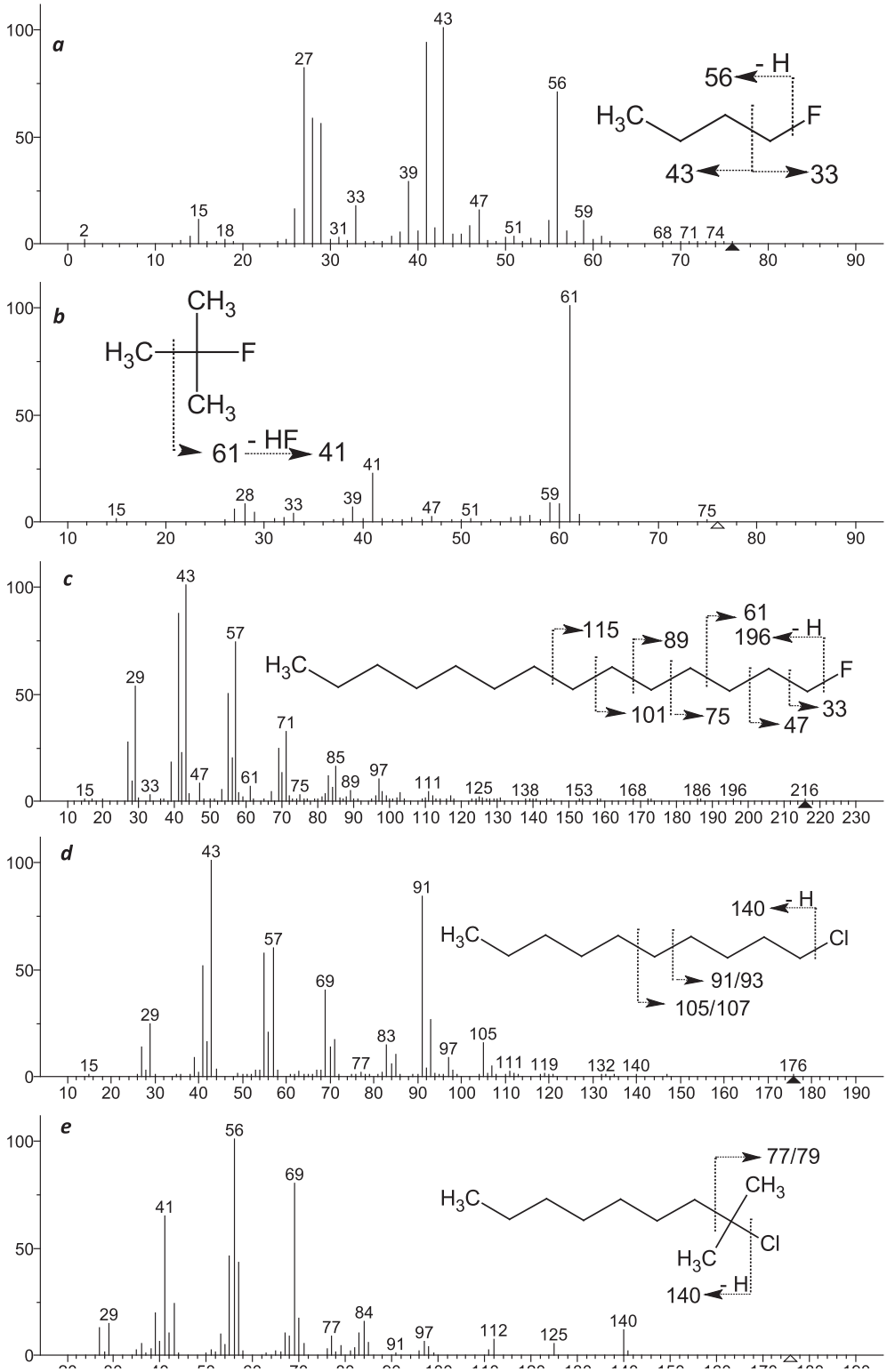

FIG. 45. Mass spectra [m/z (relative abundance, %)] of 1-fluorobutane (a), 2-fluoro-2-methylpropane (b), 1-fluorotetradecane (c), 1-chlorodecane (d), and 2-chloro-2-methylnonane (e).

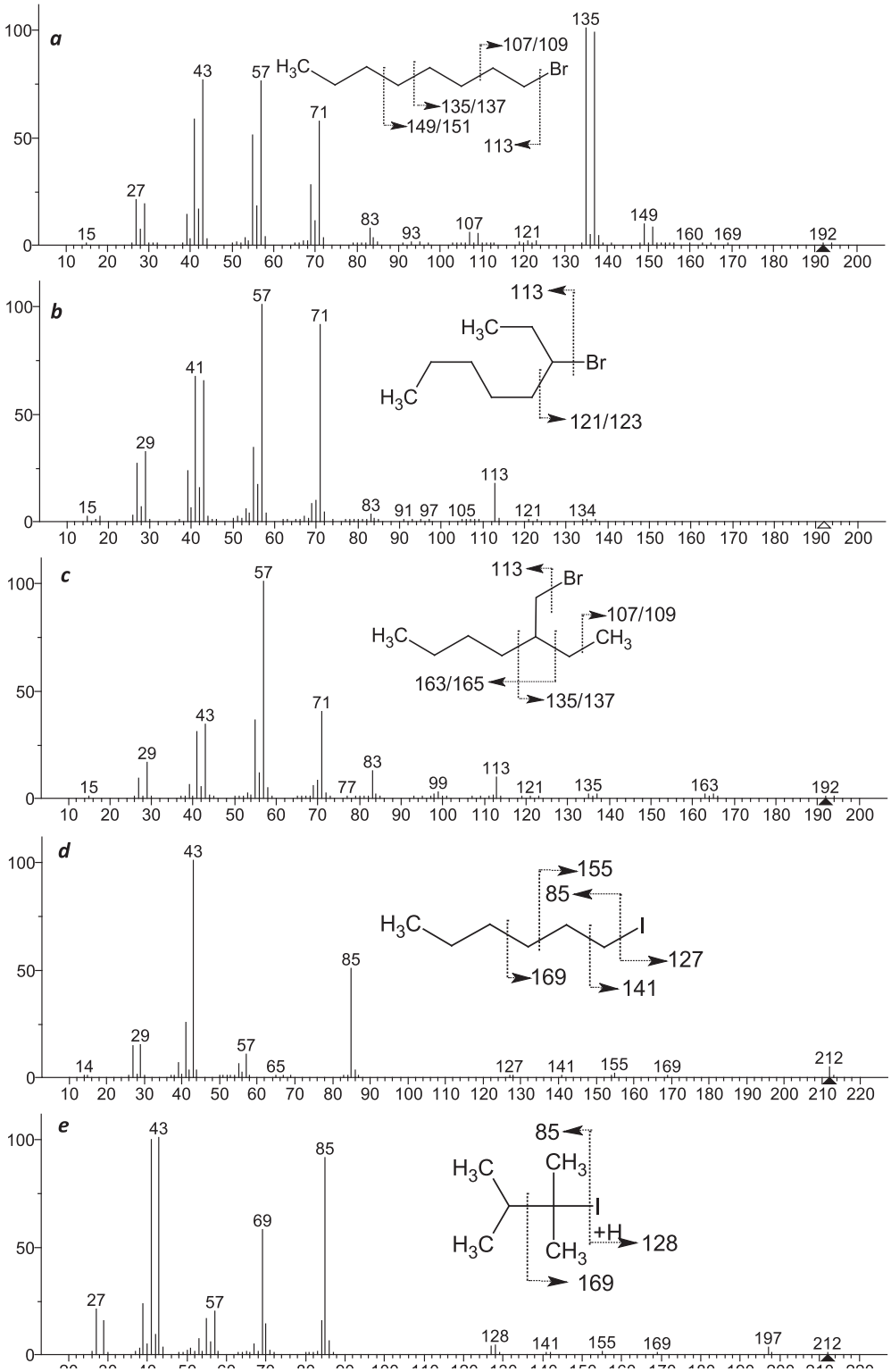

FIG. 46. Mass spectra [m/z (relative abundance, %)] of 1-bromo-*n*-octane (a), 3-bromo-*n*-octane (b), 3-(bromomethyl)-*n*-heptane (c), 1-iodo-*n*-hexane (d), and 2-iodo-2,3-dimethylbutane (e).

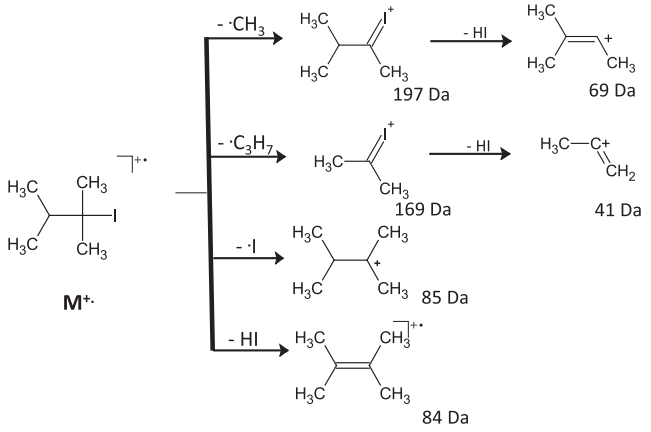

SCHEME 64. Fragmentation patterns of 2-iodo-2,3-dimethylbutane.

$M^{+\cdot}$ is associated with the loss of chlorine radical and/or hydrogen chloride. Comparison of decomposition of isomeric chlorohexenes [Figs. 47(a) and 47(b)] demonstrates competing β-cleavages relative to the double bond and the ease of formation of ions originated due to rearrangement processes, such as the $[M\text{-}C_3H_7]^+$ (75/77 Da) EE ion in the case of 1-chlorohexene [Fig. 47(b)] and the $[M\text{-}C_2H_4]^{+\cdot}$ (90/92 Da) OE ion peak in the spectrum of 6-chlorohexene [Fig. 47(a)]. Allylic cleavage enhanced by the branching is responsible for the formation of $[CH_2{=}CHCHCl]^+$ (75/77 Da) EE ions in the case of 3-chloro-1,5-hexadiene [Fig. 47(c)]. The same type of dissociation is typical for hexynyl chloride [Fig. 47(e)]. Noticeable peaks at 88/90 are observed in the latter spectrum that are the products of preliminary acetylene-allene isomerization of the $M^{+\cdot}$ followed by 1,6-shift of chlorine and the loss of an ethylene molecule (Scheme 65).

Generation of the $[CH_2(Cl)CCH{=}CH_2]^{+\cdot}$ (88/100 Da) OE ion is the major fragmentation pathway for the isomeric allene chloride ($H_2C{=}C{=}CHCH_2CH_2CH_2Cl$) that produces the base peak in its spectrum.

9.2. Aliphatic fluorocarbons

The mass spectra of lower perfluoro-paraffins usually show just traces of molecular ion peaks and starting from perfluorinated hexanes the $M^{+\cdot}$ peak becomes undetectable. The peak with the highest mass value in the spectra corresponds to $[M\text{-}F]^+$ EE ions, which can be utilized for the determination of the elemental composition. The highest intensity peaks in the spectra of perfluoroalkanes usually correspond to $[CF_3]^+$ (69 Da) EE ions.

Ionized fluorocarbons undergo carbon–fluorine and carbon–carbon bond cleavages. Sequential implementation of these parallel competing processes generates the major peaks in the spectra. Unlike hydrocarbons, much of the charge stays on the smaller part of the molecule after a C–C bond breakup. For that reason, the abundant ions in the spectra correspond to $[CF_3]^+$ (69 Da), $[C_2F_5]^+$ (119 Da), and $[C_3F_7]^+$ (169 Da) EE ions and to their defluorinated analogs, such as $[CF_2]^{+\cdot}$ (50 Da), $[C_2F_4]^{+\cdot}$ (100 Da), and $[C_3F_6]^{+\cdot}$ (150 Da) OE ions, as seen in the spectrum of perfluorohexane [Fig. 48(a)]. Unlike hydrocarbons, branching in a carbon skeleton of a fluorocarbon is not reflected in any way in their

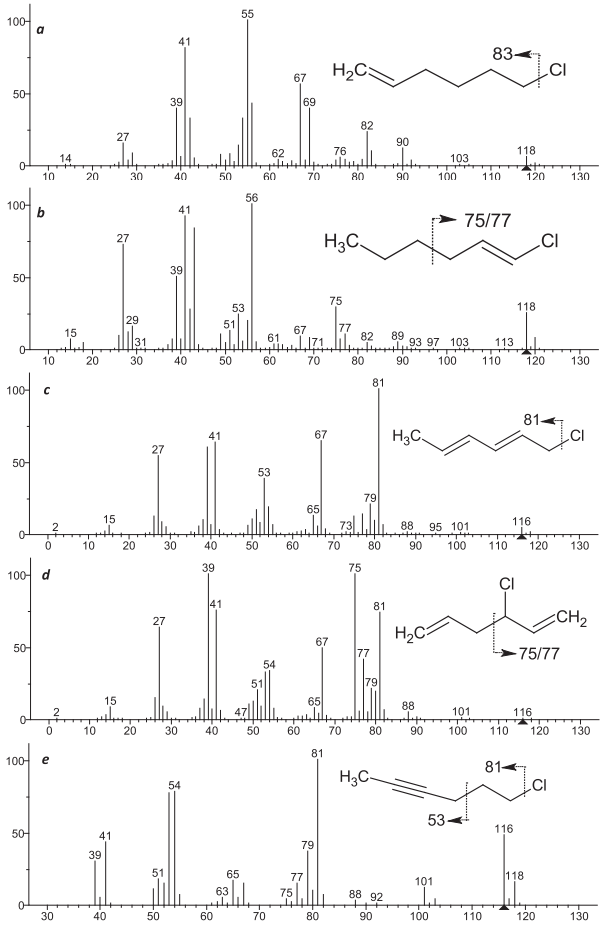

FIG. 47. Mass spectra [m/z (relative abundance, %)] of 1-chloro-5-hexene (a), 1-chloro-1-hexene (b), 1-chloro-2,4-hexadiene (c), 3-chloro-1,5-hexadiene (d), and 6-chloro-2-hexyne (e).

mass spectra. For example, the mass spectrum of perfluoroisohexane [Fig. 48(b)] does not reveal the expected $[M\text{-}CF_3]^+$ and $[M\text{-}C_3F_7]^+$ ion peaks. For comparison, the mass spectrum of the corresponding hydrocarbon—isohexane—shows an abundant $[M\text{-}CH_3]^+$ EE ion and a base peak of the $[M\text{-}C_3H_7]^+$ EE ion.

As noted above, the CF_3 end group is responsible for the base $[CF_3]^+$ ion peaks in the spectra of perfluorinated paraffins [Figs. 48(a) and 48(b)]. In the case of 1-hydro-perfluorohexane [Fig. 48(c)], containing trifluoromethyl and difluoromethyl end

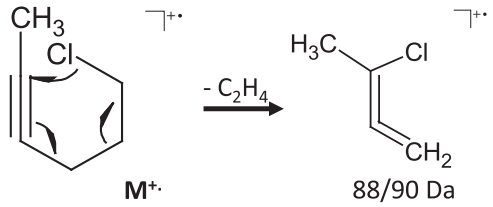

SCHEME 65. Loss of an ethylene molecule from $M^{+\cdot}$ of 6-chloro-2-hexyne.

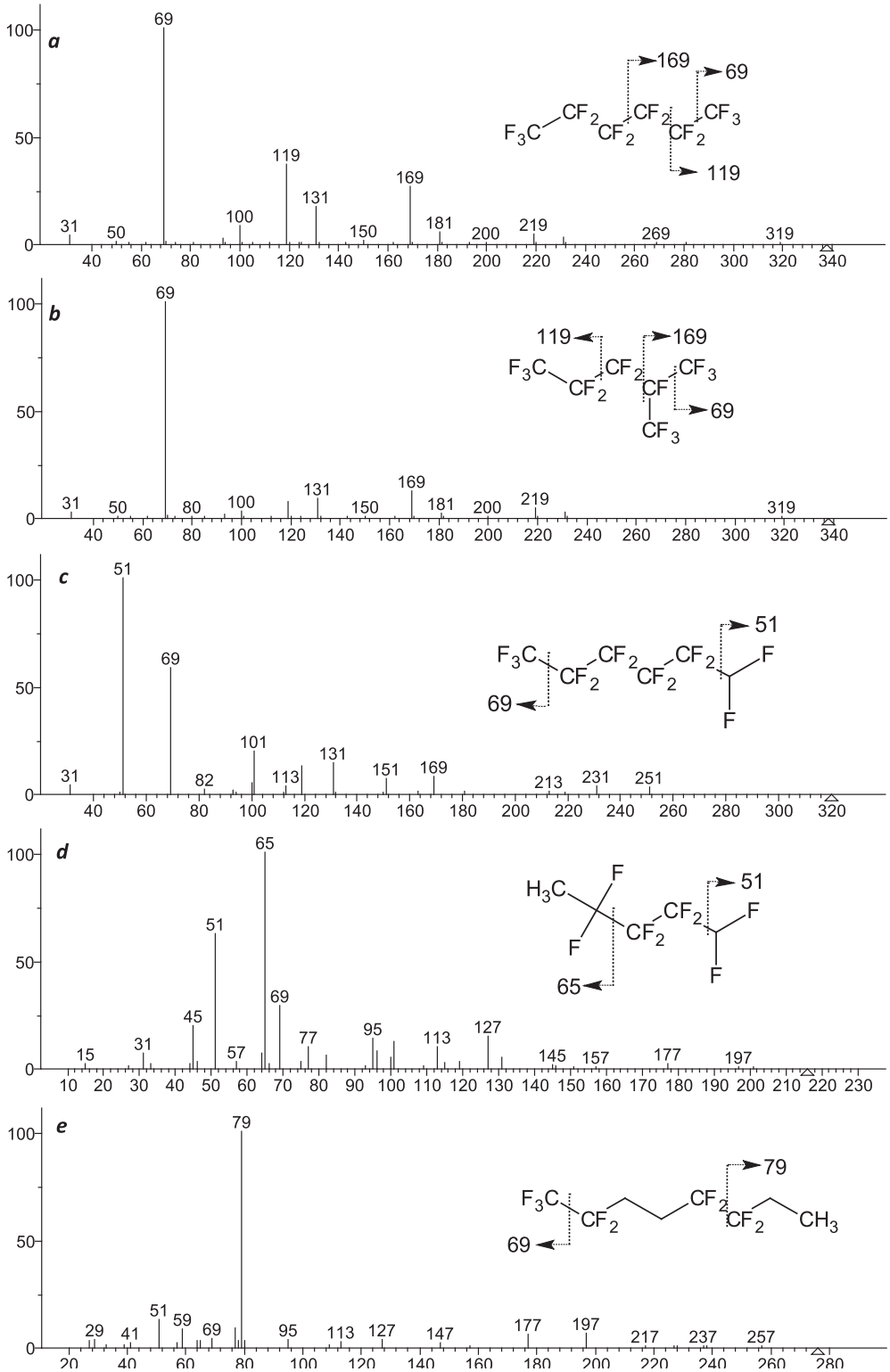

FIG. 48. Mass spectra [m/z (relative abundance, %)] of *n*-tetradecafluorohexane (a), 2-trifluoromethyl-*n*-undecafluorohexane (b), 1-hydro-tridecafluoro-*n*-hexane (c), 1,1,2,2,3,3,4,4-octafluoro-*n*-pentane (d), and 1,1,1,2,2,5,5,6,6-nonafluoro-*n*-octane (e).

groups, the base peak corresponds to the $[CHF_2]^+$ (51 Da) EE ion and the intensity of the $[CF_3]^+$ ion is about 58% rel. In the case of 1,1,2,2,3,3,4,4-octafluoropentane [Fig. 48(d)], the $[C_2H_3F_2]^+$ (65 Da) and $[CHF_2]^+$ (51 Da) EE ions characterize both terminal groups: difluoroethyl and difluoromethyl. These ions can be utilized for identification of their position in a molecule. The spectrum of 1,1,1,2,2,5,5,6,6-nonafluorooctane [Fig. 48(e)] gives evidence that the cleavage of a bond between two difluoromethylene groups is preferred. This is why the only outstanding peak in the spectrum corresponds to the $[CF_2C_2H_5]^+$ (79 Da) EE ion. In addition, it should be noted that $[CF_3]^+$ (69 Da) of various intensities can be frequently generated during dissociation of partially fluorinated hydrocarbons even if they do not contain a terminal trifluoromethyl group.

The behavior of halo-paraffins under EI may not have universal grounds for rapid structure determination. However, their general and specific dissociation rules are the key elements for making structure determination among unknowns.

Supplementary Material

See the supplementary material for mass and isotopic composition of selected naturally occurring elements that mostly build organic and organometallic molecules are incorporated in Appendix A, Table 7. A list of ions with diagnostic power for acyclic compounds is also encompassed in Appendix A, Table 8; ion structures are given as one of the tools for data visualization. Similar lists of ions with diagnostic power will be provided in Papers II-V.

Acknowledgments

The author thanks Dr. Nune Atyan, Dr. Pawel Jaruga, Dr. Jacolin A. Murray, Dr. Nino G. Todua, Dr. Kirill V. Tretyakov, Dr. William E. Wallace, Dr. Vladimir G. Zaikin, and Dr. Rebecca A. Zangmeister for discussions, assistance, review, and recommendations during preparation of this manuscript.

This research did not receive any specific grant from funding agencies in the public, commercial, or not-for-profit sectors.

Certain commercial materials are identified in this paper in order to specify the origin of experimental data adequately. Such identification is not intended to imply recommendation or endorsement by the National Institute of Standards and Technology, nor is it intended to imply that the identified materials are necessarily the best available for the purpose.

10. Author declarations

10.1. Conflict of Interest

The authors have no conflicts to disclose.

11. Data availability

Data sharing is not applicable to this article as no new data were created or analyzed in this study.

12. Appendix: Composition of selected elements and of ions with diagnostic power

TABLE 7. Mass and isotopic composition of selected naturally occurring elements and their properties

Element	Symbol	Atomic number	Number of neutrons	Mass of atom (Da)	Abundance (%)	Isotope pattern	Ionization energy[a] [kJ/mol (eV)]
Hydrogen	^{1}H	1	0	1.007 825	99.988 5	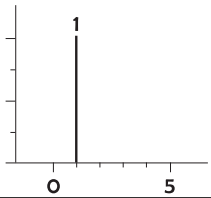	1312.0 (13.5984)
Deuterium	^{2}H		1	2.014 102	0.011 5		
Tritium	^{3}H		2	3.016 049	⋯		
Helium	^{3}He	2	1	3.016 029	0.000 137	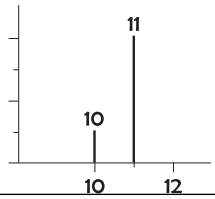	2372.3 (24.5874)
	^{4}He		2	4.002 603	99.999 863		
Boron	^{10}B	5	5	10.012 937	19.9	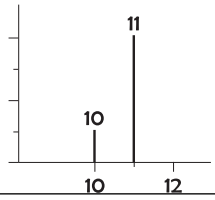	800.6 (8.298)
	^{11}B		6	11.009 305	80.1		

TABLE 7. (*Continued.*)

Element	Symbol	Atomic number	Number of neutrons	Mass of atom (Da)	Abundance (%)	Isotope pattern	Ionization energy[a] [kJ/mol (eV)]
Carbon	^{12}C	6	6	12.000 000	98.93	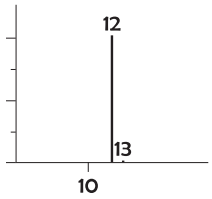	1086.5 (11.2603)
	^{13}C		7	13.003 355	1.07		
	^{14}C		8	14.003 242	⋯		
Nitrogen	^{14}N	7	7	14.003 074	99.632	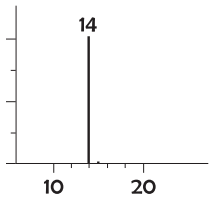	1402.3 (14.5341)
	^{15}N		8	15.000 109	0.368		
Oxygen	^{16}O	8	8	15.994 915	99.757	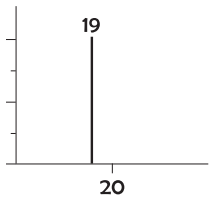	1313.9 (13.6181)
	^{17}O		9	16.999 132	0.038		
	^{18}O		10	17.999 160	0.205		
Fluorine	^{19}F	9	10	18.998 403	100	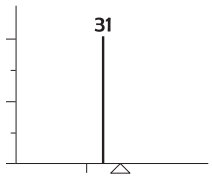	1681.0 (17.4228)
Neon	^{20}Ne	10	10	19.992 436	90.48	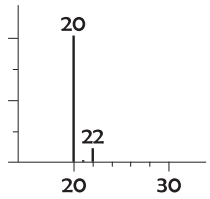	2080.7 (21.5646)
	^{21}Ne		11	20.993 843	0.27		
	^{22}Ne		12	21.991 383	9.25		
Silicon	^{28}Si	14	14	27.976 927	92.229 7	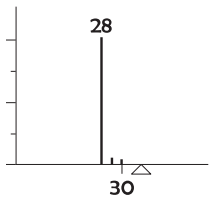	786.5 (8.1517)
	^{29}Si		15	28.976 495	4.683 2		
	^{30}Si		16	29.973 770	3.087 2		
Phosphorus	^{31}P	15	16	30.973 762	100	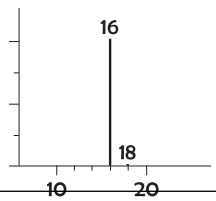	1011.8 (10.4867)

TABLE 7. (*Continued.*)

Element	Symbol	Atomic number	Number of neutrons	Mass of atom (Da)	Abundance (%)	Isotope pattern	Ionization energy[a] [kJ/mol (eV)]
Sulfur	^{32}S	16	16	31.972 071	94.93	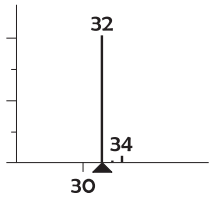	999.6 (10.36)
	^{33}S		17	32.971 458	0.76		
	^{34}S		18	33.967 867	4.29		
	^{36}S		20	35.967 081	0.02		
Chlorine	^{35}Cl	17	18	34.968 853	75.78	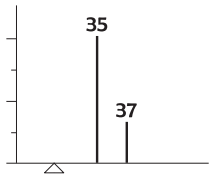	1251.2 (12.9676)
	^{37}Cl		20	36.965 903	24.22		
Argon	^{38}Ar	18	20	37.962 732	0.063 2		1520.6 (15.7596)
	^{40}Ar		22	39.962 383	99.600 3		
Manganese	^{55}Mn	25	30	54.938 05	100	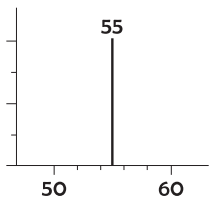	717.3 (7.434)
Iron	^{54}Fe	26	28	53.939 615	5.845	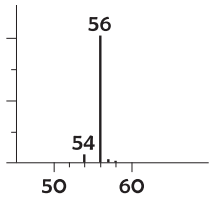	762.5 (7.9024)
	^{56}Fe		30	55.934 942	91.754		
	^{57}Fe		31	56.935 399	2.119		
	^{58}Fe		32	57.933 280	0.282		
Germanium	^{70}Ge	32	38	69.924 250	20.84	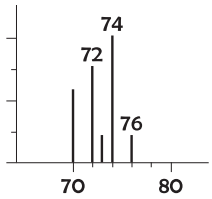	762 (7.8994)
	^{72}Ge		40	71.922 076	27.54		
	^{73}Ge		41	72.923 459	7.73		
	^{74}Ge		42	73.921 178	36.28		
	^{76}Ge		44	75.921 403	7.61		

TABLE 7. (*Continued.*)

Element	Symbol	Atomic number	Number of neutrons	Mass of atom (Da)	Abundance (%)	Isotope pattern	Ionization energy[a] [kJ/mol (eV)]
Arsenic	^{75}As	33	42	74.921 596	100	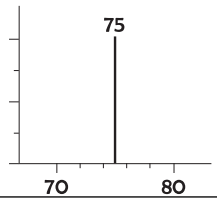	947 (9.7886)
Selenium	^{74}Se	34	40	73.922 477	0.89	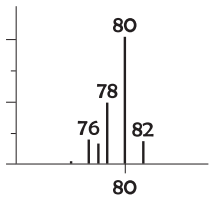	941 (9.7524)
	^{76}Se		42	75.919 214	9.37		
	^{77}Se		43	76.919 915	7.63		
	^{78}Se		44	77.917 310	23.77		
	^{80}Se		46	79.916 522	49.61		
	^{82}Se		48	81.916 700	8.73		
Bromine	^{79}Br	35	44	78.918 338	50.69	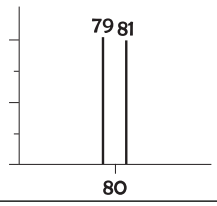	1139.9 (11.8138)
	^{81}Br		46	80.916 291	49.31		
Krypton	^{78}Kr	36	42	77.920 396	0.35	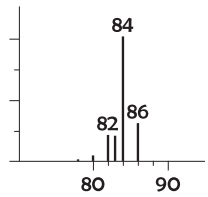	1350.8 (13.9996)
	^{80}Kr		44	79.916 380	2.28		
	^{82}Kr		46	81.913 482	11.58		
	^{83}Kr		47	82.914 135	11.49		
	^{84}Kr		48	83.911 507	57.00		
	^{86}Kr		50	85.910 616	17.30		
Tin	^{112}Sn	50	62	111.904 821	0.97	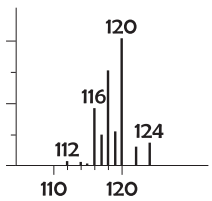	708.6 (7.3439)
	^{114}Sn		64	113.902 782	0.66		
	^{115}Sn		65	114.903 346	0.34		
	^{116}Sn		66	115.901 744	14.54		
	^{117}Sn		67	116.902 954	7.68		
	^{118}Sn		68	117.901 606	24.22		
	^{119}Sn		69	118.903 309	8.59		
	^{120}Sn		70	119.902 197	32.58		
	^{122}Sn		72	121.903 440	4.63		
	^{124}Sn		74	123.905 275	5.79		
Tellurium	^{120}Te	52	68	119.904 020	0.09	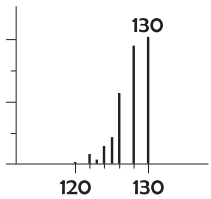	893.5 (9.0096)
	^{122}Te		70	121.903 047	2.55		
	^{123}Te		71	122.904 273	0.89		
	^{124}Te		72	123.902 819	4.74		
	^{125}Te		73	124.904 425	7.07		
	^{126}Te		74	125.903 306	18.84		
	^{128}Te		76	127.904 461	31.74		
	^{130}Te		78	129.906 223	34.08		

TABLE 7. (*Continued.*)

Element	Symbol	Atomic number	Number of neutrons	Mass of atom (Da)	Abundance (%)	Isotope pattern	Ionization energy[a] [kJ/mol (eV)]
Iodine	^{127}I	53	74	126.904 468	100	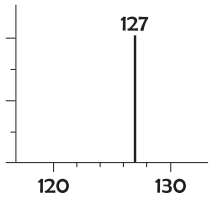	1008.4 (10.4513)
Xenon	^{124}Xe	54	70	123.905 894 2	0.09	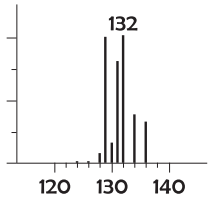	1170.4 (12.1298)
	^{126}Xe		72	125.904 281	0.09		
	^{128}Xe		74	127.903 531 2	1.92		
	^{129}Xe		75	128.904 780 1	26.44		
	^{130}Xe		76	129.903 509 4	4.08		
	^{131}Xe		77	130.905 072	21.18		
	^{132}Xe		78	131.904 144	26.89		
	^{134}Xe		80	133.905 395	10.44		
	^{136}Xe		82	135.907 214	8.87		
Lead	^{204}Pb	82	122	203.973 029	1.4	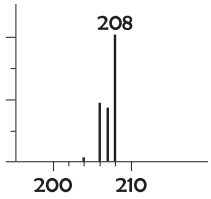	715.6 (7.4167)
	^{206}Pb		124	205.974 449	24.1		
	^{207}Pb		125	206.975 881	22.1		
	^{208}Pb		126	207.976 636	52.4		

[a] 1 eV = 96.485 34 kJ/mol; 1 kJ/mol = 0.010 364 268 8 eV.

TABLE 8. Mass values of ions of diagnostic power, composition of these ions, and list of compounds generating these ions under EI

m/z	Ion structure	Typical for the compounds
12	$[C]^+$	Lower hydrocarbons
13	$[HC]^+$	Lower hydrocarbons
14	$[N]^+$	Nitrogen, nitrogen containing compounds
	$[N_2]^{2+}$	
15	$[CH_3]^+$	Alkanes, alkenes, aliphatic chain
16	$[CH_4]^{+\cdot}$	Hydrocarbons
	$[NH_2]^+$	Nitrogen containing compounds
	$[O]^+$	Oxygen, oxygen containing compounds
	$[O_2]^{2+}$	
17	$[NH_3]^{+\cdot}$	Primary amines
	$[OH]^+$	Oxygen containing compounds
18	$[NH_4]^+$	Amines
	$[H_2O]^{+\cdot}$	Alcohols
19	$[H_3O]^+$	Alcohols
	$[F]^+$	Fluoro-compounds
20	$[HF]^{+\cdot}$	Fluoro-compounds
24	$[C_2]^+$	Acetylenes, alkadienes, alkenes
25	$[CH{\equiv}C]^+$	Acetylenes, alkadienes, alkenes, alkanes
26	$[CH{\equiv}CH]^{+\cdot}$	Acetylenes, alkadienes, alkenes, alkanes
27	$[CH_2{=}CH]^+$	Alkanes, alkenes, aliphatic chain

TABLE 8. (*Continued.*)

m/z	Ion structure	Typical for the compounds
28	$[CH_2{=}CH_2]^{+\cdot}$	Alkanes, alkenes, aliphatic chain
	$[HC{\equiv}NH]^+$	Alkylamines, ethyleneimines
29	$[C_2H_5]^+$	Ethyl esters, compounds containing ethyl moiety
	$[HC{\equiv}O]^+$	Aldehydes, ketones
	$[SiH]^+$	Silicon containing compounds
30	$[CH_2{=}NH_2]^+$	Amines, methylureas, methylthioureas
	$[N{=}O]^+$	Nitroalkanes, alkyl nitrates, alkyl nitrites, *N*-oxide-dimethyldiazenes
31	$[HN{=}NH_2]^+$	Alkylhydrazines
	$[CH_2{=}OH]^+$	Alcohols, ethers
	$[CH_3O]^+$	Methyl esters
	$[CF]^+$	Fluorinated paraffins
32	$[NH_2NH_2]^{+\cdot}$	Acyl hydrazides
	$[HN{=}OH]^+$	Oximes
	$[S]^+$	Thiols, disulfides, thioesters
33	$[NH_2OH]^{+\cdot}$	*N*-Alkoxyamines
	$[CH_3OH_2]^+$	Methyl alkyl ethers
	$[CH_2{=}F]^+$	Fluorinated paraffins
	$[HS]^+$	Thiols, thioesters
34	$[H_2S]^{+\cdot}$	Thiols, thioesters
35	$[H_3S]^+$	Thiols, thioesters
35/37	$[^{35}Cl]^+/[^{37}Cl]^+$	Chlorine containing compounds
36/38	$[^{35}ClH]^{+\cdot}/[^{37}ClH]^{+\cdot}$	Chlorine containing compounds
39	$[C_3H_3]^+$	Acetylenes, alkadienes, alkenes, alkanes
40	$[C_3H_4]^{+\cdot}$	Acetylenes, alkadienes, alkenes, alkanes
41	$[C_3H_5]^+$	Alkadienes, alkenes, alkanes
	$[CH_2{=}C{=}NH]^+$	Aldoximes, cyanoalkanes
42	$[C_3H_6]^{+\cdot}$	Alkanes, alkenes, aliphatic chain
	$[CH_2{=}N{=}CH_2]^+$	Di(alkyl)nitro amines
	$[CH_3C{\equiv}NH]^+$	*O*-Methyloximes, methylimines of alkanones
	$[CH_3N{\equiv}CH]^+$	Hydrazine derivatives
	$[CH_2{=}CO]^{+\cdot}$	Alkyl acetates
43	$[C_3H_7]^+$	Alkanes, alkenes, aliphatic chain
	$[CH_2{=}NH{=}CH_2]^{+\cdot}$	Di(alkyl)nitroamines
	$[CH_2NCH_3]^{+\cdot}$	Hydrazine derivatives
	$[CH_3CH{=}NH]^{+\cdot}$	Cyanoalkanes
	$[CH_3C{\equiv}O]^+$	Aldehydes, ketones, acetates
	$[C_2F]^+$	Perfluoroalkanes
44	$[CH_2{=}CHOH]^{+\cdot}$	Aliphatic aldehydes
	$[CH_3CH_2{=}NH]^+$	Ethyl-carbamides, amines, methylureas, methylthioureas
	$[N(CH_3)_2]^+$	*N*,*N*-Dimethylureas
	$[CH_2{=}NHCH_3]^+$	Methylamines, hydrazine derivatives
	$[N(H)C_2H_5]^+$	*N*-ethylureas
	$[NH_2{=}CO]^+$	Alkyl-carbamides
	$[CO_2]^{+\cdot}$	Alkanoic acids (decomposition product)
	$[CONH_2]^+$	Alkylureas
	$[CH_2NO]^+$	Amides
45	$[(CH_3)_2NH]^+$	Hydrazine derivatives
	$[(CH_3)N{=}NH_2]^+$	Alkyl(methyl)hydrazines
	$[CH_2{=}OCH_3]^+$	Methyl alkyl ethers
	$[CH_3CH_2O]^+$	Compounds with ethoxy moiety
	$[CH(CH_3){=}OH]^+$	Alkanols
	$[CH{\equiv}S]^+$	Dialkylsulfides
	$[HSi{\equiv}O]^+$	Trimethylsilyl alkanoates

TABLE 8. (*Continued.*)

m/z	Ion structure	Typical for the compounds
46	$[NO_2]^+$	Alkyl nitrates
	$[CH_2{=}NHOH]^+$	*N*,*N*-Dialkylhydroxylamines
	$[CH_2{=}ONH_2]^+$	*N*-Alkoxyamines
	$[CH_2{\equiv}S]^+$	Thiols, thioesters
47	$[C_2H_5OH_2]^+$	Ethyl alkyl ethers
	$([HC(OH)_2]^+$	Dialkyl acetals
	$[CH_3O_2]^+$	Acetals
	$[CH_2{=}SH]^+$	Alkanethiols, dialkylsulfides
48	$[SO]^{+\cdot}$	Methyl sulfamides, sulfoxides, sulfones
49/51	$[^{35}Cl{=}CH_2]^+/[^{37}Cl{=}CH_2]^+$	Chloroalkanes
50	$[CF_2]^{+\cdot}$	Fluorinated paraffins
51	$[CHF_2]^+$	Fluorinated paraffins
54	$[C_4H_6]^{+\cdot}$	Acetylenes, alkadienes, alkenes, alkanes
	$[C_2H_4C{\equiv}N]^+$	Nitroalkanes
55	$[C_4H_7]^+$	Alkanes, alkenes, aliphatic chain
	$[C_3F]^+$	Perfluoroalkanes
56	$[C_4H_8]^{+\cdot}$	Alkanes, alkenes, aliphatic chain
	$[HC{\equiv}CCH_2OH]^{+\cdot}$	β,γ-Alkadienoic acids
	$[CH_2{=}N{=}C{=}O]^+$	Alkyl isocyanates
57	$[C_4H_9]^+$	Alkanes, alkenes, aliphatic chain
	$[C_2H_5C{\equiv}O]^+$	Ethylalkylketones
58	$[C_2H_5CH{=}NH_2]^+$	Amines
	$[CH_3CH{=}NH(CH_3)]^+$	
	$[H_2C{=}N(CH_3)_2]^+$	
	$[C_2H_5N{=}NH]^{+\cdot}$	Semicarbazones
	$[CH_3CH{=}CH(OH)]^{+\cdot}$	α-Methylalkanals
	$[CH_2{=}C(OH)CH_3]^{+\cdot}$	2-Alkanones
	$[CH_2CONH_2]^+$	Amides
59	$[HN{=}NH(C_2H_5)]^+$	Alkylhydrazines
	$[(CH_3)_2C{=}OH]^+$	α,α-Dimethylalkanols
	$[(C_2H_5)HC{=}OH]^+$	α-Ethylalkanols
	$[CH(CH_3){=}OCH_3]^+$	Methyl alkyl ethers
	$[H_3COC{\equiv}O]^+$	Methylalkanoates
	$[H_3CC{\equiv}S]^+$	*O*-Alkylthioacetates
	$[CH_3C(O)NH_2]^{+\cdot}$	*n*-Alkanamides
60	$[CH_2C(OH)_2]^{+\cdot}$	Alkanoic acids
	$[HSCH{=}CH_2]^{+\cdot}$	Unsaturated sulfides
	$[CH_2{=}ONO]^+$	Alkyl nitrites
	$[HO{-}N(CH_3){=}CH_2]^+$	Hydroxylamines-*N*-methyl-*N*-alkyl-
	$[HNC(NH_2)OH]^{+\cdot}$	Semicarbazones
	$[C(S)NH_2]^+$	Alkane thioamides
61	$[CH_2{=}SCH_3]^+$	Methylthio-alkanes
	$[C_2H_5S]^+$	Ethylthioesters
	$[(CH_3)CH{=}SH]^+$	α-Methylalkanethiols, dialkylsulfides
	$[HC(OH)(OCH_3)]^+$	Dimethyl acetals
	$[CH_3COOH_2]^+$	Acetates of alcohols
	$[CH_2{=}N(O)OH]^+$	Nitroalkanes
62	$C_2H_5SH]^+$	Ethylthioesters
	$[(CH_2)_2(OH)_2]^{+\cdot}$	Ethylene ketals
	$[CH_2{=}N(OH)_2]^+$	Nitroalkanes
63	$[CH_2{=}SOH]^+$	Dialkylsulfoxides
63/65	$[C_2H_4Cl]^+$	Chloroalkanes

TABLE 8. (*Continued.*)

m/z	Ion structure	Typical for the compounds
64	$[SO_2]^{+\cdot}$	Methyl sulfamides, dialkylsulfates
65	$[CF_2CH_3]^+$	Fluorinated paraffins
66	$[S_2H_2]^{+\cdot}$	Alkyldisulfides
68	$[C_5H_8]^{+\cdot}$	Acetylenes, alkadienes, alkenes
	$[C_3H_6C{\equiv}N]^+$	Nitroalkanes, nitriles
69	$[C_5H_9]^+$	Alkanes, alkenes, aliphatic chain
	$[CF_3]^+$	Fluorinated paraffins, trifluoroacetates
70	$[C_5H_{10}]^{+\cdot}$	Alkanes, alkenes, aliphatic chain
71	$[C_5H_{11}]^+$	Alkanes, alkenes, aliphatic chain
	$[CH_3NHC(CH_3){=}CH_2]^{+\cdot}$	Methylimines of alkanones
	$[C_3H_7C{\equiv}O]^+$	Aliphatic hydroxamic acids, alkyl(propyl)ketones
72	$[C_2H_5CH{=}CHOH]^{+\cdot}$	α-Ethylalkanals
	$[CH_2{=}C(C_2H_5)OH]^{+\cdot}$	Alkyl(ethyl)ketones
	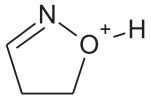	Aldoximes
	$[(CH_3)_2N{=}C{=}O]^+$	Amides
	$[CH_2CH_2C(O)NH_2]^+$	*n*-Alkanamides
	$[CH_2{=}N{=}C{=}S]^+$	Alkyl isothiocyanates
	$[CH_2{=}SCHCH_2]^+$	Unsaturated sulfides
73	$[C_3H_7O{=}CH_2]^+$	Dialkyl ethers
	$[C_2H_5O{=}CHCH_3]^+$	
	$[CH_3O{=}C(CH_3)_2]^+$	
	$[C_3H_7CH{=}OH]^+$	Alcohols
	$[(CH_3)_3Si]^+$	Trimethylsilyl ethers, thioethers, esters, thioesters, *N*-trimethylsilyl amines, -amides
	$[C_2H_5C{\equiv}S]^+$	*O*-Alkyl thiopropionates
	$[HN{=}NH(C_3H_7)]^+$	Alkylhydrazines
	$[CH_2{=}CHC(OH)_2]^{+\cdot}$	Alkanoic acids
	$[COOC_2H_5]^+$	Ethyl esters
	$[CH_3COO{=}CH_2]^+$	*n*-Alkanol acetates
	$[CH_2{=}C(CH_3)NHOH]^{+\cdot}$	Ketoximes
74	$[HSCH_2CH{=}CH_2]^{+\cdot}$	Unsaturated sulfides
	$[CH(CH_3)C(OH)_2]^{+\cdot}$	α-Methyl-alkanoic acids
	$[CH_2C(OH)OCH_3]^{+\cdot}$	Methylalkanoates
	$[C(S)NH(CH_3)]^+$	Alkane thioamides
	$[CH_3C(O)NHNH_2]^+$	*n*-Alkanoic acid hydrazides
75	$[(CH_3)_2C{=}SH]^+$	α,α-Dimethylalkanethiols, dialkylsulfides
	$[CH(OCH_3)_2]^+$	Dimethyl acetals
	$[C_2H_5COOH_2]^+$	Alkyl propionates (alkyl > C_2H_5)
	$[CH_2{=}CHSO]^+$	Vinylsulfones
	$[(CH_3)_2SiOH]^+$	Trimethylsilyl ethers, *tert*-butyldimethylsilyl ethers, esters
	$[CH_2{=}C(OH)NHOH]^{+\cdot}$	Aliphatic hydroxamic acids
	$[(CH_3)HC{=}N(OH)O]^{+\cdot}$	Nitroalkanes
75/77	$[C_3H_4Cl]^+$	1-Chloroalkenes
76	$[CS_2]^{+\cdot}$	Alkyl alkanedithioates
	$[(CH_3)HC{=}N(OH)_2]^+$	α-Methylnitroalkanes
	$[CH_2{=}ONO_2]^+$	Alkyl nitrates
77/79	$[C_3H_6{=}Cl]^+$	Chloroalkanes
78/80	$[CH_3C(O)Cl]^{+\cdot}$	Chloro anhydrides of alkanoic acids

TABLE 8. (*Continued.*)

m/z	Ion structure	Typical for the compounds
79	$[CF_2C_2H_5]^+$	Fluorinated paraffins
	$[CH_3SO_2]^{+\cdot}$	*O*-Alkyl methanesulfonates
79/81	$[^{79}Br]^+/[^{81}Br]^+$	Brominated compounds
80	$[CH_3SSH]^{+\cdot}$	Methyldisufides
80/82	$[^{79}BrH]^{+\cdot}/[^{81}BrH]^{+\cdot}$	Brominated compounds
82	$[C_6H_{10}]^{+\cdot}$	Acetylenes, alkadienes, alkenes, alkanes
	$[C_4H_8C{\equiv}N]^+$	Nitroalkanes, alkylcyanides
83	$[C_6H_{11}]^+$	Alkenes, alkanes
	$[S(OH)_3]^+$	Dialkyl sufites
84	$[C_6H_{12}]^{+\cdot}$	Alkenes, alkanes
	$[C_4H_9C{\equiv}NH]^+$	Semicarbazones, thiosemicarbazones
85	$[C_6H_{13}]^+$	Alkanes
	$[C_4H_9C{\equiv}O]^+$	Aliphatic hydroxamic acids, butyl(alkyl)ketones
	$[CH_2{=}CH{-}N{=}N(CH_3)_2]^+$	Alkanal dimethylhydrazones
86	$[C_4H_9CH{=}NH_2]^+$	α-Butyl(alkyl)amines
	$[C_3H_7C(OH){=}CH_2]^+$	Propyl(alkyl)ketones
	$[CH_2{=}CH{-}NH{-}N(CH_3)_2]^{+\cdot}$	Alkanal dimethylhydrazones
	$[HCNNHCONH_2]^+$	Semicarbazones
87	$[C_5H_{11}O]^+$	Alkanols, dialkyl ethers
	$[C_3H_7C{\equiv}S]^+$	*O*-Alkyl thiobutyrates
	$[C_3H_7COO]^+$	Alkyl butyrates
	$[CH_2{=}CHC(OH)OCH_3]^{+\cdot}$	Methylalkanoates
	$[CH(CH_3){=}CHC(OH)_2]^{+\cdot}$	α-Methyl-alkanoic acids
	$[CH_2CH_2C(O)NHNH_2]^+$	*n*-Alkanoic acid hydrazides
88	$[CH(CH_3)C(OH)OCH_3]^{+\cdot}$	Methyl α-methylalkanoates
	$[CH_2C(OH)OC_2H_5]^{+\cdot}$	Ethyl alkanoates
	$[C(CH_3)_2C(OH)_2]^{+\cdot}$	α,α-Dimethyl-alkanoic acids
	$[C(S)N(CH_3)_2]^+$	Alkane thioamides
	$[CH_2{=}CH{-}C(=OH){-}NHOH]^{+\cdot}$	Aliphatic hydroxamic acids
88/90	$[CH_3C(Cl){=}C{=}CH_2]^{+\cdot}$	Alkyne chlorides and allene chlorides
	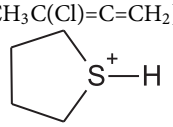	
89		Alkanethiols, dialkylsulfoxides, thioesters
	$[C_3H_7COOH_2]^+$	Alkyl butyrates (alkyl > C_2H_5)
	$[C_4H_9O_2]^+$	Acetals, ketals
	$[OSi(CH_3)_3]^+$	Trimethylsilyl esters
	$[(CH_3)_2C{=}N(OH)O]^{+\cdot}$	Nitroalkanes
90	$[(CH_3)CH{=}ONO_2]^+$	Alkyl nitrates
91	$[HS{=}Si(CH_3)_2]^+$	Trimethylsilyl-thiols
	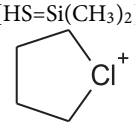	
91/93		*n*-Alkyl chlorides
	$[CH_2CH_2C(O)Cl]^+$	Chloro anhydrides of alkanoic acids
92	$[H_3CC(S)SH]^{+\cdot}$	Alkyl dithioacetates
93/95	$[^{79/81}Br{=}CH_2]^{+\cdot}$	Alkyl bromides
95	$[C_7H_{11}]^+$	Alkadienes, acetylene hydrocarbons

TABLE 8. (*Continued.*)

m/z	Ion structure	Typical for the compounds
96	$[C_7H_{12}]^{+\cdot}$	Acetylenes, alkadienes, alkenes, alkanes
	$[C_5H_{10}C{\equiv}N]^+$	Nitroalkanes, alkylcyanides
97	$[C_7H_{13}]^+$	Alkanes, alkenes, aliphatic chain
98	$[C_7H_{14}]^{+\cdot}$	Alkanes, alkenes, aliphatic chain
	$[C_3H_6C(O)NCH_2]^+$	Pyrrolidone derivatives of alkanols and alkenols
99	$[C_7H_{15}]^+$	Alkanes, alkenes, aliphatic chain
	$[C_5H_{11}C{\equiv}O]^+$	Aliphatic hydroxamic acids, pentyl(alkyl)ketones
	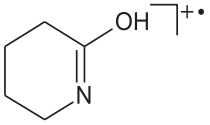	Alkyl isocyanates
	$[C_3H_6C(OH)NCH_2]^+$	Pyrrolidone derivatives of alkanols and alkenols
	$[(OH)_3S{=}O]^+$	Dialkylsulfates
100	$[C_5H_{11}CH{=}NH_2]^+$	α-Pentyl(alkyl)amines
	$[C_4H_9C(OH){=}CH_2]^{+\cdot}$	Butyl(alkyl)ketones
	$[CF_2{=}CF_2]^{+\cdot}$	Fluorinated paraffins
101	$[C(CH_3)_2{=}CHC(OH)_2]^{+\cdot}$	α,α-Dimethyl-alkanoic acids
	$[C_4H_9COO]^+$	Alkyl butyrates
	$[CH(CH_3){=}CHC(OH)OCH_3]^{+\cdot}$	Methyl α-methylalkanoates
102	$[C(CH_3)_2C(OH)OCH_3]^{+\cdot}$	Methyl α,α-dimethylalkanoates
	$[H_2C{=}N(H)Si(CH_3)_3]^+$	*N*-(Trimethylsilyl)alkylamines
	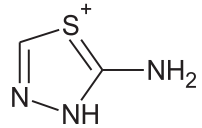	Thiosemicarbazones
103	$[C_5H_{11}S]^+$	Pentyl(alkyl)sulfides
	$[CH(OC_2H_5)_2]^+$	Diethyl acetals and ketals
	$[C_4H_9COOH_2]^+$	Alkyl butyrates
	$[CH_2{=}OSi(CH_3)_3]^+$	Trimethylsilyl ethers of alcohols
104	$[C_2H_5CH{=}ONO_2]^+$	α-(Ethylalkyl)nitrates
	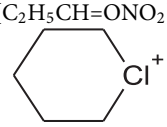	
105/107		*n*-Alkyl chlorides
106	$[C_4H_9SOH]^{+\cdot}$	Butyl(alkyl)sulfoxides
107/109	$[C_2H_4{}^{79/81}Br]^+$	Bromoalkanes
109	$[CH_2{=}O{-}S(CH_3)O_2]^+$	*O*-Alkyl methanesulfonates
110	$[C_8H_{14}]^{+\cdot}$	Acetylenes, alkadienes, alkenes
	$[CH_2{=}SO(OH)(OCH_3)]^+$	Methyl alkanesulfonates
111	$[C_8H_{15}]^+$	Acetylenes, alkadienes, alkenes, alkanes
	$[CH_2{=}O{-}S(OH)O_2]^+$	Dialkylsulfates
112	$[C_8H_{16}]^{+\cdot}$	Alkanes, alkenes, aliphatic chain
113	$[C_8H_{17}]^+$	Alkanes, alkenes, aliphatic chain
	$[C_6H_{13}C{\equiv}O]^+$	Aliphatic ketones
	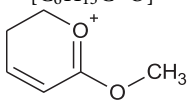	Methyl α,β-alkenoates
	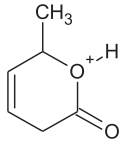	Methyl γ,δ-alkenoates

TABLE 8. (*Continued.*)

m/z	Ion structure	Typical for the compounds
	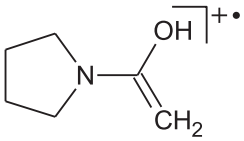	Alkanoic acid pyrrolidides
	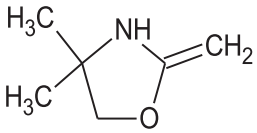	Dimethyloxazoline derivatives of alkanoic acids
115	$[(CH_3)_3CSi(CH_3)_2]^+$	*tert*-Butyldimethylsilyl ethers, esters, *N*-*tert*-butyldimethylsilyl amides
	$[C(CH_3)_2{=}CHC(OH)OCH_3]^{+\cdot}$	Methyl α,*α*-dimethylalkanoates
	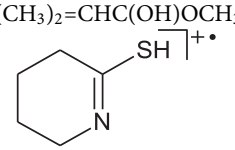	Alkyl isothiocyanates
116	$[(CH_3)HC{=}NH(Si(CH_3)_3]^+$	*N*-(Trimethylsilyl)alkylamines
	$[C(S)N(C_2H_5)_2]^+$	Alkane thioamides, *N*,*N*-diethyl
	$[CH_3C(O)NHSi(CH_3)_2]^{+\cdot}$	*N*-trimethylsilyl-*n*-alkanamides
117	$[(CH_3)CH{=}OSi(CH_3)_3]^+$	Trimethylsilyl ethers of alcohols
	$[(CH_3)_3CSi(CH_3)OH]^+$	*tert*-Butyldimethylsilyl ethers, esters
	$[CH_2{=}C(OH)O{=}Si(CH_3)_2]^+$	Trimethylsilyl alkanoates
119	$[C_2F_5]^+$	Fluorinated paraffins, pentafluoropropionates
121/123	$[C_3H_6{}^{79/81}Br]^+$	Bromoalkanes
124	$[C_7H_{14}CN]^+$	Alkyl cyanides
125	$[C_9H_{17}]^+$	Acetylenes, alkadienes, alkenes, alkanes
125	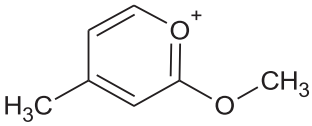	Methyl 3-methyl-2,4-alkanedienoates
126	$[C_9H_{18}]^{+\cdot}$	Alkanes, alkenes, aliphatic chain
	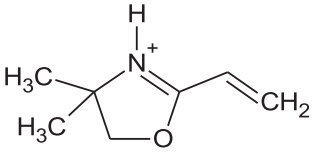	Dimethyloxazoline derivatives of *n*-alkanoic acids
127	$[C_9H_{19}]^+$	Alkanes, alkenes, aliphatic chain
	$[C_7H_{15}C{\equiv}O]^+$	Aliphatic ketones
	$[I]^+$	Iodinated compounds
128	$[HI]^{+\cdot}$	Iodinated compounds
129	$[C_6H_{11}C(OH)_2]^{+\cdot}$	Alkanoic acids
	$[C_5H_9C(OH)OCH_3]^{+\cdot}$	Methylalkanoates
	$[CH_2{=}CHC(O)O{=}Si(CH_3)_2]^+$	Trimethylsilyl alkanoates
130	$[(CH_3)_2C{=}NHSi(CH_3)_3]^+$	*N*-(Trimethylsilyl)alkylamines
131	$[(CH_3)_2C{=}OSi(CH_3)_3]^+$	Trimethylsilyl ethers of alcohols
	$[CH(CH_3){=}C(OH)O{=}Si(CH_3)_2]^+$	Trimethylsilyl *α*-methylalkanoates
	$[CH_3C(O)NHSi(CH_3)_3]^{+\cdot}$	*N*-Trimethylsilyl-*n*-alkanamides
	$[CF_2{=}CFCF_2]^+$	Fluorinated paraffins
132	$[CH_2{=}C(OH)O{=}Si(CH_3)_3]^{+\cdot}$	Trimethylsilyl alkanoates

TABLE 8. (*Continued.*)

m/z	Ion structure	Typical for the compounds
132/134	$[CH_3C(Br)=C=CH_2]^{+\cdot}$	Alkyne bromides and allene bromides
	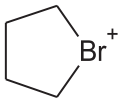	
135/137		*n*-Alkyl bromides
138	$[C_8H_{16}CN]^+$	Alkyl cyanides
139	$[C_{10}H_{19}]^+$	Alkenes, unsaturated hydrocarbons
	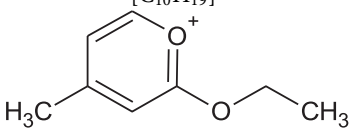	Ethyl 3-methyl-2,4-alkanedienoates
140	$[C_{10}H_{20}]^{+\cdot}$	Alkanes, alkenes, aliphatic chain
141	$[C_{10}H_{21}]^+$	Alkanes, alkenes, aliphatic chain
	$[C_8H_{17}C\equiv O]^+$	Aliphatic ketones
	$[CH_2=I]^+$	Alkyl iodides
143	$[C_7H_{13}C(OH)_2]^{+\cdot}$	Alkanoic acids
	$[C_6H_{11}C(OH)OCH_3]^{+\cdot}$	Methylalkanoates
	$[CH(CH_3)=CHC(O)O=Si(CH_3)_2]^+$	Trimethylsilyl β-methylalkanoates
144	$[(CH_3)_3CSi(CH_3)_2NH=CH_2]^+$	*N*-*tert*-Butyldimethylsilylalkylamines
	$[CH_2CH_2C(O)NHSi(CH_3)_3]^{+\cdot}$	*N*-trimethylsilyl-*n*-alkanamides
145	$[(CH_3)_3C(CH_3)_2SiO=CH_2]^+$	t-Butyldimethylsilyl ethers of alcohols
	$[CH_2=CHC(OH)=OSi(CH_3)_3]^+$	Trimethylsilyl alkanoates
146	$[CH(CH_3)=C(OH)O=Si(CH_3)_3]^+$	Trimethylsilyl α-methylalkanoates
	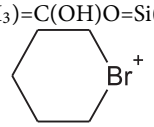	
149/151		*n*-Alkyl bromides
	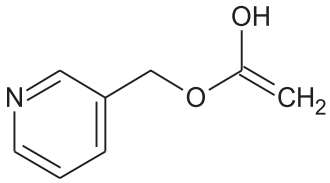	
151		Picolinyl *n*-alkanoates
152	$[C_9H_{18}CN]^+$	Alkyl cyanides
154	$[C_{11}H_{22}]^{+\cdot}$	Alkanes, alkenes, aliphatic chain
155	$[C_{11}H_{23}]^+$	Alkanes, alkenes, aliphatic chain
158	$[(CH_3)_3C\ Si(CH_3)_2NH=CH(CH_3)]^+$	*N*-(*tert*-Butyldimethylsilyl)alkylamines
159	$[CH(CH_3)=CHC(OH)=OSi(CH_3)_3]^+$	Trimethylsilyl β-methylalkanoates
	$[(CH_3)_3C(CH_3)_2SiO=CH(CH_3)]^+$	*tert*-Butylmethylsilyl ethers of alcohols
	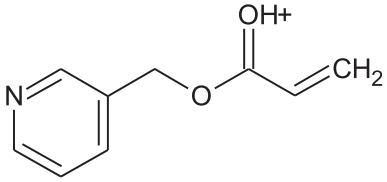	
164		Picolinyl *n*-alkanoates
166	$[C_5H_4NCH_2OSi(CH_3)_2]^+$	Picolinyldimethylsilyl ethers of alkanols and alkenols
	$[C_{10}H_{20}CN]^+$	Alkyl cyanides
168	$[C_{12}H_{24}]^{+\cdot}$	Alkanes, alkenes, aliphatic chain
	$[C_5H_4NCH_2OSi(CH_3)=OH]^+$	Picolinyldimethylsilyl ethers of alkanols
169	$[C_{12}H_{25}]^+$	Alkanes, alkenes, aliphatic chain
	$[C_3F_7]^+$	Fluorinated paraffins, alkyl heptafluorobutyrates
172	$[(CH_3)_3CSi(CH_3)_2NH=C(CH_3)_2]^+$	*N*-(*tert*-Butyldimethylsilyl)alkylamines
173	$[(CH_3)_3C(CH_3)_2SiO=C(CH_3)_2]^+$	*tert*-Butyldimethylsilyl ethers of alcohols

TABLE 8. (*Continued.*)

m/z	Ion structure	Typical for the compounds
174	$[((CH_3)_3Si)_2N{=}CH_2]^+$	*N*,*N*-bis(*N*-trimethylsilyl)alkylamines
181	$[CF_2{=}CFCF_2CF_2]^+$	Fluorinated paraffins
182	$[C_{13}H_{26}]^{+\cdot}$	Alkanes, alkenes, aliphatic chain
183	$[C_{13}H_{27}]^+$	Alkanes, alkenes, aliphatic chain
188	$[(Si(CH_3)_3)_2N{=}CH(CH_3)]^+$	*N*,*N*-bis(*N*-trimethylsilyl)alkylamines
196	$[C_{14}H_{28}]^{+\cdot}$	Alkanes, alkenes, aliphatic chain
197	$[C_{14}H_{29}]^+$	Alkanes, alkenes, aliphatic chain
202	$[[Si(CH_3)_3]_2N{=}CCH_3)_2]^+$	*N*,*N*-bis(*N*-trimethylsilyl)alkylamines
210	$[C_{15}H_{30}]^{+\cdot}$	Alkanes, alkenes, aliphatic chain
211	$[C_{15}H_{31}]^+$	Alkanes, alkenes, aliphatic chain
219	$[C_4F_9]^+$	Fluorinated paraffins
225	$[C_{16}H_{33}]^+$	Alkanes, alkenes, aliphatic chain
231	$[CF_2{=}CFCF_2CF_2CF_2]^+$	Fluorinated paraffins
239	$[C_{17}H_{35}]^+$	Alkanes, alkenes, aliphatic chain
258	$[(Si(CH_3)_2(C_4H_9))_2N{=}CH_2]^+$	*N*,*N*-bis(*tert*-butyldimethylsilyl)alkylamines
272	$[(Si(CH_3)_2(C_4H_9))_2N{=}CHCH_3]^+$	*N*,*N*-bis(*tert*-butyldimethylsilyl)-*α*-methylalkylamines
286	$[(Si(CH_3)_2(C_4H_9))_2N{=}C(CH_3)_2]^+$	*N*,*N*-bis(*tert*-butyldimethylsilyl)-*α*-methylalkylamines

13. References

[1] J. J. Thomson, "*Bakerian Lecture*: Rays of positive electricity," Proc. R. Soc. A **89**, 1–20 (1913).

[2] H. R. Stewart and A. R. Olson, "The decomposition of hydrocarbons in the positive ray tube," J. Am. Chem. Soc. **53**, 1236–1244 (1931).

[3] M. L. Gross and R. M. Caprioli, *The Encyclopedia of Mass Spectrometry. Vol. 6. Ionization Methods*, edited by M. L. Gross and R. M. Caprioli (Elsevier, New York, 2007).

[4] J. H. Beynon, R. A. Saunders, and A. E. Williams, *The Mass Spectra of Organic Compounds* (Elsevier Publishing Company, New York, 1968).

[5] H. Budzikiewicz, C. Djerassi, and D. H. Williams, *Mass Spectrometry of Organic Compounds* (Holden-Day, San Francisco, 1968).

[6] H. Budzikiewicz, C. Djerassi, and D. H. Williams, *Structure Elucidation of Natural Products by Mass Spectrometry. Volume 1: Alkaloids* (Holden-Day, San Francisco, 1964).

[7] H. Budzikiewicz, C. Djerassi, and D. H. Williams, *Structure Elucidation of Natural Products by Mass Spectrometry. Volume 1: Steroids, Terpenoids, Sugars, and Miscellaneous Classes* (Holden-Day, San Francisco, 1964).

[8] F. M. McLafferty and F. Turecek, *Interpretation of Mass Spectra* (University Science Books, Mill Valley, CA, 1993).

[9] K. Biemann, *Mass Spectrometry: Organic Chemical Applications* (McGraw-Hill, New York, 1962).

[10] Q. N. Porter and J. Baldas, *Mass Spectrometry of Heterocyclic Compounds* (Wiley-Interscience, New York, 1971).

[11] R. Ekman, J. Silberring, A. M. Westman-Brinkmalm, and A. Kraj, *Mass Spectrometry: Instrumentation, Interpretation and Applications* (John Wiley & Sons, Hoboken, 2009).

[12] M. C. Hamming and H. G. Foster, *Interpretation of Mass Spectra of Organic Compounds* (Academic Press, New York, 1972).

[13] J. H. Gross, *Mass Spectrometry: A Textbook*, 2nd ed. (Springer, New York, 2011).

[14] J. T. Watson, *Introduction to Mass Spectrometry*, 3rd ed. (Lippincott-Raven, New York, 1997).

[15] R. M. Smith and K. L. Busch, *Understanding Mass Spectra: A Basic Approach* (John Wiley & Sons, New York, 1999).

[16] M. L. Gross and R. M. Caprioli, *The Encyclopedia of Mass Spectrometry. Vol. 3. Biological Applications. Part A: Peptides and Proteins*, edited by R. M. Caprioli and M. L. Gross (Elsevier, New York, 2005).

[17] M. L. Gross and R. M. Caprioli, *The Encyclopedia of Mass Spectrometry. Vol. 2. Biological Applications. Part B: Carbohydrates, Nucleic Acids and Other Biological Compounds*, edited by R. M. Caprioli (Elsevier, New York, 2006).

[18] M. L. Gross and R. M. Caprioli, *The Encyclopedia of Mass Spectrometry. Vol. 8. Hyphenated*, edited by F. M. A. Niessen (Elsevier, New York, 2006).

[19] M. R. Litzow and T. R. Spalding, *Mass Spectrometry of Inorganic and Organometallic Compounds* (Elsevier, New York, 1973).

[20] C. M. Barshchick, D. C. Duckworth, and D. H. Smith, *Inorganic Mass Spectrometry: Fundamentals and Applications* (Marcel Dekker, New York, 2000).

[21] W. Henderson and J. S. McIndoe, *Mass Spectrometry of Inorganic and Organometallic Compounds* (John Wiley & Sons, Chichester, England, 2005).

[22] NIST/EPA/NIH Mass Spectral Library with Search Program Data Version: NIST v20, NIST Standard Reference Database-1A, 2020.

[23] F. W. McLafferty, *Wiley Registry of Mass Spectral Data*, 12th ed. DVD (Wiley, New York, 2020), available at https://www.wiley.com/en-us/Wiley+Registry+of+Mass+Spectral+Data,+12th+Edition-p-9781119171027?purchasedProduct=%2Fen-us%2FWiley%2BRegistry%2Bof%2BMass%2BSpectral%2BData%252C%2B12th%2BEdition-p-9781119171027#.

[24] Mass Frontier™ Spectra Interpretation Software, Thermo Fisher Scientific, 2020, https://mymassfrontier.com/2020/01/22/mass-frontier-8-0-demo-download/.

[25] S. Wang, T. Kind, D. J. Tantillo, and O. Fiehn, "Predicting in silico electron ionization mass spectra using quantum chemistry," J. Cheminf. **12**, 63 (2020).

[26] C. A. Bauer and S. Grimme, "How to compute electron ionization mass spectra from first principles," J. Phys. Chem. A **120**, 3755–3766 (2016).

[27] F. Hufsky and S. Böcker, "Mining molecular structure databases: Identification of small molecules based on fragmentation mass spectrometry," Mass Spectrom. Rev. **36**, 624–633 (2017).

[28] V. Zaikin and J. Halket, *A Handbook of Derivatives for Mass Spectrometry* (IM Publications, Chichester, UK, 2009).

[29] NIST Chemistry Webbook, SRD 69, https://webbook.nist.gov/chemistry/name-ser/.

[30] S. R. Heller, "The history of the NIST/EPA/NIH mass spectral database," Today's Chemist Work **8**, 45–46 (1999), available at https://citeseerx.ist.psu.edu/viewdoc/download?doi=10.1.1.474.7125&rep=rep1&type=pdf.

[31] P. Ausloos, C. L. Clifton, S. G. Lias, A. I. Mikaya, S. E. Stein, D. V. Tchekhovskoi, O. D. Sparkman, V. Zaikin, and D. Zhu, "The critical evaluation of a comprehensive mass spectral library," J. Am. Soc. Mass Spectrom. **10**, 287–299 (1999).

[32]M. Reichenbacher and J. Popp, *Challenges in Molecular Structure Determination* (Springer, New York, 2007).
[33]C. Bruno, F. Patin, C. Bocca, L. Nadal-Desbarats, F. Bonnier, P. Reynier, P. Emond, P. Vourc'h, K. Joseph-Delafont, P. Corcia, C. R. Andres, and H. Blasco, "The combination of four analytical methods to explore skeletal muscle metabolomics: Better coverage of metabolic pathways or a marketing argument?," J. Pharm. Biomed. Anal. **148**, 273–279 (2018).
[34]M. Karni and A. Mandelbaum, "The 'even-electron rule,'" Org. Mass Spectrom. **15**, 53–64 (1980).
[35]M. L. Gross and R. M. Caprioli, *The Encyclopedia of Mass Spectrometry. Vol. 5: Elemental and Isotope Ratio Mass Spectrometry*, 1st ed., edited by D. Beauchemin and D. Matthews (Elsevier, New York, 2008).
[36]D. Valkenborg, I. Mertens, F. Lemière, E. Witters, and T. Burzykowski, "The isotopic distribution conundrum," Mass Spectrom. Rev. **31**, 96–109 (2011).
[37]J. W. Bright and E. C. M. Chen, "Mass spectral interpretation using 'rule of 13,'" J. Chem. Educ. **60**, 557–558 (1983).
[38]H. E. Audier, "Ionisation et fragmentation en spectrometrie de masse—I: Sur la repartition de la charge positive entre fragments provenant de memes ruptures," Org. Mass Spectrom. **2**, 283–298 (1969).
[39]A. M. Duffield, W. Carpenter, and C. Djerassi, "The course of the electron impact-induced elimination of hydrogen sulphide from aliphatic thiols," Chem. Commun. **1967**(3), 109b–110.
[40]E. F. Saad, E. A. Hamed, and A. A. El-Bardan, "Skeletal rearrangements in 2,4-dinitrophenyl-4′-substituted phenyl sulfides and sulfones upon electron impact," Spectrosc. Lett. **24**, 413–421 (1991).
[41]A. I. Mikaia and V. G. Zaikin, "Reaction gas chromatography/mass spectrometry," Mass Spectrom. Rev. **9**, 115–132 (1990).
[42]D. R. Knapp, *Handbook of Analytical Derivatization Reactions* (John Wiley & Sons, New York, 1979).